nagra
National Cooperative for the
Disposal of Radioactive Waste

TECHNICAL REPORT 92-04

Hydrodynamic Synthesis and Modeling of Groundwater Flow in Crystalline Rocks of Northern Switzerland

December 1994

O. Voborny, G. Resele, W. Hürlimann
W. Lanyon, S. Vomvoris, W. Wilson

Hardstrasse 73, CH-5430 Wettingen/Switzerland, Telephone +41-56-37 11 11

nagra National Cooperative for the Disposal of Radioactive Waste

TECHNICAL REPORT 92-04

Hydrodynamic Synthesis and Modeling of Groundwater Flow in Crystalline Rocks of Northern Switzerland

December 1994

O. Voborny[1], G. Resele[1], W. Hürlimann[1]
W. Lanyon[2], S. Vomvoris[3], W. Wilson[4]

1) Colenco Power Consulting AG, Baden
2) GeoScience, Falmouth UK
3) Nagra, Wettingen
4) Intera Inc., Austin USA,
now at Creek Hydrogeology, Georgetown, USA

Hardstrasse 73, CH-5430 Wettingen/Switzerland, Telephone +41-56-37 11 11

This report was prepared on behalf of Nagra. The viewpoints presented and conclusions reached are those of the author(s) and do not necessarily represent those of Nagra.

ABSTRACT

This report represents the methodology and results of hydrogeological synthesis of crystalline rocks in Northern Switzerland. This synthesis concludes the regional investigation program KRI-I that was conducted by Nagra (Swiss National Cooperative for the Disposal of Radioactive Waste) during 1981-1993. The principal objective of this program is to assess the suitability of the crystalline basement as a host rock for a deep-seated repository for high-level and long-lived intermediate-level radioactive waste (HLW/ILW).

The present report provides a comprehensive hydrogeological characterization of the crystalline basement. The characterization study plays a key role in assessing the repository safety and performance, given that any release of radionuclides from a repository and further transport through the geological environment (geosphere) will occur by groundwater. The final objective of the characterization study is to provide a representative description of processes and parameters that control the flow system between the repository and the biosphere.

The hydrogeological characterization study of crystalline rocks was performed in 1991-1993 and included the following steps:

- compilation and a consistent interpretation of hydraulic borehole data
- development of the hydrogeological conceptual model of crystalline rocks
- analytic estimates of effective hydraulic properties of the defined conceptual units
- modeling and evaluation of regional flow
- modeling and evaluation of local-scale flow in a selected area of interest
- stochastic modeling of fracture flow at repository (block) scale and derivation of relevant input parameters for repository-safety assessments

The results of this multi-level synthesis study were presented in a series of Nagra internal reports. They all are integrated in this report which represents a complete background information on the hydrogeology of crystalline rocks in the basement of Northern Switzerland. The overall synthesis of all investigations performed in the scope of KRI-1 program is presented in THURY et al. (1994).

Nagra's area of interest is a strip of crystalline basement between the deep Permocarboniferous Trough in the south and the German border in the north.

This area is characterized by Nagra's deep boreholes at the sites of Kaisten, Böttstein, Leuggern and Siblingen. Because the basement is covered by Mesozoic sediments throughout the investigation area, no direct surface observation is available. Instead, studies on crystalline outcrops in the adjacent Southern Black Forest are used to complement the scarce information from boreholes.

The first step of hydrogeological characterization is the development of a conceptual model that provides a simplified but consistent description of flow through crystalline rocks. Based on the synthesis of experimental data, the crystalline basement of the investigation area is subdivided into conceptual domains. Each domain is deemed to represent a homogeneous volume of rock that can be characterized by a single mean property. The combined framework of these domains accounts for the observed spatial heterogeneity of crystalline rocks. In terms of the large-scale flow, the basement is separated into large subvertical faults acting as water conduits and irregular blocks of relatively undisturbed rock. Based on generally observed tendency, the latter are further subdivided into an upper, relatively high-permeable crystalline unit and a lower, relatively low-permeable unit. An earlier geological synthesis suggested that potentially suitable crystalline rocks occur in two sub-regions of Northern Switzerland, identified as area West (Kaisten-Leuggern-Böttstein) and area East (Siblingen). These sub-regions are also characterized by different hydraulic properties. The lower crystalline unit in area West was identified as the potential host formation for a deep repository, designated the Lower-permeability domain. In area East, which is characterized only by one borehole at Siblingen, no such crystalline-rock domain of similarly favorable properties was observed. The fundamental question is here, whether the data from the Siblingen borehole are representative for the area of interest, or whether they rather represent local hydrogeologic conditions that are specific for that site only. The conceptual model of sub-regional flow considers both alternatives as equally plausible.

At a much smaller scale of a potential repository (block scale), the flow through an undisturbed block of the low-permeable domain is controlled by a variety of discrete discontinuities. These planar features are identified as inflow points in hydraulic borehole tests and are generalized as transmissive elements in the conceptual model. They are characterized by statistical properties derived or inferred from borehole and outcrop observations.

The modeling of large-scale groundwater flow was used to confirm and improve the general understanding of the regional flow system in Northern Switzerland.

At this scale, the crystalline rocks were approximated by an equivalent-porous medium (EPM). Model results were compared with observed heads and hydrochemical evidence to test the plausibility of several conceptual hypotheses. The outcome is a set of concise statements, weighed hypotheses and alternatives that express the current conceptual understanding of regional hydrodynamic system. The robustness of the simulated hydrodynamic system was also tested by inserting discrete faults and by including long-term scenarios that consider neotectonic changes in the topography and lateral displacements of river channels.

At a smaller scale, the local flow system in area West was evaluated by means of a hybrid or "double-porosity" model. This approach allows to model explicitly the large water-conducting faults and the intervening blocks of undisturbed crystalline rocks, represented as EPM. The development of a new mesh generator was required to handle the complex geometry of arbitrarily oriented faults. A simplified geometric fault model designed by structural geology served as basis for the numerical grid. Multiple geometric variants of the hybrid model were implemented to cover the uncertainty related to the geometry and frequency of the hydraulically active faults. The two bounding patterns, referred to as the full scenario and sparse scenario, were assumed to cover the full range of possible model results and were subjected to a comprehensive analysis. The principal objective of the simulations is to evaluate the impact of major water-conducting faults on the local flow field in the intervening blocks of undisturbed crystalline rocks. The model results are evaluated from the perspective of needs for the repository safety analysis. The principal output consists in 1) the distribution of fluxes between the crystalline rock blocks and large faults, 2) the distribution of hydraulic gradients within the potential host rock as function of the fault frequency, and 3) the direction and path length of flow between the disposal location and the closest high-permeability medium. The simulated mean absolute gradients vary between 0.01 (full scenario) and 0.05 (sparse scenario). The direction and pathlength of flow within the low-permeable host rock depends on the size of the undisturbed block. It is shown that local flow systems are preserved only in large blocks. The comparison of model results with borehole observations suggests that not all faults in the geometrical network, such as identified by the structural geology, are hydraulically active. In other words, the conditions simulated in the sparse scenario (large blocks) are more plausible than those in the well-connected network of the full scenario.

The next level of modeling deals with characterization of flow through a typical

block volume of low-permeable crystalline rocks surrounding a hypothetical repository drift. According to the conceptual model, the advective flow and transport at this scale is entirely controlled by conductive fractures, termed transmissive elements. Because the hydraulic and geometric properties of these features are not known explicitly, they are incorporated into a statistical framework. These are the discontinuum models that simulate the advective flow through a fractured medium, where the contribution of the matrix flow is negligible. The models are generated as complex stochastic networks based on statistical input data derived from borehole observations.

The simulation of fracture networks encompassing a hypothetical repository serves to provide the following input for repository-performance analysis:

- Frequency, trace length and transmissivity of intersected fractures. These parameters in combination with hydraulic gradients (obtained from the local-scale model) allow to estimate the volumetric flow through a repository.
- Effective hydraulic conductivity of the modeled block. This parameter can be used as a feedback to characterize the block matrix in the hybrid models.

Evaluation of block-scale flow was performed for typical volumes of the lower crystalline rock unit in area West and East, with the final goal to provide quantitative input data for safety analysis calculations. The results are the water flow through a repository and its distribution among single transmissive elements, and the dilution potential of flow passing the repository within the near-surface aquifers and rivers in each area. Area East is less well-characterized and a substantial uncertainty is related to the evaluation of results at the block scale. Two separate datasets are derived for the safety analysis in area East, considering the two possible alternatives regarding the representativeness of Siblingen observations.

ZUSAMMENFASSUNG

Der vorliegende Bericht beschreibt die Methoden und Resultate einer umfassenden hydrogeologischen Synthese des kristallinen Grundgebirges der Nordschweiz. Diese Studie ist ein wichtiger Bestandteil eines regionalen geologischen Untersuchungsprogramms, das die Nagra (Nationale Genossenschaft für die Lagerung radioaktiver Abfälle) in den Jahren 1981 - 1993 in der Nordschweiz durchgeführt hat. Im Rahmen des schweizerischen Programms für die Entsorgung hochradioaktiver Abfälle (HAA) hat die Phase KRI-I das Ziel, die Eignung des kristallinen Untergrundes als Wirtgestein für ein tiefliegendes Endlager abzuklären.

Dieser Bericht beinhaltet eine umfassende hydrogeologische Charakterisierung des kristallinen Grundgebirges. Dieser Schritt spielt eine zentrale Rolle bei der Beurteilung der Endlagersicherheit, weil jede eventuelle Freisetzung von Radionukliden aus dem Endlager und deren Transport durch die Geosphäre nur durch fliessendes Grundwasser erfolgen kann. Aus dieser Sicht besteht das wichtigste Ziel der Charakterisierungsstudie aus einer möglichst quantitativen und belastbaren Beschreibung der relevanten hydrogeologischen Parameter und Prozesse, die das Fliessverhalten der tiefen Grundwässer in der potentiellen Endlagerregion bestimmen.

Die hydrogeologische Synthese wurde in den Jahren 1991 - 1993 durchgeführt und umfasste folgende Schritte:

- Zusammenstellung und kohärente Auswertung aller hydrogeologischen Bohrlochdaten
- Synthese der Informationen in ein konzeptuelles hydrogeologisches Modell des kristallinen Grundgebirges; analytische Abschätzung der effektiven hydraulischen Eigenschaften der konzeptuellen Einheiten
- Modellierung und Interpretation der grossräumigen (regionalen) Fliessverhältnisse
- Modellierung der lokalen Fliessverhältnisse in einem ausgewählten Gebiet
- Stochastische Modellierung von Kluftnetzwerken im Wirtgesteinblock in der Umgebung eines hypothetischen Endlagers; Ableiten der für die Sicherheitsanalyse relevanten Parameter

Die Ergebnisse der einzelnen Projektphasen wurden in zahlreichen Nagra-internen Berichten dokumentiert. Sie sind alle im vorliegenden Bericht integriert,

der deshalb als eine umfassende Synthese der hydrogeologischen bzw. hydrodynamischen Parameter und Prozesse im kristallinen Grundgebirge zu werten ist. Die Gesamtsynthese aller durchgeführten Untersuchungen im Rahmen des KRI-I Programms wird von THURY et al. (1994) behandelt.

Das engere Untersuchungsgebiet der Nagra wird im Süden durch den Nordschweizerischen Permokarbon-Trog und im Norden durch die Grenze zu Deutschland begrenzt. Auf diesem Gebiet wird das Grundgebirge vollständig von Mesozoischen Deckschichten überlagert, so dass keine direkten Beobachtungen an der Oberfläche möglich sind. Die verfügbaren Informationen aus den wenigen Tiefbohrungen in der Region werden deshalb durch Analogiestudien im benachbarten Südschwarzwald ergänzt.

Der erste Schritt jeder hydrogeologischen Charakterisierung einer Region besteht aus der Entwicklung eines konzeptuellen Modells, das eine vereinfachte aber in sich konsistente Darstellung der Grundwasser-Fliessverhältnisse in verschiedenen Grössenbereichen zum Ziel hat. Ausgehend von der verfügbaren Datenbasis wird das kristalline Grundgebirge in dreidimensionale konzeptuelle Bereiche unterteilt. Jeder Bereich repräsentiert ein hydrogeologisch homogenes Gebirgsvolumen, das mit einem typischen Eigenschaftswert (z.B. effektiver K Wert) beschrieben werden kann. Die Anordnung und Ausdehnung dieser Homogenbereiche widerspiegelt annähernd die beobachtete räumliche Heterogenität des kristallinen Grundgebirges. In bezug auf grossräumige Grundwasserströmungen wird das Grundgebirge in folgende zwei Grundelemente gegliedert: große, steilstehende Störungen, die als regionale Wasserleiter wirken können sowie dazwischen liegende unregelmässige Blöcke von relativ wenig gestörtem Kristallin. Die letzteren können aufgrund der allgemein beobachteten Tendenzen in eine obere, relativ hochdurchlässige und eine tiefere, relativ geringdurchlässige kristalline Einheit unterteilt werden. In einer früheren Phase der Studie wurde gefolgert, dass ein potentiell geeignetes kristallines Grundgebirge in zwei verschiedenen Regionen der Nordschweiz anzutreffen sei, die als Zone West (Bohrungen Böttstein, Leuggern und Kaisten) bzw. Zone Ost (Bohrung Siblingen) definiert wurden. Beide Gebiete weisen unterschiedliche hydrogeologische Eigenschaften auf. Die tiefere kristalline Einheit der Zone West wurde als potentielles Wirtgestein identifiziert und im konzeptuellen Modell explizit als "Geringdurchlässiger Bereich" bezeichnet. In der Zone Ost, deren hydrogeologische Verhältnisse einzig durch die Bohrung Siblingen charakterisiert werden können, wurde kein solcher Bereich mit vergleichbar günstigen Eigenschaften angetroffen. Die grundlegende Frage lautet

nun, inwiefern der Datensatz der Bohrung Siblingen repräsentativ für die umliegende östliche Kristallinregion ist, oder ob er vielmehr lokale hydrogeologische Verhältnisse wiedergibt, die nur am Bohrstandort selbst Gültigkeit haben. Da diese Frage ohne zusätzliche Informationen nicht schlüssig zu beantworten ist, berücksichtigt das konzeptuelle Modell beide Möglichkeiten als gleichwertige Alternativen.

Betrachtet man den viel kleineren Massstab im Bereich eines potentiellen Endlagers, so ist die Grundwasserführung in einem geringdurchlässigen Wirtgesteinblock fast ausschliesslich auf die mannigfaltigen diskreten Trennflächen beschränkt. Diese planaren Elemente wurden in den hydraulischen Bohrlochversuchen als individuelle Zuflussstellen identifiziert und im konzeptuellen Modell vereinfacht als planare wasserführende Strukturen oder transmissive Elemente idealisiert. Ihre hydrogeologische Charakterisierung (Häufigkeit, Grösse, Transmissivität) stützt sich auf statistische Auswertung von Bohrlochdaten sowie auf weitere direkte und indirekte Beobachtungen.

Die Modellierung grossräumiger Grundwasserströmungen diente zur Bestätigung und Verbesserung des generellen Verständnisses des regionalen Fliessregimes im Grundgebirge der Nordschweiz. In diesem Skalenbereich konnten die kristallinen Gesteine durch eine Annäherung als äquivalent-poröses Medium (EPM) beschrieben werden. Modellergebnisse wurden mit beobachteten hydraulischen Potentialen sowie mit hydrochemischen Aussagen verglichen, um den Glaubwürdigkeitsgrad der verschiedenen getesteten Hypothesen zu überprüfen. Das Produkt dieser Sensitivitätsstudie ist eine tabellarische Zusammenstellung von schlüssigen Aussagen und nach Glaubwürdigkeit gewichteten möglichen Alternativen, die gesamthaft das gegenwärtige konzeptuelle Verständnis des regionalen hydrodynamischen Systems zum Ausdruck bringen. Die Robustheit der simulierten Verhältnisse wurde zusätzlich durch nachträglichen Einbau von expliziten Störungen (als 3-dimensionale Elemente) sowie durch Einbeziehung von hydrogeologischen Langzeit-Szenarien, die eine neotektonisch bedingte Veränderung der Topographie und seitliche Verlagerung der Flusssysteme berücksichtigen, getestet.

Die lokalen Fliessverhältnisse in der ausgewählten Zone West wurden mittels eines sogenannten hybriden oder Doppelporositätmodells untersucht. Dieses Verfahren ermöglicht eine explizite Modellierung der regionalen wasserführenden Störungszonen und den dazwischen liegenden - relativ ungestörten - kristallinen Blöcken (konzeptuelle Bezeichnug: Matrixblöcke). Die letzteren

werden wiederum durch den EPM Ansatz charakterisiert. Hierfür musste ein neues Netzgenerierungsprogramm entwickelt werden, um die komplexe Netzgeometrie zu meistern, die sich aus Verschneidungen der beliebig orientierten planaren Störungen ergibt. Ferner wurde durch die Strukturgeologen ein vereinfachtes Störungsmodell des kristallinen Grundgebirges entworfen, das als Grundlage für die Auslegung des numerischen Netzes diente. Da jedoch die wahre Häufigkeit und räumliche Lage und Geometrie der wichtigen wasserführenden Störungen bis auf wenige Ausnahmen unbekannt ist, wurden mehrere geometrische Modellvarianten erstellt, um diesbezüglichen Unsicherheiten Rechnung zu tragen. Die beiden Extremvarianten in bezug auf räumliche Dichte der berücksichtigten Störungen wurden als VOLL-Szenario und TEIL-Szenario bezeichnet. Es wurde davon ausgegangen, dass diese beiden Varianten das volle Spektrum der möglichen Simulationsergebnisse abdecken. Die umfassende Auswertung der Modellaussagen konnte somit auf diese zwei Fälle beschränkt werden. Das Hauptziel der durchgeführten Simulationen war die Untersuchung der Auswirkungen der grossen wasserführenden Strukturen auf das lokale Fliessfeld in dazwischenliegenden Blöcken. Die Resultate wurden im Hinblick auf die Bedürfnisse der Sicherheitsanalyse ausgewertet. Die wichtigsten Aussagen sind 1. die Verteilung des Wasserflusses auf die Störungen und Matrixblöcke, 2. die Verteilung der hydraulischen Gradienten im Wirtgestein als Funktion der Störungsdichte, und 3. die Fliessrichtung und Fliesslänge des Grundwassers zwischen Endlagerort und dem nächstgelegenen hochdurchlässigen Medium. Die simulierten hydraulischen Gradienten liegen zwischen 0.01 (Mittelwert VOLL-Szenario) und 0.05 (Mittelwert TEIL-Szenario). Die Fliessrichtung und -Länge des Grundwassers im geringdurchlässigen Wirtgestein ist von der Blockgrösse abhängig. Es wurde gezeigt, dass lokale Fliesssysteme nur in grösseren Blöcken erhalten bleiben. Ein Vergleich der simulierten und beobachteten Vertikalgradienten ergab, dass nicht alle Störungen des vorgeschlagenen strukturgeologischen Modells hydraulisch wirksam sein können. In anderen Worten, die im TEIL-Szenario simulierten hydrogeologischen Verhältnisse sind plausibler als jene im hydraulisch zusammenhängenden VOLL-Netzwerk.

Der nächst kleinere Modellbereich behandelt die Beschreibung des Grundwasserflusses durch einen typischen Wirtgesteinblock, der ein hypothetisches Endlager beherbergen würde. Gemäss der konzeptuellen Vorstellung ist in diesem Massstab die Grundwasserführung ausschliesslich auf einzelne durchlässige Klüfte konzentriert, die als planare transmissive Elemente idealisiert werden. Da ihre Lage sowie ihre hydraulischen und geometrischen Eigenschaf-

ten nicht explizit bestimmbar sind, müssen diese Strukturen durch ein statistisches Netzwerk beschrieben werden. Dies ist das Prinzip der Diskontinuum-Modelle, die den advektiven Grundwasserfluss durch ein geklüftetes Medium simulieren, wobei der Beitrag der Gesteinsmatrix vernachlässigt wird. Die generierten komplexen Kluftnetzwerke werden durch statistische Eingabeparameter definiert, die aus Bohrlochdaten abgeleitet worden sind. Die Simulation der Kluftnetzwerke in der Umgebung einer Endlagerkaverne hat zum Ziel, die für den Datensatz der Sicherheitsanalyse benötigten Parameter bereitzustellen. Es handelt sich hierbei um:

- Anzahl, Spurlänge und Transmissivität der im Kavernenstollen angetroffenen transmissiven Elemente. Diese drei Grössen erlauben in Kombination mit hydraulischen Gradienten (im Lokalmodell berechnet) die Abschätzung des Volumenstroms durch die Kaverne.
- Abschätzung der effektiven hydraulischen Durchlässigkeit des modellierten Wirtgesteinblocks. Dieser Parameter kann wiederum im Hybridmodell zur Charakterisierung der Blockmatrix eingesetzt werden.

Die Untersuchung der Grundwasserführung in einem Kluftnetzmodell wurde für typische Blockgrössen der tieferen kristallinen Einheit in Zone West und Ost durchgeführt. Das Ziel war jeweils die quantitative Herleitung von relevanten Parametern für Transportmodellierung im Rahmen der Sicherheitsanalyse. Das Resultat beinhaltet Aussagen über Volumenstrom durch Kaverne und dessen Verteilung auf einzelne transmissive Elemente sowie über die Verdünnung dieses Volumenstroms in den oberflächennahen Aquiferen (Biosphäre). Die Zone Ost erwies sich erwartungsgemäss als weniger gut charakterisierbar und die Modellaussagen sind mit grossen Unsicherheiten behaftet. Für diese Zone wurden zwei unabhängige Datensätze erstellt, die auf zwei verschiedenen Interpretationen der Siblingen-Daten basieren.

RÉSUMÉ

Ce rapport donne une synthèse hydrogéologique du socle cristallin de la Suisse du Nord ainsi que la méthodologie d' investigation utilisée pour ce faire. Il clôt les études effectuées par la Société coopérative nationale pour l' entreposage de déchets radioactifs (Cédra) de 1981 à 1993. Le principal but de celles-ci était de déterminer l' aptitude du socle cristallin comme roche d'accueil pour le stockage définitif de déchets radioactifs à haute activité et de déchets à moyenne activité et longue durée de vie.

La caractérisation hydrogéologique détaillée du socle cristallin présentée dans ce rapport occupe une position clé pour l' analyse de sûreté et de performance du site, compte tenu du fait que les mouvements d' eaux souterrainnes provoquent le transfert de radionucléides entre le site d' entreposage et au travers du milieu géologique (géosphère). L' objectif final de la caractérisation est de fournir une description adéquate des processus et des paramètres qui contrôlent le système d' écoulement entre le site de stockage et la biosphère.L' étude hydrogéologique de caractérisation du socle cristallin a été accomplie de 1991 et 1993 et comprend les étapes suivantes:

- Synthèse des données hydrauliques des forages et conceptualization hydrogéologique de la roche cristalline.
- Estimation analytique des propriétés hydrauliques effectives dans le cadre conceptuel adopté.
- Modélisation des écoulements à l' échelle régionale.
- Modélisation et évaluation des écoulements à une échelle locale pour des domaines d' étude choisis.
- Modélisation stochastiques des écoulements en milieu fracturé à l' échelle du site de stockage et déduction des paramètres d' entrée nécessaires pour les études de sûreté.

Les résultats de cette étude effectuée sur différents niveaux ont été présentés dans une série de rapports techniques de la Cédra. Ce rapport en fait une synthèse et présente une description exhaustive de l' hydrogéologie des roches du socle cristallin de la Suisse du Nord. La synthèse de tous les travaux effectués dans le cadre du programme KRI-I est donnée par THURY et al. (1994).

L' intérêt de la Cédra s' est focalisé sur une bande du socle cristallin située entre la bordure du fossé au Sud et la frontière avec l' Allemage au Nord. Ce

domaine a été investigué par les forages profonds de la Cédra à Kaisten, Böttstein, Leuggern et Siblingen. Comme le socle y est recouvert par des sédiments du Mésozoïque, aucune observation de surface n'est disponible. Aussi, des études d' affleurement du socle cristallin dans la partie méridionale de la Forêt Noire sont utilisées afin de compléter les informations fragmentaires des forages profonds.

Une première étape dans la caractérisation hydrogéologique est l' élaboration d' un modèle conceptuel qui donne une description simplifiée mais cohérente de l' écoulement à travers les roches cristallines. Le socle cristallin est subdivisé en plusieurs unités conceptuelles qui constituent une représentation simplifiée du milieu en blocs homogènes caractérisés par une valeur unique moyenne des paramètres. A une échelle d' écoulement régionale, le socle est traversé par des failles subverticales occasionnant d' importantes circulations d' eau. La matrice rocheuse des blocs de taille variable situés entre ces failles est peu diaclasée. Verticalement ces blocs peuvent être subdivisés en une zone supérieure plus perméable et une zone inférieure moins perméable. Dans une synthèse hydrogéologique précédente deux régions du Nord de la Suisse ont été identifiées comme possédant une roche cristalline adéquate: à l' Ouest la zone de Kaisten-Leuggern-Böttstein, à l' Est la zone de Siblingen. Ces deux régions sont caractérisées par des propriétés hydrauliques différentes. La partie inférieure du cristallin dans la zone Ouest a été identifiée comme roche d'accueil potentielle pour un stockage profond. Dans la zone Est, caractérisée par un seul forage à Siblingen, une roche cristalline semblable n' a pas été identifiée. La question fondamentale est de savoir si les données du forage de Siblingen sont représentatives de l' ensemble du domaine considéré ou si elles reflètent plutôt des conditions hydrogéologiques locales. Le modèle conceptuel d' écoulement à l' échelle sub-régionale considère ces deux éventualités. A l' échelle du site de stockage (échelle d' un bloc) l' écoulement est contrôlé par des discontinuités discrètes. Ces structures bidimensionelles sont identifiées comme zones d'afflux lors des essais hydrauliques en forages, sont conceptualisées sous forme d' éléments transmissifs et sont caractérisées par les propriétés statistiques déduites ou induites des observations.

Les écoulements souterrains régionaux ont été modélisés afin de confirmer et d' augmenter la compréhension générale du système d' écoulement dans le socle cristallin en Suisse du Nord. A cette échelle, la roche cristalline est considérée comme milieu équivalent à un milieu poreux. Les résultats de modélisation ont été comparés aux hauteurs piézométriques observées ainsi qu' aux données

hydrochimiques afin d' analyser la plausibilité des différentes hypothèses conceptuelles. Cette étude a conduit à un tableau résumant le éléments clé et les alternatives pondérées selon leur plausibilité, donnant ainsi une vue globale du système hydrogéologique régional. La robustesse du système simulé a été testée en introduisant des fractures discrètes et en considérant des scénarios géologiques à long terme comprenant des changements topographiques néo-tectoniques et des modifications du cours des rivières.

Le régime d' écoulement local dans la zone Ouest a été évalué au moyen d' un modèle dit hybride ou à double porosité. Cette approche permet de prendre en compte de façon explicite les failles à haute perméabilité et les blocs peu diaclasés dans la modélisation. Le développement d' un nouveau générateur de maillage a été necessaire afin de prendre en compte la géometrie complexe et les orientations aléatoires des failles. Un modèle géométrique de failles simplifié a servi de base pour le maillage numérique. L' impact de différentes variantes géométriques du modèle hybride sur les résultats de simulation a été investigué afin de couvrir les incertitudes relatives à la géométrie et à la distribution statistique des failles hydrauliquement actives. Les deux situations extrêmes dénommées scénario "réseau de failles complet (RFC)" et scénario "réseau de failles réduit (RFR)" sont supposées couvrir l' ensemble des situations possibles et ont été sujettes à une analyse exhaustive. L' objectif principal des simulations était d' évaluer l' impact des failles à conductivité majeure sur l' écoulement dans les blocs du cristallin peu diaclasés à l' échelle locale. Les résultats de modèlisation sont évalués dans l' optique d' une analyse de sûreté. Les résultats principaux sont 1) la distribution des flux entre les blocs de roche cristalline et les failles, 2) la distribution des gradients hydrauliques à l' intérieur de la roche d'accueil en fonction de la fréquence des failles, et 3) l' orientation et les longueurs de cheminement de l' écoulement entre le site de stockage et le milieu fortement perméable le plus proche. Les gradients hydrauliques moyens varient entre 0,01 (RFC) et 0,05 (RFR). L' orientation et les longueurs de cheminement de l' écoulement dans la roche d'accueil peu perméable dépend de la taille des blocs peu diaclasés. Les résultats montrent que l' écoulement local n' est préservé que dans le cas de blocs de dimensions importantes. La comparaison des résultats de modélisation avec les observations effectuées par forage suggèrent que seulement un certain nombre des failles identifiées par une analyse de géologie structurale et appartenant à un réseau géométrique donné sont hydrauliquement actives. En d' autres termes, les conditions simulées dans le scénario RFR sont plus plausibles que celles du scénario RFC pour lequel l' interconnection du réseau est importante.

Dans un second temps, la modélisation a porté sur la caractérisation de l' écoulement à l' intérieur d' un bloc de roche cristalline à faible perméabilité dans lequel est positionnée une galerie de stockage hypothétique. D' après le modèle conceptuel, l' écoulement et le transport advectif à cet échelle est entièrement contrôlé par les élements transmissifs dont les caractéristiques géométriques et hydrauliques ne sont pas connues de façon déterministe mais de façon statistique. Le modèle conceptuel considéré est donc un modèle de milieu fracturé discontinu, dans lesquels la contribution de la matrice à l' écoulement est négligeable. Le réseau de fractures complexe est généré par simulation statistiques sur la base des paramètres descriptifs obtenus par observations dans les forages. La simulation de réseaux de fractures comportant une galerie de stockage hypothétique fournit les paramètres suivants nécessaires à l' analyse de performance de la galerie de stockage:

- Fréquence, longueur de la trace d' intersection et transmissivité des fractures intersectés. Ces paramètres combinés aux gradients hydrauliques (obtenus par le modèle d' écoulement à l' échelle locale) permettent l' estimation des flux volumétriques au travers de la galerie de stockage.
- Conductivité effective du bloc simulé. Ce paramètre peut être utilisé comme information a posteriori pour la caractérisation des blocs de matrice rocheuse du modèle hybride.

L' écoulement à l' échelle d' un bloc a été calculé pour des volumes de roche cristallines typiques de l' unité inférieure des zones Est et Ouest dans le but de procurer des données d' entrée quantitatives pour les simulations de l' analyse de sûreté. Les résultats obtenus portent sur les flux hydriques à travers le site de stockage ainsi que leur distribution entre les éléments transmissifs, et sur la dilution potentielle des eaux passées au travers du site dans les aquifères de surface et les rivières. Comme la zone Est est moins bien caractérisée, une incertitude importante entache les résultats d' évaluation à l' échelle d' un bloc. Deux groupes de données distincts sont obtenus pour l' analyse de sûreté de la zone Est qui prennent en compte les deux alternatives d' interprétation possibles des observations de Siblingen.

CONTENTS

FIGURES

TABLES

APPENDICES

1 INTRODUCTION

1.1 Objectives and scope of the report

The crystalline basement of Northern Switzerland is under consideration as a potential host rock for the final disposal of high-level and long-lived intermediate-level nuclear waste. Because any eventual release of radionuclides from the deep repository to man's environment (biosphere) would be by groundwater, the understanding of the hydrogeological processes and conditions at various scales is required to make a credible assessment of the suitability of such rocks to meet the safety criteria.

The crystalline rocks form the basement of the Swiss Plateau. Whereas the basement is exposed in the Black Forest massif beyond the German border, in Northern Switzerland it is covered by sedimentary rocks of several hundreds of meters thickness. The crystalline investigation program of Nagra is therefore based on seven deep boreholes, with depths ranging between 1,300 and 2,500 m, and on geophysical exploration consisting of about 700 km of seismic lines. The investigation area with borehole locations is shown in Fig. 1.1. Regional investigations of the crystalline bedrock, designated as KRI-1 program, were carried out between 1982 and 1989. All boreholes have been subjected to an extensive hydraulic testing program, comprising packer tests, different fluid-logging techniques and long-term monitoring. Furthermore, systematic sampling of deep groundwaters provided basis for extensive hydrochemical and isotope studies.

The field investigation program was concluded by a comprehensive analysis and interpretation of all experimental data. This project of an overall synthesis of crystalline data included many earth-scientific disciplines and was conducted by Nagra between 1990 and 1993. The results have been published in several background reports, such as DIEBOLD et al. (1991; synthesis of regional tectonics), SCHMASSMANN et al. (1992; hydrochemical synthesis), and PEARSON et al. (1991; groundwater-isotope synthesis). The overall results of the KRI-1 project are summarized in the main synthesis report by THURY et al. (1994).

The task of hydrodynamic synthesis of crystalline rocks, presented in this report, plays a key role within the KRI-1 synthesis project mentioned above.

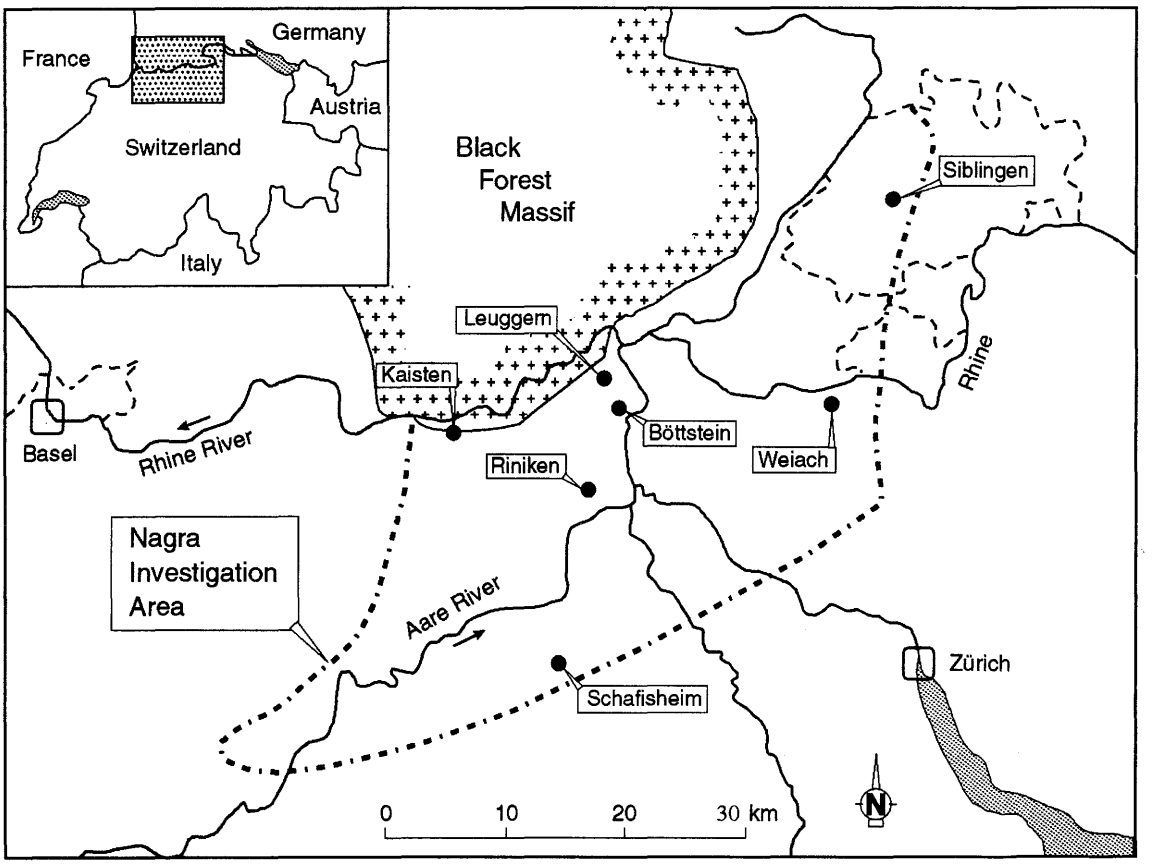

Fig. 1.1 Investigation area of crystalline basement in Northern Switzerland

The outcome of this synthesis study is a part of the required input for assessment of the repository performance. Hence, the primary objective of this study is the hydrogeologic characterization of the crystalline rocks and derivation of realistic input parameters for solute-transport calculations.

In order to describe the groundwater flow through crystalline rocks at multiple scales and to derive the required parameters, the hydrodynamic synthesis study comprises the following steps:

1) The compilation and interpretation of all hydraulic test data from Nagra boreholes, complemented by other hydrogeologic information such as water chemistry, core analyses, geothermal data, etc.

2) The development of a conceptual hydrogeological model as a simplified characterization of groundwater flow through crystalline rocks, which is consistent with physical observations at multiple scales

3) Numerical modeling of advective groundwater flow at regional, local and block scales. The modeling goes hand in hand with the iterative development of the conceptual flow model and helps to improve the understanding of the hydrodynamic regime down to the scale of a single fracture.

By describing the methods and results of the hydrodynamic synthesis, this report provides a background documentation on the hydrogeology of crystalline rocks in Northern Switzerland; the principal results of this study are summarized in the main synthesis report (THURY et al. 1994, NTB 93-01) under Chapter 8.

In accordance with the abovementioned structure of the study, the report is divided in five principal chapters that describe the synthesis of borehole data and the evaluation of hydraulic properties, followed by numerical modeling studies of groundwater flow at different scales of interest.

Chapter 2 presents the compilation and interpretation of hydraulic rock properties based on borehole data and the development of the conceptual hydrogeological model. The underlying database as obtained from hydraulic borehole tests is compiled in Appendices 1 and 2. The output of the borehole data synthesis is a reference data set of hydraulic parameters for each defined hydrogeological domain that forms a part of the conceptual model. Analytical methods are applied to the derived hydraulic and geometric parameters controlling the flow in a fractured medium in order to estimate the equivalent large-scale hydraulic property of each conceptual unit.

Chapter 3 describes the results of a comprehensive analysis of the regional groundwater-flow regime in the crystalline basement of Northern Switzerland. A numerical model was used to simulate the groundwater flow on large scale and to analyze the plausibility of various possible hypotheses regarding the relevant boundary conditions and parameters of a such large-scale flow. The outcome of this study is a conceptual description of the regional hydrogeologic system. The resulting conceptual understanding is expressed by a set of plausible hypotheses, which are classified into the most likely and alternative ones, and weighed by a degree of uncertainty. The complete set of statements and hypotheses is listed in Appendix 3 of this report.

For an appropriate characterization of the groundwater flow at the local scale, i.e., within a given sub-region that is representative for a potential repository site,

i.e., within a given sub-region that is representative for a potential repository site, two specific areas of interest were identified within the investigation region by considering the large-scale heterogeneity of the hydrogeologic system. These geographic sub-regions were designated area West and area East respectively. Chapter 4 presents the results of hydrogeologic characterization of area West that encompasses the locations of Nagra's deep boreholes Böttstein, Kaisten and Leuggern. Numerical modeling was applied to analyze the effects of major structural features (faults) on the local hydrodynamic system (at km scale) and to provide some information on the distribution of hydraulic gradients and fluxes.

Chapter 5 deals with the assessment of groundwater flow at the "block" scale (repository scale) in the area West. Discontinuum models are used to simulate flow through a block volume of typical fractured host rock that surrounds a hypothetical emplacement cavern of a deep repository. The approach and results of these stochastic fracture-network models are described. Also at this scale, the uncertainties of the conceptual model with respect to flowpath properties are tested by varying the fracture parameters in question in multiple simulations. As plausibility checks, equivalent block properties are calculated and compared with the analytical estimates derived in Chapter 2.

The analysis of the sub-regional and block-scale flow in the area East is performed in Chapter 6. In contrast to the area West, where data from three deep boreholes were disposable for developing a local model, only a sparse database from one borehole (Siblingen) is available in area East. Because a large uncertainty is attached to this data set as to its representativeness for the area in question, it was deemed inappropriate to implement a complex numerical model similar to that in area West. Instead, an alternative approach was adopted by using a modified version of the regional model (presented in Chapter 3) to estimate the sub-regional gradient distribution.

Both Chapters 5 and 6 put emphasis on derivation of results that are relevant as input for the safety assessment. A more detailed discussion on the adopted approach and the underlying assumptions is given in VOMVORIS et al. (in prep.).

The concluding Chapter 7 summarizes the general findings and conclusions that were obtained from the hydrogeological synthesis of crystalline rocks in Northern Switzerland.

1.2 Approach to modeling crystalline rocks

Suitability assessments of a potential host rock for the disposal of radioactive waste require an understanding of the hydrodynamic processes in deep underground which control the fluid movement through the geological environment (geosphere). A such understanding is acquired iteratively during the synthesis of experimental data and other hydrogeological information. The acquired knowledge is integrated into a hydrogeological conceptual model. In the present study, the conceptual model is defined as a set of basic principles and concise statements - or hypotheses respectively - that characterize the hydrogeologic system or relevant processes, being in balance with the available information and knowledge. Hence, the derivation of a conceptual model represents the basic step in a hydrogeologic characterization of a potential site area. Due to the practical limits of data acquisition and the heterogeneity of hydrogeological conditions in the area of interest, the conceptual model represents a generalized and simplified description of the "real" system. In this context, the conceptual model is used in a semi-quantitative manner to characterize the hydrogeologic framework that controls the groundwater flow.

A quantitative expression of the conceptual model are mathematical models of groundwater flow at multiple scales, which are used to test and improve the conceptual model. The inherent uncertainties of the latter are addressed by appropriate parameter variations. Because of the limited availability of hydrogeologic observations in the present study, the numerical models are used as interpretative rather than predictive tools. To cope with the need to characterize groundwater flow at different scales, a hierarchical sequence of numerical models was adopted.

A schematic illustration of this approach is shown in Fig. 1.2. On the left hand side is a sketch of the hydrogeological conceptual model of crystalline rocks of Northern Switzerland, such as derived in Chapter 2; its representation in numerical models at different scales is shown on the right.

The strategy of hierarchic modeling as illustrated by Fig. 1.2 is commented in the following.

The first stage of numerical modeling of crystalline basement investigates the large-scale groundwater flow within an area of about 1,700 km² (VOBORNY et al. 1992). At this scale, the modeled rock formations are described as an

equivalent-porous medium (EPM), by making the continuum approximation over large rock volumes. The hydraulic rock properties are characterized by an estimate of the single equivalent conductivity value for each defined rock volume (isotropic and homogeneous).

The principal objectives of the regional flow model were

1) to test various plausible alternative parameters and conditions that control the regional groundwater flow, and thereby improve the general understanding of the overall system; and

2) to provide a basis for definition of boundary conditions for smaller models at a sub-regional scale (see Fig. 1.2).

The second modeling phase is addressed to the evaluation of local groundwater-flow conditions that are likely to occur in a potential repository area in the crystalline basement. Because prominent tectonic features such as regional faults (termed major water-conducting faults, MWCF, in Fig. 1.2) dominate the flow regime at km scale, the so-called "hybrid" or double-porosity approach was adopted for this task. The hybrid approach best represents the conceptual model, because it combines the explicit treatment of large discrete faults with the continuum approximation over the intervening blocks of relatively undisturbed rock (Fig. 1.2). In order to implement such a hybrid model with its variety of arbitrarily oriented discrete features, the development of a new mesh-generating algorithm that can handle the complex geometry was required (HÜRLIMANN 1994). The hybrid models in this study are used as interpretative tools that help to characterize the local flow conditions in a designed conceptual area. In other words, the model results are not intended to reproduce or predict the "true" flow conditions at a specific geographic location.

The principal objectives of the hybrid models are

1) to improve and test the conceptual model of flow, by showing the impact of major structural features on the local flow system; and
2) to provide the "first-level" results required as input for the safety analysis, such as distribution and direction of hydraulic gradients, and distribution of specific fluxes through the faults and average rock.

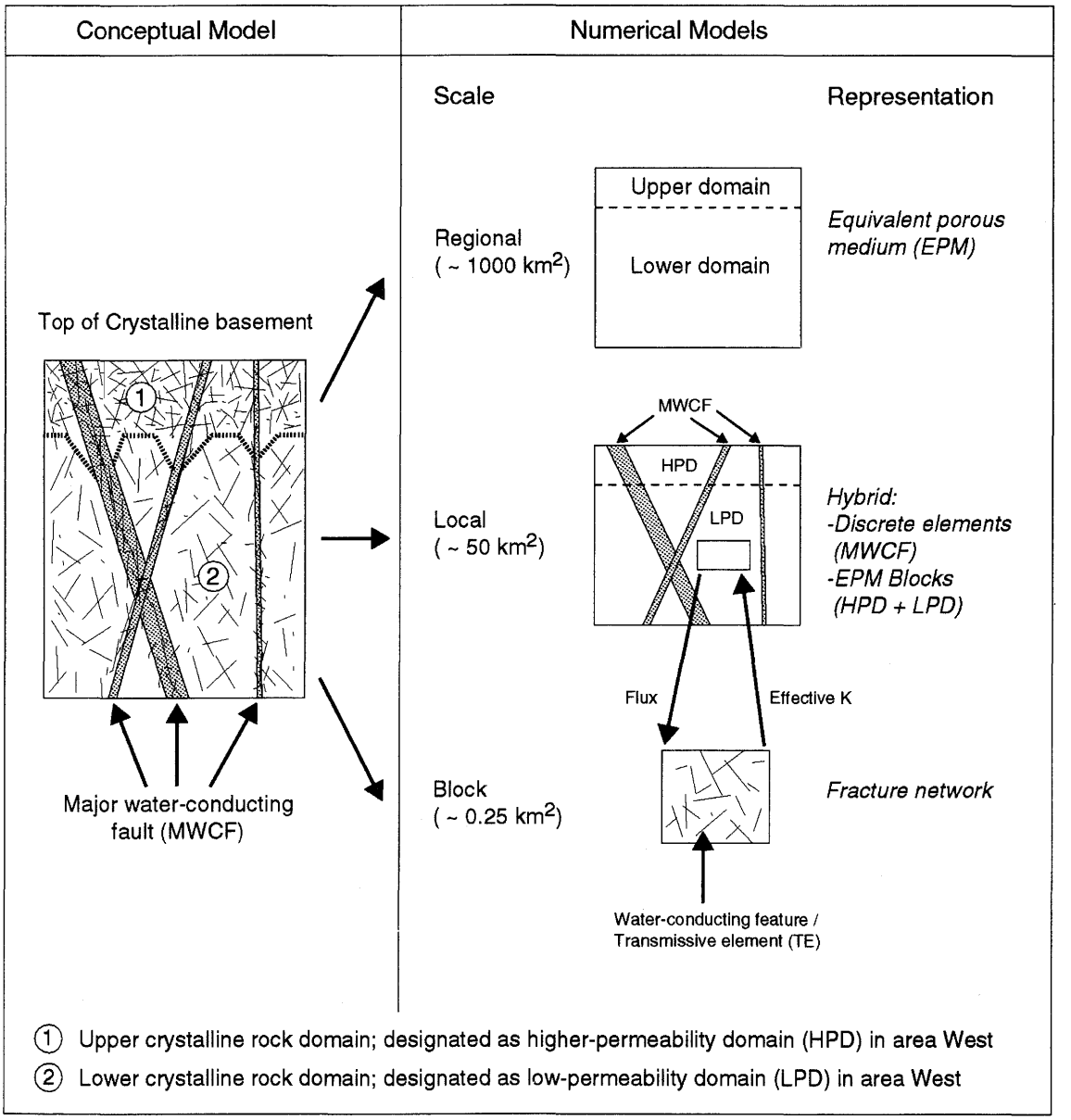

Fig. 1.2 Approach to modeling groundwater flow in crystalline basement of Northern Switzerland

The third level of numerical modeling deals with the characterization of flow through a typical block of low-permeable fractured crystalline rock that may constitute the immediate environment of a hypothetical repository. At this block scale, the groundwater flow and storage occurs primarily within the discontinuities; the contribution of the low-permeable rock matrix is negligible. Because the exact geometry and properties of the fracture system cannot be measured, generic models are used that describe the network properties stochastically. The required statistical input parameters are derived from borehole observations. By generating multiple stochastic networks with different fracture parameters, such as frequency, size and aperture, the significance of the conceptual uncertainties on the effective properties of a fracture network can be investigated. Due to the ability to simulate flow through many thousands of discrete planar features that occur within a block of the potential host rock, the fracture-network models have recently become a conventional tool in the field of repository performance assessment and site characterization.

1.3 Acknowledgments

The authors thankfully acknowledge the active support that was provided in the course of the progressing study by R. Andrews (Intera, Austin); J. Pearson Jr. (Irving, Texas) and H. Schmassmann (Liestal).

Valuable review comments and suggestions were provided by F. Pasquier (Nagra) and J. Trösch (ETH Zürich).

Special thanks go to S. Shulist and Mrs. Hussner (Colenco) who provided illustration and editorial support.

The synthesis study reported herein was performed on behalf of Nagra, the Swiss National Cooperative for the Storage of Nuclear Waste, under the project management of S. Vomvoris.

2 SYNTHESIS OF BOREHOLE DATA AND ASSESSMENT OF HYDRAULIC ROCK PROPERTIES

2.1 Introduction

The principal tasks of the hydrodynamic synthesis of crystalline rocks are to collect and analyze all hydrogeological data that were acquired by Nagra during the recently completed regional investigation program KRI-1, and to integrate these experimental data and observations into a hydrogeological conceptual model. The development of a such conceptual model is the first and the most critical step in the task of hydrogeological characterization of the crystalline basement in Northern Switzerland. The purposes of the conceptual model are: 1) to provide a simplified description of the groundwater flow at different scales of interest that is consistent with a variety of available field information, and 2) to describe the hydraulic properties of the hydrogeological system. Thus, the conceptual model forms the basis for the hydrogeological characterization of the considered host rock, for numerical studies of groundwater flow and for long-term safety assessments in the context of high-level radioactive disposal.

Therefore, the objective of Chapter 2 is twofold; first to document the approach and results of the synthesis of hydrogeologic borehole data, and second to develop a conceptual model of crystalline rocks and produce a set of representative hydrogeologic parameters that are required for safety-analysis and modeling studies. The borehole-data synthesis consisted of comprehensive hydrogeological and statistical analyses that were documented in a series of internal Nagra reports. The synopsis of these studies was provided by VOBORNY et al. (1993) and is presented as Chapter 2 in this report.

The synthesis of borehole hydraulic data is outlined in Section 2.2. The outcome is the development of the hydrogeological conceptual model of crystalline rocks in Northern Switzerland described in Section 2.3. Section 2.4 deals with the methods of characterizing the advective fracture flow. Statistical methods and conceptual considerations are applied to quantify the parameters that control fracture flow. Based on the hydrogeological domains that were defined by the conceptual model, analytical estimates of the corresponding effective hydraulic properties are performed in Section 2.5. The concluding Section 2.6 summarizes the results of the performed synthesis work and provides a reference data set of key hydrogeological parameters.

2.2 Synthesis of borehole data

2.2.1 Approach

The basic borehole data comprise the results of hydraulic tests (packer tests and fluid-logging tests) that were performed in the following four deep boreholes of Nagra's crystalline drilling program (with indicated length of drilled section in crystalline rock) north of the Permo-carboniferous trough, PCT (see Fig. 1.1): Böttstein (BOE, 1,186 m); Kaisten (KAI, 1,009 m); Leuggern (LEU, 1,466 m) and Siblingen (SIB, 1,173 m). Not included are test results from the three boreholes that are located within or south of the deep PCT.

Although the 2,480-m deep Weiach well had penetrated crystalline rocks in the lowermost section, it is not integrated in the database because of its location within the PC trough (close to the edge formed by normal faulting). The penetrated crystalline interval of 460 m is too deep below ground level to be considered as a potential host formation. In any case, the crystalline rocks at this depth were characterized by rather low conductivities in the packer tests and would, therefore, bias the statistical results toward the lower end.

The large amount of test data was subjected to an iterative process of analyses, ranging from first quick-look interpretations of raw data to assignment of definitive properties to rock intervals and identified water-bearing fractures.

In order to produce a consistent profile of transmissivity variation along a borehole with overlapping test intervals, the procedure of deconvolution (described in BLACK et al., 1987) was applied at the initial stage of analysis. The interpretation of test data focused on identification and hydraulic characterization of discrete zones in which advective flow occurs and which are observable as inflow points in the boreholes. Thus, the hydraulic data were primarily categorized into two families: the discrete *"inflow points"* and the *"matrix"*, i.e. test intervals with no observed inflow point.

This classification was iteratively improved on the basis of detailed analyses of fluid-logging results and visual inspections of cores as follows:

- The first synthesis of hydraulic test data from the boreholes was performed by LINDER & VOBORNY (1991). On the basis of deconvoluted test results

and a first classification into inflow points and matrix, linear regressions were calculated for the data set of each borehole (BOE, KAI and LEU). The results of the regression analysis and core data were used for the assignment of data points to discrete inflows or matrix intervals.

- Following several reviews of the fluid-logging and packer-test data and a complementary core analysis by MAZUREK (1990) a final identification of inflow points and matrix intervals was established by KLEMENZ (1991). The data set also included a basic petrographic characterization of the permeable features. A similar database for the SIB borehole was provided by KLEMENZ & GUYONNET (1992).

The two last mentioned reports represent the definitive compilation of hydraulic borehole data, and serve, therefore, as the basic dataset for the hydrogeological characterization and modeling of crystalline rocks in Northern Switzerland.

Once the discrete inflow points and their transmissive properties were identified in the boreholes, additional characterization studies were conducted. The approach adopted for this assessment is illustrated in Fig. 2.1 and described below. In the context of flow characterization, the small-scale geologic features (fractures, joints) that carry most of the flow and produce the inflow points in the boreholes were designated *"water-conducting features"*. The objective of the characterization studies was to describe the typical properties of these single transmissive fractures in terms of a) advective flow, and b) contaminant transport, i.e., to establish a database that serves as input to safety-analysis calculations and numerical transport models.

The compilation of all experimental data that are used in the present synthesis is given in Appendix 1 for identified inflow points and in Appendix 2 for matrix intervals. All data are summarized per borehole and include the following parameters: inflow-point number, depth below ground level (matrix: centre of interval), depth below top of crystalline rocks, and the assigned T or K value with corresponding basis-10 logarithm. In accordance to the conceptual model described in Section 2.3, the borehole data are regionalized into two geographical areas West and East. The resulting subdivision into hydrogeological domains, as described in Section 2.3.3, is also indicated in the table, in order to document the proposed zoning of the crystalline basement. The last column in Appendix 1 refers to a systematical classification of the identified features according to Section 2.2.4.

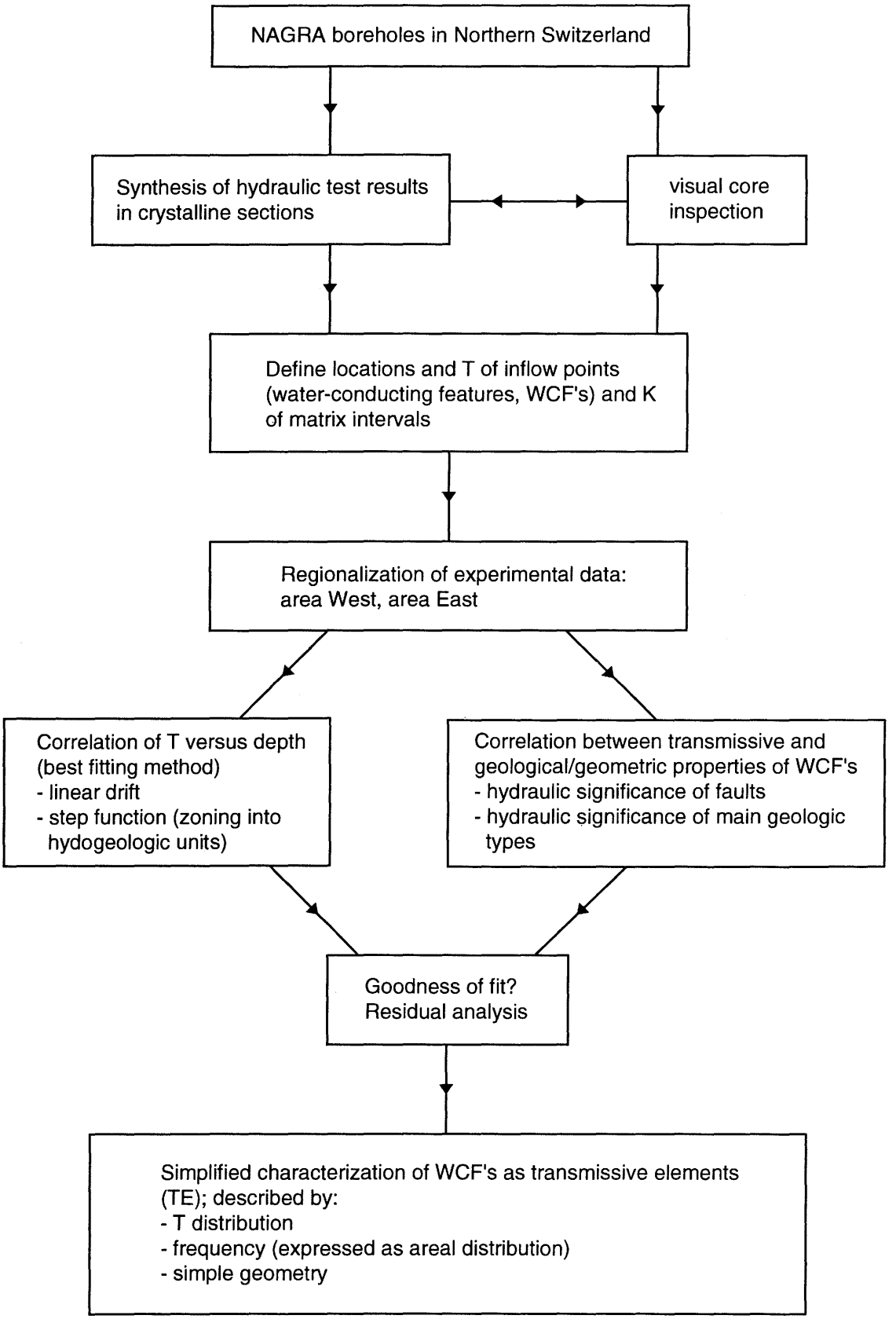

Fig. 2.1 Approach for assessment of hydraulic rock properties

2.2.2 Depth-dependent behaviour of hydraulic parameters

The basis for the statistical analyses of hydraulic properties was the definitive categorization of test data into inflow points and matrix intervals according to Appendices 1 and 2. The former data group is characterized by a discrete location and the transmissivity, the latter by the interval length and the mean hydraulic conductivity, which assumes a homogeneous porous rock within the interval. A first preliminary analysis of the depth-dependent behaviour of these parameters by LINDER & VOBORNY (1991) has suggested that the best characterization is achieved by plotting the logarithmic values of T or K against the depth below the top of crystalline rocks, given that the basement is covered by sedimentary rocks of variable thickness.

The graphical presentation of all experimental data is given as depth-related spread diagrams in Fig. 2.2. The data points are categorized by boreholes. As a general trend, both spread graphs show a decrease in parameter values with increasing depth. The matrix conductivity shows a rather uniform trend in all boreholes, regardless of the different bedrock type penetrated (granites and gneisses). The transmissivity distribution of the water-conducting features (inflow points) manifests, however, a different behaviour in some boreholes. The aforementioned preliminary analysis tried to match the observed trend by the method of linear regression, which, however, produced a large statistical scatter of data around the fitted values. A more appropriate characterization of the hydraulic variability was achieved by dividing the crystalline rocks into an upper and a lower unit, that were incorporated in a preliminary conceptual model.

The separation into hydrogeologically more homogeneous sub-domains significantly reduced the spread around the fitted regression lines. At this stage, the statistical analysis did not incorporate some "outliers", such as the high-transmissive features at LEU-1650 and KAI-700 (Fig. 2.2). The development of the definitive conceptual model, consisting in the definition of conceptual hydrogeologic units and their hydraulic characterization, is presented in Section 2.3.

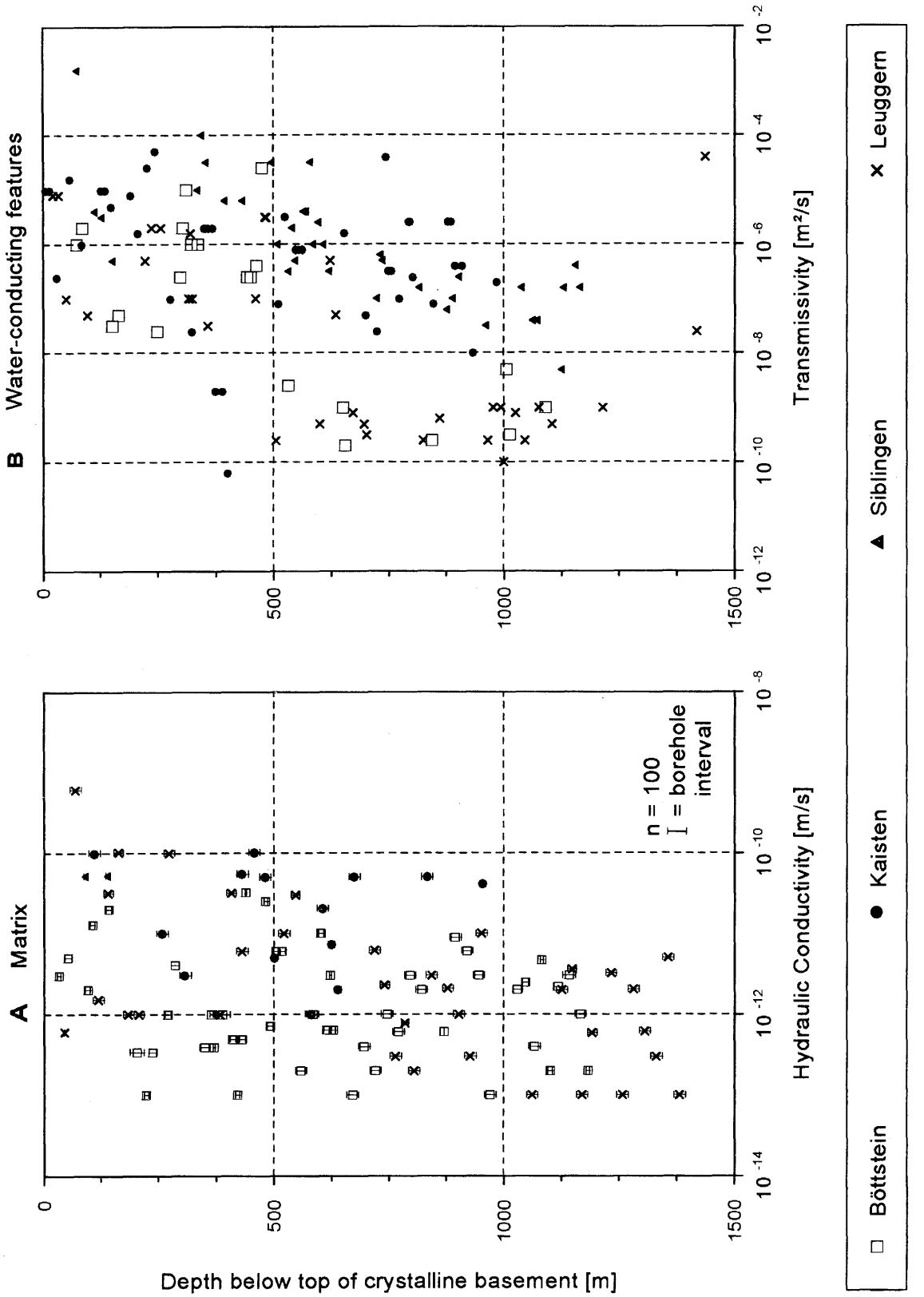

Fig. 2.2 Spread diagrams of hydraulic properties versus depth: log K of crystalline matrix (A), log T of water-conducting features (B)

2.2.3 Hydraulic significance of faults

The second step of the statistical analysis addressed the hydraulic significance of tectonically disturbed zones (faults). A correlation of structural data obtained from core analysis with fluid-logging results (AMMANN et al., 1992) stressed that about 50-60 % of all detected inflows occur in disturbed core sections, which, in turn, represent only 15-20% of the total crystalline length. Hence, the frequency of inflows in tectonically disturbed zones is 5 to 11 times higher than that in averagely fractured rock. Due to lack of other diagnostic criteria in the boreholes (caused by the one-dimensionality of observations), closely spaced disturbed core sections were combined to define a fault zone. Although such a definition is a subjective one, this pragmatic approach was applied consistently to all boreholes (AMMANN et al., 1992).

To analyze the hydraulic fault properties, all inflow points were categorized in faults and non-faults and each data set was subjected to a geostatistical analysis (JAQUET 1991b). The relationship between log T and depth was described by a linear regression (termed drift) for both data sets. Because the resulting regression lines were similar for both groups, it was concluded that the population of water-conducting features within faults (i.e., within disturbed core sections) does not have different hydraulic properties from that outside the faults. Hence, a specific differentiation of faults within the generic family of water-conducting features is not required in the hydrogeological conceptual model.

2.2.4 Systematic classification of water-conducting features

The abovementioned statistical analyses suggested that no further qualification of discrete water-conducting features is required to characterize the advective flow through these elements. However, safety-performance calculations and solute-transport models require a complete geological dataset which characterizes the flow and transport properties of single fractures that control the small-scale flow. The preliminary petrographical characterization of water-conducting features, as mentioned in section 2.2.1 (MAZUREK 1990), was tailored to individual boreholes and based partially on conservative assumptions. Hence, a new petrographical analysis of crystalline core sections in Nagra's boreholes was performed by MAZUREK (1991), to provide a consistent and realistic dataset which includes all rock types, deformational patterns and types of alteration observed in Nagra's boreholes. Emphasis was put on a simplified description of

geometrical and mineralogical properties of water-bearing features, which control the transport processes of nuclides in groundwater.

The study suggested, that - despite the complex geological conditions - the groundwater flow through fractured crystalline rocks of Northern Switzerland can be described in terms of 3 principal types of water-conducting features, defined as follows (MAZUREK 1991):

Type 1: Cataclastic zones: Faults and disturbed sections characterized by cataclastic shear deformation.

Type 2: Jointed zones: characterized by brittle deformation (tensile jointing).

Type 3: Fractured aplite and pegmatite dykes: late magmatic intrusions with a concentration of brittle deformation.

Each type was subjected to mineralogical and geochemical laboratory analyses to evaluate the petro-physical and geochemical properties that are required as input for safety-performance calculations (MAZUREK 1991).

The following two steps address the question whether the observed transmissivity of the water-conducting features (WCF) can be correlated either to their petrographical properties or to the type of the background rock. For this purpose, the identified transmissive features were first categorized into the 3 principal types as defined above and re-plotted in Fig. 2.3A. The scatter of T values shows no evident relationship to geological properties. In a second step, the same population of identified WCF's is plotted in Fig. 2.3B, now classified into two separate subsets reflecting the type of primary bedrock (granite or gneiss). The spread diagramm shows a similar trend in T distribution for the two datasets, suggesting that the hydraulic properties of WCF's in Nagra boreholes are not correlated to the type of background rock. However, the frequency of inflow points in granite is somewhat smaller than in gneisses: N (WCF granite) = 0.023 m^{-1} , N (WCF gneiss) = 0.035 m^{-1}.

It is concluded, that the hydraulic behaviour of the WCF's shows no distinct correlation neither to their geological properties nor to the type of primary bedrock. Based on this finding, the variety of discrete small-scale geological discontinuities (WCF) that control the advective flow through blocks of fractured rock can be characterized hydraulicaly by one single generic feature.To empha-

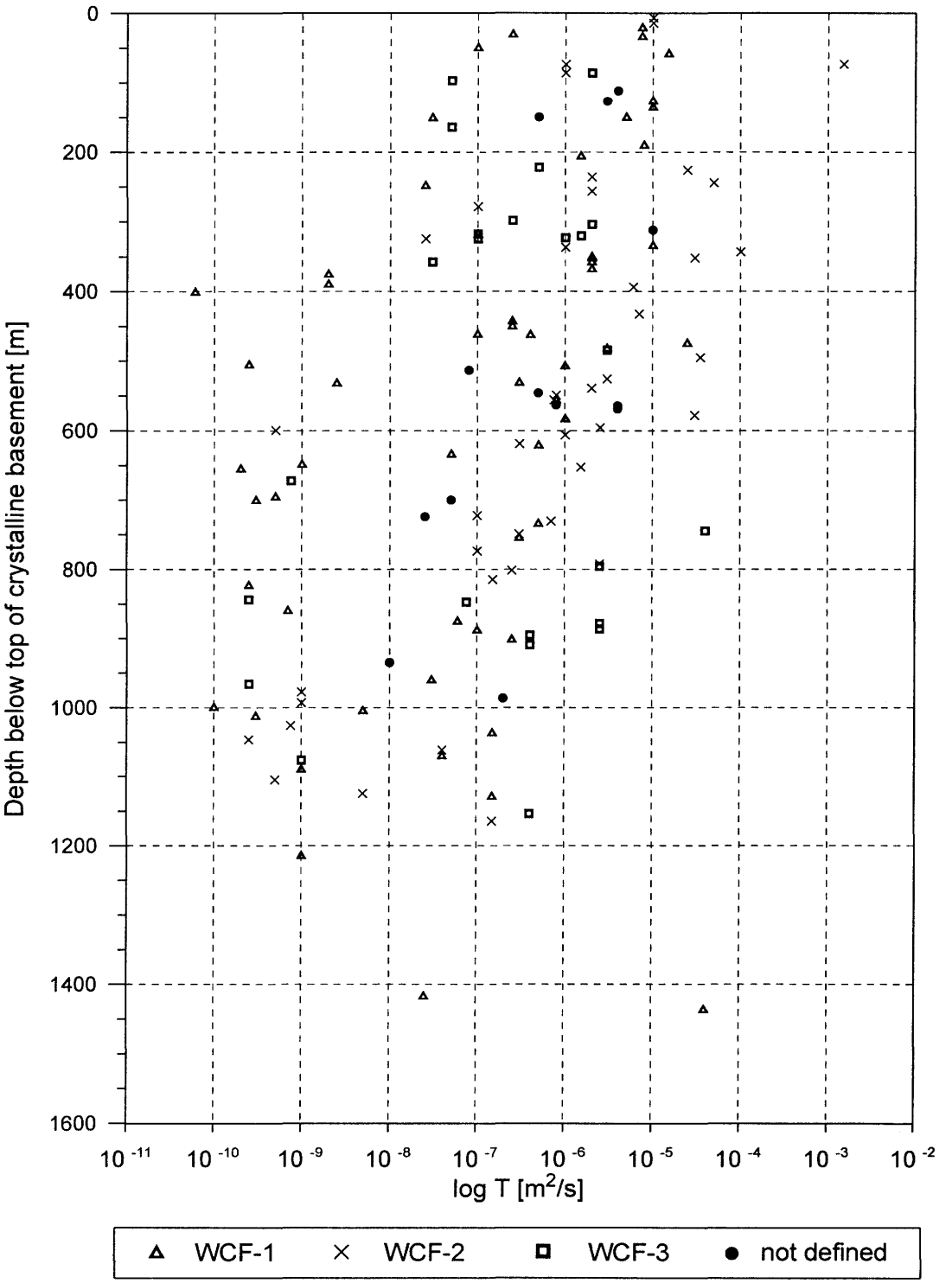

Fig. 2.3A Log T of water-conducting features (WCF) classified into main geological types

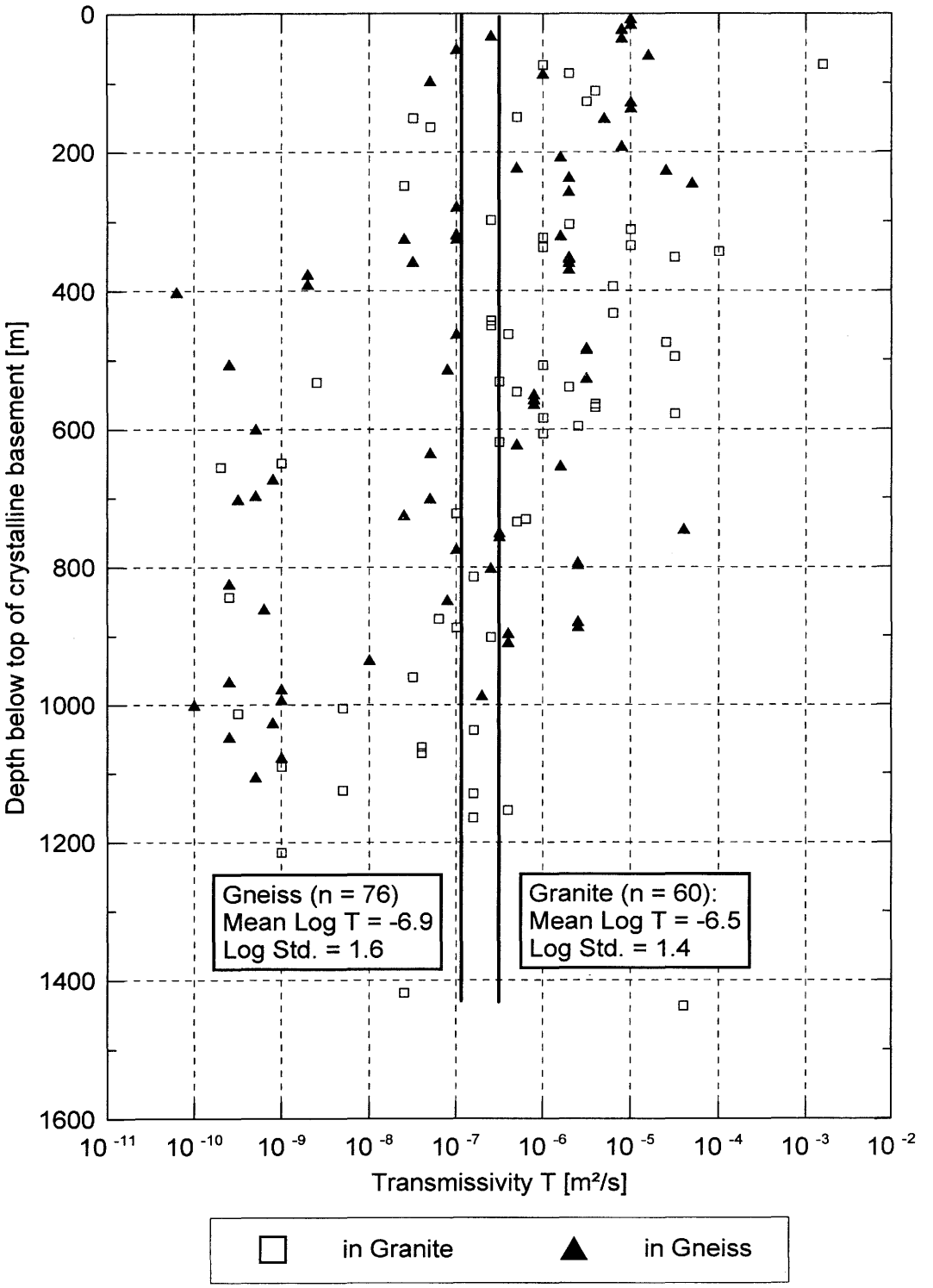

Fig. 2.3B Log T of water-conducting features (WCF) indicating occurrence in granitic bedrock or gneiss

size this step of generalization (with respect to solute transport), the term **"transmissive element"** was introduced for the use in conceptual and hydrodynamic models describing the **advective flow** in crystalline rocks of Northern Switzerland. In contrast, the term of water-conducting features remains associated with different transport properties of single fractures and is reserved for the geometric-mineralogical description of discrete flowpaths.

2.3 Conceptual hydrogeological model of crystalline rocks

2.3.1 Objectives

The key issue in the assessment of the repository performance in the considered crystalline host rocks is the potential transport of released radionuclides by groundwater through the geological environment (geosphere). The solute-transport calculations require a realistic input that has to be provided by an appropriate hydrogeological characterization of the geosphere. As a rule, such a characterization relies on simplified concepts that approximate the complex and heterogeneous hydraulic conditions of bedrock. The main task of any hydrogeological site characterization is to develop a conceptual model that represents an adequate approximation of the real system or processes. In view of the limited database available and the heterogeneity of the hydrogeologic system under consideration, the conceptual model is deemed the weakest link in the modeling chain. Mathematical models, being the next step in a characterization study, are an useful tool to test the plausibility of the conceptual model and to quantify its inherent uncertainties.

The objective of the conceptual model is to integrate the acquired experimental findings, observations and experience into a simplified[1)] but consistent description of the groundwater flow system within crystalline rocks at different scales.

[1)] preferably with a minimum number of parameters due to the sparse database consisting of 4 boreholes in a region of several 100 km^2

2.3.2 Regionalization of borehole data

The first proposal for a quantitative hydrogeologic characterization of crystalline rocks was derived by LINDER & VOBORNY (1991) based on the analysis of the hydraulic tests in Böttstein, Kaisten and Leuggern, all situated in the western part of the investigation area. It was shown that the hydraulic behaviour of crystalline rocks is depth dependent (drift) and that low-permeable conditions are likely to occur at certain depth. The subsequent analysis of hydraulic data from the Siblingen borehole in the eastern area (KLEMENZ & GUYONNET 1992) also showed a depth dependence of the hydraulic properties, but shifted towards higher values than those observed in the western area. This finding can be explained as follows: 1) the crystalline rocks in the region surrounding the SIB site do indeed exhibit different hydraulic properties from those in the western part of the investigated area, or, 2) the SIB site reflects a local anomaly and the true properties of "undisturbed" crystalline rocks surrounding the site are similar to those observed in the western part.

The first explanation is supported by geological observations indicating that the two areas have undergone a different deformation history and are situated in a different seismo-tectonic setting (see Table 4.1 in Ch. 4). There is no hard information in favour of the second hypothesis. Nevertheless, due to the structural setting of the SIB site which is dominated by extensive horst-graben tectonics, the presence or proximity of a major tectonic feature cannot be excluded.

The first hypothesis is considered "conservative" in terms of hydraulic-conductivity distribution because it does not extrapolate the observations from the western area (low-permeable crystalline rocks at depth) to the region surrounding the SIB site. It was concluded, therefore, that a primary subdivision of the investigated region into an area West (characterized by BOE, KAI, LEU) and area East (SIB) is appropriate for the quantitative characterization of sub-regional groundwater flow. The flow conditions in these areas are analyzed separately in Chapters 4 and 6 respectively. The development of the conceptual hydrogeological model is described below. The hydrogeological assessment of area East is conducted for both conceptual hypotheses which are treated as equally plausible.

2.3.3 Description of the conceptual model

Parallel to the progressing synthesis of hydraulic borehole data, the early hydrogeological characterization of LINDER & VOBORNY (1991) was iteratively developed to the actual form of the conceptual model of crystalline rocks, described herein.

The principle of the conceptual model is a binary representation of the crystalline rock mass. At the large scale of several kilometres, the rock is differentiated into two classes **"Major water-conducting faults"** and **"Block matrix"**. The latter term is used herein to address the volumes of relatively undisturbed "background" rock between the major faults. This partition in discrete flowpaths and background rock is valid at different scales of interest. Moreover, this characterization reflects the large-scale geo-mechanical heterogeneity of the crystalline basement, where the large faults are zones of major tectonic displacements and the inert rigid blocks constitute the intact rock.

The bimodal approach is characteristic for sites in hard fractured rock and has been successfully applied in the STRIPA project in Sweden (HERBERT et al. 1991) and in groundwater modeling of the Grimsel Test Site (VOBORNY et al. 1991). The principal underlying assumptions of this approach are that a) the large faults and fracture zones extending over kilometres of distance represent major conduits that govern the large-scale groundwater flow; and, b) these faults are deterministic structures that can be identified in space and explicitly included in conceptual and numerical models. The importance of these regional faults in the field of waste disposal is that they in fact define the boundaries of block volumes within which a potential repository can be sited.

At a scale larger than a few km^2, minor faults and other tectonic discontinuities cannot be treated in a deterministic manner and are accounted for by geostatistical means. They are implicitly incorporated in the Block matrix, which is characterized by the continuum approximation at this scale. Nonetheless, these permeable features significantly affect the hydraulic properties, namely the tensor of equivalent hydraulic conductivity, of the Block matrix. By making the continuum approximation, the conceptual model implies that these blocks of relatively undisturbed rock are large enough with respect to the size of included discontinuities and that a representative elementary volume (REV) exists.

Unlike the preliminary conceptual model, the bimodal approach does accom-

modate the observed occurrence of highly transmissive features at greater depths in the crystalline basement, such as observed in the bottom part of KAI and LEU. This approach represents, therefore, a further development of the earlier concept; it also maintains the vertical zoning of crystalline bedrock to account for its hydraulic heterogeneity. The difference to the former approach is that this zoning applies to the blocks of rock between the explicitly considered major faults.

A schematic illustration of the conceptual division of crystalline rocks into hydrogeologically homogeneous units is presented in Fig. 2.4. As exposed above, the bimodal characterization defines two principal domains, designated as Major water-conducting faults (MWCF) and Block matrix. In geometric terms, the MWCF's dissect the crystalline basement into a number of irregular subvertical prismas of variable sizes, constituted by the Block matrix. These blocks, in turn, are subdivided into two zones of different hydraulic properties that approximate the observed general trend of hydraulic heterogeneity in the crystalline rocks of Northern Switzerland.

The elements of the conceptual framework are described in the following. Although this framework was basically established on the basis of borehole data from the area West, its principles are also valid for the observations at SIB site. The basic differences between the two areas are discussed below. In this context, a fundamental question to be addressed by the conceptual model is whether the SIB data are representative for the characterization of that subregion or not.

The conceptual framework defines the "major faults" of the **MWCF domain** as tectonic faults of 1st and 2nd order, according to the hierarchical classification given by AMMANN et al. (1992, Tab. 2-1). At the site of KAI, a geometric correlation of structural core data with the observed tectonic pattern at the surface of the adjacent region indicates, that among the faults observed in the lower section of the borehole (below 830 m of depth) some features belong to the Eggberg fault zone of 1st order (AMMANN et al. 1992, App. 9a,b,d). Based on this positive correlation, the transmissive properties of the MWCF's were inferred from the hydraulic data in this borehole section. However, the core analysis does not provide any supporting evidence for the presence of a large fault, because there is no enhanced intensity of cataclastic deformation in the corresponding borehole section (MAZUREK in prep.). Besides major faults, the conceptual unit of MWCF also includes as members prominent **mineral and ore dykes** to

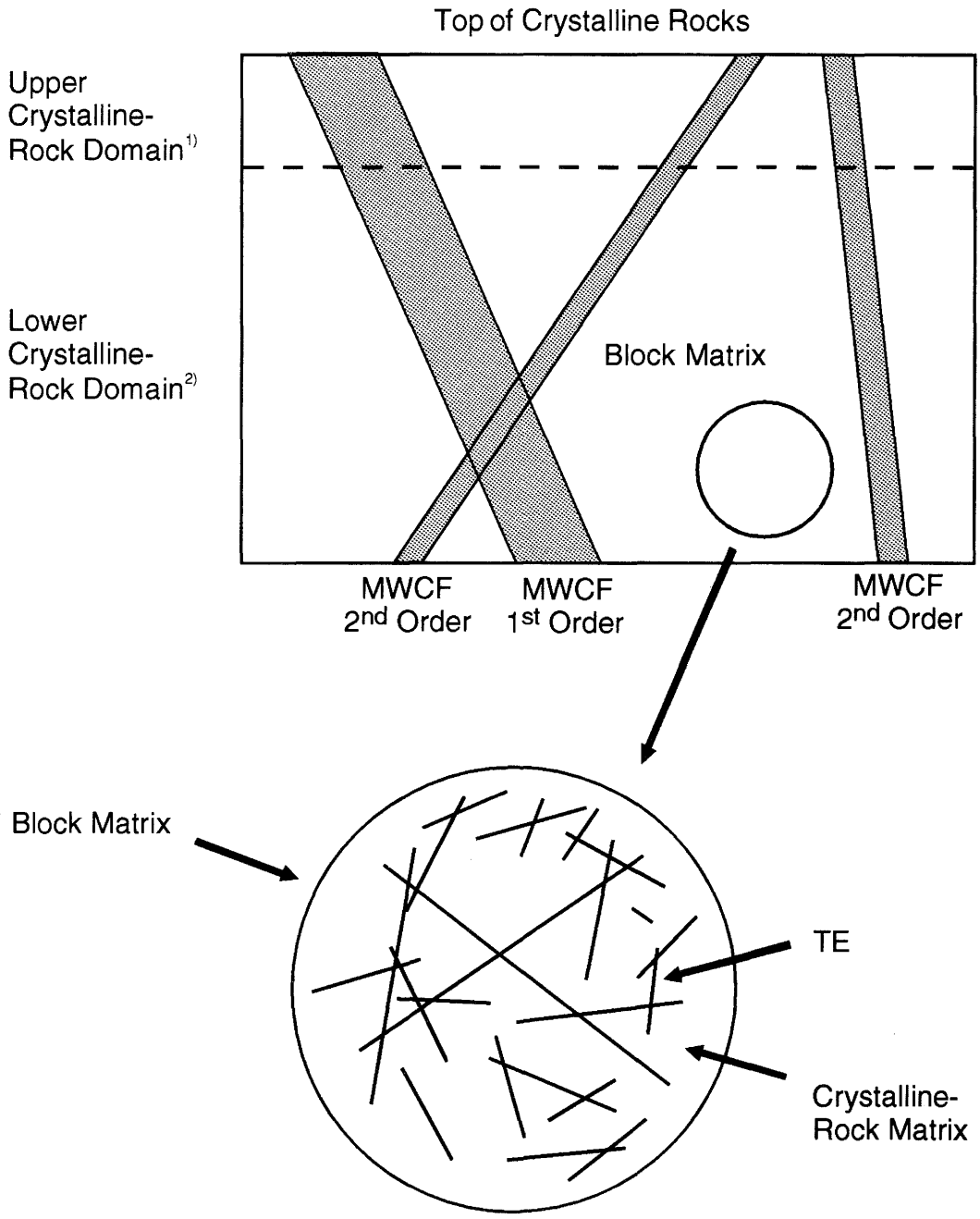

[1)] defined as HPD in area West
[2)] defined as LPD in area West

Fig. 2.4 Schema of the conceptual hydrogeological model of crystalline rocks

account for their potential capacity to carry flow. Several of such large water-bearing dykes have been reported in the southern Black Forest (see AMMANN et al. 1992, p. 51ff for references). A common property of all mineral & ore dykes is their enhanced secondary permeability resulting from leaching of ore minerals and partly from tectonic reactivation of accompanying faults. Due to their distinctive transmissive properties and a lateral extent of several kilometers, these features represent significant hydraulic conduits that require an explicit treatment in the conceptual and numerical models. In contrast, the aforementioned magmatic dykes (Section 2.2.4) are treated statistically as the Type-3 member of the small-scale water-conducting features.

Although no mineral or ore dykes have been penetrated in Nagra deep boreholes they form an integral part of the conceptual model, based on analogy with observations in the southern Black Forest. In structural terms, the dykes are attributed to north-south oriented Rhenish faults of 2nd order (Fig. 4.1). The nearest outcrop of such dykes to the Swiss crystalline basement occurs near Säckingen north of the Rhine River. In the bottom part of the Leuggern borehole (LEU-deep in Fig. 2.2B), a highly transmissive fractured zone contains abundant mineralization and dissolution cavities (vugs). The unusual concentration of vugs along preexisting fractures indicates the proximity to a mineral dyke or the presence of a such dyke in its initial stage (AMMANN et al. 1992, p. 54). In the conceptual model, the observed conditions at LEU-deep are attributed to mineral/ore dykes and, hence, they contribute to the hydraulic characterization of the MWCF unit.

The concept of MWCF is founded primarily on the observation in KAI-deep and LEU-deep intervals. Among the Nagra boreholes north of the PCT, these are the only two cases where a MWCF was positively identified, based either on a direct correlation to structural surface data (KAI) or on an indirect reference to Black Forest observations (LEU). Moreover, if the second conceptual alternative is taken into consideration, also the SIB borehole interval is interpreted as part of the MWCF dataset. In addition to the mentioned Nagra boreholes, the role of MWCF's as preferred conduits of flow is also manifested in other deep boreholes in the crystalline basement of Northern Switzerland, such as the thermal production wells of Säckingen (SAE in Fig.3.7), Zurzach (ZUR) and Rheinfelden (beyond Nagra's area of interest). Observations from these wells are implicitly considered in the conceptualization of regional flow but no hydraulic data were used for the quantitative characterization in Section 2.3.4.

The **Block matrix** represents the properties of the "average", i.e., relatively undisturbed rock. As schematically shown in Fig. 2.4 (bottom), such a block is constituted by the crystalline rock matrix and a large variety of structural features. The latter are per definition classified as minor, i.e., smaller than faults of 2nd order, and include fractures, joints, vugs, magmatic dykes and veins. The flow-carrying members of these structures are the water-conducting features or transmissive elements (TE) as defined in Section 2.2.4, which, in turn, are "visible" as inflow points in the hydro tests and particularly as peaks in fluid-logging. Thus, the effective hydraulic properties of a volume of crystalline rock that constitutes a hydraulic domain are defined by the permeability of the crystalline matrix and by the density and transmissivity of the constituent WCF's. As mentioned above, the conceptual model characterizes the Block matrix by a single average property by using a continuum approximation over that block volume.

Fig. 2.4 shows the subdivision of the Block matrix into two hydrogeological units, of which each can be characterized by homogeneous hydraulic properties. This differentiation of the relatively undisturbed blocks of crystalline rock accounts for the depth-related variability of transmissivity of water-conducting features that is evident in all deep boreholes of the investigation area (Fig. 2.3).

In the **area West**, this vertical zoning is characterized by a sharp decrease in transmissivity at a depth of 400 to 600 m below the top of crystalline rocks (see also Fig. 2.5). However, this boundary between the two zones has no evident physical significance (such as the lower limit of weathering, for example). The relative depth of this hypothetical boundary to the top of crystalline basement varies between 500 m in BOE, 370 m in KAI and 650 m in LEU, according to the dataset presented in Appendix 1. The conceptual and numerical models assume a mean (and constant) thickness of the Upper crystalline unit of 500 m, i.e. the observed variability in BOE, KAI and LEU is ±150 m. An alternative approach to this bimodal representation of the crystalline basement was tested in the regional groundwater model (drift in run V22, see Fig 3.6).

The **area East**, represented only by the borehole of SIB, shows consistently higher transmissivities and frequencies of water-conducting features than the observed values in Area West (see parameter compilation in Table 2.2). Hence, the principal question, addressed in Section 2.3.2, was whether the sampled experimental data at SIB are representative of a relatively undisturbed Block matrix in area East or whether they rather represent some site-specific disturbed conditions. Due to lack of additional information, the conceptual model has to

consider both alternatives as equally plausible.

The two hypotheses of the conceptual model East read as follows:

1) The first hypothesis, saying that SIB data represent the typical properties of the Block matrix in area East, implies that the latter is characterized by generally high effective conductivities. Hence, the "intact" Block matrix represents a well-connected permeable system for the groundwater flow. Due to lack of other indications, this hypothesis also assumes that the transmissive properties of Major water-conducting faults, which were not observed in SIB borehole, are similar to those of the Block matrix. With other words, there is no significant hydraulic contrast between the two conceptual elements, MWCF and Block matrix. This assumption is based on expert judgment and is considered justified by the high permeability values encountered in SIB as a whole. Due to this large bulk permeability of the rock, the large tectonic faults do not represent a major controlling factor for the regional groundwater flow in area East.

2) The second conceptual hypothesis considers the SIB data to be non-representative of the undisturbed Block matrix in area East. According to this hypothesis, the observed conditions correspond to a local anomaly that is attributed to a major tectonic fault accompanied with hydrothermal activity. The SIB site is located in an area dominated by 2nd-order faults that belong to a Hercynian horst-graben system. In this case, the SIB data cannot be used for the characterization of the typical Block matrix in area East, rather they represent a MWCF condition that can be encountered anywhere in the crystalline basement of Northern Switzerland. Hence, SIB data are lumped with those from KAI-deep and LEU-deep to form one single dataset that characterizes the MWCF domain.

2.3.4 Hydraulic characterization

It was concluded in the process of borehole-data synthesis (Fig. 2.1) that a hydraulic characterization of crystalline rocks is best accomplished by the derivation of two independent parameter sets, designated West and East, and that a larger degree of uncertainty is attached to the dataset East (Section 2.3.2). The parametric characterization of the defined conceptual domains is developed in the following. The derivation of the parameter sets West and East

according to the first conceptual hypothesis (SIB data representative for East, see above) is given in Section 2.3.4.1 and 2.3.4.2 respectively. The implications of the second conceptual hypothesis (SIB data non representative) are evaluated in Section 2.3.4.3.

2.3.4.1 Area West (BOE, KAI, LEU)

Figure 2.5 illustrates the transmissivity distribution of all observed TE's in that area. The spread diagram on top shows the T vs. depth behaviour of TE's categorized into conceptual domains as defined above. The data points corresponding to the Block matrix exhibit a distinct clustering, and are separated accordingly into an Upper and a Lower domain. For the purposes of the hydrogeologic synthesis of Nagra's KRI 1 investigation phase, these two units of area West are defined in hydraulic terms as the **Higher-permeability domain, HPD**, and the **Low-permeability domain, LPD**. The latter unit features favourable hydrogeologic properties and has been identified as the potential host unit for a deep HLW repository. An effective hydraulic conductivity of about 10^{-10} m/s is associated with the definition of LPD. Because the limit between these domains is defined at a different level in each borehole, some overlapping of data points occurs. The graph suggests that no hydraulic contrast is present between the HPD and MWCF domains as both display the same range of transmissivities. The bottom graph of Fig. 2.5 shows the probability distribution of log T values of observed TE's in area West. Except for one value, the range is from $1 \cdot 10^{-10}$ m^2/s to $1 \cdot 10^{-4}$ m^2/s. The distribution shows a distinct bimodal shape in accordance to the two clusters of HPD/MWCF and LPD indicated in the top diagram.

The proposed parametric characterization of conceptual domains in area West is derived in Fig. 2.6. Each of the three defined domains represents a homogeneous volume of rock that is described by a single hydraulic property, in this case the mean log T of the transmissive elements, shown as solid line in the graphs. An underlying assumption of this characterization is that all T values are log-normally distributed (see Fig. 2.5 bottom). Hence, the transmissivity of TE's in each domain is described by two distribution parameters, the log mean, μ, and the log standard deviation, σ. The former is the geometric mean of T, whereas the latter defines the spread of observed data around the mean value (referred to as residuals) and is assumed to have a Gaussian distribution. The statistical meaning of the residual value σ is that 95.5% of all data points occur within the range of $\pm 2\sigma$ with respect to the mean of log T.

The left diagram of Fig. 2.6 shows the characterization of the MWCF domain as derived from the observations in KAI and LEU boreholes. The geometric mean of T is $4.8 \cdot 10^{-7}$ m^2/s. The right-hand diagram shows the hydraulic characterization of the HPD and LPD that constitute the Block matrix, i.e., the undisturbed crystalline blocks between major faults. The contact between the two domains is approximated at 500 m depth below the top of crystalline rocks, although its location varies among the individual boreholes. The HPD is described by a geometric mean of $T = 8.8 \cdot 10^{-7}$ m^2/s, which is similar to that of MWCF. The LPD is characterized by a mean T of $5.8 \cdot 10^{-10}$ m^2/s, which is by full 3 orders of magnitude less than in the other domains.

The similarity in the parametric description of MWCF and HPD confirms the hydraulic affinity between these two domains. This justifies the earlier simplification that MWCF have the same hydraulic properties as HPD that was used for derivation of a preliminary input dataset for safety assessment and model calculations in 1991.

The fact that the MWCF's exhibit even at greater depths similar hydraulic properties as the HPD (see summary in Table 2.8) supports the conceptual hypothesis that the bulk groundwater movement through crystalline basement at the depth of a planned repository occurs within the MWCF's.

The residuals, i.e., the scatter of observed data around the fitted mean value are analyzed for each domain in Fig. 2.7. The shape of histograms suggests that the observed data are distributed symmetrically around the fitted value. Exception is the HPD unit (centre) that includes two "outliers" with very low T values, also evident in Fig. 2.6. Noteworthy is the small variability (scatter) of experimental data around the mean value within the LPD unit, which suggests relatively homogeneous hydraulic conditions within this domain.

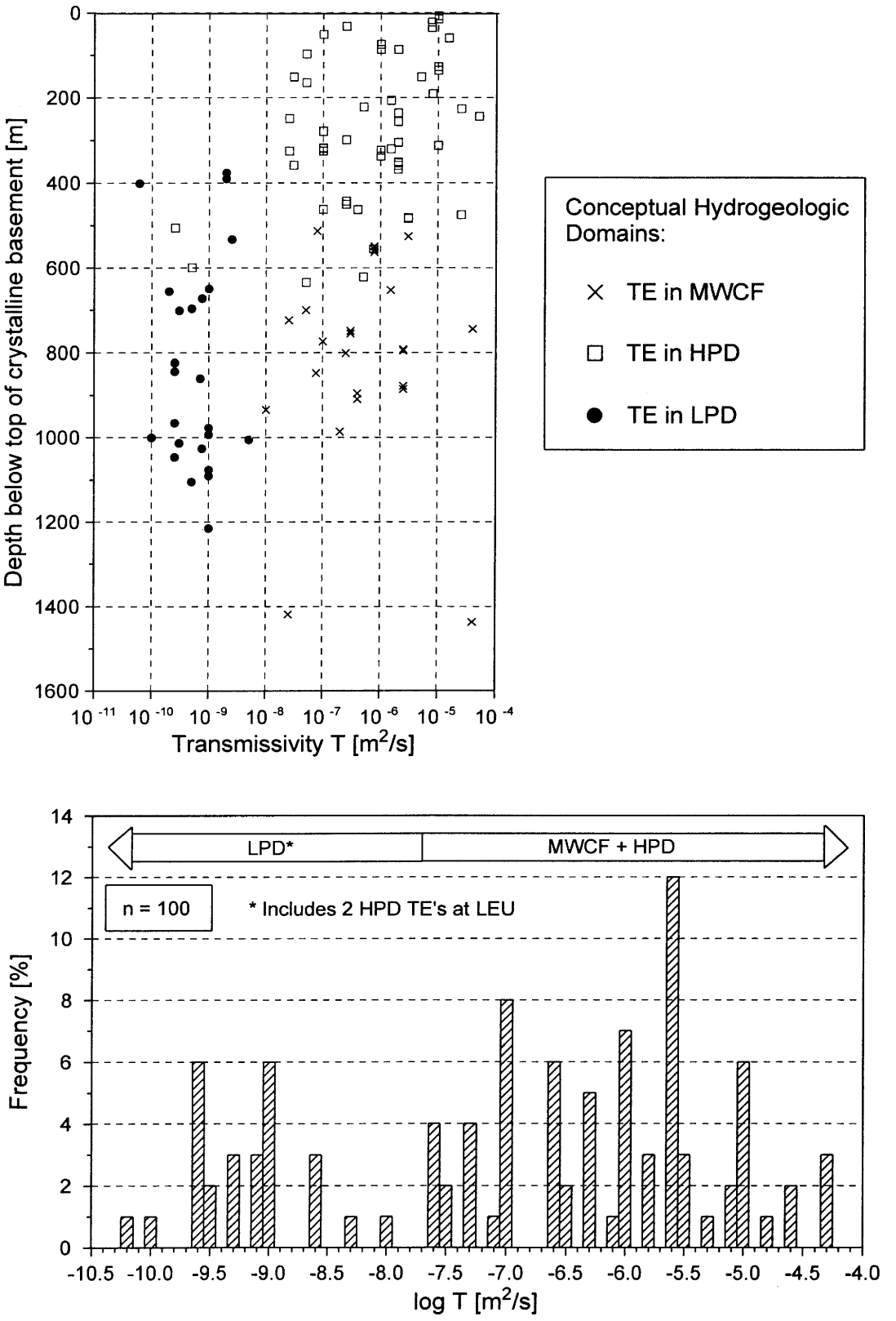

Fig. 2.5 Area West: T distribution of TE's categorized in hydrogeologic domains: spread diagramm *(top)*, histogram of log T *(bottom)*

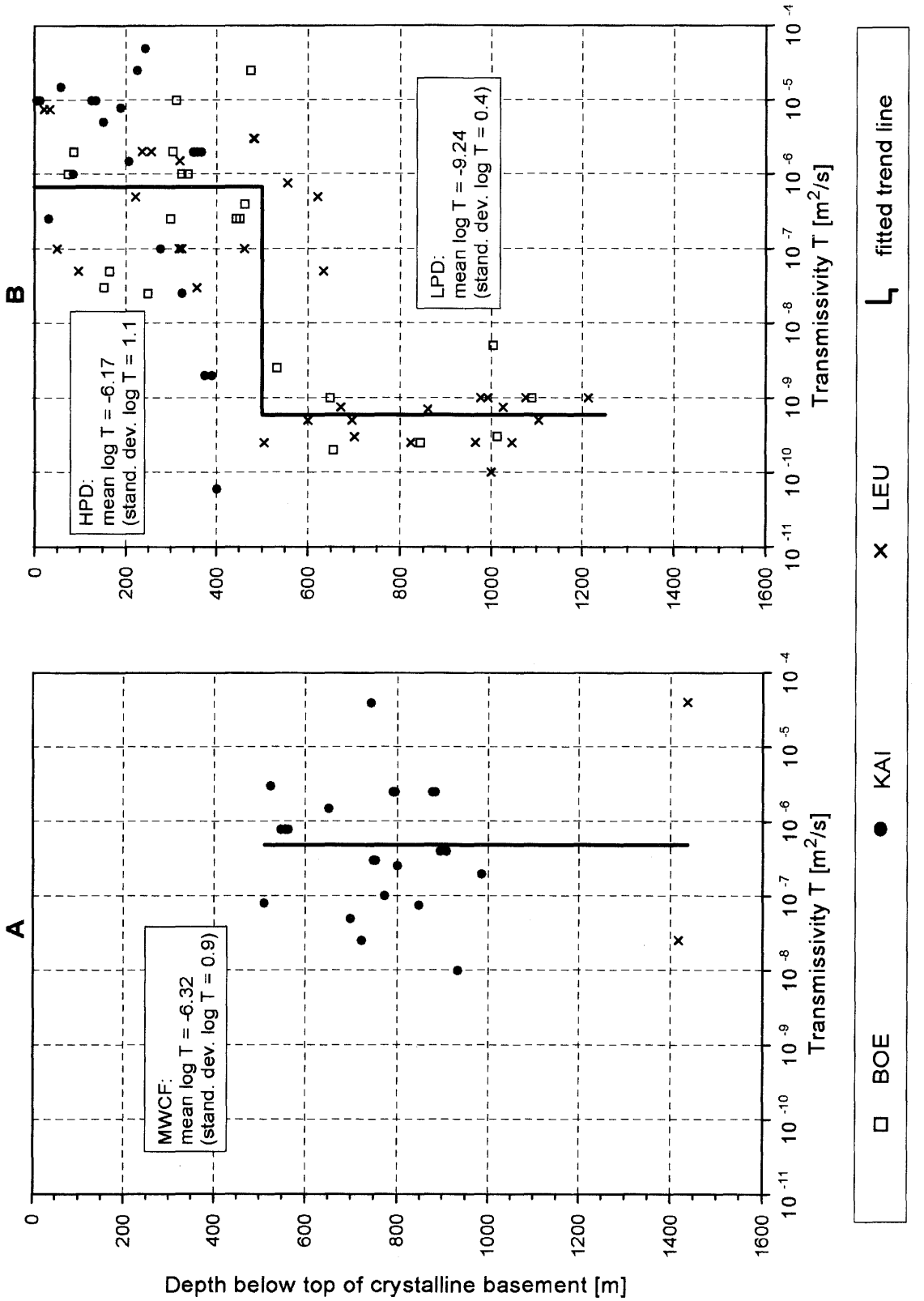

Fig. 2.6 Hydraulic characterization of conceptual units West: Major water-conducting faults MWCF (A); Block matrix divided in HPD & LPD (B)

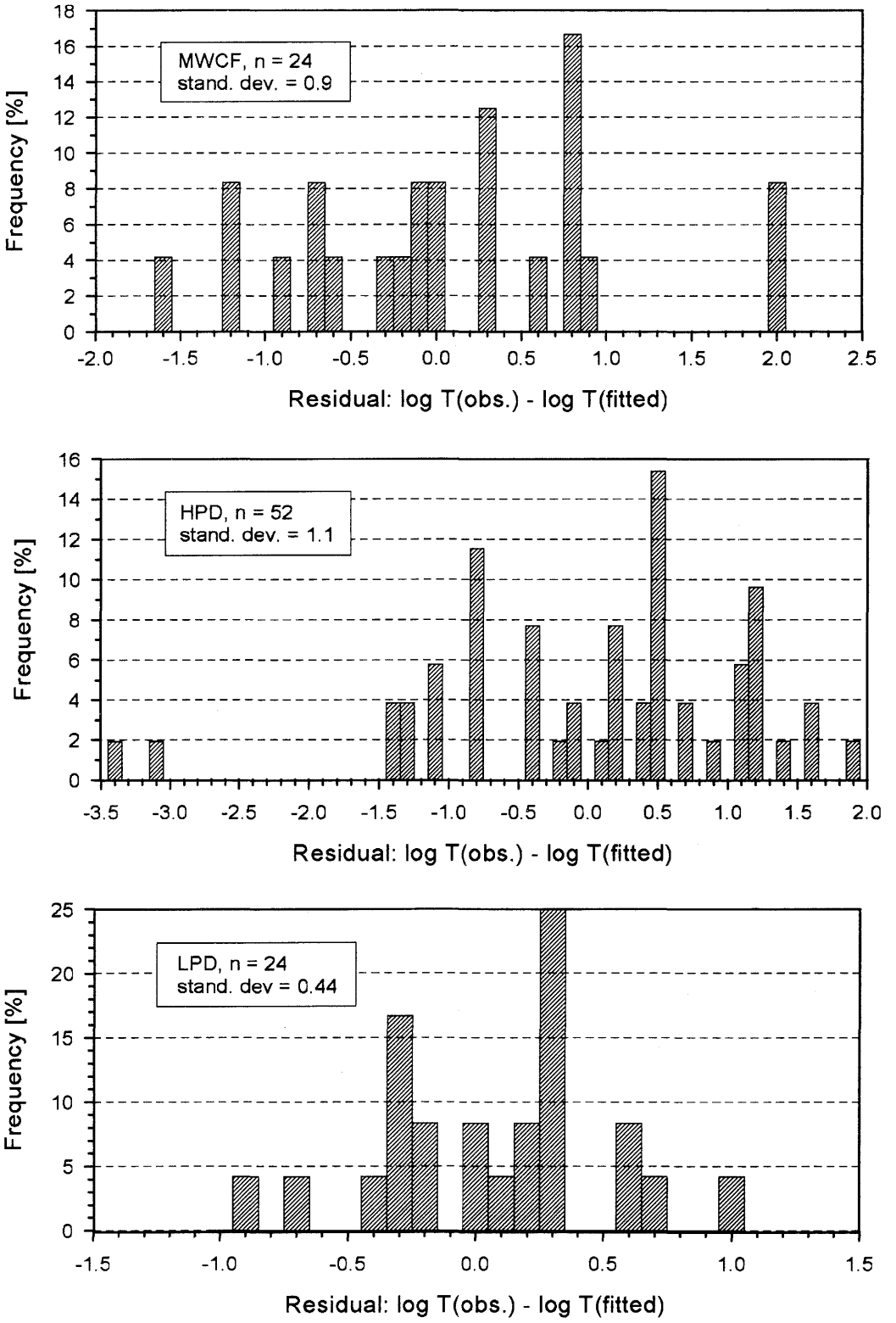

Fig. 2.7 Area West: distribution of residuals between observed and fitted T values of TE's for the defined hydrogeologic domains

2.3.4.2 Characterization of area East

As exposed above, the hydraulic characterization of the area East is more uncertain as the available database is derived from one borehole only. This uncertainty was addressed by defining two alternative conceptual hypotheses in Section 2.3.3. In the following, the parametric description of the conceptual model East is developed separately for the two alternatives.

Hypothesis 1

The hydraulic characterization of the area East, as described herein, is derived entirely from observed T values at SIB under the assumption that these data represent the typical properties of the Block matrix in this area.The T distribution of all transmissive elements at SIB is depicted in Fig. 2.8. The spread diagram (top) shows an inverse correlation of T with depth; i.e., the presence of a drift. The histogram of log T (bottom) indicates that most values are in the range between 10^{-8} and 10^{-4} m^2/s, with an outlier at each extreme.

The T trend shown in Fig. 2.8 (top) can be approximated by two possible fitting methods displayed in Figures 2.9 and 2.10 and commented in the following.

Figure 2.9 addresses the depth-related behaviour of log T by using the linear regression, i.e., drift (top); no further division of the crystalline blocks into homogeneous sub-domains is made. The slope of the regression line indicates a decrease of the mean transmissivity by a factor of 0.002 ($=10^{-2.7}$) per each 1,000 m of depth. The spread of observed data around the fitted regression line is given by the residual value $\sigma = 0.7$, indicating that the most data points occur within a factor of 25 with respect to the fitted value. The distribution of residuals around the mean value is plotted in the bottom graph of Fig. 2.9.

However, in the context of repository-performance assessment, it is desirable to provide a parametric characterization of the potential host-rock formation surrounding the repository and not of the bulk crystalline column. Therefore, the depth-related variability of transmissivities of TE's is fitted by a step-wise drift function, in analogy to area West. As shown in Fig. 2.10A the crystalline column is divided into horizontal layers that can be characterized by a single mean property.

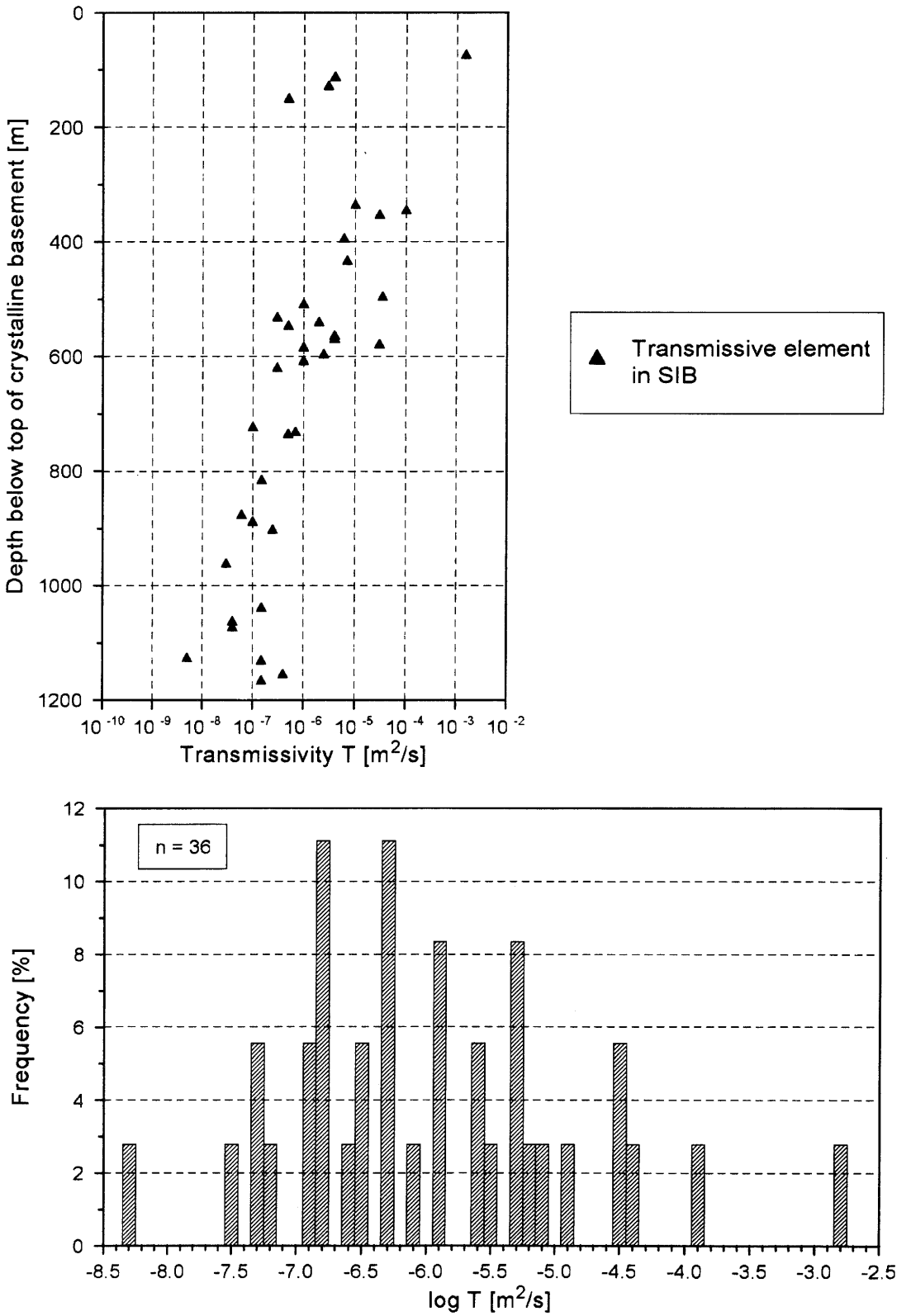

Fig. 2.8 Log-T distribution of transmissive elements in area East: spread diagram *(top)*, histogram *(bottom)*

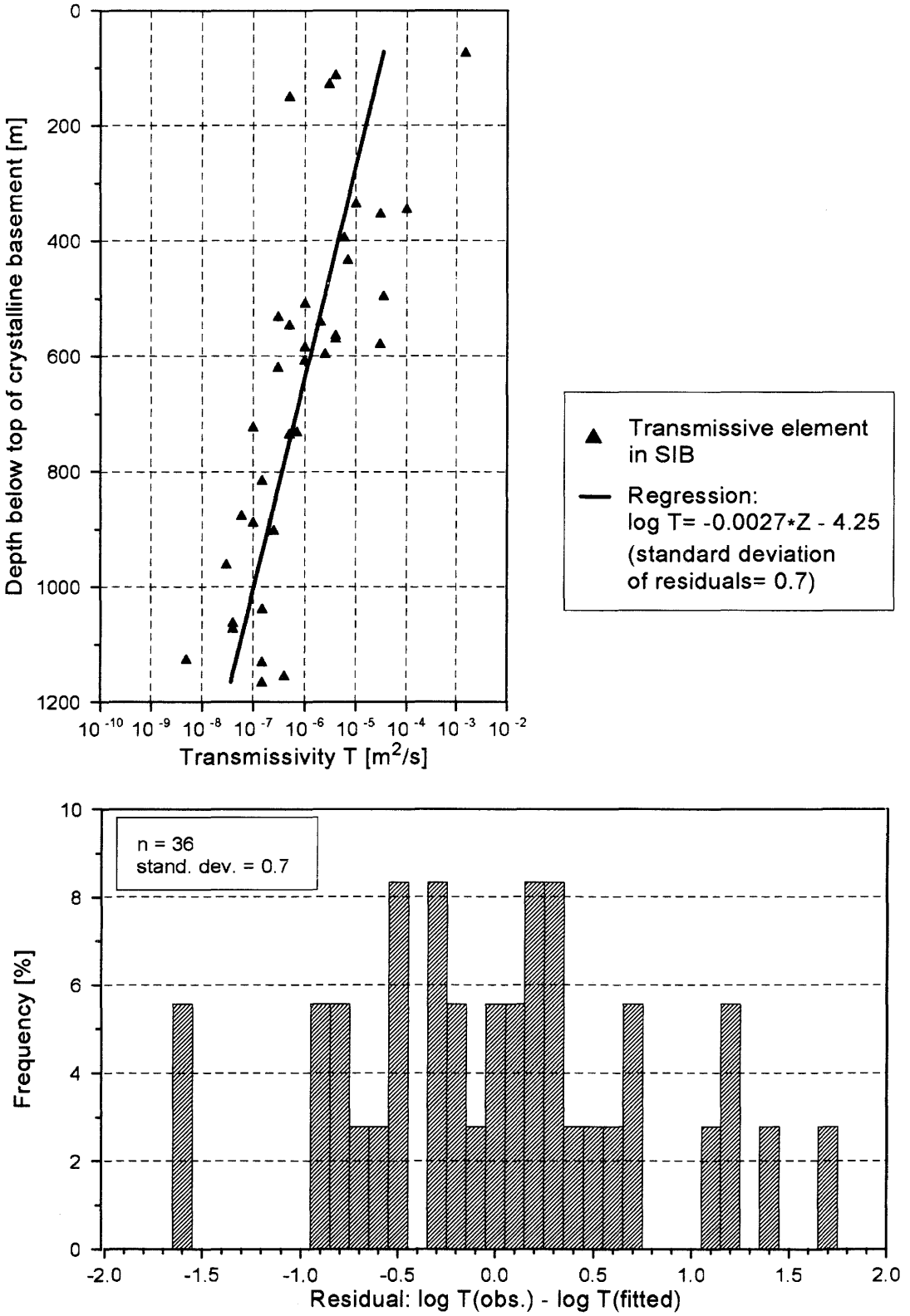

Fig. 2.9 Area East: Possible characterization of Block matrix by linear drift of T(TE); spread diagram *(top)*, distribution of residuals *(bottom)*

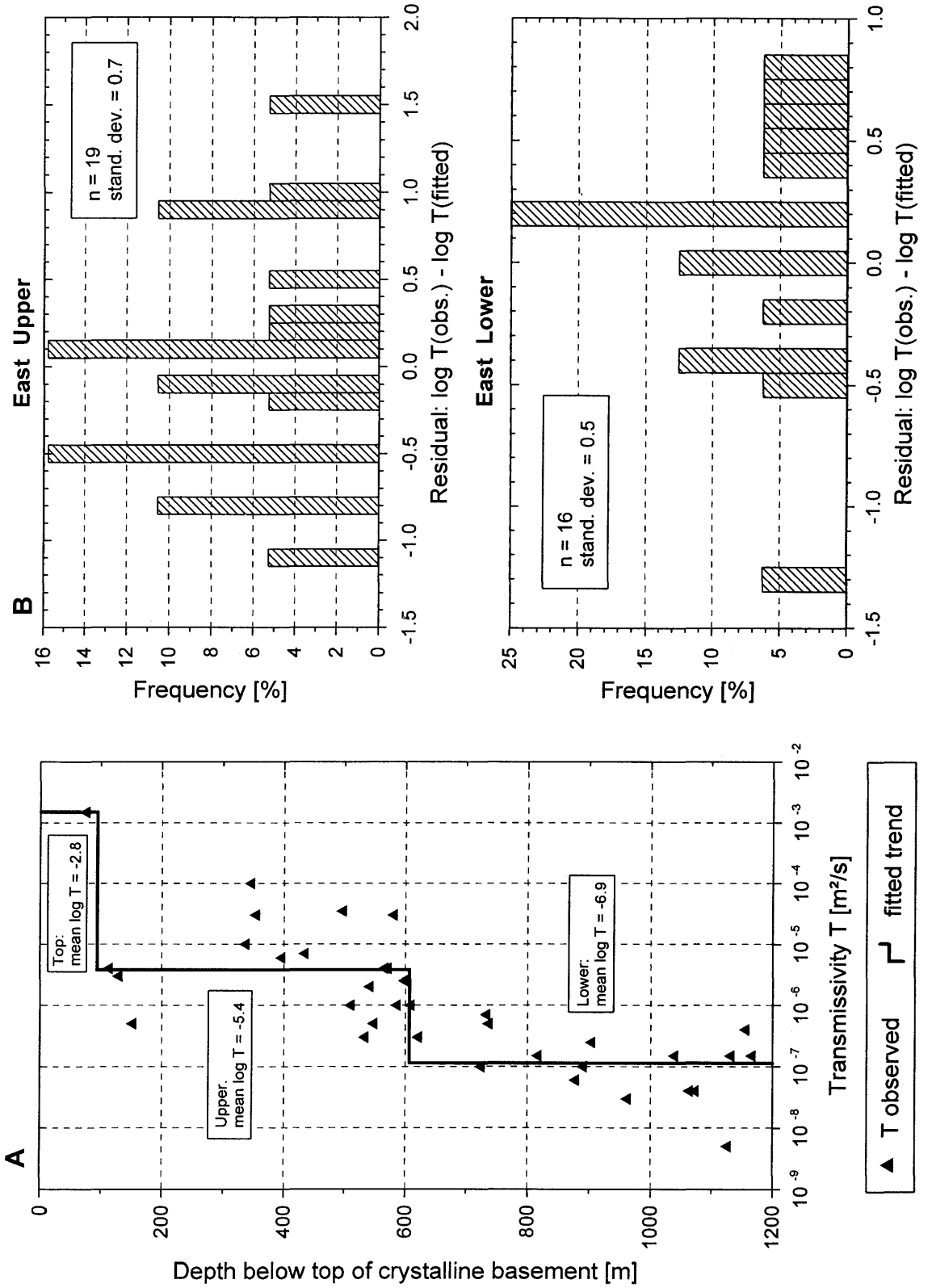

Fig. 2.10 Area East, Hypothesis 1: Proposed characterization of Block matrix by step-wise drift (A); distribution of residuals (B)

The proposed characterization for area East defines the following homogeneous hydraulic domains:

a) a contact-near **Top unit** to accommodate highly transmissive conditions that were observed in two packer-test intervals CR1 & CR2 (KLEMENZ & GUYONNET 1992) in the uppermost part of crystalline rock (depth interval 348.6 - 442.4 m below ground level)

b) an **Upper unit**, characterized by a relatively high permeability, extending from 94 m to 606 m below top of crystalline rock (442.4 - 955 m b.g.l.); and

c) an **Lower unit**, characterized by a somewhat lower permeability relative to the overlying unit, extending from 606 m to 1,173.4 m below the top of crystalline rock (955 - 1,522 m b.g.l.).

In geometrical terms, the division into an upper and a lower unit is similar to the area West. However, the hydraulic characterization of these conceptual domains shows significant discrepancies between the two areas, as will be shown below. The principal conceptual differences between the two sub-regions are as follows:

- The Major water-conducting faults are not a relevant element of the conceptual framework East (see section 2.3.3).

- The Low-permeability domain - such as defined in area West in its quality as a potential host rock - does not exist in the East according to SIB evidence.

The two upper units in Fig. 2.10A constitute about 50% of the total thickness of crystalline rock penetrated in SIB, but the water-conducting features in this section contribute 99.8 % of the overall transmissivity. In turn, the lower unit constitutes the lower half of the crystalline-rock interval, but its contribution to the bulk transmissivity of the crystalline column is negligible (KLEMENZ & GUYONNET 1992). This relationship emphasizes the dominant role of the two upper units for the bulk groundwater flux through the crystalline rocks at SIB, in contrast to the lower unit which has little hydraulic significance.

Hence, the step-wise approximation of the depth-dependent variability of T, as proposed in Fig. 2.10A, adequately describes the hydraulic zoning as observed in the borehole tests. This fit also provides a better statistical description of the

flow distribution within the crystalline column than the alternative method by linear regression, shown in Fig. 2.9.

Again, the goodness-of-fit is expressed by the distribution of residuals shown in Fig. 2.10B for the upper and lower unit. In comparison with the linear-drift residuals (Fig. 2.9), a significant reduction of spread was achieved for the lower unit. The value of $\sigma = 0.5$ suggests that most of observed transmissivities are within a factor 10 from the proposed geometric mean of T.

Hypothesis 2

In the following, the second hypothesis is applied for integration of SIB into the conceptual model. The underlying assumption here is that the SIB borehole is affected by the presence or proximity of a major tectonic feature (Section 2.3.3, Fig. 3.1) and, in fact, represents MWCF-like conditions.

The consequences for the conceptual characterization of crystalline rocks are twofold:

1) The highly transmissive conditions as observed at SIB can occur as MWCF anywhere in area "West and East". An example for similar conditions is the uppermost crystalline interval at Zurzach.

2) Undisturbed volumes of crystalline rocks (Block matrix) of similar quality to those in area West do also exist in the area surrounding the SIB site; i.e., the LPD is present throughout the region.

The integration of SIB observations into a single conceptual model "West & East" is presented in Fig. 2.11. A comparison with Fig. 2.5 and 2.6 (West only) shows that the transmissivities of TE's at SIB match reasonably well the characterization of MWCF as derived from KAI-deep and LEU-deep. The respective mean log-T value shifts merely from -6.3 (West, Fig. 2.6) to -6.1 (West+East, Fig 2.11), the error range (log standard deviation, not shown) increases slightly from 0.9 to 1.0. Moreover, as will be shown below, the intensity of inflows in SIB is also comparable to that within MWCF-West.

It is concluded that the second conceptual hypothesis about SIB has little impact on the parametric characterization of conceptual units that was derived under

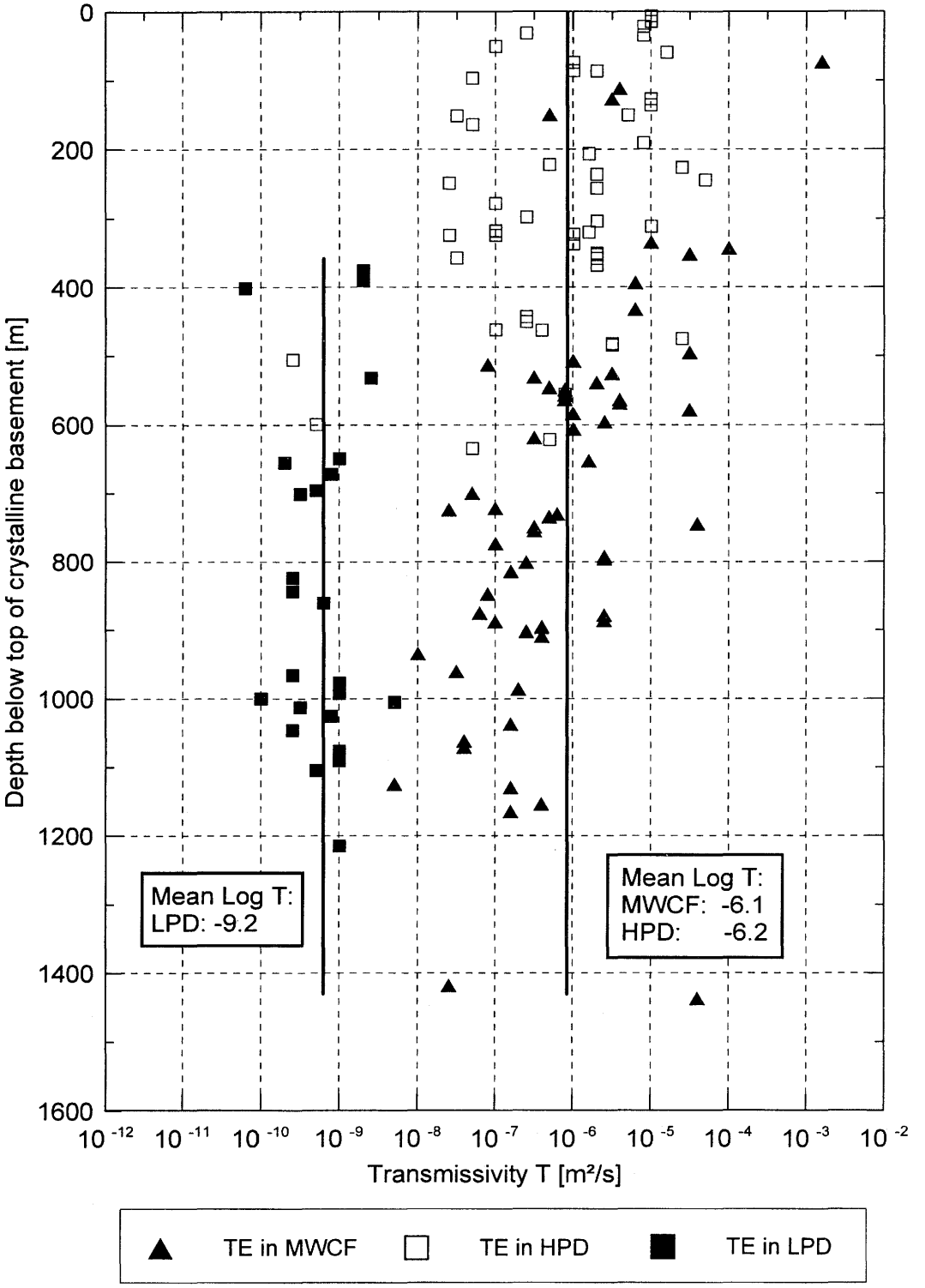

Fig. 2.11 Hypothesis 2: Hydraulic characterization of conceptual units "West & East"

Hypothesis 1. The most important implication of the 2nd hypothesis is the inferred presence of LPD-like conditions in the eastern area, which is favourable from the perspective of safety assessment and availability of potential host rock.

2.3.4.3 Comparison of Block-matrix properties West-East

A comparison of TE properties of Block matrix "East" (Fig. 2.10A) with those of Block matrix "West" in Fig. 2.6B reveals that the TE transmissivities in SIB are consistently by at least one order of magnitude larger than those observed in area West. In particular, the deeper, generally low-permeable portions of crystalline rocks, identified as the potential host rock in the West (LPD), show a large contrast in hydraulic properties between West and East. In the East, TE's in the Lower unit are not only more permeable by a factor of about 200 on the average, but they also occur at a higher frequency (factor of 2-3, see Table 2.2). The combination of these two parameters results in a substantial increase of the effective hydraulic conductivity of the Lower crystalline unit in area East, as will be shown in Section 2.5

Assuming that the conceptual Hypothesis 1 is valid, an evaluation was made to determine whether the SIB data could be fitted into one single dataset that is representative of the Block-matrix properties in the entire region of interest (i.e. East and West). For this purpose, the transmissivity data representing the Lower domain in SIB were combined with those representing the LPD in area West in Fig. 2.12. Both diagrams, a scatter plot of T vs. depth (top) and a histogram (bottom), show clearly that the data sets "East" and "West" form two separate clusters. When considering also the significant contrast in frequency of TE's described in the following Section 2.4 (Table 2.2), it is evident that the SIB data cannot be averaged with those from area West to form a single parameter set that characterizes the hydraulic property of the "undisturbed" Block matrix in the crystalline basement of Northern Switzerland.

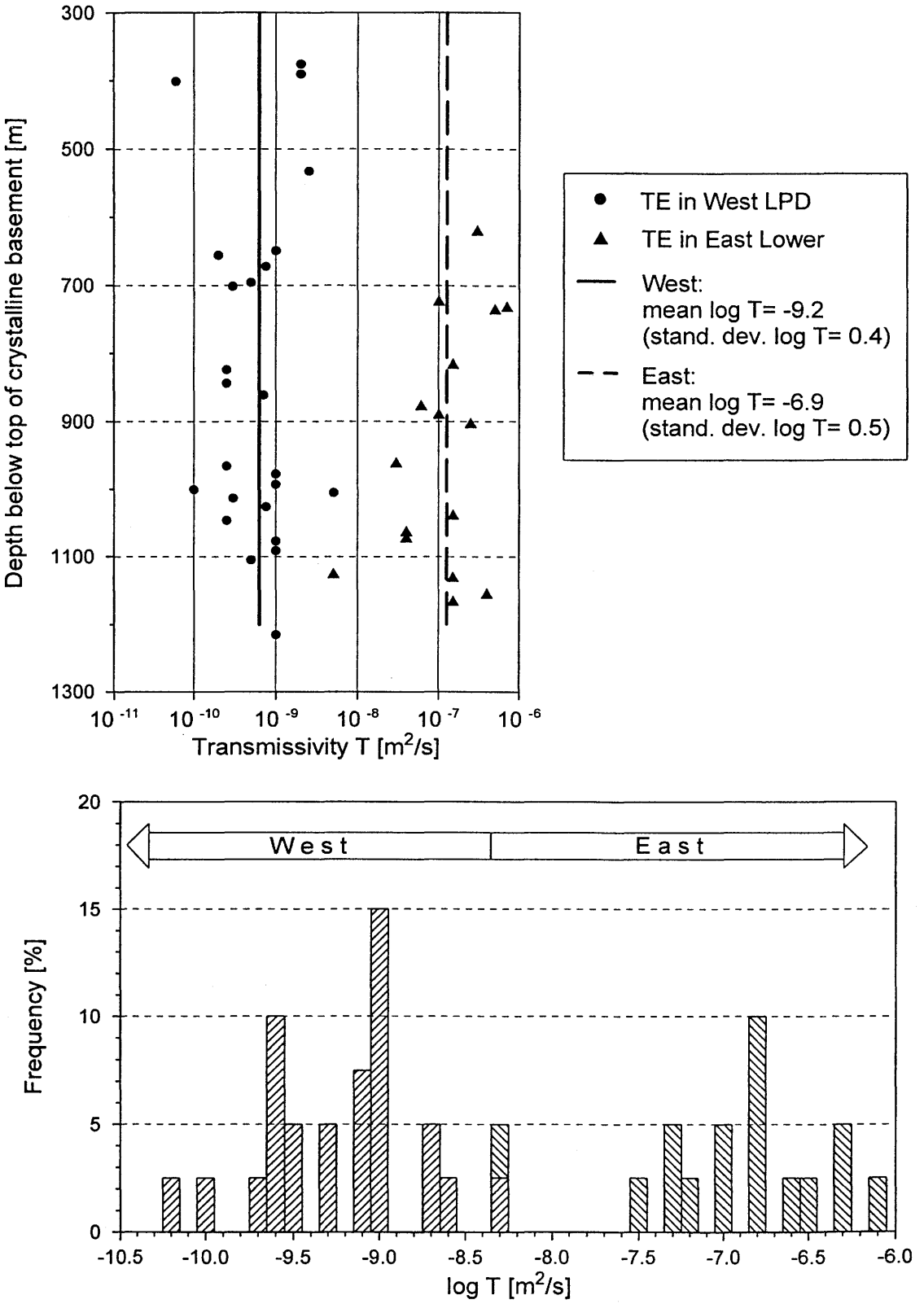

Fig. 2.12 Comparison of observed TE transmissivities in the Lower domains of area West and area East. Spread diagram *(top)*, histogram *(bottom)*

2.3.4.4 Rock matrix (BOE, KAI, LEU, SIB)

The hydraulic conductivity of the undisturbed crystalline rock matrix was obtained from packer intervals without discrete inflow points. The depth-dependent behaviour of the matrix conductivity shows in all boreholes where it was explicitly tested[2)] a consistent linear decrease (drift) by approximately one order of magnitude per 1,000 m of depth. The fitted regression line is shown in Fig. 2.13 (top). Due to the gentle slope of the regression line, the drift can be neglected and replaced by a depth-independent characterization of the matrix conductivity. Fig. 2.13 (bottom) shows a log-normal distribution that was fitted to the observed values. The spread of $\sigma = 0.86$ around the mean value in this distribution is only slightly greater than the residuals of the linear-drift fitting method shown in the above graph ($\sigma = 0.80$). The results of the statistical analysis might be affected in this case by the fact that the lower detection limit of K (that can be measured in the hydraulic tests) is relatively close to the average conductivity value of the matrix; this implies that the resulting database is biased toward high values.

[2)] Note that in SIB the testing program focused on the characterization of the transmissive elements rather than of the rock matrix

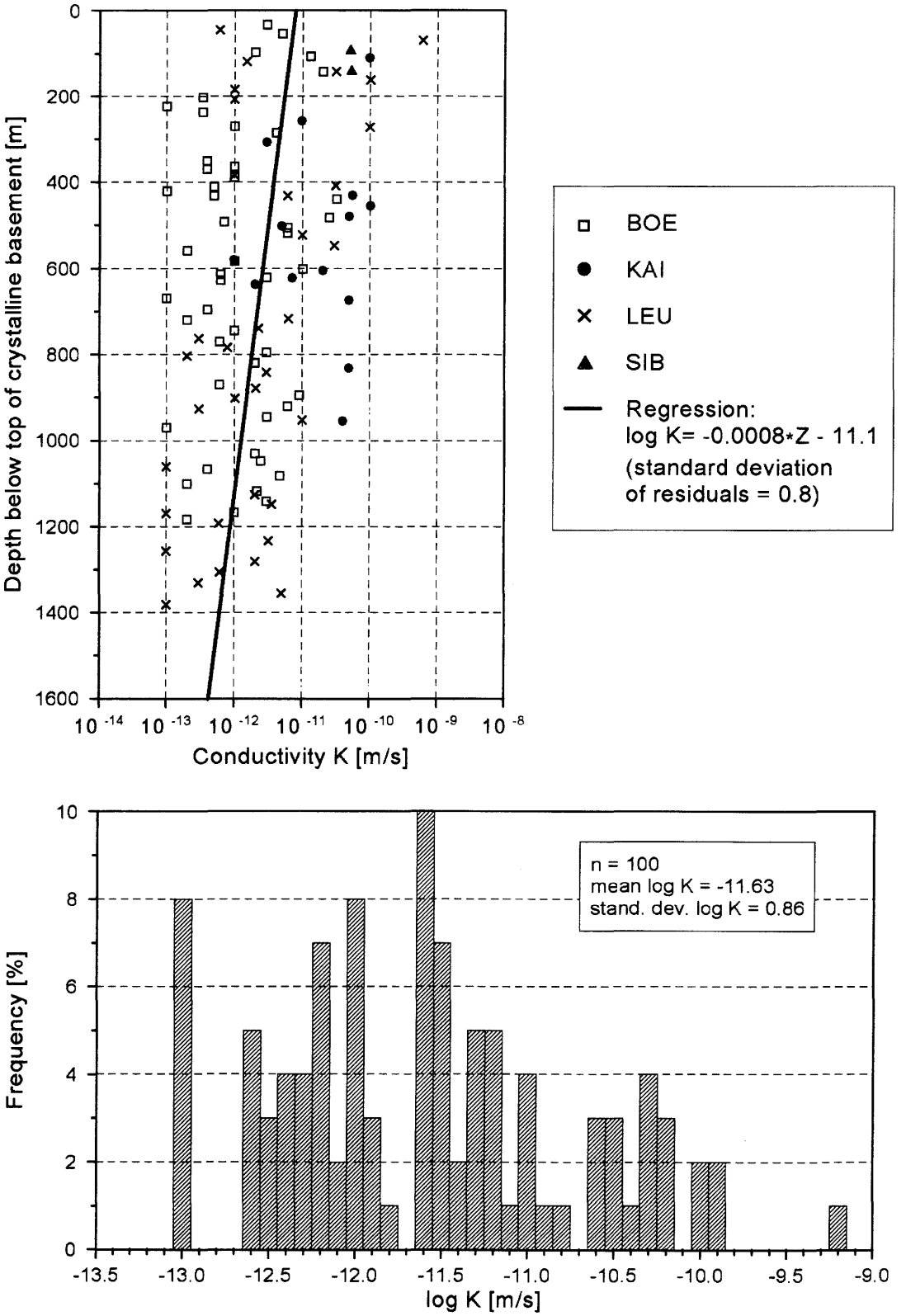

Fig. 2.13 Observed K values of matrix intervals (West and East): Characterization by linear drift *(top)*, and by log-normal distribution *(bottom)*

2.4 Characterization of fracture flow

After deriving the hydrogeological conceptual model of the crystalline basement of Northern Switzerland, it is of interest to describe groundwater flow through the fractures in a low-permeable crystalline rock that is considered as a potential host formation. Also at this scale, simplifying conceptual considerations are required to integrate the few available experimental data and associated uncertainties into a coherent characterization of the fracture flow processes. The following sections document the statistical and conceptual assessments that were performed in the context of the borehole data synthesis of KRI-1 study.

2.4.1 Statistics of planar features intercepted by boreholes

In low-permeable fractured rock the water movement and storage is controlled by discrete fractures that constitute complex geometrical networks. The key parameters describing the fracture flow are the fracture intensity ("abundance"), length and hydraulic aperture/transmissivity.

The frequency of planar features intersected by vertical boreholes depends on their spatial intensity, their size and their orientation. In the context of numerical fracture modeling, the fracture intensity is also expressed as the density of centre nodes of fractures with given dimension within a test volume (GRINDROD et al. 1991).

An alternative measure for quantifying the density of planar structures is the so-called "areal fracture intensity", or P_{32}-measure, defined by DERSHOWITZ (1984). The application of this parameter within the context of Nagra's borehole data synthesis was discussed by RESELE & JAQUET 1992. Compared to other measures, such as the centre-node density, the P_{32}-measure is more directly linked to observable geometrical properties, such as the mean fracture frequency along boreholes. In fact, P_{32} is the preferred fracture-density measure, since it is scale independent and invariant with respect to the distribution of fracture size, as shown by DERSHOWITZ (1984)[3].

---

[3] The mathematics related to the P_{32}-measure are extensively discussed in RESELE & JAQUET (1992).

The principal definitions and relations are:

θ	dip of the structure ($\theta = 90°$: vertical)
N	Frequency: Number of structures intersected by a vertical borehole per unit length of borehole section [m^{-1}]
$N(\theta)d\theta$	Frequency: Number of structures with dip [θ , $\theta+d\theta$] intersected by a vertical borehole per unit length of interval, [m^{-1}]
P_{32}	Total areal fracture intensity: Total area[4)] of structures whose centroid (centre of gravity) is inside a test volume of rock, divided by that actual volume, [m^{-1}]
$P_{32}(\theta)d\theta$	Total area of structures with dip [θ , $\theta+d\theta$], whose centroid is inside a test volume of rock, divided by that actual volume, [m^{-1}]

The basic relations read as follows

$$N(\theta) = P_{32}(\theta) \cdot \cos\theta \tag{1}$$

$$P_{32} = \int_0^{\pi/2} P_{32}(\theta)d\theta = \int_0^{\pi/2} \frac{N(\theta)}{\cos\theta} d\theta \tag{2}$$

$$N = \int_0^{\pi/2} N(\theta)d\theta = \int_0^{\pi/2} P_{32}(\theta)\cos\theta\, d\theta \tag{3}$$

These relations show that, given the observed mean frequency of planar features along a vertical borehole, the value of P_{32} can be determined if the distribution of the dip angle (range) of the structures is known or can be inferred from indirect information. No information on size, shape or strike direction is

---

4) The features are assumed to be planar, i.e., the thickness is negligible when compared to other dimensions. Therefore, the "area of a structure" is defined as its surface area, e.g., a square feature of 10 m side length has an area of 100 m^2.

required.

The performed analysis is based on the following definition for $P_{32}(\theta)$, according to RESELE & JAQUET (1992):

"A dip distribution of a set of planar structures of arbitrary size is considered to be uniform within the dip interval [a,b] - a and b being dip angles - if their $P_{32}(\theta)$-measure is equal to the $P_{32}(\theta)$-measure of a set of planar structures with the following properties:

- *equal size of all structures of the set*
- *dip of all structures within the interval [a,b]*
- *uniform density of the stereographically projected poles of structures on the half sphere within the [a,b] interval*

According to this definition, the equations (1) to (3) above read for uniform dip distributions within the dip interval [a,b] as follows:

$$P_{32}(\theta) = \begin{cases} p_{[a,b]} \cdot \sin\theta & a \le \theta \le b \\ 0 & \text{else} \end{cases} \tag{4}$$

$$P_{32} = p_{[a,b]} \cdot (\cos a - \cos b) \tag{5}$$

$$\begin{aligned} N &= p_{[a,b]} \cdot \frac{1}{2} \cdot (\cos^2 a - \cos^2 b) \\ &= P_{32} \cdot \frac{1}{2} \cdot (\cos a + \cos b) \end{aligned} \tag{6}$$

where $p_{[a,b]}$ is a constant that can be determined from the total fracture frequency N by using eq. (6). The relationship between P_{32} and the frequency N for various assumptions regarding the limiting dip angles a and b are shown in Table 2.1.

The occurrence of identified transmissive elements in the crystalline rocks of Northern Switzerland was analyzed statistically for each hydraulic domain in the area West and East. The analysis is based on:

- The observed TE frequency in the boreholes Böttstein, Kaisten, Leuggern and Siblingen, calculated from the compiled data in Appendix 1; and

- The assumption that the dip angles of the TE's are uniformly distributed within the interval [45°,90°] in area West and within the interval [60°,90°] in area East.

Table 2.1 Relationship between P_{32} and N for different dip distributions

Dip distribution	**Equation relating P_{32} and frequency N**
Uniform within [0°,90°]	$P_{32} = 2 \cdot N$
Uniform within [45°,90°]	$P_{32} = 2\sqrt{2} \cdot N = 2.8 \cdot N$
Uniform within [45°,70°]	$P_{32} = 1.9 \cdot N$
Uniform within [45°,80°]	$P_{32} = 2.3 \cdot N$
Uniform within [30°,90°]	$P_{32} = 2.3 \cdot N$
Uniform within [60°,90°]	$P_{32} = 4 \cdot N$
Clustered around 45°	$P_{32} = \sqrt{2} \cdot N$
Clustered around 60°	$P_{32} = 2 \cdot N$

The results of statistical analysis are given in Table 2.2 in terms of the areal fracture intensity, P_{32}. It should be noted that the analysis is based on the mean frequency of water-conducting features (TE's) **observed** in the boreholes. Hence, the resulting P_{32} values reflect the intensity of the "visible" features that were carrying flow at the intersection with the borehole, rather than the total density of all fractures in a unit volume of rock. This notation corresponds to the **conductive-fracture intensity**, $\mathbf{P_{32C}}$, introduced by DERSHOWITZ (1984) and derived from the frequency of conductive fractures in the boreholes. The potential consequences of flow channeling; i.e., of the fact that the flow might be restricted only to a small portion of the fracture area, which has only a small probability of being intersected by a borehole, is discussed in Section 2.4.2.

The **confidence level** of the calculated P_{32} values depends on 1) the statistical reliability of the basic data set, 2) the variability of fracture density in space, and 3) the degree to which the assumption on the dip-angle distribution is correct and has an impact on the result.

The relations between the fracture frequency N and P_{32}, shown in Table 2.1 above, suggest that the source of uncertainty attached to the use of indirect information on the dip distribution can be quantified as a factor of $\sqrt{2}$ or 40%.

Table 2.2 Statistical analysis of all TE's identified in the boreholes in area West and East. The P_{32C} values assume uniform distribution of dip angles within the interval of: West = [45°,90°], East = [60°,90°]

Borehole section	Hydraulic domain	Depth interval [m]	Length of interval [m]	No. of identified TE's	mean spacing of TE's along borehole [m]	frequency N [m^{-1}]	P_{32} [m^{-1}]
I. AREA WEST							dip [45°,90°]
Kaisten deep	MWCF	790.0 - 1305.8	515.8	22	23.5	0.043	0.121
Leuggern deep	MWCF	1640.0 - 1688.9	48.9	2	24.5	0.041	0.116
Böttstein high	HPD	315.3 - 801.3	486	14	34.7	0.029	0.081
Kaisten high	HPD	296.5 - 665.5	369	18	20.5	0.049	0.138
Leuggern high	HPD	222.8 - 881.4	658.6	20	32.9	0.03	0.086
Boettstein deep	LPD	801.3 - 1501.3	700	7	100	0.01	0.028
Kaisten interm.	LPD	665.5 - 790.0	124.5	3	41.5	0.024	0.068
Leuggern interm.	LPD	881.4 - 1640.0	758.6	14	54.2	0.018	0.052
Total area West	All MWCF		564.7	24	23.5	0.043	0.12
	All HPD		1513.6	52	29.1	0.034	0.097
	All LPD		1583.1	24	66	0.015	0.043
II. AREA EAST (without SIB top)							dip [60°,90°]
Siblingen high	Upper	442.4 - 955.0	512.6	19	27	0.037	0.148
Siblingen deep	Lower	955.0 - 1522.0	567	16	35.4	0.028	0.112
III. WEST & EAST (SIB = MWCF, HPD and LPD same as West)							dip [45°,90°]
All region	All MWCF		1738.1	60	29	0.035	0.098

The **spatial variability** of P_{32} was estimated from a comparison of the results for the three boreholes in the area West. For the Upper domain, HPD, the calculated P_{32} values range between 0.081 m^{-1} and 0.138 m^{-1}, i.e., within -20% to +40% with respect to the average value of 0.097 m^{-1} (Table 2.2). For the Lower domain, LPD, the corresponding range is between -35% and +60%. Given the fact that the maximum deviation of +60% was derived for the borehole section "Kaisten interm." from a poor statistical database (n=3, see Table 2.2), the spatial variability on the km scale is estimated to be smaller than 30% to 40%.

Compared to these degrees of uncertainty, the purely statistical standard deviation of P_{32} as calculated from the borehole observations is of similar magnitude. For a uniform distribution within the dip interval [a,b], the variance of P_{32} can be calculated as

$$\frac{\mathrm{Var}(P_{32})}{P_{32}^{\,2}} = \frac{1}{n}\,\frac{\ln(\cos a \,/\, \cos b)}{\cos a - \cos b}\,\frac{\cos a + \cos b}{2} \qquad (7)$$

with n = number of features intersected within the borehole interval

which reduces to the ratio $\mathrm{Var}(P_{32})/P_{32}^{\,2} = 1/n$ for $a \approx b$.

According to eq. (7), the purely statistical standard deviation is logarithmically divergent for $b \to 90°$. Because this divergence is weak and real features are never exactly planar and vertical, it is sufficient for practical purposes to assign b a value slightly below 90°, say 88°, to get:

for the interval [45°,~90°]
for the interval [60°,~90°] } Std. dev. $(P_{32})/P_{32} \leq 1.3/\sqrt{n}$

which corresponds to a variation coefficient of 0.4 if 10 TE's are identified and to a coefficient of variation of 0.3 if the number of transmissive elements is 20.

Based on the analysis, it is concluded that the **conductive-fracture intensity, P_{32c}** (related to TE's observed in the hydraulic tests) can be determined within a confidence interval of ± 50% around the mean value as follows:

Area	Conceptual domain	P_{32C} of TE's
West	Major faults = MWCF	0.12 m^{-1}
	Upper = HPD	0.10 m^{-1}
	Lower = LPD	0.04 m^{-1}
East (Hyp. 1)	Upper domain	0.15 m^{-1}
	Lower domain	0.11 m^{-1}
W + E (Hyp. 2)	MWCF (KAI,LEU,SIB)	0.10
	HPD, LPD	as above

It bears noting that the intensity of TE's in the LPD of area West is significantly smaller than that of all other domains. This property contributes - together with the low transmissivities observed - to the favourable characterization of this domain in its quality as a prospective host formation for a deep repository. In contrast, area East (SIB) is characterized by a large TE intensity throughout, which is comparable to that of MWCF in area West.

2.4.2 Effects of fracture-plane heterogeneity (or "channeling")

2.4.2.1 Conceptual considerations

A fundamental premise of flow analysis through fractured rocks is that only a fraction of the fractures present in the rock are water conducting. This phenomenon, termed channeling (BOURKE 1987; TSANG & TSANG 1987), refers to the fact that water flow in discrete planar elements like fractures is not evenly distributed over the entire fracture area but rather is restricted to individual flow paths or channels, due to local variations in aperture and infilling. Consequently, a hydraulic test in a well that intersects only a small area of the fracture surface may sample a high- or a low-conductive part of the same feature. The probability of sampling the highly transmissive portion of the fracture area is small if the flow is strongly channeled, i.e., if only a small fraction of the fracture area carries water.

In general, when a hydraulic gradient is imposed upon a fracture, the flow follows pathways of minimum resistance, avoiding low-conductive portions. Generic simulation studies based on statistical variations of fracture aperture (transmissivity) show that the principal flow usually occurs through only a few prominent channels in the fracture plane (MORENO et al. 1988; TSANG & TSANG 1987, etc.). Several field experiments at the Stripa site suggest that channels are distributed in clusters and that there are consistently only a few channels which carry most of the water flow (ABELIN et al. 1987; 1994). The field observations are supported by numerical solute-transport simulations with stochastic channel-flow models. These indicate that the majority of particles takes fast flow paths, characterized by a fast and early rise in the breakthrough curves (MORENO et al. 1988). A further indirect evidence for the presence of fast channels within a fracture zone in crystalline rocks is the observed tritium in the Stripa mine at a depth of 300 m below surface. This observation implies that the groundwater has moved more than 300 m from the surface in 30 years, hence travelling rapidly along preferred channels within the fracture zone.

The water-conducting features - or transmissive elements, TE's - are *per definition* discrete elements that carry most of the water flux through the crystalline block matrix. Hence, the statistical analysis of TE's in this study (previous section) includes the **observed conductive fractures** only and the derived P_{32} measure corresponds to the conductive fracture intensity, P_{32C}, rather than to the total areal intensity of all fractures. It is likely, however, that the boreholes intersected many other structural elements that were non-conductive at the point of intersection, but which carry flow at larger scales. On the other hand, fractures may also be conductive locally but do not contribute to flow at larger scales. Such a condition was evidenced in the borehole interval BOE deep (see Table 2.2 and Appendix 1, inflows No. 15-21), where a highly saline and obviously stagnate groundwater was sampled, suggesting that the intersected TE's are not participating in the large-scale flow.

As a net effect, it is probable that the reported P_{32C} values underestimate the true frequency of conductive fractures. This bias, however, is compensated by the circumstance that the areal intensity of **conductive** fractures is derived by considering the total fracture area, which implies that the entire square area (e.g., 100·100 m in the conceptual model) is open for flow.

Several conceptual models of the channeling phenomenon are plausible, as is schematically illustrated in Fig. 2.14 and described below.

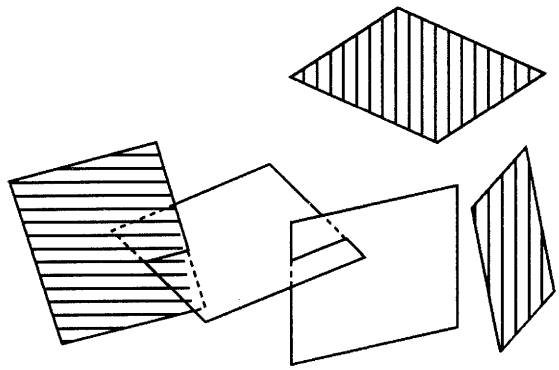

a) Concept Nr. 1

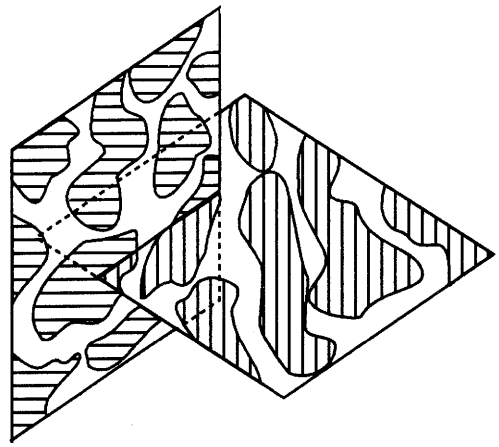

b) Concept Nr. 2

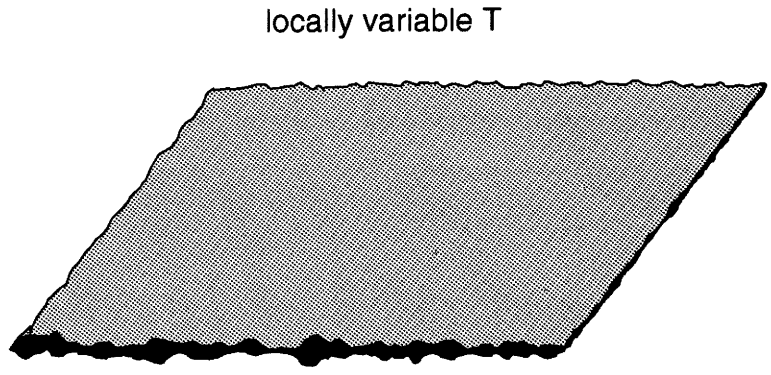

c) Concept Nr. 3

Fig. 2.14 Schematic conceptual model of channeling

The first channeling model discriminates between elements that are entirely non-conductive (i.e., with no hydraulic contrast to the background rock) and elements that are at least locally conductive. This conceptualization is not considered further because such non-conductive planar features are not TE's per definition and have no hydraulic significance, even if they have the same phenomenological origin as the transmissive elements.

The second conceptual model separates the fracture-surface area (on a decimeter- to decameter-scale) into conductive "channels" and low-permeable "islands" surrounded by the channels. The conductivity of the islands is similar to that of the background rock and substantially lower than that of the channels. In this channeling model, the local fracture transmissivity can be described by a bi-modal probability distribution, with a higher mode for the channels and a substantially lower mode for the islands.

In the third channeling concept, the local T of TE's (averaged on the cm-to-dm scale) is assumed to be more-or-less continuous with a uni-modal (e.g., a log-normal) probability distribution and a spatial correlation. The impact of the different concepts on the analysis of effective properties is discussed below. The underlying assumption is that the channels indeed are pathways of preferential flow; this is only possible if they form an interconnected network. The following discussion assumes that each sampled channel is connected to the network and thereby contributes to fracture flow.

2.4.2.2 Consequences of concept No. 2: channels and islands

Depending on the typical geometrical size of the islands and the width of the channels, two effects may have an influence on the observations and hydraulic test results in boreholes:

- If the islands have a substantially larger surface area than the borehole diameter, the number of identified TE's (those in which the borehole intersects a conductive channel) is smaller than the number of physically intersected (but undetected) TE's. The percentage of TE's not sampled is roughly equal to the areal fraction of islands with respect to the total surface area of the fracture. The ratio of the number of geometrically intersected TE's and the number of hydraulically identified (observed) TE's (i.e., intersected in a channel) is called the "channeling factor", C. The

higher the channeling factor, the larger is the total intensity of intersected TE's for a given frequency of observed (= locally conductive) TE's along a borehole.

- The test results are influenced either by individual channels or areal averages, depending on the exact location of the borehole intersection with the channel system, on the length of individual channel segments between two intersection points, on the hydraulic properties of the channels and on the duration of the hydraulic test.

If the spatial range of the test is smaller than the distance to the next intersection point of two channels, the resulting transmissivity T is that of a single channel; further, if the range is larger than the width of the channel, the test result would show a 1-d characteristic (i.e., linear flow).

If the range is much larger than the typical distance between channel intersection points, the results would show a 2-d or higher-dimensional flow characteristics and the resulting T-value corresponds to an areal average of the fracture surface, including channels and islands.

In any case, according to concept No. 2, the results of hydraulic tests categorized as "inflow-point tests" in the analysis (water-conducting features in Appendix 1) reflect the properties of individual channels or of averages of the channel/island system, but they never describe the property of the "no-flow" islands. Because the geodynamic processes that control the development of channels and islands (i.e., erosion, dissolution and precipitation) are only active under an imposed external hydraulic gradient, it is concluded that the probability of two individual channels being interconnected at the intersection of two fracture planes is somewhat larger than the purely statistical probability. It is evident from the genetic point of view, that a fracture opening can only develop to an active water conduit (channel) if it was at some time connected to other channels upstream and downstream, and thereby had formed a part of the flow network.

2.4.2.3 Consequences of concept No. 3: Uni-modal permeability distribution

If the TE's have an uni-modal transmissivity distribution, the latter can be assumed to be spatially correlated so that the higher transmissive areas have a tendency to be linked and thus to form channels (TSANG & TSANG 1987).

If the range of hydraulic tests in boreholes is smaller than the spatial correlation length of the local T-value, the tests yield a distribution of measured T-values that reflects the spatial distribution of the local TE transmissivity. Tests with a range larger than the correlation length provide a spatial average of T.

According to concept No. 3, the test results provide a continuous distribution of the transmissivity, ranging from very low (i.e., with virtually no contrast to the rock matrix) to high values. The identification of individual TE's requires the definition of a lower bound for T of TE's as a cut-off to separate a continuous T distribution into a group labelled as "inflow-point tests" (App. 1) and a group labelled as "rock-matrix tests" (compiled in App. 2). The latter also includes TE's intersected at a location of low local transmissivity.

If the cut-off subdivides the T distribution at the low-end tail, only a small fraction of geometrically intersected TE's is not sampled, and the corresponding test is classified as "rock matrix test". The observed intensity of TE's would be a good approximation of the "reality" with only a little distortion.

If, however, the cut-off value truncates the distribution near its mode value or even toward the high-end tail, the resulting apparent T distribution of identified TE's would be strongly skewed with the mode at the low-end side. This is obviously not the case for the analyzed TE's according to the process described in Section 2.2 and the results of residuals analysis shown in Figs. 2.7 and 2.10. The latter indicate a symmetrical, non skewed spread of observed T values around the mean; i.e., no truncation effects at either end of T distribution are evident.

2.4.2.4 Assumptions for the proposed conceptual model of fracture flow

The available borehole data and additional information do not permit designation of a currently preferred concept for crystalline rocks, although concept No. 2 appears to be more plausible in view of the observations (i.e., the resulting T distribution is not skewed with the mode at the low-end side). Moreover, this concept represents a conservative approach if the measured T's are interpreted as average values for channel/island-systems. This assumption yields a higher density of TE's and higher average transmissivities than the alternatives.

Predicting the degree or magnitude of channeled flow is difficult. The flow pat-

terns and mechanisms are not well known and there are no well developed investigation techniques. Very few investigations have been made regarding the flow and transport patterns in deep crystalline rocks. Hence, only very few direct observations are available on the channeling phenomenon; i.e., on the geometrical extent of the islands and on the proportion of channels. Useful semi-quantitative information was provided by channeling experiments involving drilling of boreholes along a fracture plane (BOURKE 1987, ABELIN et al. 1994) and by the Stripa 3D experiment (ABELIN et al. 1987, summary in NERETNIEKS et al. 1990). By drilling 5 boreholes along a fracture surface, BOURKE identified channels with lengths at meter scale and widths of a few decimeters. The total channel area was about 20% of the fracture surface. In the Stripa 2D experiment (ABELIN et al. 1985), natural water flow was monitored in three fractures intersecting tunnel walls; most of the flow occurred in about 20% of the total trace length. Channeling at a scale larger than a single fracture was evidenced by the Stripa 3D experiment, which investigated water flow and tracer migration through a low-permeable fractured granite in a 100-m long drift. An area of 750 m^2 in the ceiling of the drift was monitored by plastic sheets for more than two years. At this scale, a strong concentration of flow in a few areas was observed: 50% of the total inflow occurred in about 3% of the monitored area, and 90% of inflow was restricted to 10% of the area. In the remaining portion of the monitored surface, large dry areas extending over many tens of meters were observed. The irregular distribution of water flow and the presence of tritium in two of six samples observed in the drift best illustrates the channeling effects in low-permeable crystalline rocks at 100-m scale.

The mentioned field observations indicate that the phenomenon of channeling occurs on very different scales. It was deduced from this fact that the relevant spatial correlation length, which is responsible for the channeled flow in each case, is on the same order of magnitude as the scale of observation (MORENO et al. 1988).

Despite the extensive experimental research in the field of tracer transport in fractures with variable properties (see ABELIN et al. 1994 for recent summary and discussion), it is not possible to provide an unequivocal answer to the key question how much of a fracture area is open to flow. Similarly, the overall impact of channeled flow on the properties of the real fracture network is ambiguous. On one hand, the borehole information on the frequency of flowing features does probably underestimate the true density of conductive fractures (see above), on the other hand, the variable aperture across a fracture has a

reducing effect on the overall network connectivity and the total flow rate through the fracture. It was shown independently in Stripa channeling experiments (ABELIN et al. 1994) and in stochastic fracture-flow simulations (TSANG et al. 1988) that the flow rate or pressure drops respectively are determined by the smaller apertures (pinch points) along the flow path.

In view of the inherent ambiguity in interpreting the impact of channeling on fracture flow, and given the definition of the areal density of conductive fractures, P_{32C} which includes the total cross-sectional fracture area, the following conclusions were adopted for the conceptual model in the present study:

- It is recognized that flow in a single TE may be restricted to only a fraction - say about 20% - of the total surface area. Nevertheless, the application of an arbitrarily defined "correction factor" (e.g. 5) for the effects of channeling is not deemed appropriate for the reasons stated above.

- The conceptual model thus assumes that the conductive-fracture intensity - as derived from borehole observations in Section 2.4.1 - is in fact similar to the effective fracture intensity which determines the flow through the fracture network.

With regard to further analyses and modeling studies in the scope of the hydrogeologic synthesis KRI-1, it is concluded that P_{32C} - or the total area of **conductive** fractures in a unit volume of rock - is the quantity of interest rather than the total areal intensity of <u>all</u> fractures, P_{32}(full). The full fracture intensity is related to the former through the linear correction factor C for the proportion of non-conductive fracture area (that is, area having transmissivity below a defined threshold): $P_{32}(full) = C \cdot P_{32C}$ Note that the transmissivity distribution for the P_{32}(full) also includes those low T values below the defined threshold. The ratio of the respective area of the T distribution below this threshold to that of T distribution above the threshold should be proportional to the correction factor C.

2.5 Analytical assessment of effective properties

2.5.1 General

The final task of the borehole-data synthesis deals with derivations of effective hydraulic properties of the previously defined hydrogeologic domains. The analytical approach is presented herein. Section 2.5.2 considers a single fracture whereas an analytical approach for a system of fractures is derived in Section 2.5.3. Numerical estimates of K(eff) are provided in Chapter 5 describing the fracture-network modeling of a typical block of low-permeable crystalline rock.

2.5.2 Equivalent permeability of a single fracture considering various geometries of the open porespace

A water-conducting feature - or transmissive element, TE - may be conceptualized, for the purposes of performance assessment of the geosphere, as being composed of flowpaths with simple geometries. A parallel plate or a tube-like flowpath represent two of the common conceptualizations of the flow geometry within a TE. This section considers the hydraulic implications of the various geometries; that is, what is the effective hydraulic conductivity (or, equivalently, transmissivity) of a TE composed of continuous "openings" of certain geometries.

Initially, three simplified geometries are considered: fractures with parallel plates, tubes with circular cross-sections and tubes with more general ellipsoidal cross-sections. The assumption of laminar viscous flow in such openings is made; the results follow then from the Navier-Stokes equations and their simplified Poiseuille form.

The expressions for the equivalent hydraulic conductivity of a single feature described by these geometries are as follows:

Parallel Plate (Cubic Law)

$$K = \frac{b^2}{12} \cdot \frac{\gamma}{\mu} \qquad (8)$$

Circular Cross-Section

$$K = \frac{r^2}{8} \cdot \frac{\gamma}{\mu} \qquad (9)$$

Elliptical Cross-Section

$$K = \frac{a^2 \cdot b^2}{4 \cdot (a^2 + b^2)} \cdot \frac{\gamma}{\mu} \qquad (10)$$

where,

a, b are the major and minor axes of the ellipse.

r is the radius of the circle.

b is the spacing in the parallel-plate model.

γ is the specific gravity.

μ is the kinematic viscosity.

Table 2.3 shows a range of values for each one of these systems (for water at 20 °C $\gamma/\mu = 9.8\ 10^6\ m^{-1}s^{-1}$).

Table 2.3 Equivalent hydraulic conductivity of a single feature for different geometric properties

Parallel Plate		Circular Cross-Section		Elliptical Cross-Section		
b (m)	K (m/s)	r (m)	K (m/s)	a (m)	b (m)	K (m/s)
1 E-6	8.2 E-7	1 E-6	1.2 E-6	1 E-7	1 E-5	2.45 E-8
1 E-5	8.2 E-5	1 E-5	1.2 E-4	1 E-6	1 E-5	2.42 E-6
1 E-4	8.2 E-3	1 E-4	1.2 E-2	1 E-6	1 E-4	2.45 E-6
1 E-3	8.2 E-1	1 E-3	1.2	1 E-5	1 E-4	2.42 E-4
1 E-2	82	1 E-2	122	1 E-5	1 E-3	2.45 E-4
--	--	--	--	1 E-4	1 E-3	2.42 E-2
--	--	--	--	1 E-4	1 E-2	2.45 E-2
--	--	--	--	1 E-3	1 E-2	2.42
--	--	--	--	1 E-2	1 E-1	242

Of interest is also the equivalent hydraulic conductivity of a block volume having a cross section of an unit area (for example 1 m^2) and encompassing a certain number of these features. The **effective hydraulic conductivity,** K_{eff}, of the unit cross-sectional area can be thought of as the arithmetic average of the hydraulic conductivities of the open features and the matrix.

The corresponding expression is:

$$K_{eff} = \frac{N \cdot A \cdot K + (1 - N \cdot A) \cdot K_m}{1} \qquad (11)$$

where

N is the number of features in the unit area,

K is the hydraulic conductivity of the various single features (Table 2.3),

K_m is the hydraulic conductivity of the matrix (background rock),

A is the area of a feature, that is

$b \cdot 1$ (m^2) - parallel plate flowpath (assuming a $1 \cdot 1$ m^2 cross-section)
$\pi \cdot r^2$ (m^2) - circular cross-section flowpath
$\pi \cdot a \cdot b$ (m^2) - elliptical cross-section flowpath.

The following three tables summarize the resulting K_{eff} for a system of 1, 10 or 100 features in a matrix of constant hydraulic conductivity of $K_m = 10^{-10}$ m/s.

Table 2.4 Effective hydraulic conductivity for parallel-plate flowpaths

b (m)	K_{eff} (m/s)		
	N = 1	N = 10	N = 100
1 E-6	1.0 E-10	1.1 E-10	1.8 E-10
1 E-5	9.1 E-10	8.2 E-09	8.1 E-08
1 E-4	8.1 E-07	8.1 E-06	8.1 E-05
1 E-3	8.1 E-04	8.1 E-03	8.1 E-02
1 E-2	8.1 E-01	--	--

Table 2.5 Effective hydraulic conductivity for circular flowpaths

r (m)	K_{eff} (m/s)		
	N = 1	N = 10	N = 100
1 E-6	1.0 E-10	1.0 E-10	1.0 E-10
1 E-5	1.0 E-10	1.0 E-10	1.04 E-10
1 E-4	4.8 E-10	4.0 E-09	3.8 E-08
1 E-3	3.8 E-06	3.8 E-05	3.8 E-04
1 E-2	3.8 E-02	3.8 E-01	3.8

Table 2.6 Effective hydraulic conductivity for elliptical flowpaths

a (m)	b (m)	K_{eff} (m/s)		
		N = 1	N = 10	N = 100
1 E-7	1 E-5	1.0 E-10	1.0 E-10	1.0 E-10
1 E-6	1 E-5	1.0 E-10	1.0 E-10	1.0 E-10
1 E-6	1 E-4	1.0 E-10	1.0 E-10	1.0 E-10
1 E-5	1 E-4	1.0 E-10	1.07 E-10	1.7 E-10
1 E-5	1 E-3	1.07 E-10	1.7 E-10	8.7 E-10
1 E-4	1 E-3	7.7 E-09	7.6 E-08	7.6 E-07
1 E-4	1 E-2	7.7 E-08	7.7 E-07	7.7 E-06
1 E-3	1 E-2	7.6 E-05	7.6 E-04	7.6 E-03
1 E-3	1 E-1	0.76	7.62	76.2

The numerical values shown in the tables above assume that the openings are of constant cross-section in the whole TE and that no interaction among the different flowpaths exist (so-called network effects). In this sense they represent upper bounds for the inferred properties. Various studies in the literature (e.g. GELHAR 1987) have examined the effective properties of fractures with continuously variable aperture, for example. The resulting properties would be indeed smaller than the ones inferred above. A detailed review of these results is beyond the scope of this study.

2.5.3 Equivalent permeability of systems of fractures: analytical methods

The tensor of equivalent conductivity of an interconnected system of fractures embedded in a low-permeable matrix can be calculated according to

$$K_{eff,ij} = G_{ij} \cdot \overline{T} \cdot P_{32C} \cdot C + K_{mat} \qquad (12)$$

$K_{eff,ij}$ ij-component of the diagonal effective K-tensor, [m/s]

G_{ij} geometric factor, [-]

$\bar{T}$ relevant average T value of fractures, [m^2/s]

P_{32C} **conductive**-fracture intensity according to definition in section 2.4.1, [m^{-1}]

C correction factor for channeling (see section 2.4.2), [-]

K_{mat} geometric mean of matrix conductivity, [m/s]

This equation yields an estimate for the theoretical maximum effective conductivity of an infinite-fracture system, designated herein K_{eff}(infinite). "Infinite" in this context means that the fractures are large compared to the considered test volume of rock. By implying a perfect interconnectedness, this approach neglects the possible network effects on the hydraulic bulk properties of a real fracture system. The equation further assumes that there is no correlation between fracture orientation and transmissivity and that fracture intersections have no particular hydraulic properties.

The first term on the right hand side of Equation (12) represents the contribution of the fracture system, such as derived by LANYON (1992a) and VOBORNY et al. (1993). As a difference, the above equation denotes the conductive fracture intensity, P_{32C}, whereas the former notations considered the full fracture intensity, P_{32}, i.e., the total area of all contributing fractures. Note that the full fracture intensity is $P_{32C} \cdot C$ according to Section 2.4.2. An additional conceptual difference is that the former definitions assume a so-called *purely fractured medium* where the contribution of matrix to advective flow is negligible. In contrast, the above equation does consider the contribution of a low-permeable matrix to total flow through the test volume. This contribution is additive as no interaction between the fractures and the matrix is assumed to occur. Note also, that a correct quantity that describes the contribution of volumetric matrix flow is the matrix conductance, $C_{mat} = K \cdot A_{mat}$, which includes the cross-sectional area of flow, A_{mat}. In equation (12), the conductance, C_{mat} [m^3/s], is implicitly normalized to an unit area (i.e., $A_{mat} = 1\ m^2$), in analogy to the first term that represents the fracture-system contribution per unit volume (according to definition of P_{32} in Section 2.4.1).

Equation (12) was applied to calculate the tensors of equivalent conductivity for each defined conceptual domain. The impact of the possible relevant types of average T values, defined below, on the resulting effective property is illustrated in Table 2.7 that summarizes the directional tensors of effective conductivity. The input data for the calculations in Table 2.7 were obtained as follows:

G_{ij} according to LANYON (1992) or VOBORNY et al. (1993):
area West: G_{xy} = 7/12, G_z = 5/6 for dip interval 45-90°
area East: G_{xy} = 13/24, G_z = 11/12 for dip interval 60-90°
isotropic dip distribution: G_{iso} = 2/3

P_{32C} from Table 2.2 in Section 2.4.1

$\bar{T}$ means from fitted log-normal distributions (Sections 2.3.4.1 and 2.3.4.2) according to definitions given below

C Correction factor for "channeling" (see Section 2.4.2): 1 as default value in this study according to conclusions of Section 2.4.2

K_{mat} Mean from fitted log-normal distribution in Section 2.3.4.4

As discussed in VOBORNY et al. (1993), three different types of average transmissivity values, $\bar{T}$, are deemed relevant for the analytical estimate of the equivalent conductivity of a fracture system. They are characterized as follows:

$$\bar{T} = T_{geo} \quad (13)$$

geometric mean, μ, = mean from log-normal distribution: if the fractures are small and the fracture flow exhibits a 2-d characteristics.

$$\bar{T} = T_{ar} = e^{(\mu + \frac{\sigma^2}{2})} \quad (14)$$

arithmetic mean derived from log-normal distribution, defined by $\log_e$ mean, μ, and $\log_e$ standard deviation, σ: if the fractures are of larger or similar extent as the typical distance in the model using the equivalent K value as input parameter

$$\bar{T} = T_{3D} = e^{(\mu + \frac{\sigma^2}{6})} \quad (15)$$

if the fractures are small and the fracture flow exhibits a 3-d characteristics.

The first expression above (geometric mean) has been shown to hold theoretically if the fracture-aperture distribution is a stationary random field (GELHAR 1987). The other two expressions, developed for porous media, are considered herein as representing the bounding values of average T.

The significance of the calculated values for $K_{eff,ij}$ is determined by the validity of the applied conceptual model and its assumptions, and also by the significance of the input parameters used in the equation for K_{eff}. The significance is definitely smaller than what is suggested by the first decimal digit given in Table 2.7 below. The latter (e.g., 1.4E-11) is only included to illustrate the impact of selecting different input parameters and to quantify the anisotropy.

Table 2.7 Directional effective conductivities of conceptual domains estimated analytically

Conceptual area and domain	relevant mean T	C = 1 *) K_{hor} / K_{ver}
West Faults = MWCF	T_{ar} T_{geo} T_{3D}	2.8E-07 / 4.0E-07 3.4E-08 / 4.8E-08 6.8E-08 / 9.8E-08
West Upper = HPD	T_{ar} T_{geo} T_{3D}	9.8E-07 / 1.4E-06 4.0E-08 / 5.6E-08 1.1E-07 / 1.6E-07
West Lower = LPD	T_{ar} T_{geo} T_{3D}	2.0E-11 / 3.0E-11 1.4E-11 / 2.0E-11 1.6E-11 / 2.2E-11
East (Hypothesis 1) Upper	T_{ar} T_{geo} T_{3D}	1.1E-06 / 1.9E-06 3.0E-07 / 5.2E-07 4.8E-07 / 8.0E-07
East (Hypothesis 1) Lower	T_{ar} T_{geo} T_{3D}	1.3E-08 / 2.2E-08 6.8E-09 / 1.2E-08 8.6E-09 / 1.4E-08
West & East (Hypothesis 2) MWCF	T_{ar} T_{geo} T_{3D}	6.0E-07 / 8.5E-07 4.2E-08 / 6.0E-08 5.7E-08 / 8.2E-08
West & East (Hypothesis 2) HPD / LPD		same as West

*) resulting K_{eff} are directly proportional to assumed C

The anisotropy depends only on the geometric factors (resulting from dip distribution and orientation relative to a vertical borehole) and is

$K_{hor} : K_{ver}$ = 0.7	area West	(Dip interval 45-90°)
= 0.6	area East	(Dip interval 60-90°)
= 0.7	West & East	(assumed dip 45-90°)

The significance of the anisotropy is substantially larger than that of the absolute values of K_{eff}.

The most important aspects of the conceptual model and the strongest assumptions associated with the derivation of results presented above are the following:

- the applicability of the equation derived for fracture systems of infinitely extended fractures to real systems of limited fractures

- the perfect interconnectedness of the fracture system; i.e., no network effects

- the perfect hydraulic connection of channels at intersections of fractures; i.e., no dead-end channels

- the interpretation of measured T-values and derived mean $\bar{T}$-values as spatial averages for channels and islands areas within a fracture plane

All of these assumptions are conservative and lead to an overestimate of the true equivalent property. The sensitivity of some of these assumptions regarding the fracture-controlled flow was addressed by numerical studies considering a typical block of crystalline rock at the repository scale, discussed in Chapter 5.

2.6 Hydraulic data synthesis: summary and conclusions

The synthesis of experimental hydraulic data from Nagra boreholes provides the basis for hydrogeologic characterization of the crystalline basement of Northern Switzerland. The available information and knowledge is integrated into a conceptual model of crystalline rock. The rock heterogeneity - showing in spatial variability of hydraulic properties - is addressed by separating the crystalline basement into conceptual areas and domains. The latter are assumed to repre-

sent hydraulically homogeneous rock volumes that can be described by a single average property.

The outcome of the hydrogeologic characterization of the conceptual units is presented in Table 2.8. This compilation of key parameters represents a **reference dataset** that is required as input for safety-analysis calculations and for numerical models of groundwater flow as presented in the following chapters. The dataset is derived for both conceptual hypotheses concerning the SIB data.

Table 2.8 Summary of principal parameters derived from borehole data
(see below for explanation)

		Hypothesis 1					Hypo 2
		AREA WEST			AREA EAST		W & E
		Faults (MWCF)	Upper (HPD)	Lower (LPD)	Upper	Lower	MWCF (*)
I TE properties							
Frequency, N	[m^{-1}]	0.043	0.034	0.015	0.037	0.028	0.0345
Intensity P_{32C}	[m^{-1}]	0.120	0.097	0.043	0.148	0.112	0.100
mean $\log_{10}$ T, μ		-6.32	-6.17	-9.24	-5.42	-6.94	-6.14
(std $\log_{10}$ T, σ)		(0.9)	(1.1)	(0.4)	(0.7)	(0.5)	(1.0)
mean T (ar)	[m^2/s]	4.1E-06	4.4E-06	9.4E-10	1.3E-05	2.0E-07	5.8E-06
II K (Matrix)	[m/s]	mean $\log_{10}$ K = -11.63 (0.9), K(geo) = 2.3E-12 K(ar) = 1.7E-10 (± 6.3E-11)					
III K(eff) inf.	hor	2.9E-07	2.5E-07	4.0E-11	1.1E-06	1.2E-08	3.4E-07
[m/s]	ver	4.1E-07	3.6E-07	4.9E-11	1.8E-06	2.1E-08	4.9E-07
	iso	3.2E-07	2.8E-07	4.2E-11	1.3E-06	1.5E-08	3.9E-07

Explanations:

* Hypothesis 2: only MWCF reported, HPD and LPD same as area West

N: mean frequency of conductive fractures (=TE's) along borehole

P_{32C}: areal intensity of conductive fractures (derived from N and dip distribution)

T(ar): obtained directly from experimental data in App. 1, i.e., **not** calculated from fitted distribution according to Eq. (14). T(ar) for Hypo 2 is without TE SIB-top.

K: defined as T/L in all packer intervals with no discrete inflow (TE), see App. 2

K(eff): Effective hydraulic conductivity for system of infinite fractures estimated analytically according to Eq. 12. Input: G according to Section 2.5.3; P_{32C}, T(ar) and K(ar) from above. The **isotropic** values of K(eff) define the input parameters used in the hybrid modeling study of area West, described in Chapter 4.

The proposed values for effective directional conductivities are the outcome of several analytical and numerical analyses (VOBORNY et al. 1993). The given estimates of K_{eff} correspond to the maximum theoretical conductivity for an infinite-fracture system and are thus a conservative approximation of the "true" equivalent network property. As was discussed in Section 2.4, different types of average transmissivity values and different correction factors for channeling can be used in accordance to the applied conceptual model of fracture flow. The impact of the different parameters on the effective conductivity was illustrated in Table 2.7.

The conceptual model of fracture flow as adopted in this study is based on several principal assumptions and simplifications which are summarized with possible alternatives in Table 2.9. The main conclusions regarding the fracture-controlled flow through a low-permeable crystalline block are as follows:

- It is concluded that the use of the arithmetic mean of observed transmissivities is appropriate given the relatively large size of water-conducting features (including minor faults of several 100 m length) with respect to the considered block volume of rock encompassing a hypothetical repository.

- By using C=1 in Equation (12) to derive the reference dataset of Table 2.8, the conceptual model assumes that the **conductive fracture intensity, P_{32C},** derived directly from borehole observations is the appropriate quantity to approximate the actual intensity of conduits that contribute to fracture-network flow. An eventual underestimate of the true density of transmissive features is balanced by an overestimate of the system connectivity. The latter is a result of neglecting the "bottleneck" effects which constrain the fracture flow in a "real" network.

- It is also understood that the use of a) the arithmetic mean of TE transmissivity, and b) the infinite-fracture approach for estimating the effective property probably is sufficiently conservative to account for the conceptual uncertainty related to the channeling effect. The application of an arbitrary correction factor for channeling, C, to the resulting K_{eff} would lead to a further cumulation of conservative assumptions and was therefore not implemented in the conceptual model and the resulting reference dataset.

The impact of some of these uncertainties on the effective flow properties of a typical block of potential host rock was investigated in independent numerical-studies by fracture-network models. The results are summarized in Chapter 5.

Table 2.9 Summary of adopted and alternative conceptual assumptions

Subject	assumed in conceptual model	Plausible alternatives
Variability of T: · channeling · within single channel · among channels	 yes, concept No. 2 no yes (distributed)	 no / yes, concept No. 3 yes -
Characterization of T: · type of distribution · interpretation as	 log-normal surface average value	 normal; Poisson channel property
Size of WCF = TE (fracture length)	"infinite" (i.e., large with respect to considered block volume)	variable, defined by a distribution
Hydraulic properties of TE's in major faults (MWCF)	W: from KAI- & LEU-deep E: not relevant (Hypothesis 1)	W+E: from KAI, LEU & SIB (Hypothesis 2)
Impact of channeling: 1) increase of P_{32} 2) connectivity at fracture intersections 3) constrictivity of channels	 no (C=1) perfect none	 yes (e.g. C=5) reduced yes (difficult to apply)
Occurrence of LPD blocks (potential host rock)	only in area West (Hypothesis 1)	in West and East (Hypothesis 2)

3 CHARACTERIZATION OF REGIONAL FLOW

3.1 Scope and objectives of the study

The understanding of the groundwater flow through the crystalline basement of Northern Switzerland requires hydrogeological information on different scales. The large-scale hydrogeology defines the regional pattern of groundwater flow, characterized by the locations of recharge and discharge areas, the extent and properties of hydrogeological formations and the presence of major tectonic features as potential water conduits at large scale. This large-scale flow field, in turn, defines the boundary conditions for the sub-regional flow system, which represents the flow conditions in the specific area of a potential repository site.

This Chapter presents the results of a comprehensive modeling study of the regional groundwater flow in Northern Switzerland. The findings of the modeling study, together with other hydrogeological information and experience available, are integrated into a conceptual description of the regional flow system in the basement of Northern Switzerland. Due to sparse observations available, many uncertainties are inherent to this conceptual model. As a result, our current understanding of the considered system is expressed by a set of statements and hypotheses which are weighed by the associated degree of uncertainty. A compilation in the form of a table is given in Appendix 3.

The regional modeling study had two principal objectives as follows:

1) To test and improve the conceptual understanding of the regional flow in crystalline rocks with respect to boundary conditions, identification of discharge areas and consistency with hydrochemical evidence (method of particle tracking of advective flow); and

2) to provide a basis for establishing hydraulic boundary conditions for smaller sub-models at local scale.

The primary technique that was used to evaluate the regional flow system was numerical modeling. In this context, numerical modeling is an useful tool for implementing and testing various complex relationships that exist among different parameters that govern groundwater flow in a three-dimensional regime. These parameters are principally hydraulic head, hydraulic formation properties

and groundwater flux. Because of the large model scale and relatively sparse information on the spatial distribution of hydraulic rock properties, the modeled hydrologic units were represented by an "equivalent porous medium" (EPM). By making the continuum approximation for relatively large blocks of rock, it is assumed that a representative elemental volume, REV, exists within the modeled scale, with hydraulic properties being equivalent to those of a homogeneous porous medium. This implies that these properties do not depend on the explicit knowledge of fault and fracture geometry, frequency and transmissivity.

This investigation of regional groundwater flow was conducted iteratively in three modeling stages, designated KRI1, KRI2, and KRI3. The preliminary results of the first stage, KRI1, were summarized in an internal report and submitted to a broad review by hydrochemists, structural geologists and hydrogeologists (VOBORNY 1992). The outcome served as a base for an updated model version KRI2 (VOBORNY et al. 1992). Moreover, in an additional effort to improve simulation results, a few discrete tectonic features (faults) were incorporated into the model in the KRI3 phase. This Chapter describes the model development, evaluations and results obtained during the KRI2 and KRI3 modeling phases.

The EPM model described herein is intended to be an interpretive model to test various factors that affect the groundwater-flow regime in the region. This testing was done by varying certain input parameters and boundary conditions within a range of plausible values and assumptions, and then comparing the results with observed hydraulic heads. The principal bases for establishing the ranges of input parameters and for comparing heads were data obtained from hydraulic testing and from long-term monitoring of NAGRA boreholes in the region. The comparison of simulated and observed heads was the means of checking the reasonableness of the model. Because of the sparseness of field data, no formal calibration was performed; however, this step was not deemed necessary due to the primarily interpretative purpose of the modeling study.

In addition to improving understanding of the regional flow system, results of this study are also intended to provide a basis for defining boundary conditions for smaller local models. These models are not deemed location-specific, but would rather represent conditions that are representative for a certain area of interest. Moreover, due to the different numerical discretization of both models, it would not be appropriate to transfer specific boundary conditions directly from the EPM model to the local hybrid models. Instead, the insight gained on flow

directions, hydraulic gradients and fluxes, as well as the influence of certain boundaries, such as rivers and structural troughs, would be applied in defining the boundary conditions of the hybrid models (Section 3.5.3).

3.2 Outline of regional hydrogeology

3.2.1 Geological setting

Nagra's investigation region of crystalline bedrock in Northern Switzerland is limited to the south by the geological boundary of a deep sedimentary trough and to the north by the political border to Germany. In this area, the crystalline basement is covered entirely by a series of Mesozoic sediments. The crystalline rocks are exposed at surface in the adjacent Black Forest massif north of the Rhine and Wutach River. A comprehensive geological and tectonic characterization of the crystalline basement is given in DIEBOLD et al. (1991). An assessment of available geological and structural information for the specific needs of hydrodynamic modeling was provided by AMMANN et al. (1992).

The geological development of the crystalline basement complex of Northern Switzerland was dominated by the Variscan orogeny. The basement has undergone an intense, deep-reaching brittle deformation caused by Late Paleozoic tectonic events. The Permian faulting was accompanied by extension and differential subsidence of the basement, resulting in the development of large sedimentary troughs in the Late Paleozoic. During the Mesozoic age, the basement complex remained relatively stable. In the middle Miocene, a large dome, the Black Forest - Vosges massif began to rise and this process still seems to be active. The Miocene doming, accompanied by subsidence in the Molasse Basin, resulted in a tilt of the entire area toward SSE and in reactivation of the Late Paleozoic fault zones.

The crystalline basement in the underground of Northern Switzerland represents a continuation of the southern Black Forest, so that similar geological conditions were expected. Indeed, the crystalline rocks observed in Nagra's deep boreholes consist basically of old (Prevariscan) gneisses that are intruded by Variscan granites of several types, related to those of southern Black Forest. Additionally, the borehole data revealed new information on the intensity and effects of hydrothermal alterations that had affected the crystalline rocks.

The principal tectonic features in the area of northern Switzerland and southern Black Forest are depicted, together with the contour of the regional model, in a schematic tectonic map in Fig. 3.1. Evident at this scale are some large faults that dissect the crystalline basement of Black Forest. The predominant direction of NW to SE belongs to the hercynic fault system. An approximately north-south trending system of normal faults, developed particularly in the sediments of the Tabular Jura, is related to the tertiary subsidence of the Rhine Graben structure at the west border of the map. The extent of the Late Paleozoic sedimentary trough, termed the Permocarboniferous Trough, PCT, is not evident on the map because of the mesozoic cover (see Fig. 4 in DIEBOLD et al. 1991).

In a marginal zone north of the deep trough, the crystalline rocks are overlain by Permian sediments of a relatively small thickness (few 100 m), which geometrically represent a shallow shoulder of the trough. Farther north, toward the updoming Black Forest massif, the Mesozoic Buntsandstein unit overlies transgressively the weathered surface of crystalline rocks.

3.2.2 Summary of hydrochemical synthesis

Results of a comprehensive hydrochemical synthesis of Buntsandstein-Permian-Crystalline aquifers in Northern Switzerland are reported in SCHMASSMANN et al. (1992). The isotope data were analyzed by PEARSON et al. (1991).

The following types of deep groundwater occur in northern Switzerland on the basis of hydrochemical properties and isotopic data:

1) Buntsandstein water (where Buntsandstein aquifer is isolated from the crystalline aquifer): low-mineralized, Na-sulphate and Na-chloride water, widely distributed from Weiach in the east to Grenzach in the west; different from all other types of deep groundwater.

2) Rotliegend water (Permian sediments of the deep PCT and trough shoulder): highly saline Na-chloride deep groundwater, similar to conditions of some salt lakes. Indications for very small circulation, i.e., stagnant waters.

3) Crystalline low-mineralized water: Widespread flow system from the southern Black Forest to the region north of the PCT. The hydrochemical evo-

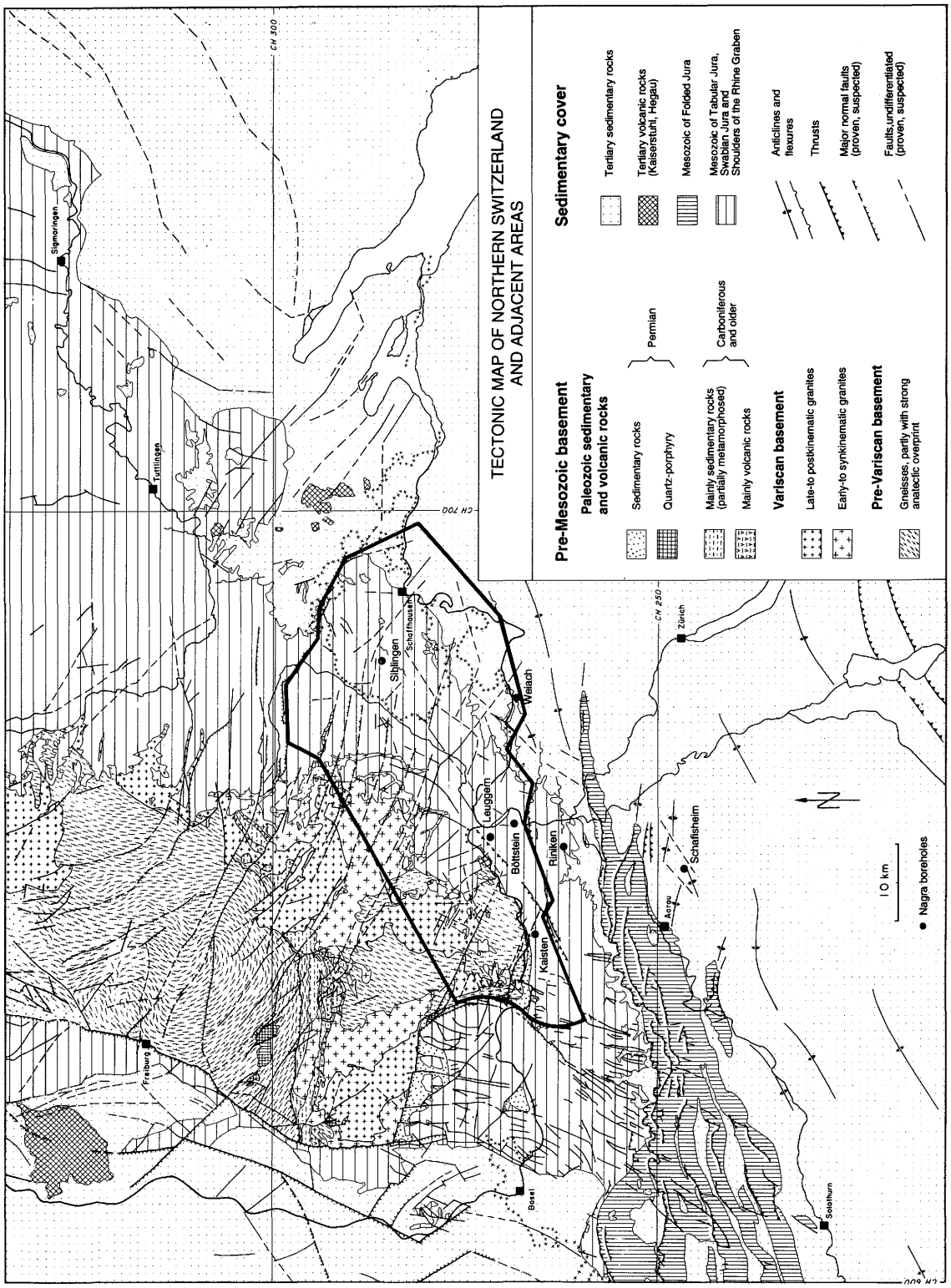

Fig. 3.1 Tectonic map of Nothern Switzerland and Southern Black Forest with area of the regional model KRI2

lution sequence extends from recent Black Forest water (alkali-earth bicarbonate type) to a higher-evolved Na-bicarbonate groundwater, observed at SIB, and finally to Na-sulphate water, widely distributed between Zurzach, BOE, LEU, KAI and Säckingen. This water type is slightly influenced by Na-chloride deep groundwater from the domain of the PCT. The smallest influence of saline components is observed at KAI; the influence increases successively at Zurzach, LEU, BOE and Säckingen, where it is the greatest.

4) Crystalline highly-mineralized water: Na-chloride deep groundwater beneath and beside the PC trough, with evidence for its origin from the more saline Rotliegend waters (type 2). The components indicate a dilution sequence from Rotliegend water (2) to crystalline water (3). The Na-Cl-deep groundwater was observed in WEI (under trough), BOE-deep (lower crystalline section, beside trough), Schafisheim (beside trough?) and Säckingen (beneath trough shoulder).

3.2.3 Reference set of hydraulic heads

The first phase of Nagra's crystalline investigation program was completed in 1989 with drilling and testing of the Siblingen borehole, the last of seven deep wells. After completion of the testing program, all boreholes were equipped with multiple long-term monitoring systems, which are providing information on the static hydraulic pressures (heads) in selected monitoring intervals. A comprehensive synthesis of the existing data set was conducted by PASQUIER et al. (1993), providing an actual and consistent "reference set" of head values. This information, in turn, represents the principal database required for the "calibration" of the hydrogeologic conceptual model and of numerical groundwater models described in this report.

In this context, the relevant data from this reference set are summarized in Table 3.1 below. The table includes only those Nagra boreholes that are located north of the PCT. Moreover, only monitoring intervals in the paleozoic basement - consisting of crystalline rocks (CR) and permocarboniferous rocks (PC) - and in the Buntsandstein layer (BS) are considered, because the overlying mesozoic cover is not included in conceptual and numerical models. For comparison purpose, the compilation includes two different types of hydraulic head which are defined as follows:

Table 3.1 Hydraulic heads in Nagra boreholes north of PCT (from PASQUIER et al. 1993, explanation see text)

Zone	Depth to Center of Interval (m)	Tested formation	Freshwater Head, H_f, (m)	Environmental Head, H_e, (m)
BOETTSTEIN (elev. 347.5 m a.s.l)				
Z2	429.2	CR	365.3	364.1
Z3	742.5	CR	363.7	363.5
Z4	972.4	CR	364.7	365.3
Z5	1150.9	CR	406.0	406.8
Z6	1329.0	CR	405.2	406.0
Z7	1368.8	CR	406.3	407.1
Z8	1408.5	CR	407.0	407.9
KAISTEN (elev. 320.4 m a.s.l.)				
Z1	103.5	BS	294.6	294.8
Z2	180.2	PC	298.7	298.2
Z3	549.3	CR	323.0	322.2
Z4	649.8	CR	343.5	342.9
Z5	743.5	CR	350.3	349.9
Z6	1008.3	CR	349.2	350.0
Z7	1266.7	CR	347.2	350.0
LEUGGERN (elev. 358.8 m a.s.l.)				
Z1	708.0	CR	362.4	362.2
Z2	923.2	CR	361.4	361.8
Z3	1176.7	CR	359.9	361.6
Z4	1472.1	CR	357.0	361.5
Z5	1606.5	CR	355.8	361.9
WEIACH (elev. 368.7 m a.s.l.				
Z2	987.5	BS	418.7	415.8
Z3	1116.1	PC	441.1	437.2
Z4	1408.2	PC	441.1	431.1
Z5	2134.7	CR	402.6	413.9
Z6	2215.0	CR	391.4	405.4
Z7	2350.6	CR	384.9	403.6
SIBLINGEN (elev. 574.4 m a.s.l.): open hole from 490.4 to 1522.0				
Z1	1004.3	CR	440.2	440.0

- The Freshwater Head, H_f, represents the elevation of a freshwater column at standard temperature and pressure (STP) conditions that corresponds to the calculated downhole pressure;

- The Environmental Head, H_e, is the elevation of a water column having the same density profile as the in-situ groundwater, calculated from the downhole pressure.

The environmental head is useful for evaluation of vertical groundwater flow in formations with different salinities. The freshwater head is relevant for evaluating the horizontal flow gradients. Note, that the numerical groundwater models, described in the following sections, use a constant fluid density of 1,000 kg/m^3 and calculate therefore the freshwater heads.

3.3 Characteristics of the regional model KRI2 (1991)

3.3.1 Approach of Finite-Element modeling

The groundwater modeling was performed with the Finite-Element code FEM301, described by KIRALY (1985). The algorithm calculates the steady-state saturated water flow (3-D) in an equivalent porous medium, under the assumption of a constant specific weight of the flow phase (i.e., fresh water). The principal procedure of numerical groundwater modeling consists of three main parts outlined below. The sequence is shown as flow chart in Fig. 3.2.

The **preprocessing phase** involves the compilation of all model-specific information into a conceptual model, followed by the generation of the finite-element grid. A coordinate file and an element file are required by the code to define the 3-D mesh. The hydraulic properties of the modeled hydrogeologic units as well as the required boundary conditions are given in a parameter file.

The second step is the **computational phase** that produces a result file as output. The code calculates a hydraulic head at every node of the mesh, except for those nodal points with prescribed external heads (boundary condition). In such cases, the resulting volumetric flux (inflow or outflow) is computed, which is representative for the vicinity of the node concerned.

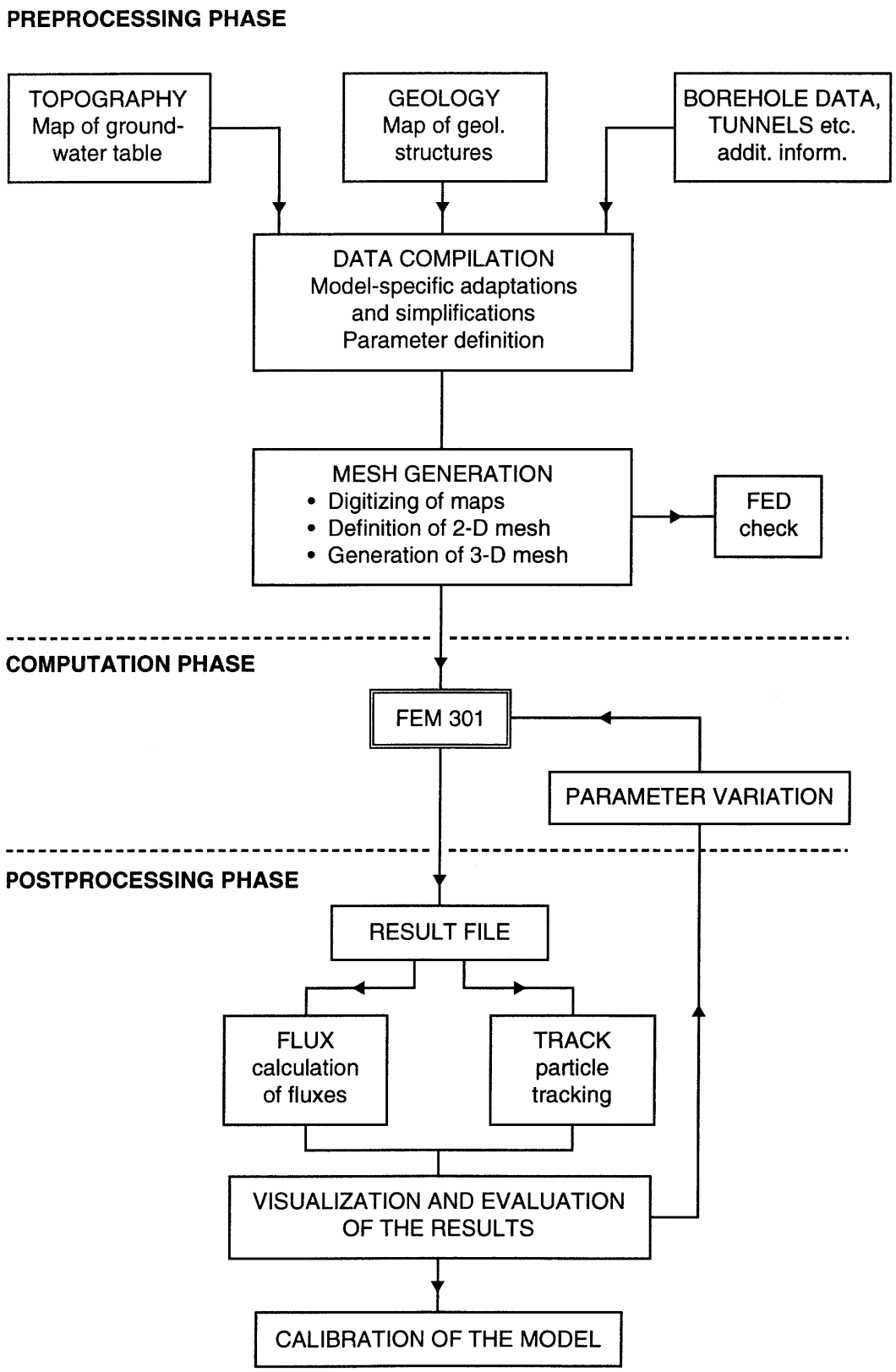

Fig. 3.2 Flow chart of numerical groundwater modeling

The last, **postprocessing phase** includes the visualization of results by means of FED (Finite Element Display) and additional calculations of water fluxes (code FLUX), particle flow paths and travel times (particle tracking code TRACK).

3.3.2 Model structure and area

The model area and the regional tectonic framework are illustrated by a tectonic map in Fig. 3.1. As exposed in Section 3.1, the numerical model is a strong simplification of the real system. Because of the sparse information distributed over large area, the geometry and material properties of the complex hydrogeologic framework are not known explicitly. Large volumes of crystalline rocks are approximated by an equivalent porous medium (EPM approach) and described by a single property, the K_{eff}. Similarly, the geometry of the modeled *hydrogeological units* is simplified in order to limit the number of finite elements. Fig. 3.3 displays the model geometry and principal boundary conditions in a schematic north-south section. To account for the generally observed trend of decreasing conductivity with greater depth (drift, see Section 2.3), the crystalline rocks are separated into an *Upper crystalline unit* (UC), with a relatively large permeability, and an underlying *Lower crystalline unit* (LC), characterized by a relatively small permeability (see vertical model sections shown in Fig. 3.3 below). Note that the major water-conducting faults, being an element of the hydrogeologic framework as defined in Section 2.3.3, are implicitly included in these EPM units. Therefore, the effective properties of the latter (listed in Table 3.2) are not identical to those derived for the conceptual domains in Chapter 2.

The crystalline rocks adjacent to the deep Permocarboniferous Trough (PCT) in the south are expected to be strongly affected by multiphase tectonic deformation processes that formed the PCT (DIEBOLD et al. 1991, p.182). The tectonically complex border zone is schematically represented in the model by a *Disturbed Zone* (DZ) as a first-order fault of 500 m width. This zone of enhanced permeability was introduced to accomodate the ascending flux of deep groundwater that was postulated by RYBACH et al. (1987) on the basis of geothermal observations.

The sediments included in the model comprise the shallow shoulder of the Permo-carboniferous Trough (PCTs) and the Buntsandstein aquifer (Bs), which is represented by 2-dimensional elements due to its small thickness.

Where possible, the model area is limited by natural geological boundaries. In the south, the Permocarboniferous Trough of several km depth is considered as a flow boundary. The trough itself is beyond the area of interest within the crystalline program; however, its possible influence on the flow regime in the adjacent crystalline basement has been investigated in the model by variations of the corresponding boundary conditions (see below). Toward the east and the west, the model is bounded by the regional 1st-order faults of Randen and Wehra respectively (see map in Fig. 3.1). No natural flow boundary was followed in the north where the model is limited by an arbitrary line across the slope of the southern Black Forest. In this case, allowance is made for recharge into the model from the adjacent Black Forest massif (fixed-head condition).

The numerical model covers an area of 1,300 km^2 and is discretized into 2,046 elements with 7,320 nodes. The grid structure is shown in Fig. 3.4 as a perspective 3-d view and in two north-south cross sections that are typical for the model geometry in the western part (section W-W') and in the Siblingen region (section E-E'). Indicated are the locations of deep boreholes and positions of horizontal sections used for display of model results.

The adopted model assumptions regarding the boundary conditions, geometry and properties of modeled units were assessed as the "best-guess", representing the most probable or plausible condition or value, and implemented in the Base-case scenario, designated V20. This configuration is also referred to as the initial case with default parameters, which serves as reference basis for the sensitivity study performed with the KRI2 model. The base-case scenario incorporates the experience and recommendations resulting from the preliminary phase KRI1 (VOBORNY 1992). The assigned model parameters and boundary conditions are described in the following sections.

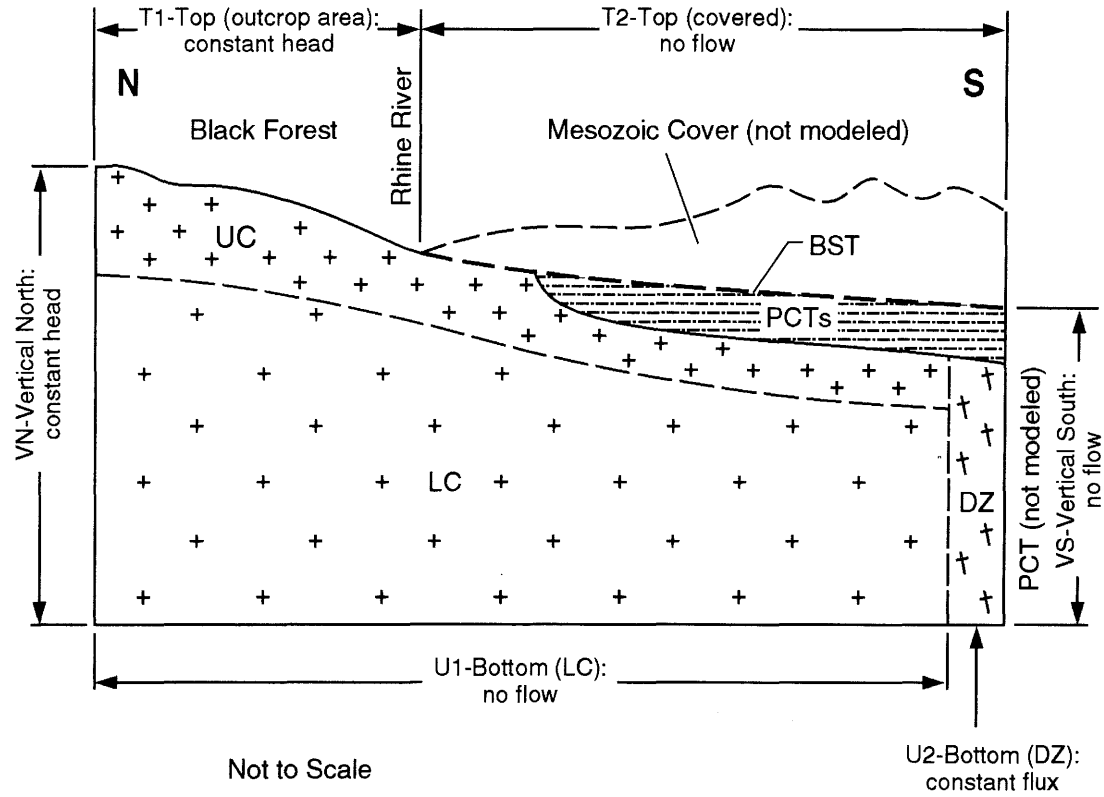

Hydrogeological units (see Table 3.2)

Bs Buntsandstein aquifer (2-d)
PCT Permo-Carboniferous Trough (not modeled)
PCTs Permo-Carbonif. Trough (shoulder)
UC Upper crystalline rock unit
LC Lower crystalline rock unit
DZ Tectonically disturbed zone (MWCF-1)

Additional boundary conditions
(not shown above)

VW Vertical West: constant flux
VE Vertical East: constant flux

Fig. 3.3 Regional model KRI2: schematic section with hydrogeological units and boundary conditions, base-case scenario

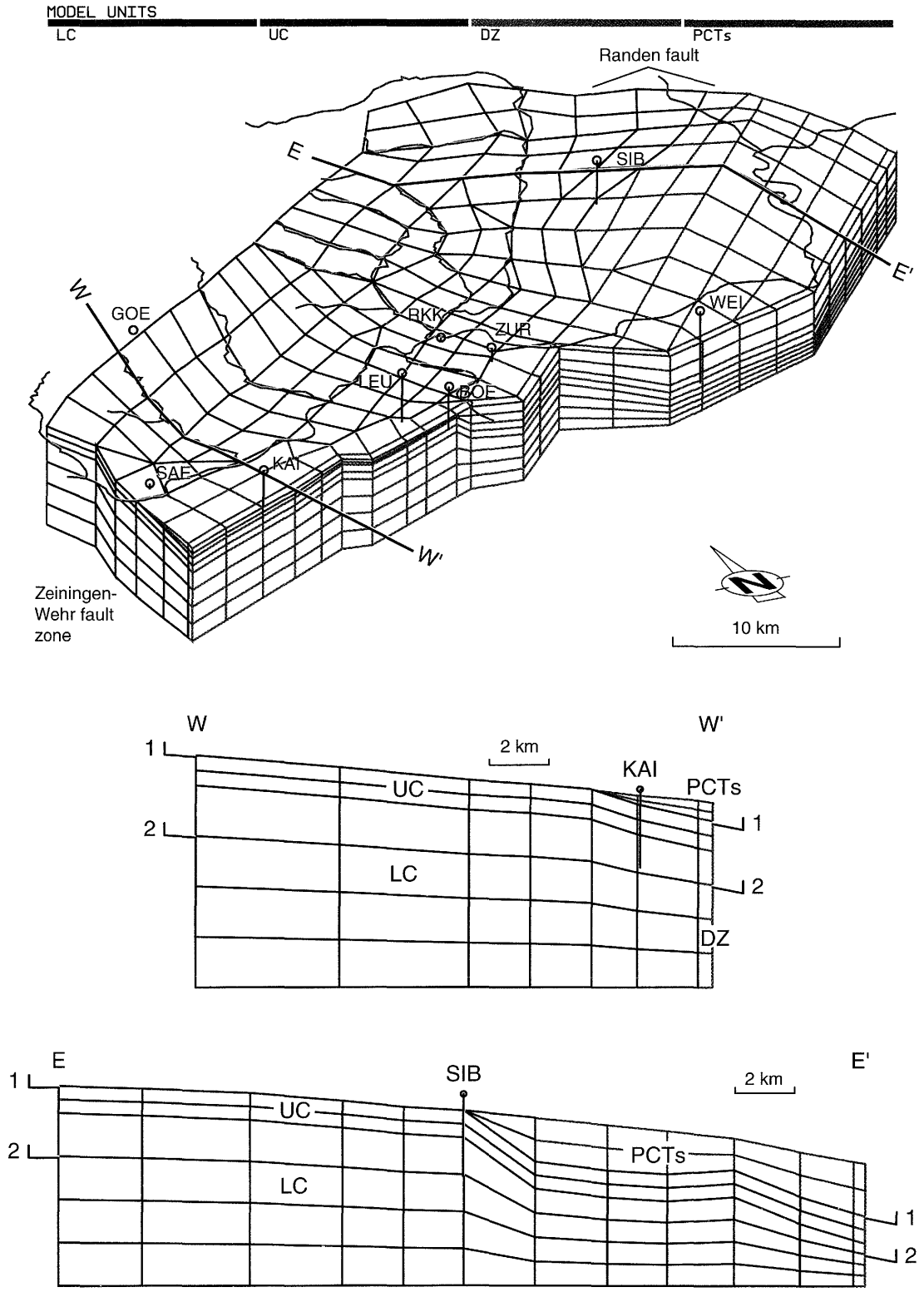

Fig. 3.4 FE grid of the regional model KRI2: 3-d view (*top*) and typical vertical sections (*bottom*), both vertical exaggerated 2x

3.3.3 Hydraulic parameters

As exposed in Section 3.1., the modeling of regional flow uses the continuum approximation over large volumes of crystalline rocks, which are described as an equivalent porous medium and characterized by a single hydraulic property, the equivalent conductivity, K_{eff} (isotropic). Since the experimental data (borehole tests) only provide information on the small-scale hydraulic properties (m to tens of m), rough estimates are required to characterize the equivalent conductivity of large rock volumes. Moreover, the synthesis of hydraulic borehole data (presented in Chapter 2) was not yet completed at the begin of the regional modeling study; hence, only preliminary estimates of effective properties were made.

The hydraulic model parameters assigned to the default scenario V20 ("best guess") are summarized in Table 3.2 and commented below.

Table 3.2 Hydraulic parameters of KRI2 model (Base case)

Model unit	Code	Property	Value
Buntsandstein	Bs	T [m^2/s]	1.5·E-05
Perm (shoulder of PCT)	PCTs	K [m/s]	1·E-09
Upper crystalline unit	UC	K [m/s]	1·E-07
Lower crystalline unit	LC	K [m/s]	1·E-09
Disturbed Zone to PCT	DZ	K [m/s]	1·E-07

Buntsandstein, Bs

Buntsandstein represents a thin regional aquifer in Northern Switzerland. In areas north of the PCT and its shoulder, PCTs, it was deposited directly on top of the weathered crystalline rocks and forms together with these an important hydrogeological unit. Due to its large hydraulic conductivity Buntsandstein exhibits horizontal flow and can thus be represented by 2-D elements, characterized by transmissivity. This property is derived from the average hydraulic conductivity of K=1·E-06 m/s, as observed in the boreholes of Böttstein, Kaisten, Riniken and Weiach, and from average thickness of 15 m.

Perm (Rotliegendes of PCT shoulder, PCTs)

The Rotliegendes sediments represents a highly heterogeneous and anisotropic sequence with respect to hydraulic properties. Packer-test data indicate a wide conductivity range from 1·E-07 to less than 1·E-11 m/s. The conceptual model considers this formation as a generally low-permeable layer that separates the Bs aquifer from the underlying crystalline rocks. This is justified by the low vertical permeability of the layered sequence and by hydrochemical evidence. Observed higher-permeable zones in the boreholes (inflows) are deemed to represent local flow systems in coarse-grained horizons. The assigned mean isotropic K value is a model assumption and its sensitivity was tested in the initial modeling phase KRI1.

Upper crystalline unit, UC

The assigned model value was derived at an early stage of the synthesis study from a preliminary assessment of effective properties (referenced in VOBORNY et al. 1993). Its application to the equivalent porous medium of the KRI2 model assumed that the contribution of large faults to the regional flow through the high-permeable UC unit can be neglected (i.e., no correction is required).

Lower crystalline unit, LC

The aforementioned preliminary assessment of effective properties suggested a value of K_{eff} = 9·E-11 m/s for a typical block of the Low-permeable domain. At the regional scale, however, the groundwater flow is deemed to occur mainly within large permeable faults of 1st and 2nd order. As a rough estimate, a scaling-up factor of 10 was applied to the effective block property derived above to include implicitly the regional faults into the modeled continuum system. This correction between the 1-km scale and 10-km scale yields the order-of-magnitude estimate of K_{eff} = 1·E-09 m/s for the Lower crystalline EPM unit.

Disturbed zone, DZ

The Disturbed zone, modeled as a major fault (MWCF) of 1st order, was assigned the same EPM property as the Upper crystalline unit, UC; both units were identified as similar already in the preliminary stage of parametric characterization. This similarity was confirmed by the definitive assessment of hydraulic properties in Chapter 2 (see Table 2.8).

3.3.4 Boundary Conditions

The model area was defined in such a way that the limits follow natural flow boundaries where possible. Nonetheless, significant uncertainties are attached to hydraulic conditions of some individual boundaries, which were subjected to a sensitivity analysis.

The "best guess" boundary conditions were implemented as default in the Base case V20. Principally, the hydraulic boundaries are closed (no-flow condition), or open, with prescribed heads or fluxes at the corresponding nodes. The assignment of the default boundary conditions and possible alternatives tested in the model are described herein. The derivation of discrete flux values for flow boundaries is documented in Table 3.3.

3.3.4.1 Model Top

T1 (exposed crystalline rocks): constant heads.

The constant-head boundary is defined by a digitized groundwater table in the area of exposed crystalline basement, i.e., in southern Black Forest. A particular emphasis was given to the assignment of exact elevations for all nodes located in the river valleys in order to reproduce the correct discharge conditions. In hilly regions between the river valleys, the assumed groundwater table follows approximately the topography (h=z simplification).
Alternatives: none

T2 (basement under Mesozoic cover): no flow, q=0

According to the basic conceptual assumption, no vertical flow occurs through the Mesozoic cover of the Lower and Middle Muschelkalk in the investigated region. The hydrothermal well of Zurzach is open by default (prescribed head). Several exceptions to the no-flow condition have been considered as follows.

T3 (leaky Mesozoic cover): non-zero flux, q>0

Exception to T2 condition beneath the Wutach River valley: although the crystalline rocks are covered by a layer of low-permeable sediments of the Lower Muschelkalk unit under the bottom of the Wutach valley, the latter is assumed

open along a continuous section reaching from the model boundary down to Eggingen (elev. 410). Along this stretch, external-head conditions are prescribed at corresponding river nodes. This assumption implies that the Buntsandstein-Crystalline (Bs/UC) aquifer is hydraulically connected to the valley bottom at various locations. The channel of the Wutach River, after the last glaciation, has eroded into the underlying sediments of Lower Muschelkalk in the reach south of Stühlingen. These layers, between 40 and 50 m in thickness, generally have small permeability, but they are dissected at many places by faults (see tectonic map of Fig. 3.1). According to model assumption, some prominent normal faults of the hercynian horst-graben systems are likely to provide pathways for discharge from the Bs/UC groundwater into the Wutach River.

Alternative: Wutach valley closed: no flow boundary, in **V203**

The scenario of leaky Mesozoic cover was further tested in the area of Tabular Jura between BOE and KAI (T3 boundary in Fig. 3.5 *top*). The Runs **V25/V250** simulate a locally limited leakage along a major discrete fault in the sediments ("Mandach scenario"). A non-zero flux, q_v, was fixed at the nodes within the T3 area of Fig. 3.5 *top*, according to the derived value in Table 3.3 below.

3.3.4.2 Model Bottom

B1: no flow as general condition
B2: prescribed non-zero flux, q_0 (= basal flux)

The open bottom boundary B2 (Fig. 3.5 *bottom*) corresponds to the bottom of the Disturbed zone, DZ, of 500 m width that extends alongside the deep PCT from south of Zurzach to the western model boundary. The flow rate imposed at this boundary was defined in accordance to the ascending volumetric flow that was suggested by RYBACH et al. (1987, p.529) on the basis of an observed geothermal anomaly. The derivation of this flow condition is given in Table 3.3. The application of the postulated flux along the Disturbed zone results in a volumetric flow of Q = 1·E-07 m^3/s per linear meter of axial length of DZ, or in a Darcy flux of q = 2·E-10 m/s per unit area. The latter value was prescribed to each node within the "open" DZ area. Given the K value of 1·E-07 m/s of this unit, the prescribed Darcy flux corresponds to an upward gradient of 0.002.

Alternative: no flow in B2, in **V205**

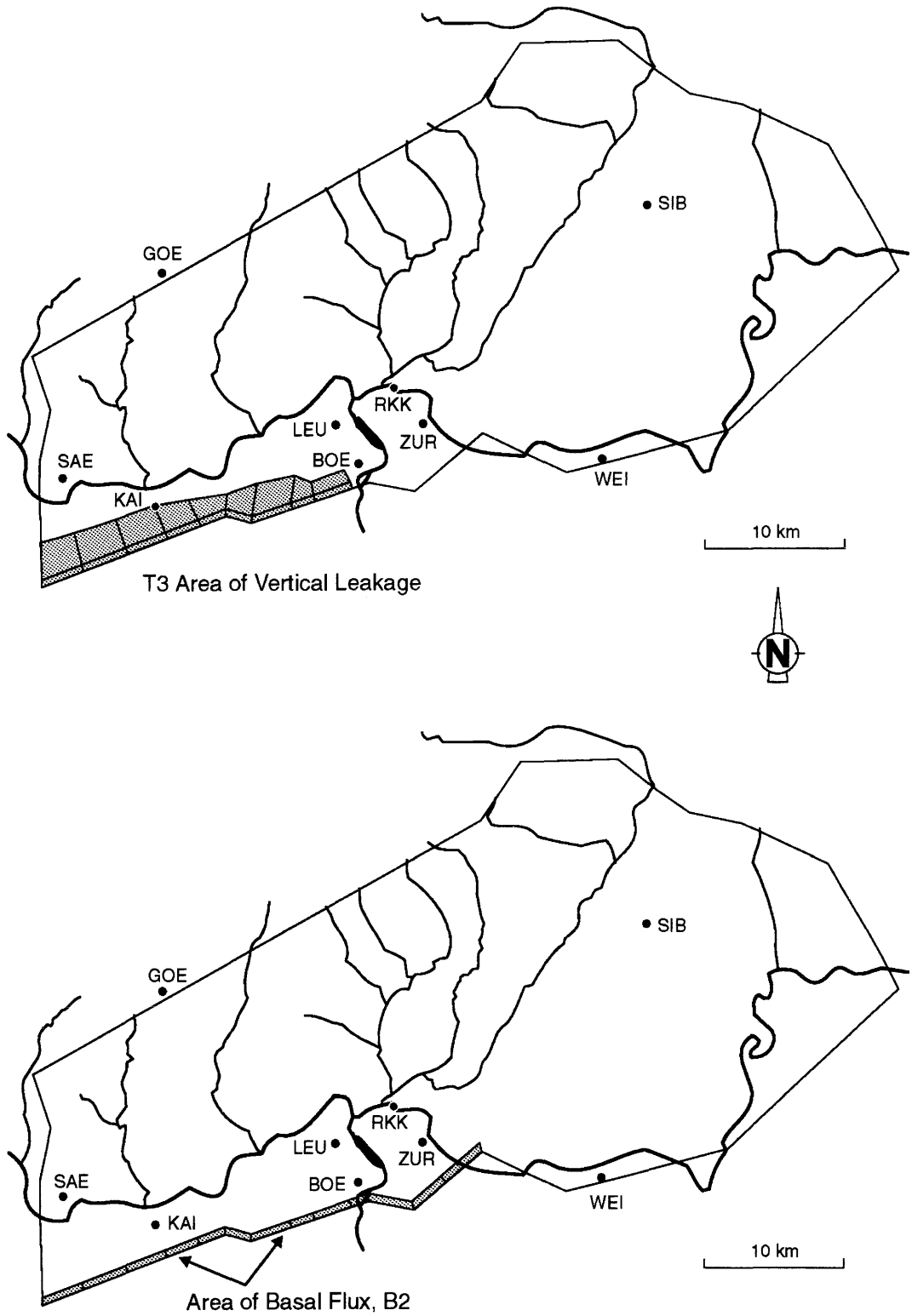

Fig. 3.5 *Top:* Area of downward leakage in V25 (T3 top boundary)
Bottom: area of active basal flux (B2 bottom boundary)

Table 3.3 Derivation of flux-boundary conditions in KRI2 model

1. Default scenario: Basal flux, Q_0 (all runs excl. V205, V23-V26)	
Assumptions based on RYBACH et al. (1987): · uprising volumetric flow beneath the trough: · flux component ascending along N margin (50%): Model KRI2: Width of Disturbed zone DZ = 500 m; i.e., resulting Darcy flux at B2 boundary, q_0: (= prescribed flux at each node of B2) DZ length = 35.9km; total volumetric flow in B2, Q_0:	 2·E-04 kg/sec per linear m, or 2·E-07 m^3/s Q = 1·E-07 m^3/s per 1m, or 0.1 l/s per 1km length of DZ q_0 = Q/A = 2·E-10 m/s per 1m 3.6 l/s, corresponds to i_v = 0.002
2. Alternative scenarios **2.1 Lateral flux from PCT, Q_{south} (Run V24)**	
Lateral inflow through south boundary, VS: · flow area A=1·E+8 m^2; assumed total inflow, Q_s: · resulting Darcy flow (in all nodes of VS), q_s:	 5 l/s = 0.005 m^3/s 5·E-11 m/s per unit area
2.2 Leaky Mesozoic cover, vertical flux Q_{vert} (V25) (Scenario "Mandach fault)"	
Vertical infiltration through top boundary T2: · flow area A = 5.7·E+07 m^2; assumed inflow, Q_v: · resulting Darcy flow as BC (all nodes of T2), q_v: · Variation in V250: q increased by factor 5, q'_v:	 4 l/s (same as Q_0 above) 7·E-11 m/s per unit area 3.5·E-10 m/s

3.3.4.3 Lateral boundaries

a) North boundary VN: constant head

The vertical north boundary, VN, is an arbitrary line running across the southern slopes of the Black Forest massif. Consideration was given to extending the model area farther north to the actual water divide in order to obtain a natural no-flow boundary. Such modification, however, would require a shift of the north boundary by 20 km north to the Feldberg massif and would almost double the model area. Instead, the same net effect of allowing for groundwater flow from central Black Forest into the model was achieved by opening the existing lateral boundary VN. For this purpose, external constant heads were assigned to all nodes along this vertical boundary by taking the topographic elevation (h=z) and assuming a zero vertical gradient over the boundary face.
Alternative: no flow, **V204**

b) South boundary VS: no flow

Under default conditions, the deep sedimentary trough that extends south of the modeled area serves as a no-flow boundary. However, the possibility of a limited lateral migration of highly saline groundwater into the adjacent crystalline basement cannot be excluded on the basis of hydrochemical observations (e.g. NaCl water in BOE, see Sect. 3.2.2).

Alternative: prescribed flow from South, q_s, in **V24,** see Table 3.3
An alternative boundary condition was implemented in V24 by substituting the former basal flux, Q_0, by a lateral flux Q_{south} across the PCT. The derivation of this boundary condition is given in Table 3.3. Due to the larger cross-flow area, the prescribed Darcy flux at the boundary nodes is four times smaller than the corresponding basal flux.

c) East boundary VE: constant heads in UC (scenario "low")

In KRI2, the condition of low heads in crystalline rocks in the east is considered as a default scenario, in accordance to the results of preliminary KRI1 simulations. This allows the groundwater to flow from the Bs/UC unit across the Randen fault into the adjoining Muschelkalk aquifer with a generally low head regime (H = 500 to 400 m a.s.l.).

Alternatives:
- Boundary fault as no-flow condition, in **V202**
- Constant heads in UC, scenario "high", in **V206**
- ditto, scenario "very low", in **V207**

d) West boundary VW: constant heads in UC south of Rhine R. (scenario "low")

Alternatives:
- Fault as no-flow condition, in **V201**
- Constant heads in UC south of Rhine River, scenario "high", in **V209**, assuming possible flow within the UC unit from west into the model (area south of Rhine River only)

3.4 Summary of model simulations

Starting from the Base case scenario V20, defined above, a comprehensive sensitivity study was conducted with the KRI2 model. A first series of model variations was assigned to testing the significance of alternative boundary conditions. A second phase investigated the sensitivity of hydraulic model parameters. An overview of the complete sensitivity study is given in Fig. 3.6.

3.4.1 Sensitivity analysis of boundary conditions

Preliminary simulations with the KRI1 model suggested that the greatest uncertainties regarding the model assumptions are associated with the boundary conditions. Therefore, a primary objective of the new simulations was to test various plausible boundary concepts, such as identified in Section 3.3.4, and to quantify their significance or impact on the simulated flow regime. Hence, the first phase of sensitivity analysis addressed the hydraulic role of the individual boundaries by varying one boundary condition at a time and checking its impact on the model results.

The variations of the West boundary comprised no-flow conditions in run **V201** that simulated the Wehra fault as a flow barrier, and high heads in UC south of the Rhine River in run **V209**. The North boundary was closed in **V204**, assuming no lateral inflow from central Black Forest.

Due to the large range of uncertainty associated with the eastern boundary conditions, VE, four different concepts were tested. As a default condition (V20), the "low head" alternative was adopted based on results of the preliminary KRI1 phase. This scenario considers a possible short-circuiting of crystalline groundwater across a (permeable) major tectonic feature to the aquifer of Upper Muschelkalk (e.g., via Randen fault or any similar structure related to the Bonndorf-Bodensee graben system). The potentiometric surface of the Muschelkalk is characterized by abnormally low values in the region of Lake Constance. Earlier observations of this anomaly (LEMCKE, 1984) have been recently confirmed in south Germany by borehole data compiled by STOBER & VILLINGER (1994). The head depression has been observed mainly in the region north of Lake Constance; its extent south and west of the lake, however, is unknown.

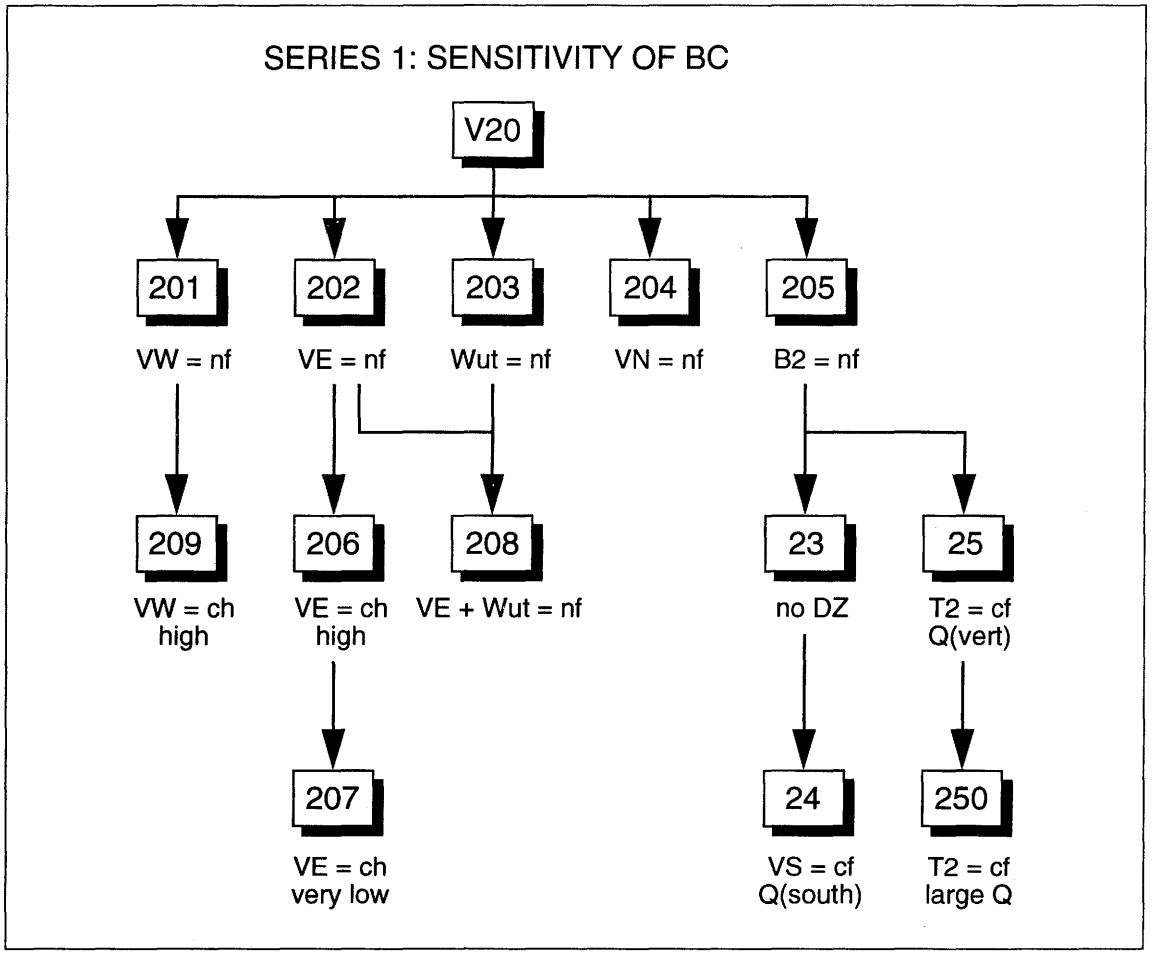

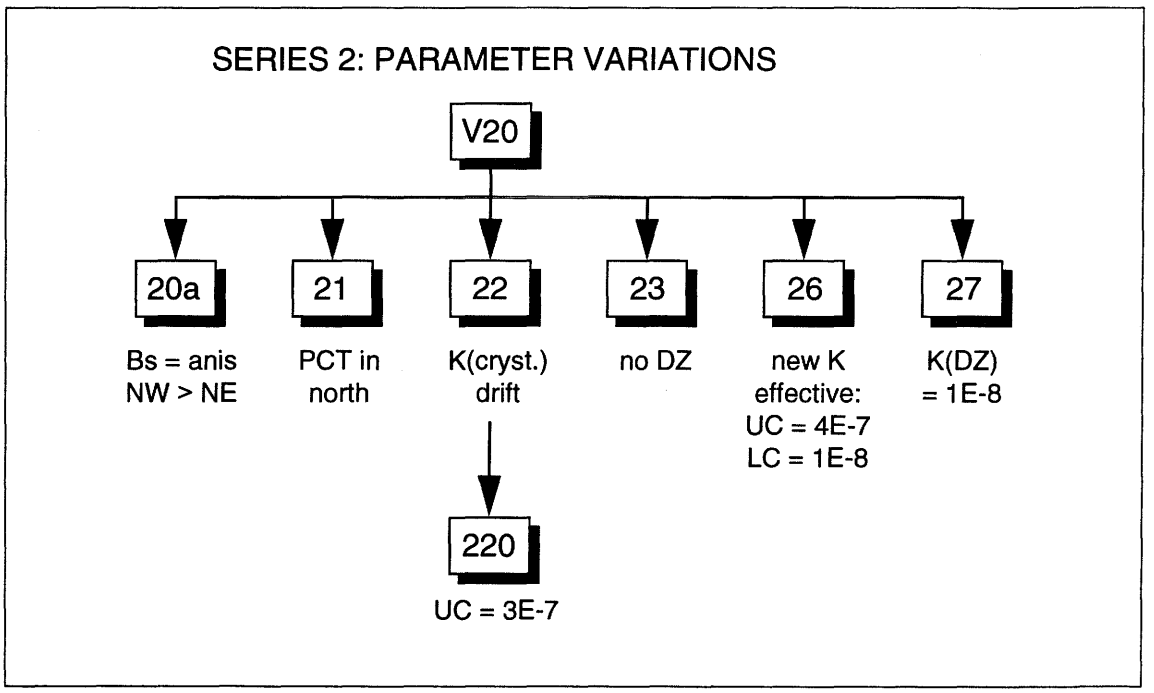

Fig. 3.6 Summary of KRI2 simulations

The simulated head distribution for the Upper crystalline unit along the VE boundary in the initial run V20 is depicted in Fig. 3.7 (*top*). In this case, hydraulic connection is assumed to the Upper-Muschelkalk unit along the southeastern extent of the fault, where the largest downward gradients between the two units are likely to occur. Another possible connection between the Bs/UC and Muschelkalk aquifers is as lateral flow across the fault farther north (east of SIB), where the two aquifer units abut against each other due to the fault throw (SCHMASSMANN internal communication 1991). A "very low" scenario was considered in run **V207** by assuming that the Muschelkalk-head depression extends farther west. To simulate this condition, the fixed heads along the southeastern edge of the model were further reduced to a minimum of 300 m. The objective of this simulation was to test what potentiometric conditions are required in the southeastern corner of the model to force groundwater from the SIB area to flow toward the Lake Constance (and beyond to the Neckar River as the possible discharge area of the Muschelkalk aquifer). No such effects are assumed in run **V206**, which represents the "high head" alternative. Fig. 3.7 *bottom* shows the corresponding head contours in the eastern part of the model area. As a fourth variation, no-flow conditions were considered in run **V202.**

The significance of the Wutach River valley as boundary was investigated in run **V203** by imposing a no-flow condition there.

The open bottom boundary, B2, with a prescribed basal flux as default condition (Fig. 3.5 *bottom*), was closed in run **V205.** The runs V24 and V25 test two alternative concepts of replacing the basal flux, q_0, by either 1) a lateral infiltration, q_s, from the adjacent deep PC trough (V24), or 2) a vertical seepage, q_v through the Mesozoic cover (V25, V250; see Table 3.2 for definition of flux conditions). In **V24**, the vertical southern boundary VS was considered permeable by means of a prescribed areal flux from the south. At the same time, the permeable Disturbed zone was "switched off" to prevent a direct drainage of the introduced flux along the permeable strip. The lateral extent of the permeable section in the east-west direction and the total volumetric flow introduced correspond to those of the basal flux boundary B2 in V20 (see Fig. 3.5 *bottom*). The vertical flux, q_v, along the model-surface boundary T3 in run **V25** was specified only at selected grid elements in order to simulate a local leakage through the Mesozoic cover. Such leakage is assumed to occur along a discrete (permeable) fault in areas of relatively high hydraulic heads in the Upper Muschelkalk. As a possible example, the Mandach fault in the Tabular Jura between BOE and KAI was considered for this scenario (Fig. 3.5 *top*). The volume of

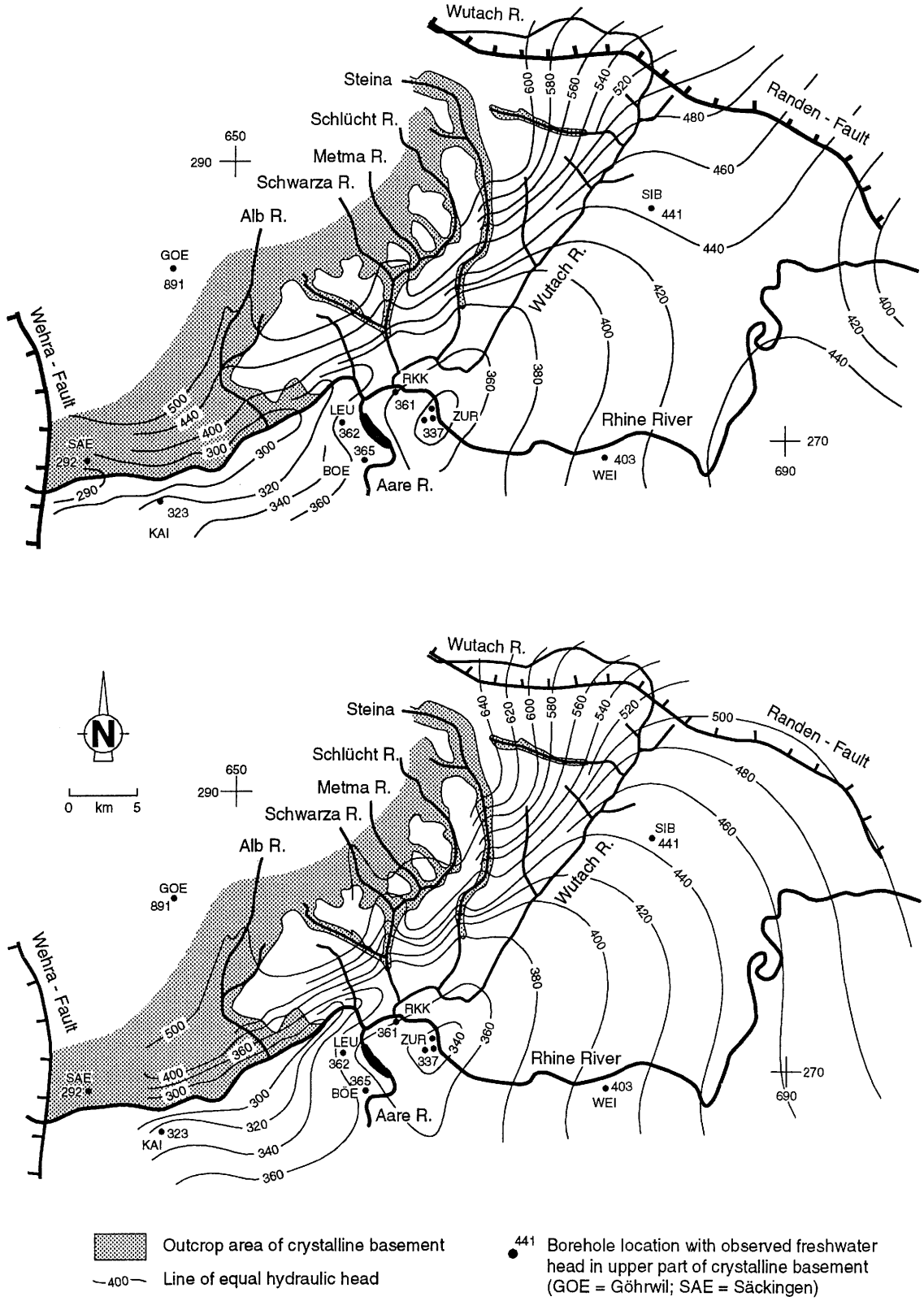

Fig. 3.7 Assumed head distribution in Upper crystalline unit for derivation of VE boundary conditions. *Top*: Base case (V20); *Bottom:* V206

infiltration in this area was again defined such as to replace the basal flux in the DZ, i.e., $q_v=q_0$. To enhance the impact of such downward leakage in terms of a sensitivity test, the prescribed areal flux and the conductivity of the trough shoulder were increased in run **V250**.

The effect of the Zurzach well as a boundary condition was tested for several scenarios (labelled with 'z', e.g., **V20z**) by "closing" the thermal well; i.e., by imposing the no-flow condition on this node instead of fixed head at 337 m.

3.4.2 Parameter variation study

The purpose of the second set of model simulations was to consider parameter variations and modifications of the model geometry and to test how much the model results would be affected by such additional model adjustments (i.e., how stable is the reproduced flow regime?).

Run **V20A** introduces a horizontal anisotropy within the Bs layer (2-d); the transmissivity parallel to the hercynic structures (NW to SE) was assumed to be greater than the transmissivity in the perpendicular direction (NE to SW).

Run **V21** accounts for a modified extent of the deep Permocarboniferous trough (PCT). The default geometry of the PCT in KRI2 mesh was based on an "older" interpretation of a seismic section through SIB (Fig. 30A in DIEBOLD et al., 1991). Reprocessing of the same line suggested the existence of a deep PCT segment south of Siblingen (Fig. 30B in DIEBOLD et al., 1991). In accordance with this interpretation, a segment of deep trough was introduced into the model in the region between Siblingen and the Rhine River. This modified model geometry is illustrated in Fig. 3.8.

An alternative conceptual model with respect to permeability distributions in the crystalline rocks was tested in run **V22**. Instead of a binary division into the Upper (UC) and Lower (LC) crystalline units with a sharp contrast in hydraulic conductivity at the contact, a step-wise decreasing permeability with depth was considered. In accordance with the observations in most of the deep boreholes, a K decrease of one order of magnitude per 1,000 m of depth was assumed. As a minor modification of this run, the K-value of the Upper crystalline unit was increased by a factor of 3 in **V220,** in order to reproduce the observed outflow in ZUR. A last variation of crystalline hydraulic properties was realized in run **V26**

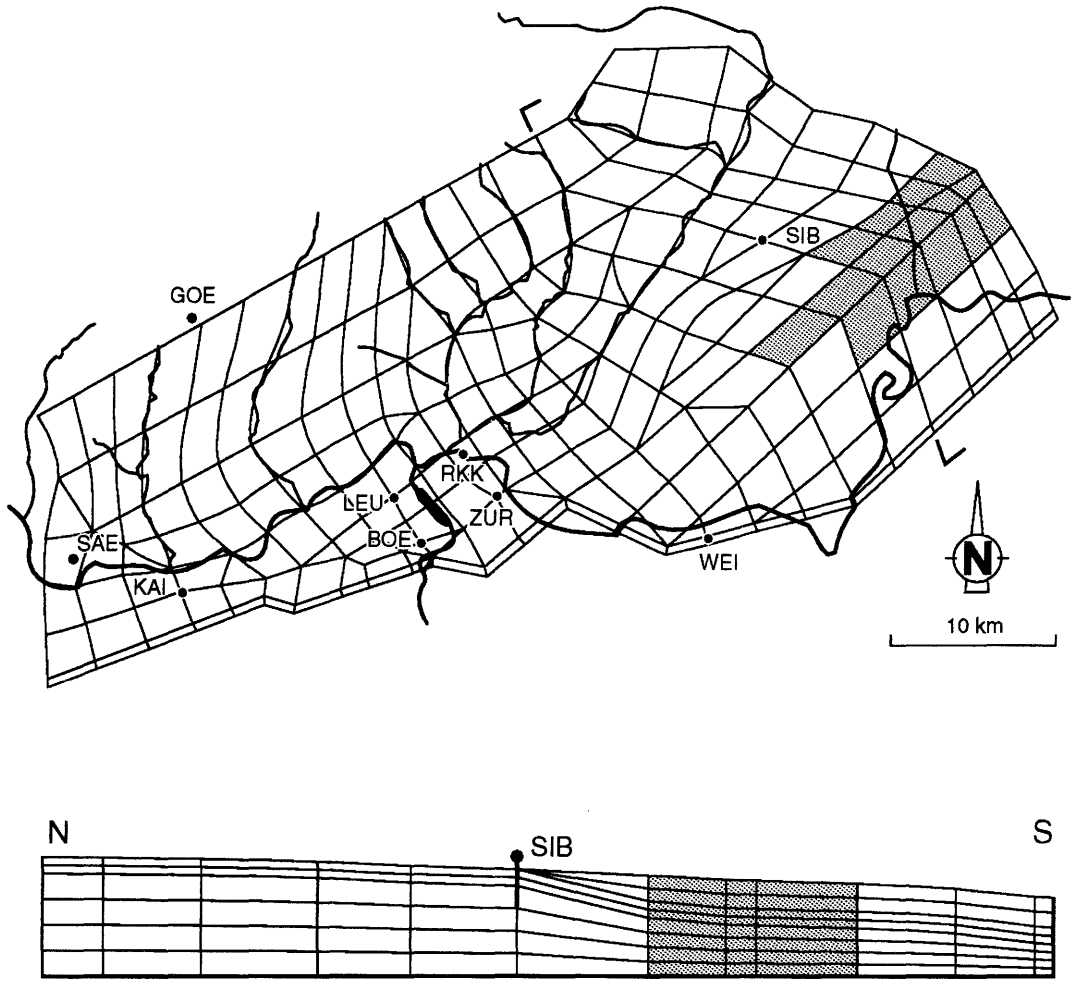

Fig. 3.8 Modified model geometry in Run V21: Northern branch of deep PCT in plan view (*top*) and cross section (*bottom*)

that considers possible upper bounds for the effective continuum properties of Upper and Lower crystalline units (increase of K by factor of 4 and 10 with respect to default values).

Runs **V23** and **V27** test the impact of the assumed Disturbed zone, DZ, on the regional flow of deep groundwater in the area BOE-LEU-KAI. In V23, this zone is made inactive by adjusting its K to that of LC; run V27 simulates a reduced conductivity of DZ by a factor of 10 with respect to V20 but maintains the same basal flux as boundary condition.

3.5 Results: Description of regional flow

3.5.1 General

This Section describes the regional groundwater flow regime in Northern Switzerland on the basis of model results and observed hydrologic conditions. The discussion of the model results is based on graphic presentations of head distributions (displayed as contour maps) or flux distributions (displayed as Darcy vectors) and of flowpath lines resulting from particle tracking. These results are shown in plan view and vertical sections. Due to similar trends in most of the runs, only the base case, V20, and some significant variations are illustrated.

As a general plausibility check of the model, the hydraulic heads in realized model simulations are compared to observations of heads in deep Nagra boreholes. The observed and simulated values are compiled in Table 3.4.

3.5.2 Default conditions: Base case V20

The regional flow pattern in the Upper crystalline unit is illustrated by horizontal head distribution in Fig. 3.9. In the area of exposed crystalline rocks in the southern Black Forest, the head contours reflect the prescribed groundwater table as boundary condition and show distinctly the significance of the river valleys as discharge areas for local flow systems. The model area of covered crystalline rocks shows a general flow direction from the northeast to the southwest, with a principal discharge area along the Rhine River valley. The corre-

sponding plot of resulting Darcy vectors (Fig. 3.10 *top*) provides an information on the direction and magnitude of the flow within the Upper crystalline unit. Because the K value is constant throughout the model, this plot also mimics the distribution of hydraulic gradients. As shown by the vectors, the groundwater divide between the discharge in the Rhine River valley in the west and the Lake Constance area in the east is located east of SIB.

The vectors also indicate the origin of flow that is intercepted in the deep boreholes: ZUR receives water that has infiltrated in southeastern Black Forest and passes through SIB area, BOE is supplied mainly by water with origin from the DZ in southeast, and RKK, LEU and KAI receive directly water from adjacent Black Forest slopes. The magnitude of the vectors shows the highest fluxes (and thus gradients) in the Black Forest area where the local flow system dominate. Generally low flow velocities are present in the area of covered basement south of the Rhine and Wutach River. The vertical short vectors east and west of KAI indicate the regional discharge area along the Rhine River.

An analogous vector map of the Darcy flux in the LC unit would show virtually the same horizontal flow directions but with flux magnitudes reduced by two orders of magnitude. However, it is of interest to display only the vertical component of Darcy flow in this unit, in order to discriminate areas with prevailing upward flow (discharge condition) or downward flow (recharge condition). Fig. 3.10 (*bottom*) shows such a contour map of vertical flux component in LC unit: the negative components depict areas with recharge condition (downward flow in LC) and positive components those with discharge regime. The map shows that infiltration into the Lower crystalline unit is limited to the hilly areas of southern Black Forest. The Black Forest river valleys and the Rhine River are important discharge areas. The region of covered crystalline basement south of the Rhine valley and Wutach valley is characterized by very low vertical flux components that correspond to vertical gradients between 0 to 0.005 (upward).

The vertical head distribution throughout the model is illustrated in Fig. 3.11 by three north-south trending sections AA' (through LEU and BOE), BB' (through RKK and ZUR) and CC'(SIB) and also by the longitudinal section DD' extending from West to East (see Fig. 3.9 for locations). Notable in the north-south sections are the very small gradients in the southern model area (south of Rhine River); visible is the effect of water inflow from the bounding DZ (basal flux). Also evident is the discharge flow condition beneath the Rhine River (covered by Mesozoic sediments in section BB') and at the open ZUR well. The longitudi-

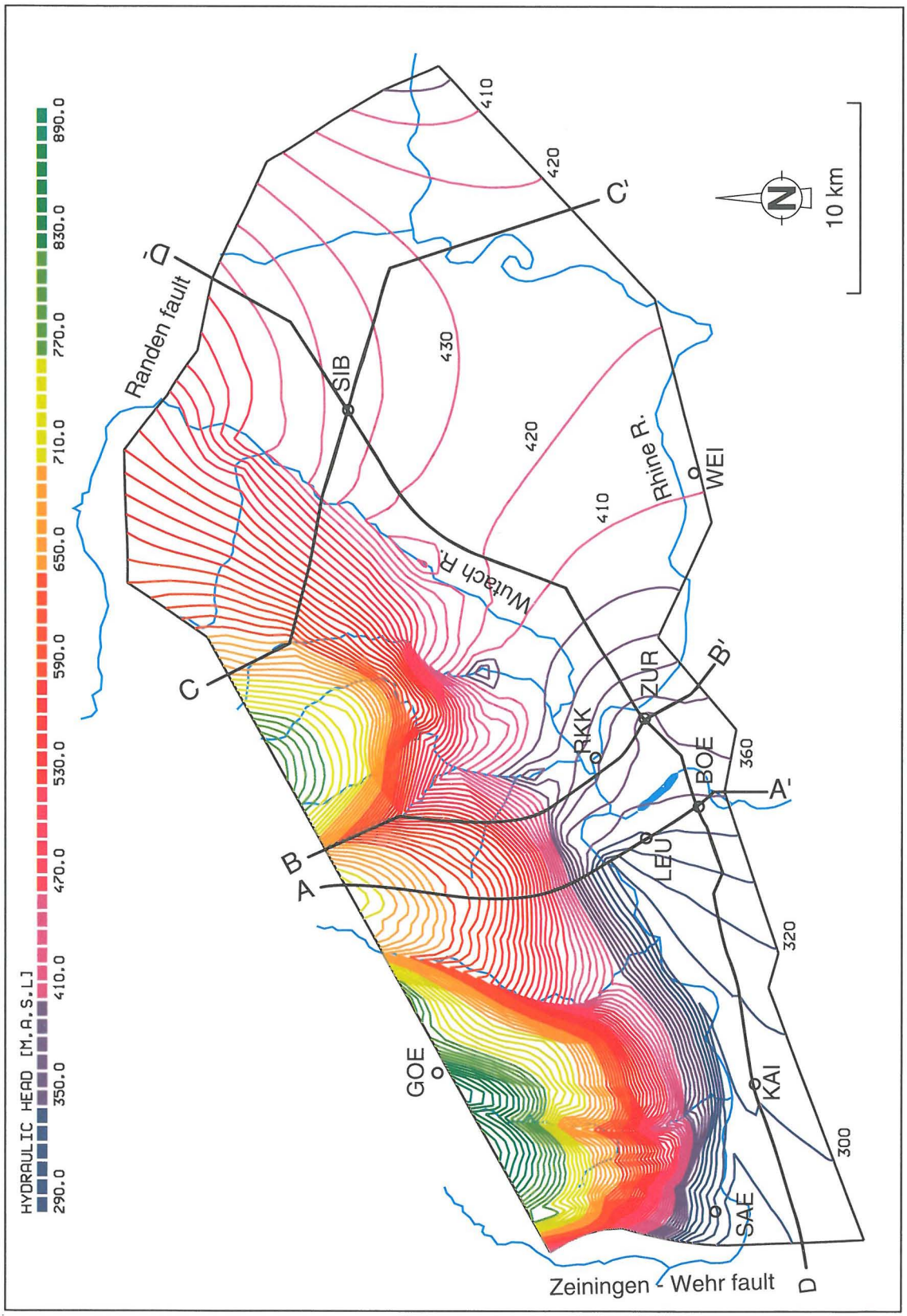

Fig. 3.9 Base case V20: Contour map of simulated head in UC unit (level 1 in Fig. 3.4.), indicating location of vertical sections

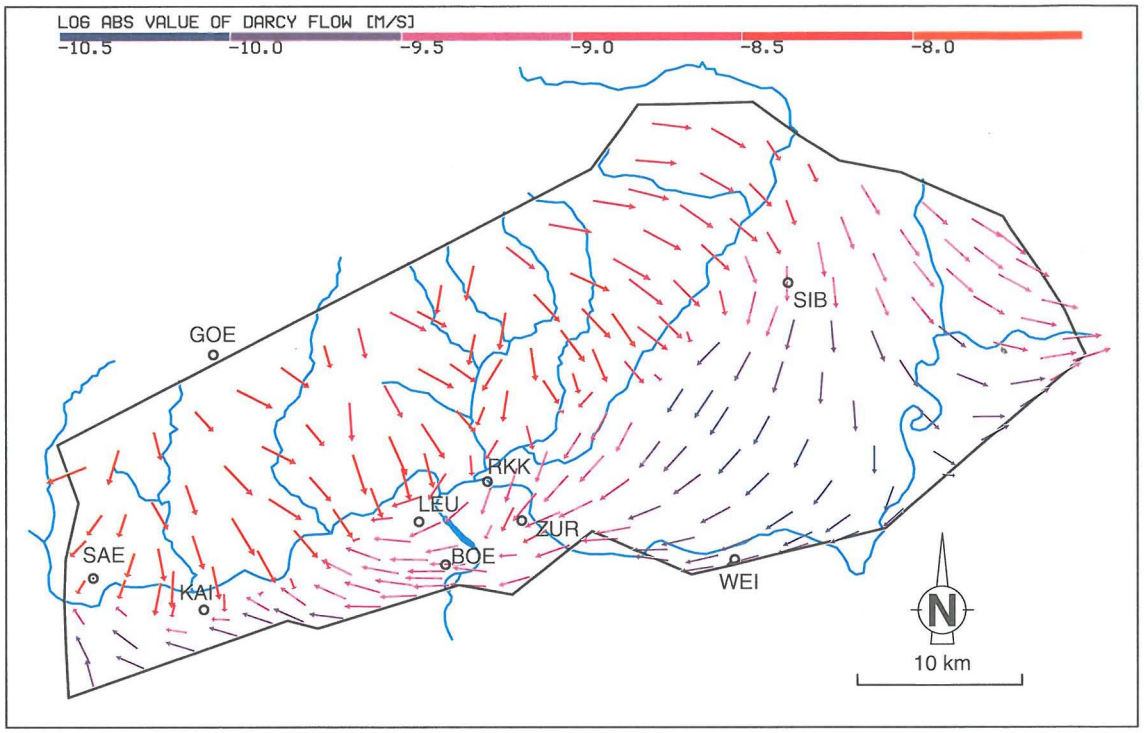

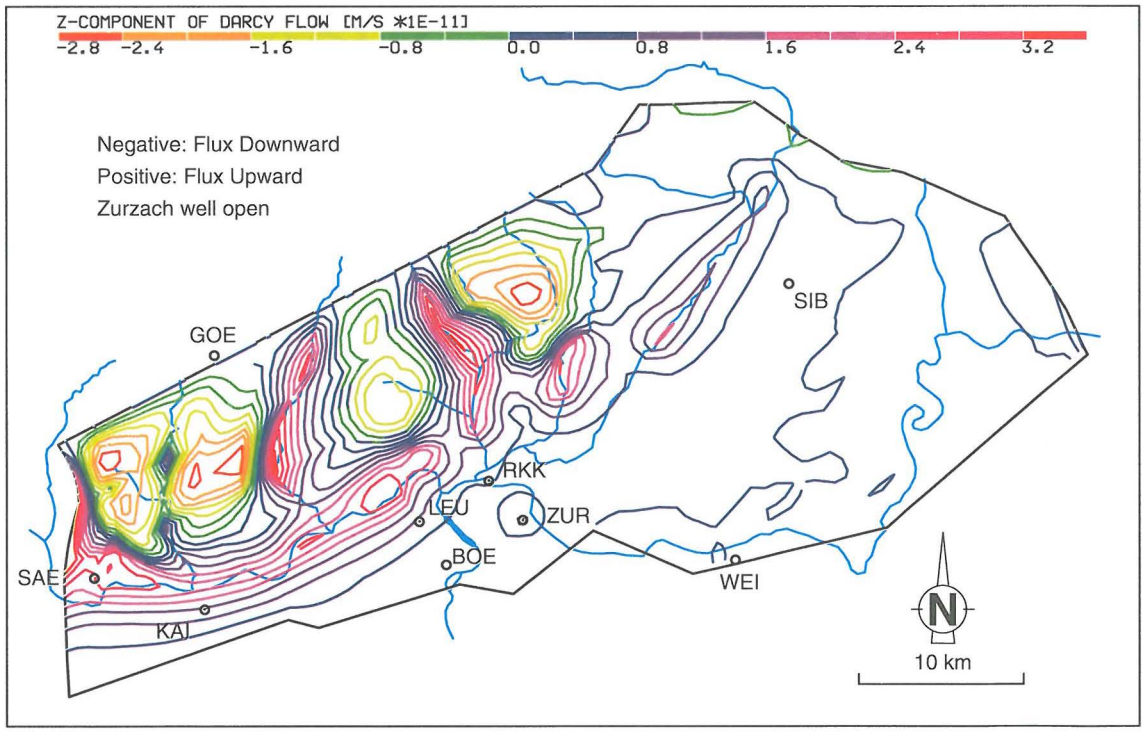

Fig. 3.10 *Top*: V20, Darcy flux vectors in UC unit
Bottom: V20, contours of vertical flux component in LC unit

nal section DD' indicates generally low head gradients with a predominant horizontal flow in the eastern part that is oriented perpendicular to the cross section in the area of SIB. Discharge regime is observed again at ZUR and in the western part of the model.

Additional insight on the advective groundwater flow in the model was obtained from particle tracking. Because near-surface flow lines in Upper crystalline unit reflect basically the local flow systems between the recharge areas and discharge in the adjacent river valleys, only the deep-lying pathlines are of interest. Fig. 3.12 shows the resulting flow lines for the initial run V20z (ZUR closed). The release points of the fluid particles are located within the Lower-crystalline unit at all nodes along a hypothetical vertical plane parallel to the northern (VN) and eastern model boundary (VE), assuming that the recharge of these particles occurs in the central part of Black Forest, beyond the modeled area. Further release points are distributed along the open B2 bottom boundary in the south, representing the entering basal flux. Both the Rhine River and the open reach of the Wutach valley are significant discharge areas for crystalline groundwater from the adjoining slopes of the Black Forest. The general flow pattern is similar to that displayed by the Darcy vectors in Fig. 3.10 (*top*). The boreholes of SIB and ZUR receive groundwater from southeastern Black Forest, whereas RKK, LEU and KAI are supplied more directly from the nearby slopes north of the Rhine valley. The borehole of BOE receives most of its water from the DZ in the southeast.

3.5.3 Effect of boundary conditions

A series of runs was dedicated to the testing of different boundary conditions and their effects on model results. All runs are derived from the initial run V20 and use identical input parameters.

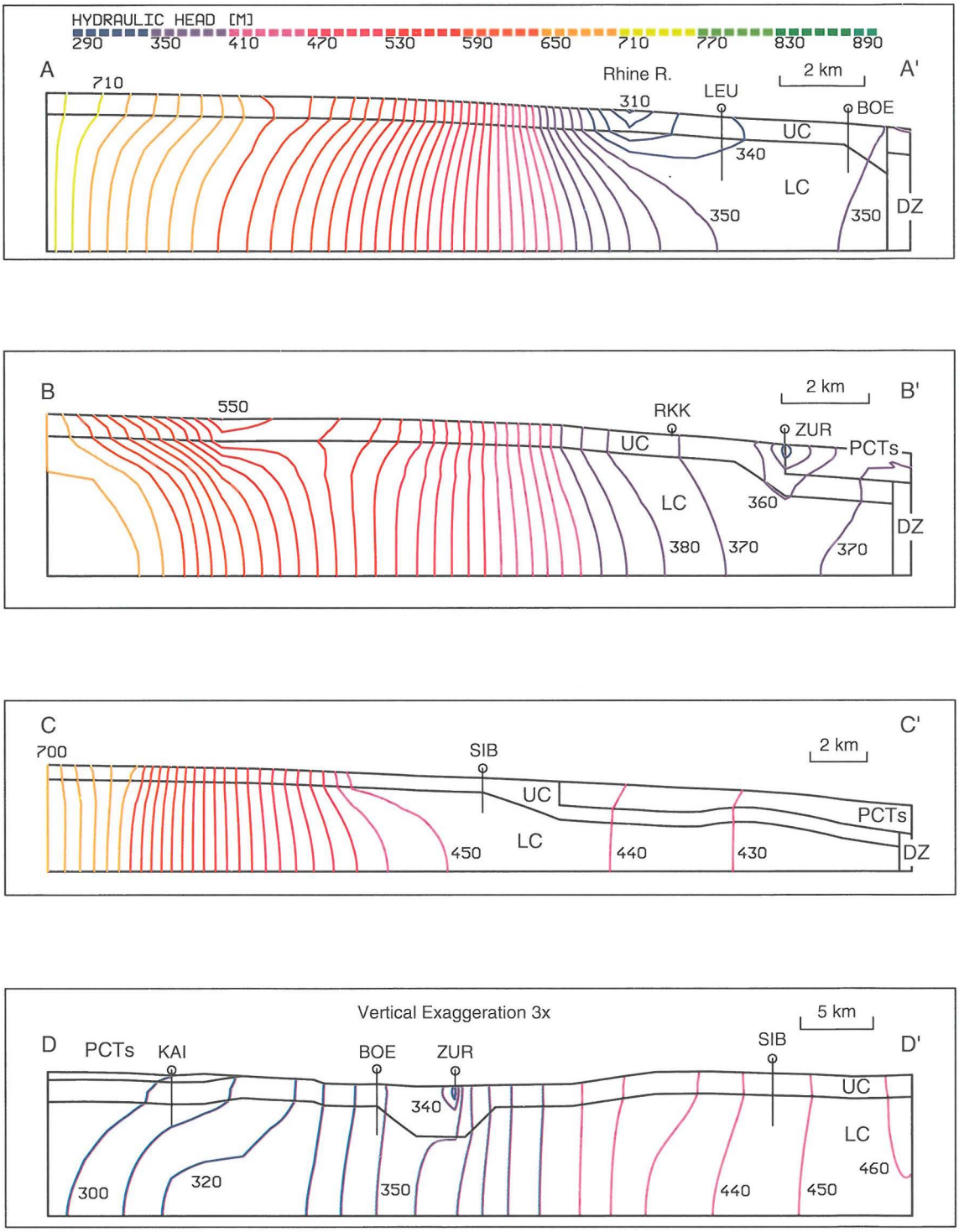

Fig. 3.11 Base case V20: Simulated head in vertical sections (see Fig. 3.9 for location), contour interval 10 m

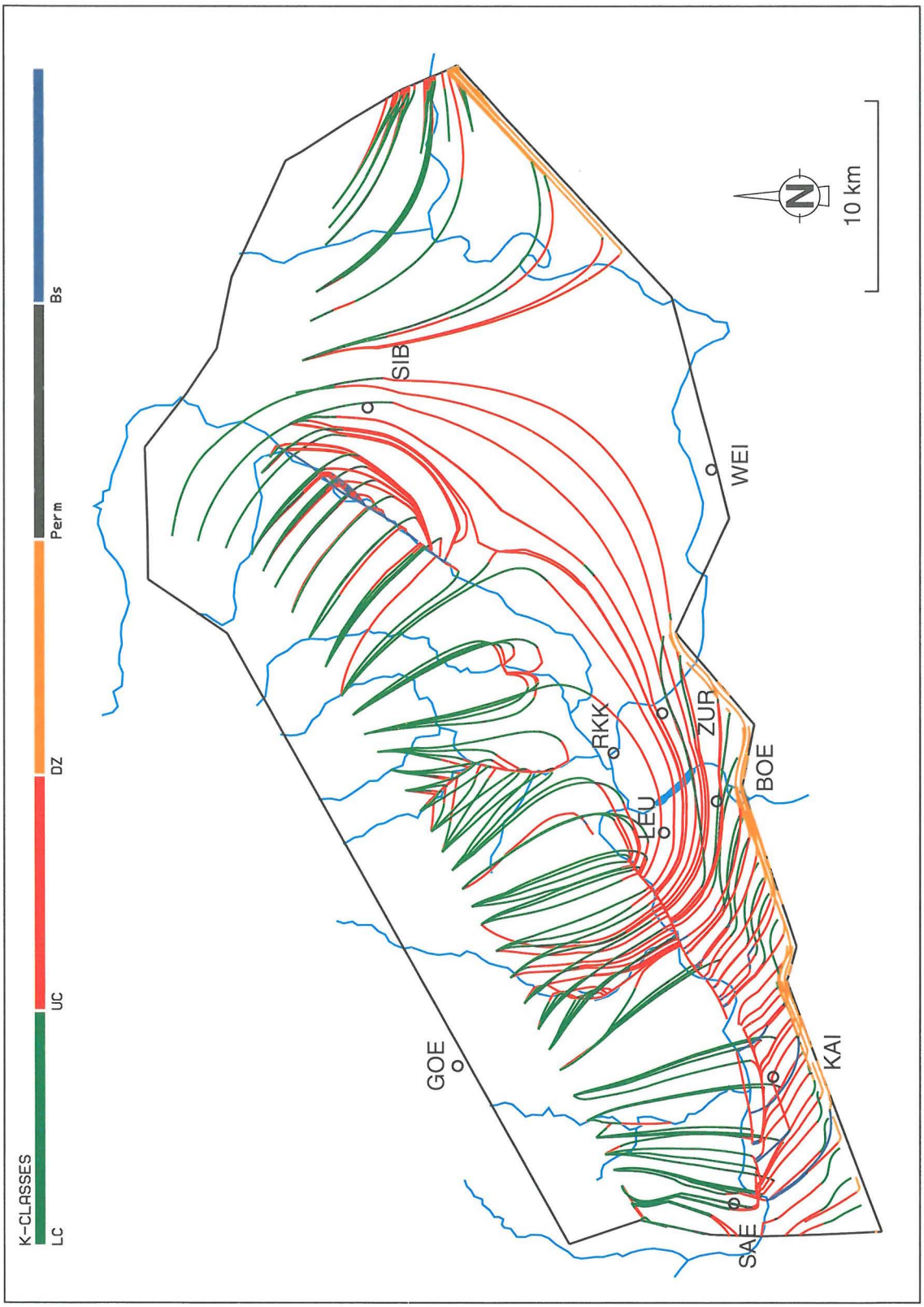

Fig. 3.12 Base case V20z: Flowpaths of particles released within the LC unit along VN, VE and B2 boundary

3.5.3.1 West boundary, VW (Wehra fault)

The closing of the VW boundary in the area between the Rhine River valley and the southern border in run V201 had a small impact on the head distribution in the adjacent model area. The head increase in UC by several meters affects only the first two element rows next to the boundary; no impact is observed at KAI. A similar effect is induced by a modified head condition in run V209, where a "reversed" flow direction from west to east is simulated in UC. The inflowing water is readily drained toward the Rhine River without affecting the heads.

3.5.3.2 North boundary, VN

The vertical VN boundary, which is open over its whole area as default, also proved to have only small effects when closed in V204. The suppressed lateral inflow into the model caused a head decrease in UC/LC units of maximum 140 m; however, the reduction was induced only in the element column adjacent to the boundary. This head change is rapidly dissipated in the model and the remaining part is not affected. When compared to V20, the deficit in recharge is about 44 l/sec, or 8% of the total water turnover in the model. These observations suggest that the resulting lateral inflow across the north boundary is not significant with respect to the total surface infiltration into the UC aquifer unit.

3.5.3.3 East boundary, VE (Randen fault)

The sensitivity of the assumed head conditions at this boundary was tested by first closing the boundary in run V202. The impeded outflow through the eastern corner of the model toward Lake Constance produced an increase of head of 50 m in this corner. Due to sufficient drainage capacity of UC unit toward the west, this higher head (with respect to V20 conditions) is dramatically reduced within short distances, as indicated by simulated heads in WEI (+5 m) and in SIB (+2 m, see Table 3.4). The remaining model area is not sensitive to this modification.

An alternative scenario of open VE boundary with prescribed high crystalline heads was tested in run V206. As a consequence, a significant increase in heads occurred in the region between the Wutach River valley and the southern and eastern model borders. The calculated heads at SIB and WEI exceed the

observed UC values by about 20 m. Again, the model area west of ZUR shows no sensitivity to this boundary variation.

The last alternative of the VE variations, V207, evaluated potentiometric conditions that are required in the east to force the groundwater from SIB to flow toward the Lake Constance and the Neckar River valley (as the possible discharge area for Muschelkalk). The prescribed heads along the VE boundary were iteratively varied from the intersection with the Wutach valley toward south. Due to the draining effect of the open Wutach valley that deflects the flow lines from SIB toward west, a substantial reduction of the heads at the southeastern boundary was required to divert the water flow from the site of SIB to the east. The lowest fixed head in the southeastern corner is 300 m, which is only 40 m above the observed Muschelkalk head at Konstanz. The consequence of this boundary condition is a significant reduction of heads in the region between SIB and WEI. The simulated UC head in the SIB borehole is now 4 m below the observed value; at the site of WEI, this simulation yields the best match with observed heads in the crystalline basement. The western model area (west of ZUR) is not affected by this variation.

3.5.3.4 Wutach valley

The significance of the Wutach River as a possible discharge area for crystalline groundwater is evident from the comparison of simulated heads between the initial run (V20, open conditions) and run V203, in which no communication is allowed (Table 3.4). The impact on the head distribution in the SIB-WEI area is even greater than that of run V206, in which heads at the VE boundary were increased by 100 m. Discharge of groundwater into the Wutach is impeded by an imposition of no-flow conditions, resulting in an increase of heads at corresponding Wutach nodes by maximum of 60 m. At SIB, the head increase is +30 m and at WEI, +17 m. It is concluded that the Wutach boundary condition significantly affects the head distribution in the SIB-WEI area, or in other words, the simulated heads in area East are very sensitive to the Wutach condition.

3.5.3.5 Zurzach well (ZUR)

Based on the initial run V20 (open well condition), the impact of the production well at Zurzach was assessed by closing the well in run V20z. A comparison of both head distributions shows that at the well location, the prescribed head of 337 m corresponds to a drawdown of 49 m with respect to the "undisturbed" head of 386 m simulated in V20z. This drawdown yields a flow of 3.8 l/s, or 38% of the observed value. However, the observed yield of the thermal well can be easily reproduced in the model by increasing the conductivity of UC by only a factor of 3 (run V220). The simulated effects of the induced drawdown at ZUR are visible at the sites of WEI (-6 m), BOE (-11 m) and LEU (-6 m). However, this simulated condition should be interpreted with caution, due to the limitations of the regional-scale EPM model (e.g. schematic discretization and absence of discrete water-conducting faults that control the hydraulics at the ZUR site).

3.5.3.6 Basal flux (B2 boundary)

RYBACH et al. (1987) have proposed upward circulation of deep groundwater as a mechanism for explaining the observed geothermal anomaly in the vicinity of the PCT. The EPM model provides a basis for investigating the impact of such basal flow on the hydrologic regime of the region. An investigation of density-related effects on groundwater flow was carried out in an independent study using a two-dimensional coupled thermo-hydraulic model (RIVERA & RESELE, 1992).

According to the hypothesis of RYBACH, a basal groundwater flux was imposed at the bottom boundary B2 (Fig. 3.5 *bottom*) as a default condition. The effects of the introduced flux into the model are relatively small, as indicated by comparison of simulated heads between the initial case (V20) and the run V205, with zero basal flux (Table 3.4). The maximum head reduction in the case of zero basal flux is 8 m at BOE (bottom). Also the contribution of the basal flow to the total turnover in the model is with about 1% not significant (compare V20 with V205 in Table 3.4).

Generally, heads in the area of BOE-KAI-LEU, south of the Rhine valley, which were already too low under default conditions, now are even further decreased. One consequence is that the vertical hydraulic gradients in this area are reduced to a very low value. This particular model area is bounded by three no-

flow boundaries, at the top, bottom, and in the south. Thus, no significant source of inflow exists, and very small gradients result. Although not dramatic, the effect of incorporating the basal flux generally improves the model results with respect to simulated heads and gradients of crystalline groundwater. Its significance in terms of volumetric flow (influence on mixing of groundwaters) is discussed in Section 3.6.

Because of the uncertainty attached to the basal flow, alternative scenarios to "replace" this flux were tested in the following runs.

3.5.3.7 Leaky Mesozoic cover (T3 boundary)

As an alternative hydrogeological scenario, a locally occurring downward leakage from the Upper Muschelkalk to the Bs and UC aquifers was simulated in the area south of BOE and KAI in run V25 (T3 boundary, see Fig. 3.5 (*top*) for areal extent). This scenario was postulated on the basis of observed high Muschelkalk heads in southern part of the Tabular Jura. The introduced flow rate, q_v (see Table 3.3), at the top boundary had only a small influence on the crystalline heads, because the imposed infiltration was easily drained by Buntsandstein. When compared with run V205 (initial case, but without basal flux), the heads in UC and LC units are raised by 2 to 4 m at the sites of BOE, LEU and KAI (see Table 3.4).

As a sensitivity check, the prescribed vertical leakage flux, q_v, was increased by a factor of 5 in the modified run V250; simultaneously, the conductivity of the Perm layer was also increased by one order of magnitude. Under these conditions, the vertical leakage through the Mesozoic cover has a more substantial effect on the head distribution in UC and LC units, as indicated by the simulated values at BOE (+9 m), LEU (+5 m) and KAI (+17 m). This scenario produced the highest heads at the site of KAI (Table 3.4); however, the results contradict the observed large upward gradient from UC to Bs unit at this site. Furthermore, such assumption of a vertical downward leakage is not consistent with hydrochemical evidence. The Muschelkalk aquifer and the Buntsandstein/Rotliegend aquifer represent different hydrochemical systems. The generally more saline Muschelkalk groundwater is part of an isolated flow system, and there are no hydrochemical indications for hydraulic communications with the deeper Buntsandstein/Perm or crystalline aquifers in the BOE-LEU-KAI area (SCHMASSMANN et al. 1992, PEARSON internal communication 1991).

Hence, it is concluded that this scenario is not a plausible alternative to the basal flux in the BOE-LEU-KAI area.

3.5.3.8 Flux from south (VS boundary)

Based on run V23, which has no Disturbed zone alongside the PCT (i.e., K(DZ)=K(LC)), the vertical southern boundary, VS, was opened in run V24 to allow groundwater to flow laterally into the model from the south. The purpose was to check the simulated effects with the hydraulic and hydrochemical observations. The introduced amount of water had only a negligible effect on heads in UC unit, due to its relatively large draining capacity; however, the change resulted in a substantial increase of heads in the low-permeable LC unit. At the site of BOE, the difference is up to 18 m with respect to V23 (B2+VS=nf) and 11 m when compared to V20, with active basal flux. Also, the site of KAI shows a significant improvement in the match with observed LC head. The head difference LC-UC, as a measure of the simulated vertical gradient, is 16 m as compared to 10 m in V20 (observed: 28 m). Therefore, this model version provides in the target area of BOE-LEU-KAI a generally better match with observed head conditions than the Base case V20 (basal flux), or than the alternative scenario V25 with assumed vertical leakage in the same model region. The only chemical sample that is representative for the deep Lower-crystalline groundwater is from BOE 1,326 m; its chemistry shows affinity to PCT waters and is thus compatible with the concept of saline (PCT) water components in the Lower crystalline unit at this site (PEARSON 1991, internal communication). Flux-balance calculations and estimates of saline-water components are presented in Section 3.6.

3.5.4 Effect of parameter variations

The main objective of the performed parameter variations was to test the "robustness" of the KRI2-model results; i.e., to show how much the simulated flow regime is sensitive to the assumed hydraulic material properties.

3.5.4.1 Anisotropy of Buntsandstein

Simulation of anisotropic flow conditions within the 2-D layer of Buntsandstein (V20a) had a negligible effect on the resulting head distribution in the underlying crystalline basement. The area of BOE-LEU-KAI showed a slight reduction in heads (max. 1.5 m at BOE), whereas the model region southeast of the Wutach (between WEI and SIB) showed higher heads by about the same amount. Both trends are explained by the preferential flow direction from southeast to northwest in western part of the model, and vice versa in the area of SIB.

3.5.4.2 Lateral extent of deep PC trough

In accordance with recent interpretations of seismic data (DIEBOLD et al., 1991), a northern branch of the PCT was introduced into the model in the area southeast of SIB (Fig. 3.8) in run V21. Although this feature represents a potential barrier for the deep groundwater flow from Black Forest toward the region of WEI, it produced only a minor impact on the simulated flow field in this region. As a general effect, the heads at the "upstream" side of the introduced northern trough are slightly higher (SIB: +2 m), and those at the "downstream" side in the south are lower (WEI: -3 m). The remaining major part of the corresponding area is not affected by this modification.

3.5.4.3 Permeability of the crystalline rocks

The hydraulic properties of the crystalline rocks were subjected to variations in runs 22, 220 and 26. Run V22 tests the alternative concept of a gradual, depth-dependent decrease of K in the crystalline basement. The division of the Lower crystalline unit, LC, into four K-classes has a distinct impact on head distribution within LC. This tendency is best described as an enhanced effect of the surface topography on the heads in deeper parts of the crystalline rocks (LC unit). In the region of the southern Black Forest, this effect shows a relative increase of LC heads by about 10-20 m beneath the hills and a corresponding decrease beneath the river valleys. As a result, the horizontal gradients in the Lower crystalline unit generally are increased, whereas the vertical gradients, which in the initial case already are too small, are further reduced (LEU and KAI). Thus, the general effect of this parameter variation on model results is small and points in the wrong direction with respect to the match of heads and vertical gradients in

the LC unit. The flow conditions of UC unit are not affected. As an additional minor modification to V22, the K(UC) was slightly increased in run V220, in order to simulate the observed discharge flow at the thermal well of Zurzach (ZUR). As indicated in Table 3.4, this version yields a head reduction by a couple of meters in the BOE-LEU-KAI area and shows no effect on the remaining part of the model. The substantial increase of the total water flow through the model (Table 3.4) is attributed to increased significance of the local flow systems in the Black Forest region.

In order to cover the possible range of the effective hydraulic properties of crystalline rocks, the upper bounds for the equivalent hydraulic conductivity of the crystalline units were assigned to run V26. The increased equivalent conductivity of LC unit accounts for the relatively high areal density of prominent tectonic features such as suggested by the geometric structural models in AMMANN et al., 1992. The increase of the overall crystalline conductance shows in the total turnover through the model (Q_{tot} in Table 3.4), but has little impact on the head distribution.

3.5.4.4 Disturbed zone, DZ

After switching off the basal flux in V205, the Disturbed zone, DZ, was completely omitted in run V23. This narrow permeable zone along the border of the PCT had a channeling effect on the flow in the low-permeable LC unit. Based on a comparison of the simulated heads with those in V205 (Table 3.4), the absence of this feature in V23 has virtually no effect on the results.

Run V27z is a modification of the initial run V20z, in which the conductivity of DZ is reduced by factor of 10 and the basal flux is maintained. The reduced overall conductance of DZ results in its limited drainage capacity in the east-to-west direction. The effect is a slight increase of heads in boreholes located in southern part of the model. The most substantial change is observed at BOE-deep, where heads increased by +7 m (Table 3.4). The result is an increased upward gradient in KAI and BOE, which yields a better fit to available observations in these boreholes. Therefore, this parameter variation has a positive impact.

The effects of the numerous parameter variations performed in this sensitivity study are summarized in the following section.

Table 3.4 Model KRI2: Comparison of observed and simulated heads

	Φ obs[1].	V20	V20z	V202	V203	V205	V206	V207	V208	V21	V22	V220	V23z	V24z	V25	V250	V26z	V27z
SIB	UC 440	445	446	448	476	445	460	436	496	447	446	445	446	446	445	444	447	446
	LC 440	446	446	449	476	445	461	436	496	448	446	445	446	447	446	444	448	447
WEI	Bs 416	412	418	417	429	410	427	402	445	409	413	414	418	421	410	411	421	421
	P 432	"	"	"	429	"	"	401	445	"	"	"	"	"	"	"	"	"
	UC 414	"	"	"	428	"	"	"	444	"	"	"	"	"	"	"	"	"
	LC 404	"	"	"	428	"	"	"	444	"	"	"	"	"	"	"	"	"
ZUR (337)	Q=10 l/s	3.8 l/s	386	3.8 l/s	4.2 l/s	3.3 l/s	4.0 l/s	3.6 l/s	4.4 l/s	3.7 l/s	4.0 l/s	11.2 l/s	381	390	3.4 l	4.0 l	386	388
	LC -	368	387	368	371	363	369	366	373	369	366	363	382	394	364	367	387	391
RKK	UC 362?	371	380	371	372	369	372	371	373	371	372	370	378	381	370	372	381	381
	LC -	371	386	378	379	375	378	377	380	377	373	371	384	388	370	379	387	387
BOE	UC 364	347	358	348	349	341	348	347	350	347	348	344	351	362	344	356	357	360
	LC 407	348	359	348	349	341	348	347	351	348	348	344	352	365	344	356	357	361
	LC 408	349	360	349	350	341	350	349	352	349	349	344	353	372	344	357	358	367
LEU	UC 362	338	344	338	339	335	339	338	340	338	340	337	341	34	33	343	345	344
	LC 362	338	351	345	345	341	345	344	346	345	340	337	347	6354	7343	350	351	352
KAI	Bs 295	300	300	300	300	298	300	300	300	300	301	299	298	300	305	321	300	299
	P 298	301	301	301	301	299	301	301	301	301	302	299	299	302	304	320	301	300
	UC 322	302	302	302	302	300	302	302	302	302	304	301	300	303	303	319	303	302
	LC 350	312	312	312	312	308	312	312	312	312	307	304	309	320	312	328	312	314
Turn-over	Qtotal (m^3/s)	0.540 100%	0.540	0.484 90%	0.529 98%	0.536 99%	0.541 100%	0.491 91%	0.475 88%	0.539 99.6%	0.588 109%	2.137 396%	0.535 99%	0.541 100%	0.540 100%	0.560 104%	2.190 400%	0.539 100%
	Remarks	**Base case KRI2**	ZUR well closed	VE=nf	Wutach closed	q_0=0	VE=ch "high"	VE=ch "x-low"	VE+ Wutach closed	north. branch of PCT	linear drift[2]	=V22 modif.	DZ off q_0=0	DZ off q_{south}= 5E-11	q_{vert}= 7E-11 m/s	V25 modif[3]	new Keff[4]	as V20 K(DZ) =1E-8

1) Environmental heads from long-term monitoring of Nagra boreholes (see Table 3.1)
2) drift: gradual decrease of K(cryst.) from 1E-07 to 5E-10 m/s. V220: K(UC) increased to 3E-07
3) q(vert) increased to 3.5E-10 m/s (factor 5); K(Perm)=1E-08 m/s (factor 10)
4) new effective properties of cryst.: K(UC)=4E-07, K(LC)=1E-08, K(DZ)=5E-08 m/s

Sensitivity analysis of boundary conditions: runs V201-V209 and V24-V25/250
Variation of hydraulic parameters: runs V20a, V21-V23, V26-V27 are not included in the table due to identical results with V20
V20a (anisotr. in Bs), V201 (VW=nf), V209 (VW=ch high), V204 (VN=nf)

3.5.5 Summary of the sensitivity study of regional flow

The objective of the performed sensitivity analyses was to test the impact of various model (and conceptual) assumptions on the simulated regional flow regime.The results of the sensitivity study are summarized in Tables 3.4 and 3.5, overall conclusions are presented in Section 3.7.

As a means of plausibility checks, Table 3.4 compares the simulated heads at borehole locations to the observed freshwater heads. Another method of consistency checks by means of particle tracking and hydrochemistry is presented in Section 3.6. Note that a formal model calibration was not envisaged in this study, given the sparse database available and the interpretive (i.e., not predictive) character of the regional model.

Head measurements in deep boreholes within the investigation area are used to estimate the direction and magnitude of vertical gradient in the borehole vicinity and of horizontal gradients between the boreholes and outcrop areas. The comparison of observed and simulated heads in Table 3.4 shows deviations of the latter by several meters in most of the boreholes. The observed discrepancy between model and "reality" is due to the following principal reasons:

- Spatial variability of hydrogeological properties, responsible for the presence of local flow condition that are not meant to be reproduced by the large-scale EPM model.

- Effect of boundary conditions: several of the simulated boreholes are located in the vicinity of model boundary (KAI, BOE, WEI) where the flow field is governed by the imposed boundary condition.

- Idealized hydrological processes: the numerical model simulates a steady-state flow of water with unit density. Variable-density effects were addressed elsewere (RIVERA & RESELE 1992) and are neglected in this study. They may have an effect of a few meters in the very deep observation intervals (such as WEI).

- Errors in experimental data: The estimated head values from packer intervals are generally associated with an uncertainty of several meters. Some deep intervals in Nagra boreholes BOE and WEI have errors of up to 10 m for freshwater head and 20 m for environmenal head (PASQUIER et al. 1993).

The response of the simulated hydrodynamic system to parameter variations is summarized in Table 3.5. The impact on the simulated head field is shown separately for the western and the eastern part of the model. The former is characterized by discharge conditions (area of BOE, KAI, LEU, SAE), the latter rather by recharge conditions covering the area between SIB and WEI. Table 3.5 indicates that the simulated system is not sensitive to most of the imposed variations. The simulated head changes at borehole location were generally less than 3 m compared to the base case (see Table 3.4). Significant changes were induced only locally in boreholes affected by a particular boundary condition (V203, V24, V250). Some modifications had a negative impact on the match between simulated and observed heads, as compared to the base case. In the region of WEI the match could be further improved only when prescribing very low constant heads (minimum of 300) at the eastern boundary (variant B6 in Table 3.5).

In the area West, an improved match was achieved (i.e., by increasing the simulated heads at borehole locations) by the following variations with respect to the base case:

1) Zurzach wells closed (B9);
2) Prescribed non-zero flux along the southern boundary VS (B13);
3) Large downward leakage through the top boundary (B12);
4) Significant increase of the equivalent property of crystalline rock units (A5); and
5) Reduction of K(effective) of disturbed zone DZ, simultaneously maintaining the basal flux (A7).
   The above variations B13 and A7 yield the largest vertical gradients at the sites of KAI, BOE and LEU.

Closing of the ZUR well is "visible" at BOE, LEU, RKK and WEI. The simulated "undisturbed" head at ZUR is 386 m (i.e. 50 m above the actual draw-down level); this elevation would fit well into a linearly interpolated undisturbed head surface between WEI (403) and BOE/LEU (365). The observed production flow rate at ZUR was reproduced by a slight increase of the effective conductivity of the UC unit.

The observed upward hydraulic gradient in area West can be reproduced only when flow is introduced into the Lower crystalline unit from the south, i.e., from PCT (B13).

Table 3.5 Results of sensitivity analyses with the regional model KRI2

Modified model parameter or condition	General impact on head distribution in crystalline units (compared to base case)[1]	
	Area West (BOE-KAI-LEU)	Area East and Southeast (SIB and WEI)
A. Geometry or property of material unit		
1. Anisotropy in BST	-	-
2. Integration of northern PCT	-	-
3. Gradual decrease in K(LC) with depth	UC: - LC: ↓ (KAI, LEU)	-
4. Small increase in K(UC)	UC: - LC: ↓	-
5. Large increase in K of UC, LC and DZ	↑ (BOE, LEU)	↑ (WEI)
6. DZ inactive, no basal flux	-	↑ (WEI)
7. K(DZ) reduced	↑ (BOE, LEU)	↑ (WEI)
B. Boundary conditions		
1. VW closed (no flow)	-	-
2. VE closed (no flow)	-	↑ (WEI)
3. VN closed (no flow)	-	-
4. High head at VW	-	-
5. High head at VE (500 m)	-	↑
6. Very low head at VE (300)	-	↓
7. Wutach valley closed (nf)	-	↑
8. Wutach and VE closed	-	↑
9. Zurzach wells closed	↑ (BOE, LEU)	↑ (WEI)
10. No basal flux (B2 no flow)	↓	-
11. Small local downward leakage (area KAI-BOE)	-	-
12. Large downward leakage, increase of K(PCTs)	↑	-
13. VS open, no DZ	UC: ↑ (BOE, LEU) LC: ↑	-

1 - head change not significant, head increase (↑) or decrease (↓), generally by 3-10 m, maximum change 50 m

3.6 Analysis of specific fluxes

One of the important contributions that was expected from the regional model was information on volumetric flow through a specific area of interest. The principal issue, expressed in review comments and internal discussions, was the origins and proportions of highly mineralized deep groundwater that is mixed with low-mineralized water of the Black Forest province in the area between the boreholes BOE, LEU and KAI, south of the Rhine valley. The identification of such specific fluxes in the model enables thus a comparison of the simulated groundwater regime with the observed hydrochemical system. This comparison provides a plausibility check of the model results. The hydrochemical characterization of the deep-groundwater system in the crystalline basement of Northern Switzerland was summarized in Section 3.2.2.

3.6.1 Approach

The objective of the flux-balance calculations was to discriminate among different water components according to their origins in the model area represented by BOE and LEU. For this purpose, a small element box comprising the Upper and Lower crystalline unit was selected as a sub-model in the area of interest.

Two types of analyses were performed. In the first, the technique of backtracking was applied, in which each flow particle that enters the box is traced backward in upstream direction to its point of origin. This technique allows visualization of the advective flowpaths of waters that are intercepted by the box. However, these particle travel paths are not stream tubes, i.e., they are in no relation to volumetric flow. Thus, the display of the flow lines contains no information on volumetric proportions and serves only for a qualitative identification of potentially saline or non-saline flow components.

In the second analysis, a flux balance (inflow and outflow) was calculated for each face of the box for selected runs (Table 3.5). By comparing the total turnover through the box with estimated volumes of water intercepted from different origins (identified by backtracking, e.g. Black Forest, PCT), the proportions of potentially saline components in the box were estimated.

In the analyses, water in the box was assumed to consist of either low-

mineralized water or highly mineralized (i.e., saline) water, or a combination of both. Consistent with the understanding of the flow regime that has been derived from hydrochemistry (Section 3.2.2), low-mineralized water is assumed to have originated as recharge in the southern Black Forest massif and to have travelled relatively short flow paths. This water is hereafter termed "Black Forest water". Saline water is assumed to have three potential sources: 1) water that was recharged in the Black Forest but that has travelled relatively long flow paths, resulting in an advanced degree of chemical evolution; 2) basal flux, introduced from below along the western section of DZ; and 3) water entering laterally from the PCT in the south. The first type has flowpaths that follow the northern border of deep PCT and pass through the Weiach area, and thus is hereafter termed "Weiach water".

Weiach water enters the DZ at its eastern end near Zurzach; the basal flux enters the DZ through its open bottom section B2 (Fig. 3.4 *bottom*); and PCT water is allowed to enter the DZ laterally along its open southern boundary in Run V24, which has the same longitudinal extent as the B2 zone. All these saline waters are assumed to have similar chemistry as groundwater type (4), according to Section 3.2.2.

As described below, various model runs were selected that emphasize or eliminate the various potential sources of saline water, in an effort to define the scenario that best accounts for observed hydrochemical conditions.

3.6.2 Flowpath description

The location of the box and the resulting flow patterns for two selected simulations are shown in Fig. 3.13. Backtracking was done from the eastern and southern box boundaries that intercept all deep groundwater entering the box.

Fig. 3.13A shows the base case V20z (ZUR well closed) with active basal flux. Most flow lines follow relatively direct routes from the Black Forest to the eastern boundary of the box, indicating that the major flux component consists of the low-mineralized Black Forest water. The LEU area, for example, intercepts only Black Forest water from the north. Another group of flow lines originates in the northeastern corner of the model (in the region of the upper Wutach valley), passes through the SIB and ZUR area and enters the box between BOE and LEU. A third group of flow lines that enters the box in the BOE area and through

the southern boundary originates directly from the DZ. This southeastern flux component into the box is assumed to consist of a combination of saline Weiach water and basal flux (also saline).

A different flow pattern is simulated in a case with zero basal flux but with DZ present (V205z, Fig. 3.13B). The area of BOE is now also supplied directly by Black Forest from the north. Without the basal flux as driving force, the DZ water enters the box only along the southern boundary. In this case, the DZ water originates in the upper Wutach River valley and represents chemically more evolved water from SIB. Therefore, the intercepted DZ water has significantly shorter flowpaths than the Weiach water in the base case (Fig. 3.13A), and, consequently, is likely to exhibit a lower degree of hydrochemical evolution (and thus salinity). Consequently, the DZ water in this case more likely resembles the chemistry of the Black Forest water than that of Weiach water and basal flux.

In the case of Run V23z (not shown), with zero basal flux **and** inactive DZ, both the eastern and southern box boundaries are supplied by Black Forest water with travelpath of different length. Also in this scenario, no saline water enters the box from the southeast. However, this does not exclude the possibility that the chemistry of the southern-most flowlines is influenced by the adjacent PCT.

The effect of prescribed lateral flow into the model was investigated in Run V24z. This is the only case in which saline water from the PCT enters directly the box. The water introduced along the VS boundary affects the flow regime only in the low-permeable LC unit where it generates a relatively large local gradient from south to north. The backtracking results suggest, that this saline component is present over the entire box area.

3.6.3 Flux-balance calculations

The balance calculations shown in Table 3.6 provide a basis for estimating the relative contributions of the saline-water component to the total turnover in the box. The table shows for some of the selected runs the flux across each face of the box within the Upper and Lower crystalline unit, the total fluxes, and the resulting net balance.

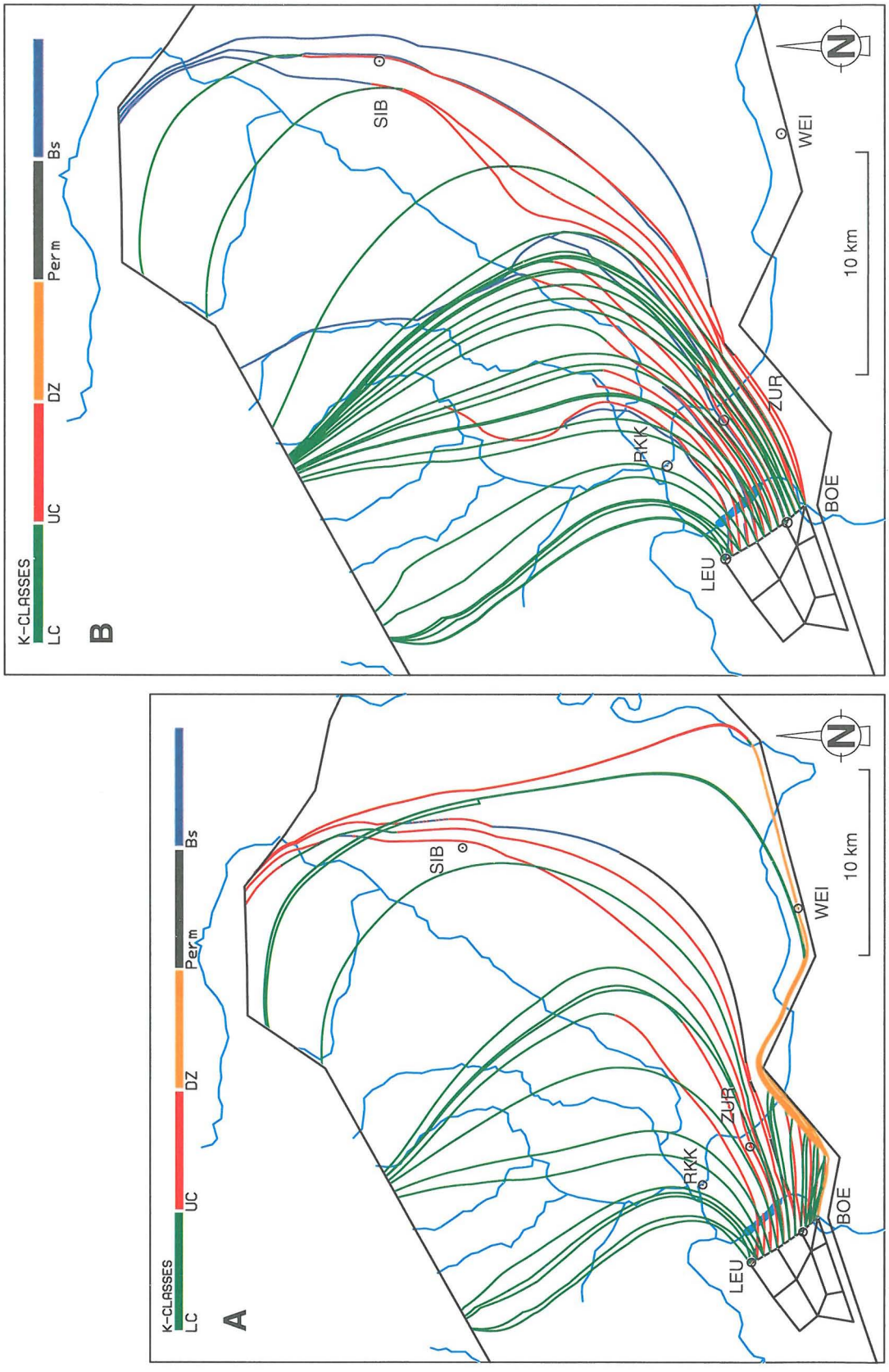

Fig. 3.13 Backtracking results in V20z (A) and V205z (B)

Table 3.6 Results of flux-balance calculations in KRI 2 sub-model (box)

Upper unit (UC)	V20z ($q = q_0$)		V205z ($q = 0$)		V23z (no DZ, no q)		V24z (q south)	
	in (l/s)	out (l/s)	in (l/s)	out (l/s)	in (l/s)	out (l/s)	in (l/s)	out (l/s)
North	0	-1.621	0	-1.291	0	-1.269	0	-1.732
South	0.702	0	0.247	-0.060	0.097	-0.003	0.517	0
West	0	-0.681	0	-0.602	0	-0.600	0	-0.678
East	1.454	0	1.492	0	1.543	0	1.517	
Top	0.243	-0.264	0.279	-0.196	0.331	-0.173	0.287	-0.259
Bottom*)	0.062	0	0.048	-0.002	0.048	-0.003	0.305	0
TOTAL UC:	**2.461**	**-2.566**	**2.066**	**-2.151**	**2.019**	**-2.049**	**2.626**	**-2.668**

Lower unit (LC)	V20z ($q = q_0$)		V205z ($q = 0$)		V23z (no DZ, no q)		V24z (q south)	
	in (l/s)	out (l/s)	in (l/s)	out (l/s)	in (l/s)	out (l/s)	in (l/s)	out (l/s)
North		-0.031	0.006	-0.019	0.006	-0.018	0	-0.056
South	0.052		0.007	0	0.003	0	0.374	0
West		-0.034	0	-0.029	0	-0.028	0	-0.056
East	0.065		0.070	0	0.073	0	0.041	-0.015
Top*)		-0.062	0.002	-0.048	0.003	-0.048	0	-0.305
Bottom	0.003		0	0	0	0	0.001	0
TOT. LC:	**0.120**	**-0.127**	**0.085**	**-0.096**	**0.086**	**-0.095**	**0.415**	**-0.432**

TOTAL):**	**2.519**	**-2.631**	**2.101**	**-2.197**	**2.053**	**-2.092**	**2.736**	**-2.796**
BALANCE	-0.112 (4%)		-0.096 (5%)		-0.039 (2%)		-0.059 (2%)	

*): for numerical reasons, fluxes through the internal boundary between Upper/Lower crystalline units are assigned values computed at Top LC

**): Total turnover in UC+LC excluding flux through internal boundary (Bottom UC and Top LC)

The following observations are made from balance calculations in Table 3.6:

- Flow enters the box from the east and from DZ in the south and leaves to the north and west toward the regional discharge area at the Rhine River;

- Flow through the LC unit contributes less than 5 percent to the total turnover in the box;

- The numerical precision of flux integrations is expressed by the resulting balance.

Based on these balance calculations, the percentage of total turnover in the box that is saline was derived from the evaluation of specific areal fluxes, as schematically illustrated by Fig. 3.14 below.

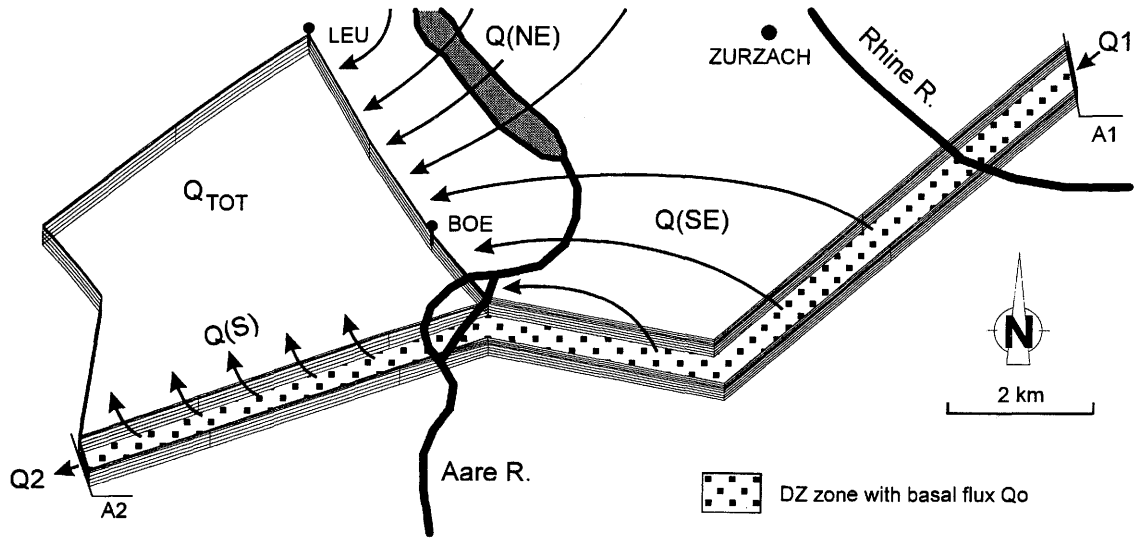

Q_{TOT}:	Total turnover in the box
Q(NE):	predominantly Black Forest water
Q(S,SE):	predominantly saline water;
Q1, Q2:	integrated flow, see text

Fig. 3.14 Evaluation of flux components intercepted by the box

The volumetric contributions of the different flow components are calculated as follows:

Q0: Portion of basal flow, Q_0, entering DZ within the relevant reach situated upstream and south of the box; obtained by integration of prescribed Darcy flux, q_0, over the relevant bottom area of DZ.

Q1: Weiach water, entering DZ from the east; integrated over the hydraulic cross section A1

Q2: Saline water (of Weiach plus basal origin) leaving DZ toward the west (thus, it does not appear in the box balance); calculated by integration over the hydraulic cross section A2

The total turnover in the box consists of Black Forest water (BF) and saline-water components, as follows:

$$Q_{TOT} = Q_{BF} + Q_{SAL}$$

According to Fig. 3.14, the saline-water components, Q_{SAL}, in the box consist of 1) Q(SE), which comes from the DZ upstream of the box and enters through E boundary; and 2) Q(S) which enters directly from DZ through S boundary. Both inflows, Q(SE) and Q(S), may be a mixture of the basal flow and Weiach water. Therefore, the net volume of saline water in the box is:

$$Q_{SAL} = Q(SE) + Q(S) = Q0 + Q1 - Q2$$

Q0, Q1 and Q2 values were obtained in Fig. 3.14 above from flux integration over the corresponding cross-sectional areas. Q(S) was obtained directly from the box balance in Table 3.6 and Q(SE), which is the a priori unknown saline component of inflow through the E boundary, is the remaining portion of the total saline water volume (Q0+Q1-Q2). The results of these mixing-ratio evaluations are summarized in Table 3.7 below.

The results of Table 3.7 show that the contribution of saline groundwater to the total turnover ranges from presumably a few percent (not determinable) in runs V205 & V23 to more than 60 percent in V20, V24 & V27. Based on the observed chemistry of groundwater from the UC unit in the box area (LEU, BOE), about 3-4 percent of the water is estimated to be saline (SCHMASSMANN, personal communication 1991). Thus, the simulated volumetric proportions in Table 3.7 are substantially greater than expected for all model realizations with prescribed external fluxes. The calculated large percentages of saline water are the net result of 1) the relatively small total volume of water flow through the box, due to the low hydraulic gradients that the model simulates in this area; and 2) the relatively large prescribed saline inflow, either as basal flux or as lateral flux from the south. Even run V26z, with a significantly increased total turnover due to a larger conductance of crystalline rocks still shows a high proportion of saline water (18%).

Table 3.7 Estimation of saline-water components in the box

	V20z Q0=5 l/s DZ=1E-7	**V205z** Q0=0 DZ=1E-7	**V23z** Q0=0 no DZ	**V24z** Qs=5 l/s no DZ	**V27z** Q0=5 l/s DZ=1E-8	**V26z** Q0=5 l/s new Keff
1. Q_{TOT} (l/s) =turnover	2.6	2.1	2.1	2.8	2.6	9.2
2. Q0 (l/s) =Q(basal)	1.63	0.0	0.0	1.9 Q(south)	1.6	1.5
3. Q1 (l/s) =Q(DZ) in	0.50	0.7	-	-	-	0.4
4. Q2 (l/s) =Q(DZ) out	-0.53	-0.5	-	-0.1	-	-0.2
Net Q_{SAL} (l/s)	1.6	< 0.2[1)]	--[2)]	1.8	1.6	1.7
vol. % of total	61.5	< 9.0[1)]	--[2)]	64	61.5	18

1) Flowpath analysis (Fig. 3.13B) shows that the water entering the box through S boundary consists mostly of Black Forest water. A possible minor admixture of saline Weiach-type water cannot be identified explicitly.

2) Because both DZ and basal flux are non-existent, all water that enters the box along the E and S boundary comes from Black Forest in NE. Although some might be a highly-evolved Weiach-type water due to long travel paths, its proportion cannot be determined separately.

On the other hand, for both scenarios with zero basal flux (and no flow along VS), V205 and V23, no saline-water component can be identified in the box, which is supplied only by Black Forest water from the northeast. For this water, some flow paths from the Black Forest are longer than others. It is thus reasonable to assume that also in these cases, minor amounts of highly-mineralized water enter the box, although this volume can be evaluated neither by the flux balance calculations nor by the flowpath analysis (stream-tube technique required). Hence, these model realizations, which have no specifically defined saline-water components in the Upper crystalline unit in the BOE-LEU area, provide the best match with hydrochemical observations. The same simulations, however, fail to fit the observed head and gradient conditions in that area (see Table 3.4). It is conceivable that a) the box volume and b) the EPM approach are not adequate to provide a representative description of the overall flow conditions (see also comments below).

The simulated proportions of the saline flux with respect to the total turnover apply to the box as a whole. On the basis of the origins of water entering the box, some qualitative judgments can be made about the distribution of saline waters within the box. The general trend, displayed by the flow pattern in the base case V20z, indicates that the water within the box could range from "all saline" along the southern edge to "all Black Forest type" in the area of LEU (Fig. 3.13A). These mixing conditions are schematized in Figure 3.15 below.

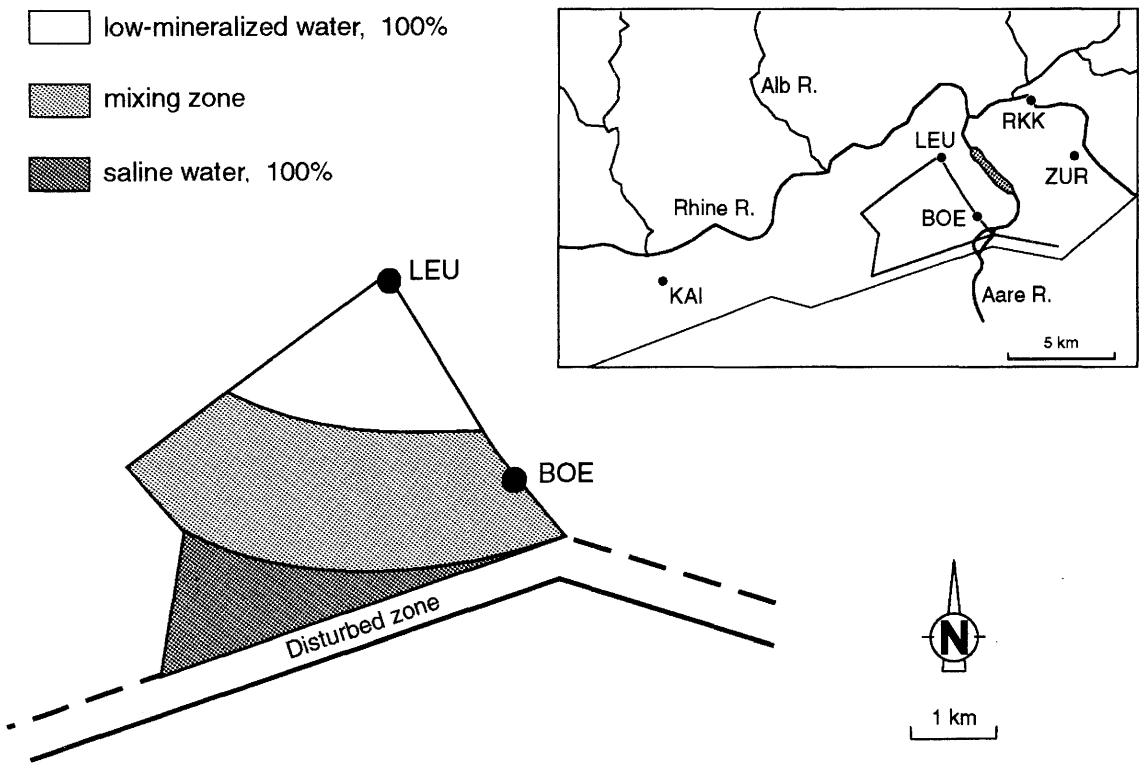

Fig. 3.15 Areas of saline-water components in the box

According to this pattern of mixing, the aforementioned high proportions of saline-water components, simulated in runs with prescribed external fluxes, apply mainly to the area of BOE (Fig. 3.13A). Thus, the model results contradict the observed groundwater chemistry at this site (see Section 3.2.2).

On the other hand, the simulated flow pattern in the vicinity of the LEU site - as displayed by Darcy vectors in Fig. 3.10 (*top*) or by particle tracking results in Fig. 3.13A - indicates the presence of low-mineralized Black-Forest water only, i.e., no mixing with saline components. Thus, in this area, the model simulations are consistent with the observed hydrochemistry (but not with the observed heads).

3.6.4 Conclusions from flowpath and flux analyses

From the evaluations of the flowpath pattern and of the flux calculations given in Tables 3.6 and 3.7, the following conclusions are made:

1) Saline groundwater in the box has three potential sources: the deep-seated basal flux, the highly evolved "Weiach"-type water, and PCT water;

2) The model simulates a large percentage of saline-water components in the box in all runs that have imposed external fluxes as boundary condition. This effect is the combination of 1) the relatively small total turnover, which in turn is caused by the small hydraulic gradients that the model simulates within the area south of the Rhine River valley; and 2) the relatively large prescribed basal flux or lateral PCT flux;

3) The simulated occurrence of saline water coming from the south and south-east in the Upper crystalline unit of the BOE area contradicts the observed water chemistry at that site. Hence, this result argues against the existence of a basal flux or a lateral inflow from the PCT, or, at least against the assumed magnitude. A reduction of the imposed basal flux by a factor of 10 or more would be required to reproduce a more realistic proportion of saline water in the box;

4) The conditions simulated in runs that have no external fluxes (V205, V23) most closely match observed conditions. The existence of a transmissive DZ alongside the deep PCT is not contradicted by these results, given that the flow regime in DZ is dominated by an axial flow from E to W. Thus, under this scenario, only minor amounts of saline Weiach-type water do enter the BOE area.

3.7 Conclusions based on KRI2 results

Based on the presented evaluations of KRI2 modeling results and on comparison with available hydrologic observations, the following conclusions are made with respect to the processes and parameters that govern the regional flow of deep groundwater in the crystalline basement of north-eastern Switzerland. The conclusions are summarized under project-specific subjects that were explicitly addressed in the study.

3.7.1 Boundary conditions

1. Groundwater flow in the SIB area is influenced primarily by the hydraulic connection with the Wutach valley. Observed heads in SIB and WEI are best reproduced by the model when Wutach valley is open (discharge condition!).

2. To a lesser extent, the groundwater flow in the SIB area is also influenced by the imposed draining condition of the East boundary, VE. The induced eastward flow due to drainage across a large normal fault (Randen) to the Upper Muschelkalk and the existence of an corresponding groundwater divide is consistent with the resulting head distribution in the model and with observed horizontal gradients in the Upper crystalline unit in the SIB-WEI area. This scenario of eastward flow across the Randen Fault has not been initially considered in the conceptual model of regional groundwater flow, it was rather included as a result of model simulations.

3. The conditions at the West, North and East boundary are not sensitive with respect to head distribution in the western target area between BOE, LEU and KAI.

4. The geothermal well of ZUR is a sensitive boundary condition in the model. The open well (i.e., free outflow at elev. 337 m) as a default condition produces a drawdown of 49 m with respect to undisturbed condition, affecting BOE (-11 m), RKK (-9 m), WEI (-6 m), and LEU (-6 m).

5. Heads in the western area of interest, delimitated by the sites of BOE, LEU and KAI, cannot be satisfactorily reproduced by the EPM model, despite several efforts that specifically addressed this issue. The simulated head distribution, in particular the very small gradients, proved insensitive to all model variations, except to those with prescribed external fluxes into the model in this area. This insensitive response to parameter variations is related to the particular hydrologic setting of this area, which is bounded from three sides by no-flow boundary conditions (model top, bottom, and vertical south boundary).

6. Among the realizations with prescribed external fluxes the version with lateral flux from the adjacent PCT best simulates the observed vertical gradients between the LC and UC unit at the sites of BOE and KAI. More-

over, the assumption of a basal flux that accounts for an observed heat-flow anomaly (RYBACH et al., 1987) is also consistent with the head distribution. However, both boundary conditions produce a high volumetric proportion (mixing ratio) of these fluxes in the investigated area of BOE, which is in contradiction to the observed water chemistry (see No. 8 and 9 below).

3.7.2 Parameter variations

7. Variations of model parameters resulted in no substantial impacts on the simulated flow regime, indicating that the general flow pattern reproduced by the model is relatively insensitive to parameter variations. This insensitivity is attributed partly to the effect mentioned above (No. 5) and partly to the generally large conductance of the Upper crystalline EPM unit, persistent throughout all model variations. Such a large conductance, defined as the product of the K value and the cross-sectional flow area, allows for compensation of all changes introduced to the system.

3.7.3 Flux balance

8. The model results indicate that large saline-water components occur within the Upper crystalline unit in area of BOE, which contradicts the hydrochemical evidence. The calculated large proportion of saline waters is due to the relatively high prescribed saline fluxes (boundary condition) with respect to the total turnover. In the area of LEU, the model results match the observed water chemistry.

9. The flux calculations allow the following conclusions:
   - The flux-analysis results argue against the presence of the basal flux (see No. 6) or a lateral flux from the south. The realizations with zero external fluxes provide the best match with observed conditions.
   - The existence of a highly transmissive DZ is not contradicted by the model results.

3.7.4 Regional flow system

10. The model results generally support the conceptual model of regional flow that is governed by groundwater recharge in the southern Black Forest and a principal discharge area along the Rhine River. Furthermore, the simulations disclosed the potential significance of some hydrologic conditions that were not envisioned in the initial concept, such as the possible discharge condition in the Wutach valley and the occurrence of a groundwater divide east of Siblingen.

11. Whereas the simulated flow directions and horizontal gradients are reasonable, the model generally could not reproduce the vertical gradients observed in the deep boreholes, in particular at the sites of BOE and KAI. As expected, the model simulates upward flow beneath the discharge area of the Rhine River valley but not in the adjacent region in the south. The observed vertical head distribution at the sites of BOE and LEU may, in reality, reflect local flow conditions that are not representative for the area. At the site of LEU which is located near the principal discharge area, the observations indicate constant head conditions along the borehole, that contradict the generally expected (and simulated) discharge regime in this area.

3.8 Impact of discrete major faults: Model KRI3 (1992)

3.8.1 Background

Given the inability of the KRI2 model to reproduce the observed vertical hydraulic gradients in the area of interest (BOE-LEU-KAI), the question was raised as to what extent the real hydrologic system of that area and throughout the region is dominated by discrete large-scale tectonic features, such as the Eggberg and Vorwald faults, which were not explicitly considered in the EPM model. To address this question, a third phase of the regional groundwater modeling study, designated KRI3, was launched. This stage represents an intermediate step between the regional continuum (EPM) model and the hybrid model at next smaller modeling scale according to Fig. 1.2. The implementation of the KRI3 model required a posterior insertion of new and arbitrarily oriented faults into the existing 3-D mesh of the KRI2 model. This task, which is by no means a trivial

one, required a substantial effort in software development. For this purpose, the brand new mesh generator FRACMESH (HÜRLIMANN 1994), which was currently being developed for the specific needs of the forthcoming hybrid study (Chapter 4), was extended by an additional option, the INSFRAC algorithm, to address this problem.

3.8.2 Model characteristics

The KRI3 model has the same structure as KRI2 but it additionally incorporates several faults of first order that are reproduced explicitly as 3-D elements. Beside the well-known and mapped faults of Eggberg and Vorwald in the western part, five less certain structures were considered toward the east, in accordance with the structural map of southern Black Forest in DIEBOLD et al. (1991, Appendix 40). These prominent faults represent in fact the limiting planes of major tectonic blocks in the crystalline basement and are, from mechanical standpoint, the major planes of displacement. The location of the inserted faults in the model is displayed in Fig. 3.16 *top*. The spatial orientation of these faults, as seen from west to east in Fig. 3.16, is indicated in Table 3.8. A detail of the resulting Finite-element mesh KRI3 is displayed in a perspective view (looking from South) in Fig. 3.16 *bottom*, showing the western model part. Because all faults are inclined and transect many existing vertical element columns, a large number of new Finite elements had to be generated at the intersections.

The modeled faults were assigned a default thickness of 500 m, which is the average of the expected range for 1st order faults according to definition in AMMANN et al (1992). The hydraulic properties of the faults were assumed to be virtually identical with those of the Upper crystalline unit, in accordance with the borehole-data synthesis. All but one model parameter and all boundary conditions were adopted without change from the run V20z as the base case scenario in KRI3, designated as V30z. The exception is due to the explicit treatment of faults (instead of EPM approximation), which leads to an increase of the total conductance of the model in the Lower crystalline domain. Therefore, the equivalent permeability of the LC unit was reduced by a factor of 5 to compensate the presence of high-permeable faults.

In order to depict the numerical complexity of a regional-scale model that includes discrete tectonic features, the characteristic parameters of the numerical models KRI2 and KRI3 are compared in Table 3.9 below. This table documents

the drastic impact of the inserted faults in KRI3 mesh on the total number of nodes and elements and its consequences for the required computational effort, expressed in terms of disc space and CPU time.

Table 3.8 Orientation of first-order faults in KRI3 model

Fault Zone N°	Name	direction of dip (°)	Dip (°)
FZ 1	Eggberg	204	55
FZ 2	Vorwald	204	70
FZ 3	"generic"	204	80
FZ 4	Hotzenwald N	024	80
FZ 5	Häusern-Graben S	024	80
-	Häusern-Graben N	not modeled	
FZ 6	Bonndorf-Graben S	011	80
FZ 7	Bonndorf-Graben	011	80

Table 3.9 Comparison of model characteristics between KRI2 and KRI3

	Model KRI2 (91)	**Model KRI3 (92)**
Model area	1,300 km^2	1,300 km^2
Number of nodes	7,320	19,641
Number of elements	2,046	14,096
Size of equation file	22.5 Mbytes	145.2 Mbytes
CPU time (STARDENT)	150 sec	2,160 sec

3.8.3 KRI3 results

The principal objective of the KRI3 modeling phase was to evaluate whether an integration of some prominent faults into the regional model would have a significant impact on the simulated flow system. Therefore, only a few runs were realized with the KRI3 model.

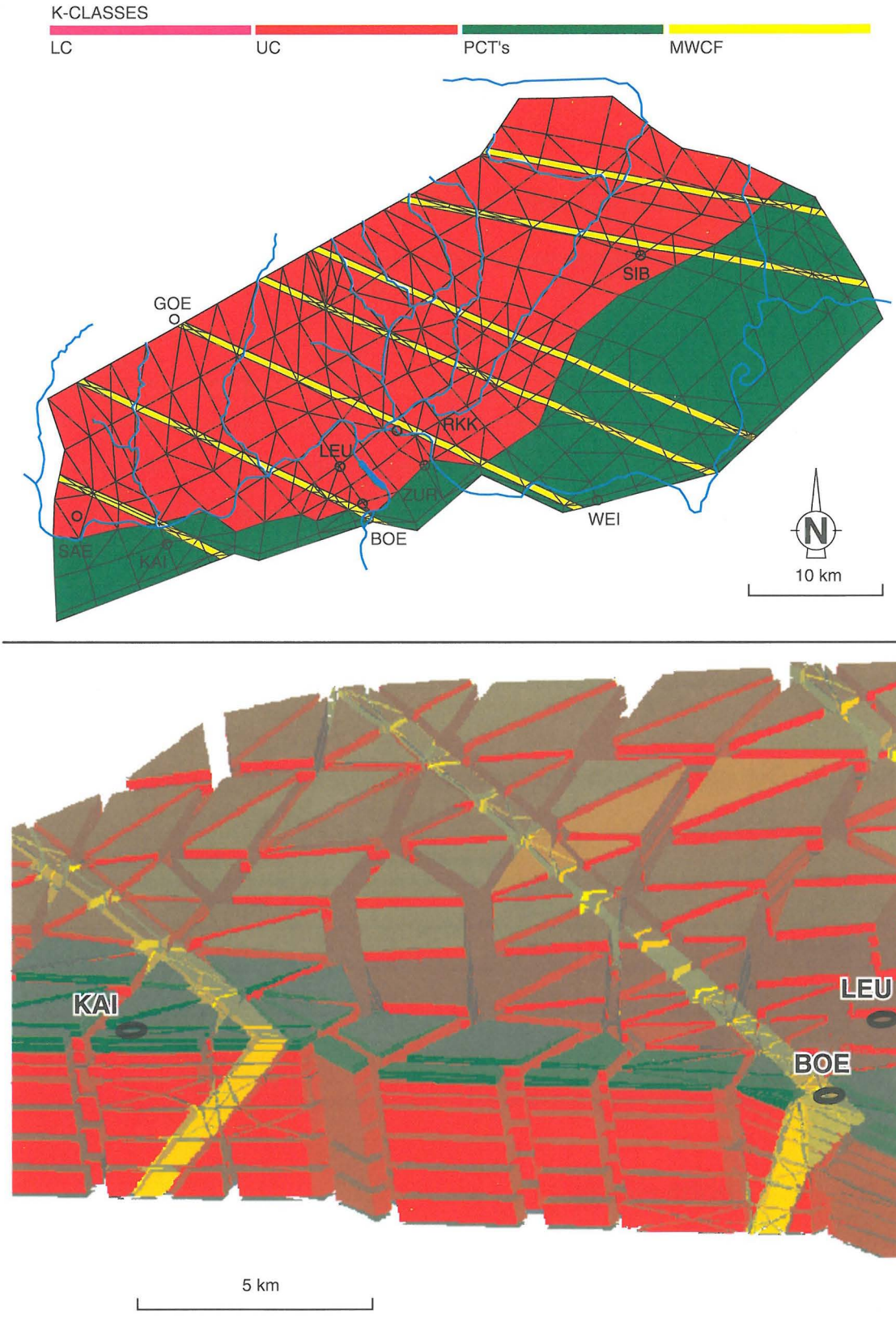

Fig. 3.16 Model KRI3: Location of explicitly modeled major faults of 1st order *(top)*, detail of the resulting FE mesh *(bottom)*

In the Base case **V30z**, all discrete fault zones are hydraulically active, with a prescribed conductivity K = 1·E-07 m/s; i.e., identical to the UC unit and the DZ in KRI2. Thus, the faults have no impact on the hydraulic properties of the Upper crystalline unit nor on the head distribution in that unit.

In the next run **V31z**, the fault zones were "switched-off" by adjusting their conductivity to those of the intersected background rock (LC unit, DZ, or Perm). Hence, this run is identical to the Base case V20z of KRI2 and serves for comparison purposes.

An additional sensitivity run was realized in **V32z** that considers the Vorwald fault as a barrier for the flow within the Upper crystalline unit and also in the DZ. The permeability of this fault was reduced to 1.0E-09 m/s, whereas all other faults have the default properties.

The simulated regional flow pattern in the Base case V30z is illustrated in Fig. 3.17 by means of areal head distribution (*top*) and particle paths lines (*bottom*). Because the faults have no hydraulic significance in the Upper crystalline unit, the head-contour map is plotted onto a horizontal section within the Lower crystalline unit (level 2 in Fig. 3.4). In areas of steep hydraulic gradients, distinct kinks in the contour lines indicate a channeling of flow into the fault zones. The water movement within the faults is mainly in the axial direction; the faults, therefore, produce a flow anisotropy in the NW-SE direction. The general head distribution, however, is not significantly affected by the presence of faults.

The bottom map of Fig. 3.17 shows the impact of faults on the advective particle transport. The release points for the flow particles are the same as in Fig. 3.12 of KRI2 model. The inserted permeable faults turn out to act as a hydraulic trap for the incoming particles by draining almost all water from upstream. Only few flowlines in Upper crystalline unit and Buntsandstein pass across the faults and reach the western model area in the vicinity of ZUR, BOE and LEU boreholes. A such anisotropy effect on the flowpath routing is somewhat unexpected, given that the faults have the same hydraulic property as the UC unit representing background rock. It bears noting that this simulation effect is in contradiction to the hydrochemical evidence. It is concluded, therefore, that not all regional faults are hydraulically active.

The effects of faults on the vertical head distribution are depicted in two cross sections in Fig. 3.18. In order to show the impact of two prominent regional

faults in Northern Switzerland, section WW' through the site of KAI was selected in Fig. 3.18 *top* (see Fig 3.4 and 3.17 for location), illustrating the head distribution across the Vorwald fault (left, dominated by recharge conditions) and the Eggberg fault (right, under discharge conditions with upward flow). Fig. 3.18 *bottom* shows section BB' through the sites of RKK and ZUR (see Fig. 3.17), which can be compared to Fig. 3.11 of KRI2. As a general trend, the faults produce a slightly higher heads in the Lower crystalline unit in the recharge areas and have the reverse effect in discharge areas, due to enhanced drainage capacity. The head differences in the LC unit induced by the presence of permeable faults are, however, only a few meters, as can be seen from the comparison of simulated and observed heads in the boreholes in Table 3.10 below.

A comparison of simulated heads in the Base-case scenarios of KRI3 and KRI2 models in Table 3.10 shows that the integration of faults into the model in V30z produces higher heads in all boreholes, except for KAI-deep which is affected by the Eggberg fault (see Fig. 3.18 *top*). The vertical hydraulic gradients between the LC and UC units are further reduced by the faults, due to the increased total conductance of the Lower crystalline unit.

When "switching-off" the faults in run V31z, i.e., simulating the same conditions as in KRI2 model, the heads remain still a few meters above those in V20z. This difference is assumed to be caused by numerical modifications of the KRI3 grid that resulted in somewhat different vertical coordinates of the nodes and, hence, in different boundary conditions at the top (h=z condition).

The simulation of a low-permeable fault zone (Vorwald) in V32z shows a significant impact only at BOE, i.e., locally near the intersection with the DZ. Here, the Vorwald fault cuts-off the flow within the DZ zone and produces a local increase of heads.

Table 3.10 KRI3: Comparison of simulated heads with borehole observations

	observed head	KRI2 v20z	KRI3 V30z	V31z	V32z
SIB	UC 440 LC 440	446 446	452 453	448 449	453 453
WEI	Bs 416 P 432 UC 414 LC 404	418 " " "	423 " " "	420 " " "	425 424 " "
ZUR	Q=10 l/s LC -	386 387	394 396	390 391	399 400
RKK	UC 362? LC -	380 386	393 402	386 391	395 404
BOE	UC 364 LC 407 LC 408	358 359 360	363 364 364	362 363 363	371 372 372
LEU	UC 362 LC 362	344 351	351 358	348 355	352 360
KAI	Bs 295 P 298 UC 322 LC 350	300 301 303 312	301 302 304 308	300 301 302 310	301 302 304 308
Flux	Total (m^3/s)	0.539 100%	0.530 =98%	0.483 =90%	0.514 =95%
	Remarks:	KRI2 base case	KRI3 base case: all FZ active	same as KRI2, all FZ inactive	Vorwald F. as barrier

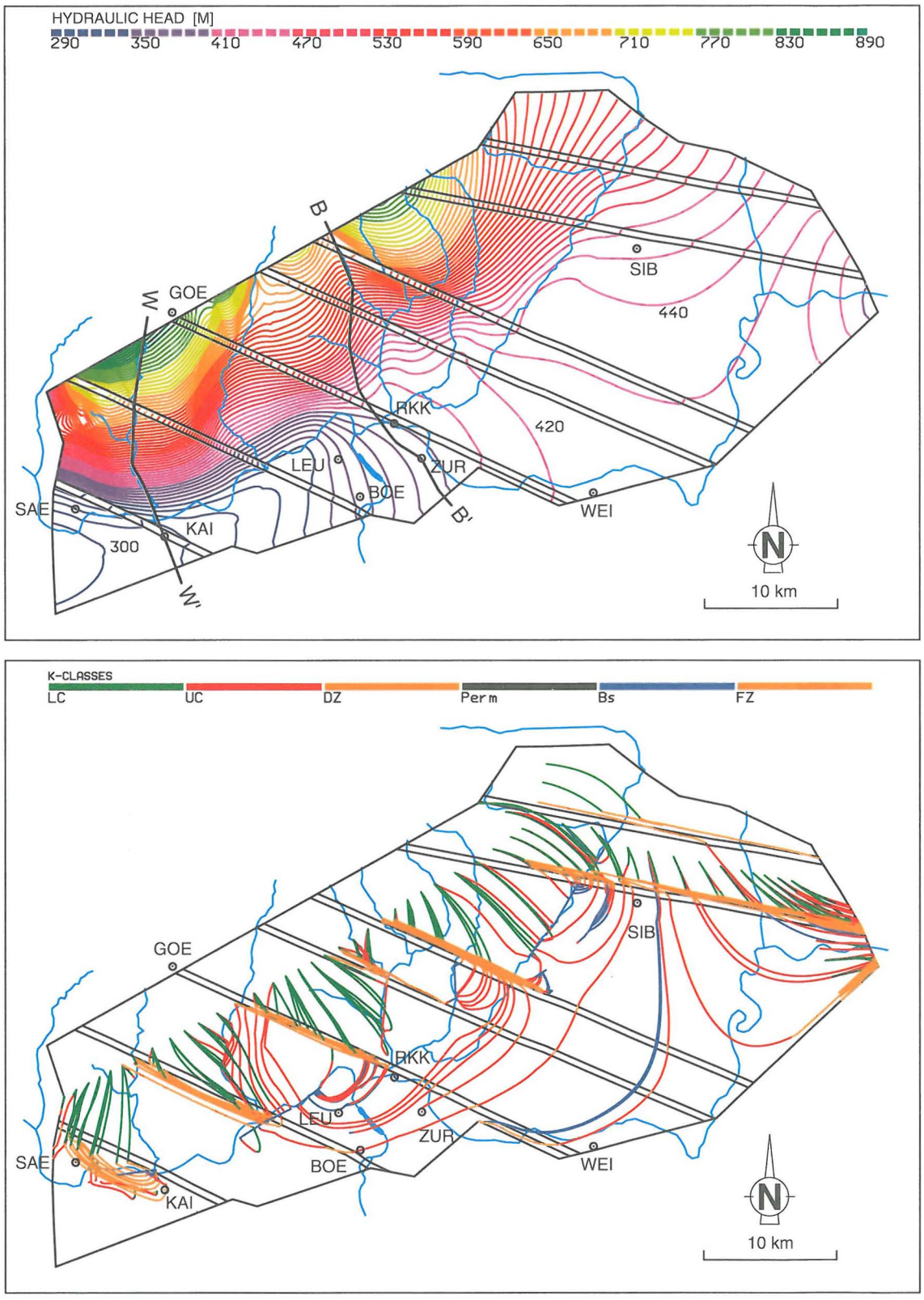

Fig. 3.17 KRI3, Base case V30z: Head contours in the LC unit *(top)*, results of particle tracking *(bottom)*

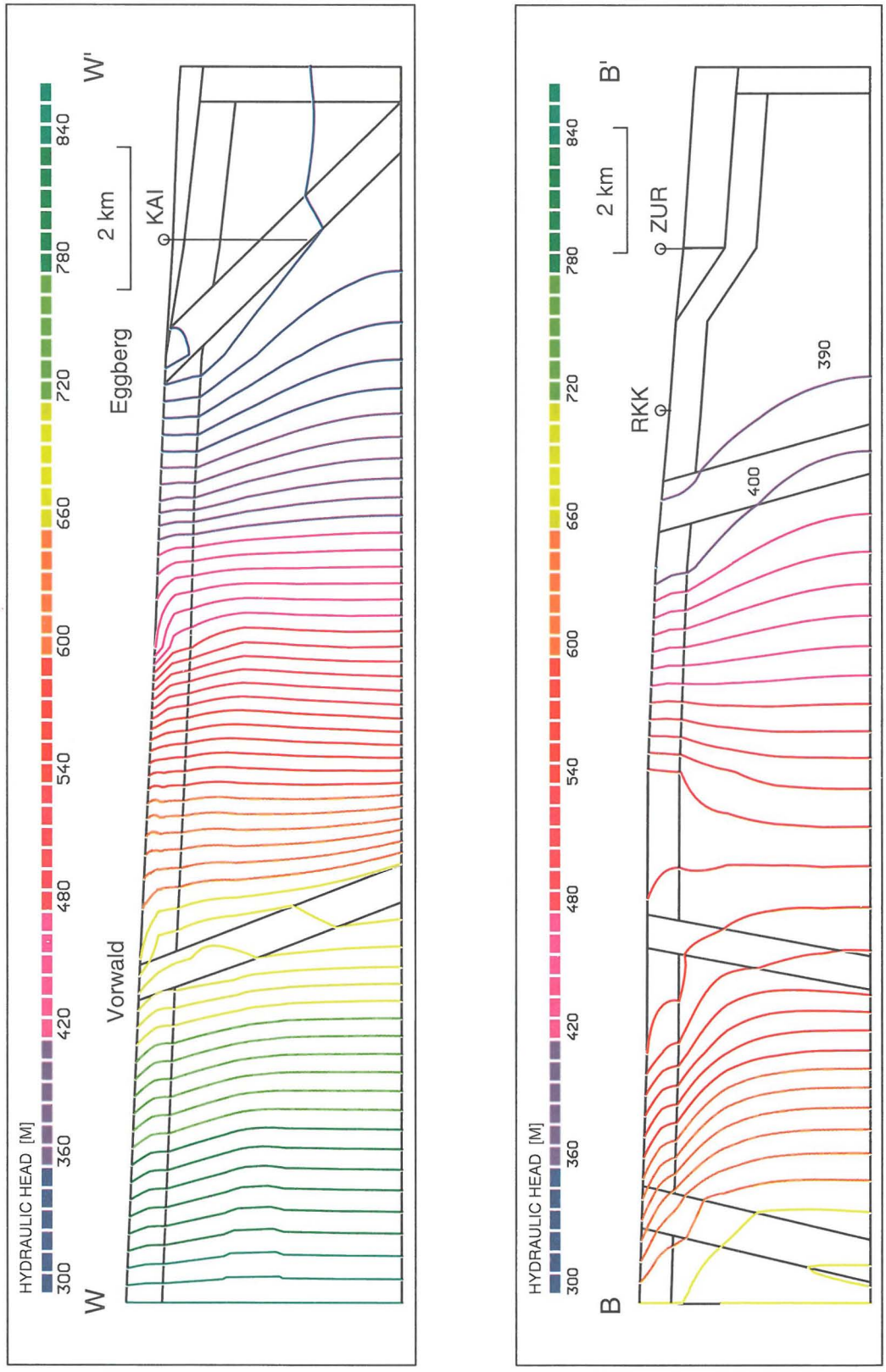

Fig. 3.18 KRI3, V30z: Head contours in Section WW' (*top*) and BB' (*bottom*). See Figure 3.17 for section location

3.8.4 KRI3 Conclusions

- Incorporation of some prominent tectonic features (i.e., transmissive faults of 1st order) into the existing EPM model did not have a significant impact on the simulated head distribution in the model. As a consequence, the match between the observed and simulated head condition in the area of interest between BOE, LEU and KAI was not improved under the given boundary conditions. In this sense, the KRI3 phase of regional modeling confirms the general conclusion of the KRI2 study on the overall insensitivity of the simulated system to considered parametric and structural variations. Other conceptual variations may well produce the desired impact but they would not be supported by geological evidence.

- On the other hand, the introduced faults affect the results of particle tracking by diverting large portions of groundwater flow in direction of the fault. This anisotropy contradicts the hydrochemical evidence, indicating that not all regional faults are likely to be hydraulically active.

- The KRI3 phase, which comprised the implementation of discrete faults on a regional scale, represents a valuable modeling exercise that included the development of new software. The KRI3 study demonstrates the numeric complexity of such large-scale models that explicitly describe discrete tectonic features and it also shows the computational restraints attached to the problem.

- The EPM approach that was adopted at the beginning of this study is justified at this scale of modeling, considering the substantial effort that was required to implement a complex regional model with discrete faults, and considering the small impact that inclusion of the faults had on the model results.

3.9 Possible long-term variations of regional groundwater flow

3.9.1 Background

A modified version of the regional model KRI2 was used to assess the impact of geological long-term processes on the large-scale groundwater-flow regime in the region of northern Switzerland. The underlying assumption is that over a geological time-scale of, say, one million years, the ongoing geological processes may significantly change the topology and hence hydraulic boundary conditions of the study area. This implies that the present-day characteristics of the geological environment (which may be favourable for a planned repository site) cannot be necessarily extrapolated in geological times that are relevant for the performance of a long-living radioactive-waste repository.

The present study defines the following processes to be relevant for the long-term behaviour of the regional flow regime:

1) **Regional uplift of the Black-Forest massif** (continuation of the observed updoming process). The centrum of the updoming area (maximum uplift rate) is located beneath the Feldberg mountain beyond the modeled area, the periphery (zero uplift rate) is defined by the boundary to the PCT in the south. For numerical modeling, the uplift geometry is defined as follows: maximum uplift of 1,000 m with respect to the datum level of the Rhine graben near Basel, linear attenuation toward 0 m along the margin of the PCT, resulting in a "tilting" of the surface toward south. This mechanism results in an uplift of about 200 m in the area of KAI and LEU boreholes and 500 m in the region of SIB.

2) **Fluvial erosion**. The regional uplift is accompanied by enhanced erosion activity of the rivers. The rivers cut deep into the bedrock to form deep valleys; the southvergent tilting of the surface results in a lateral drift of the Rhine and Wutach River toward south. The modeling assumes that the depth erosion of major rivers is in balance with the uplift rate; i.e., the bottom of these river valleys remains at today's elevation.

3) **Glacial erosion**. The third relevant process is the areal removal of Mesozoic sediments by abrasion of the glaciers. The net effect is an increased area of exposed crystalline rocks at the surface (boundary conditions!).

Other erosion effects, such as removal of the quaternary alluvions in the valleys or a general areal erosion of the relief (assumption: 50 m at maximum) are not considered as relevant in this study.

The implementation of the above scenarios in the numerical model required several modifications of the existing KRI2 model as outlined in the following.

3.9.2 Modified regional model KRI2h

The "long-term version" of the regional model, designated KRI2h, includes variations in grid topology and in boundary conditions according to the scenarios defined above. For the sake of simplicity, the existing numerical mesh of KRI2 was adapted to the long-term topography by adding the relative uplift rates to the present surface nodes. Assignment of the uplift rates to individual nodes was based on interpolation from simplified and digitalized contour lines of equal uplift rate. In a second step, selected nodes representing major river valleys were relocated back to their original elevation, in accordance to the assumption 2) above. This pragmatic approach permitted to avoid a costly design and digitalization of a new topography as model surface.

The boundary conditions were adapted to the new topography and outcrop conditions. No-flow boundary was maintained for the model surface beneath Mesozoic cover. Fixed heads (h=z) were prescribed to the area of exposed crystalline rock which was significantly enlarged with respect to the present extent. Fig. 3.19 compares the outcrop areas of the Bs/UC aquifer in the KRI2 and KRI2h models. In difference to KRI2, the eastern and western lateral boundaries, VE and VW, are closed (i.e., with imposed no-flow condition) in the KRI2h scenario, because the long-term hydraulic role of the regional faults Randen and Wehra is not evident a priori.

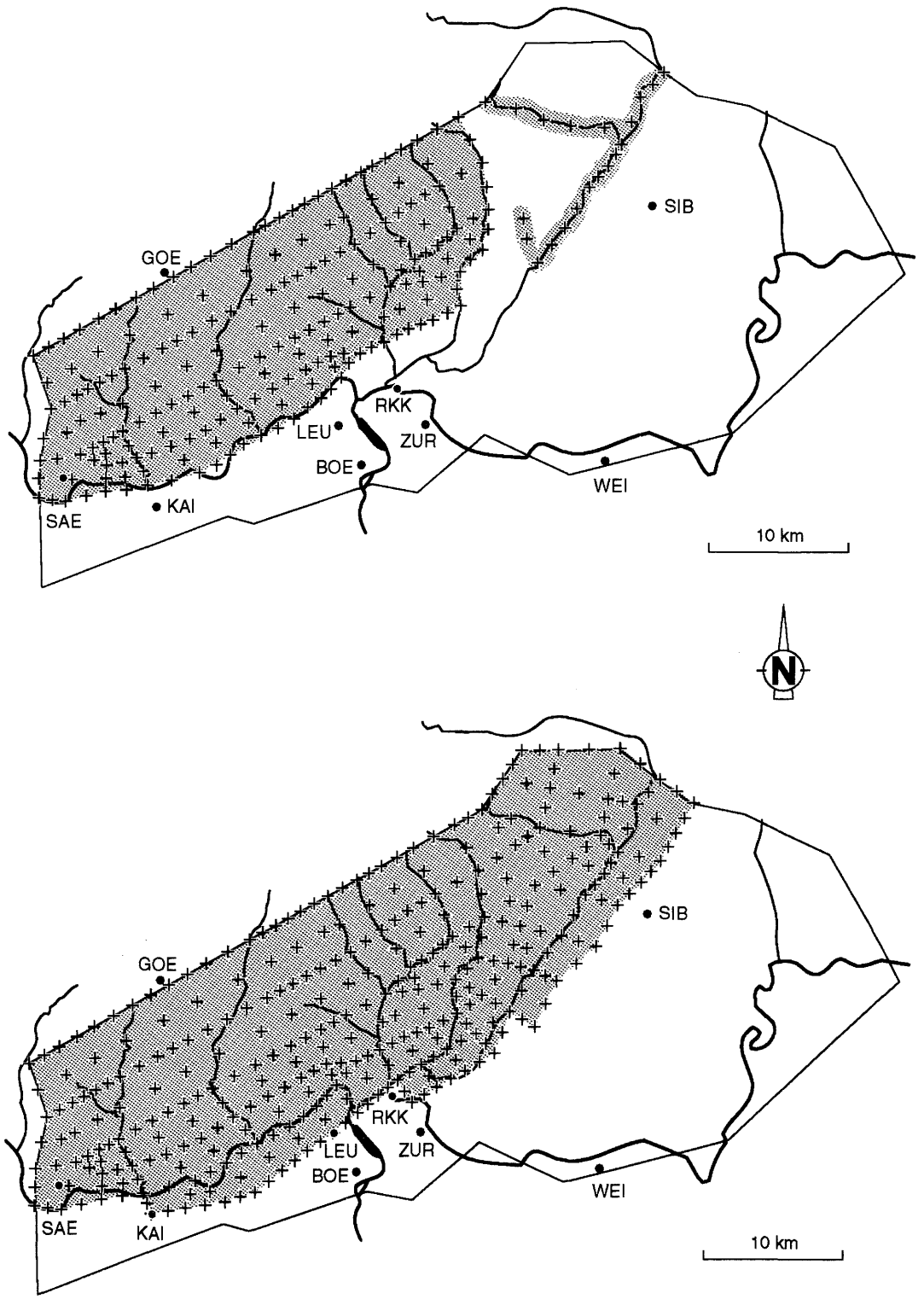

Fig. 3.19 Modeled outcrop areas of crystalline basement. *Top*: present-day scenario (KRI2). *Bottom*: long-term scenario (KRI2h).

3.9.3 Results

The long-term scenario was simulated in one run, V20h, that corresponds to the base case of the KRI2 model, except for modified boundary conditions mentioned above. The model results are displayed as a horizontal contour map (Fig. 3.20) and in two vertical sections that are representative for the western and eastern model area (Fig. 3.21).

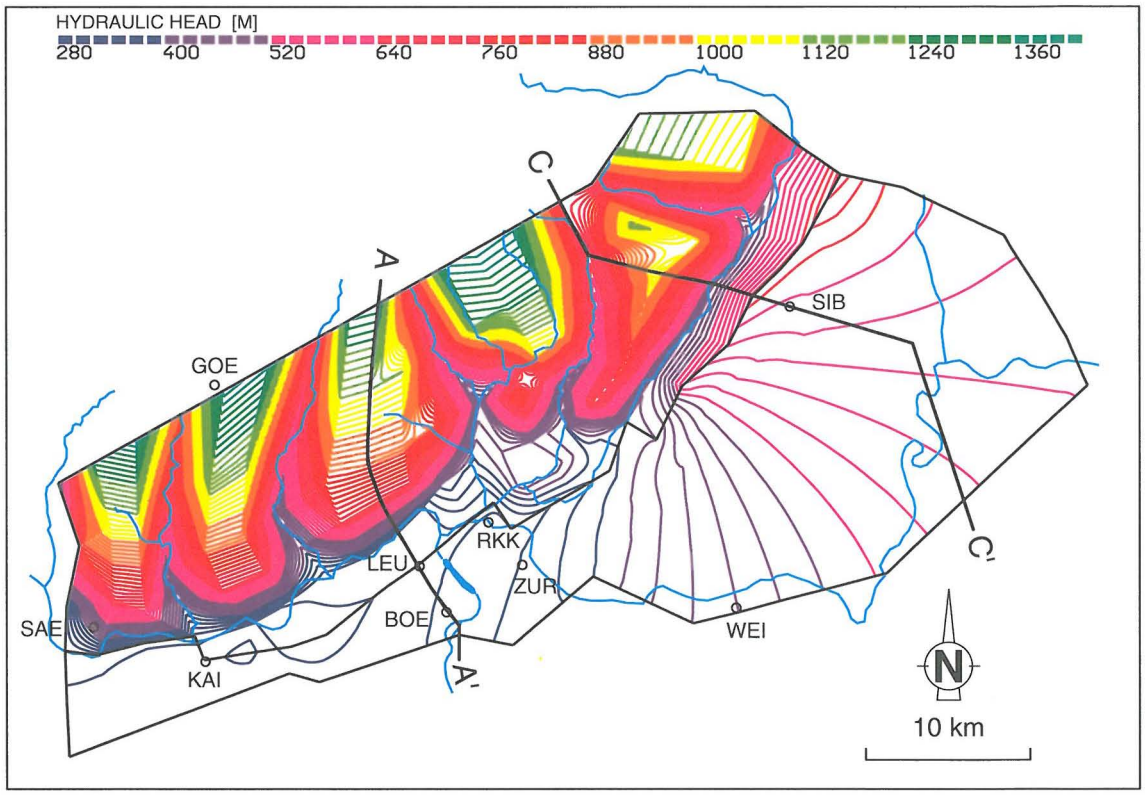

Fig. 3.20 Long-term scenario (KRI2h): areal distribution of simulated heads in UC unit

The contour map in Fig. 3.20 reflects the modified topography in the area of exposed crystalline basement. The southern Black Forest features a very strong relief with deep river valleys. The groundwater flow here is dominated by local (i.e., shallow) flow systems with large horizontal gradients. The significance of these local flow systems shows in an increase of the total turnover through the model from about 0.5 m^3/s in KRI2 to 1.7 m^3/s. The southern limit of the crystalline-outcrop area is located south of the present Rhine and Wutach valley. It shall be noted that the model topology accounts for the depth erosion of the rivers; however, it ignores a possible lateral drift toward south due to the coarse discretization of the existing KRI2 mesh.

The investigation area West (BOE-KAI-LEU), situated between the Rhine River and the PCT, is affected only by minor uplift rates. However, the southern limit of exposed basement is shifted south approximately to the line defined by the RKK, LEU and KAI boreholes (see Fig. 3.20). The removal of the low-permeable Mesozoic cover that confines the BS/UC aquifer results in new discharge conditions in that area. The shifted southern outcrop line represents now the lowest free surface for crystalline groundwaters in Northern Switzerland. This implies that area West fully includes a principal regional discharge zone, resulting in larger hydraulic gradients upward and shorter flow paths to the biosphere. The dominant discharge condition is illustrated in section AA' through LEU and BOE in Fig. 3.21a (to be compared with Fig. 3.11 in KRI2).

The groundwater flow in the region of SIB (area East) is dominated by the Wutach River that cuts deep into crystalline rocks and represents an important discharge area. The significant uplift of this area produces an infiltration regime south of the Wutach valley (Fig. 3.21b). In the present model, the groundwater divide to the Wutach discharge area is located north of the SIB site, resulting in still relatively long flowpaths from this area to the discharge into the Rhine River (although shorter than in KRI2 model). However, this simulated flow regime can change radically by a lateral drift of the Wutach valley toward south (not modeled), which results in a direct discharge of the SIB area into this river.

3.9.4 Conclusions regarding the long-term scenario

Simple modifications were implemented on the existing regional model KRI2 in order to simulate simplified geologic scenarios that are assumed to occur over the next one million of years. The objective of this modeling step was to investigate possible impacts of these long-term scenarios on the regional groundwater flow, such as evaluated in the KRI2 study, or, in other words, to test the validity of the established conceptual model of regional flow within a time space that is relevant for repository performance assessment.

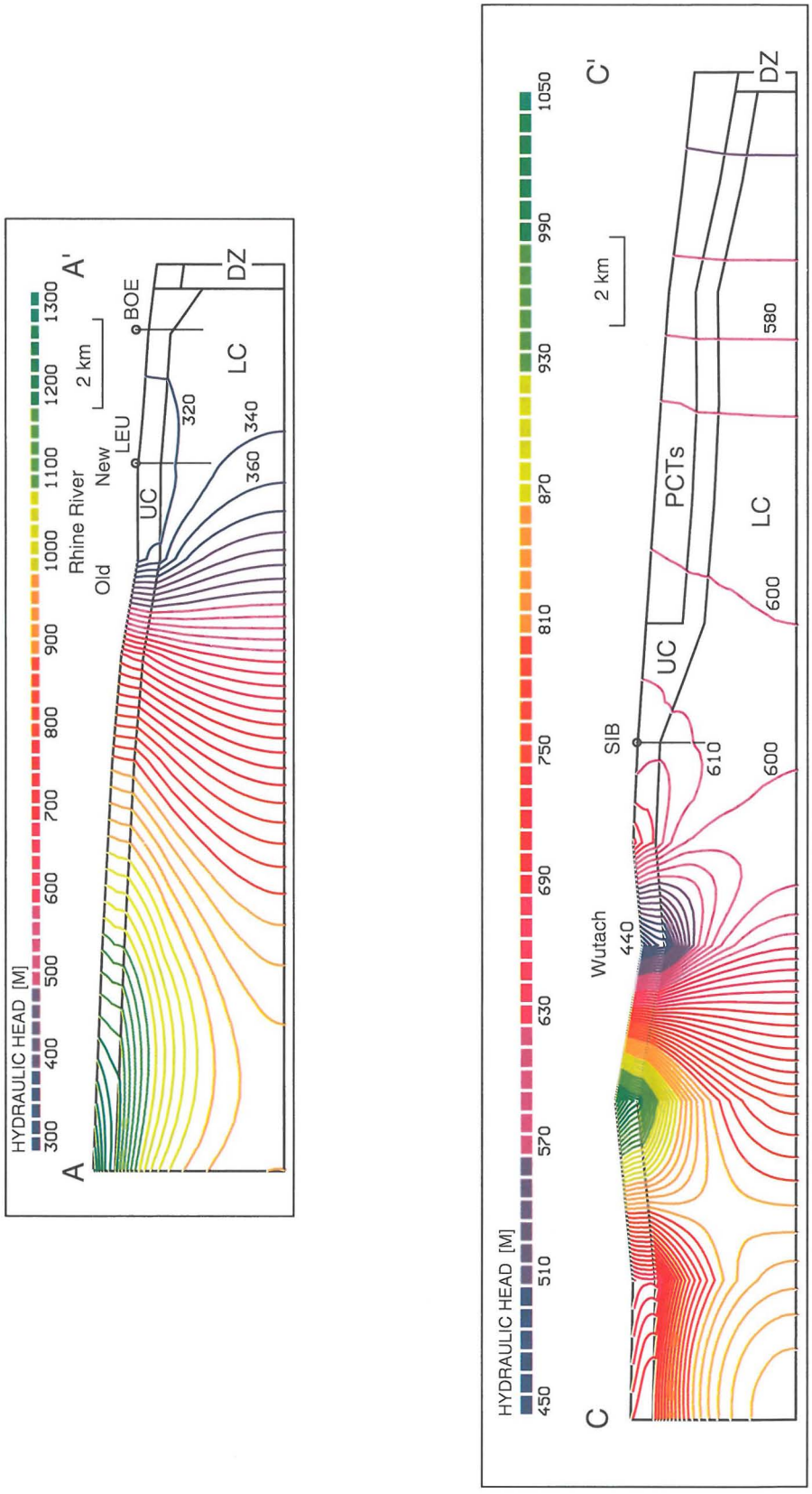

Fig. 3.21 KRI2h: effects of the simulated long-term scenario in two vertical sections AA'(a) and CC'(b). See Fig. 3.20 for section location

The modeling results lead to the following conclusions:

1) The eastern area of interest (represented by SIB site) is susceptible to fundamental variations in the hydrodynamic regime, ranging from recharge conditions with relatively long flowpaths to the biosphere (simulated in model) to extreme discharge conditions with direct exfiltration into the deep-eroded Wutach River migrated to the south (not modeled). As consequence, a potential repository area should be sited as far south of the present Wutach River valley as possible in view of the restricting presence of the northern branch of deep PCT south of the SIB site.

2) For the area West (sites of BOE, KAI, LEU), no major change in the present-day flow conditions is anticipated. The general tendency is that the present discharge regime will be enhanced, that is, the vertical upward gradient will increase and the travel paths of groundwater through the geosphere into the Rhine alluvions will be reduced.

3) Despite the dominant discharge regime in area West, the above conclusions speak in favour of this sub-region. Here, the present-day conditions can be extrapolated in geological times with greater confidence than in the area East, where a complete reversal of the present trend may occur, and, as a consequence, jeopardize the actual assessment of repository performance.

3.10 Summary of KRI modeling study: Conceptual model of regional flow system in Northern Switzerland

One of the main objectives of the regional modeling study was to improve understanding of the large-scale groundwater flow system. As stated in the introductory Section 3.1, the principal issue is to combine the findings of the modeling study with other hydrogeological information and professional experience to form a consistent conceptual model of the regional hydrologic system. Such a conceptual model is formulated as a set of hypotheses in **Appendix 3**.

The conceptual understanding of the relevant processes and parameters is expressed in terms of ***currently preferred hypotheses (CPH)*** and ***plausible alternative hypotheses (PAH)***. The term "currently preferred" is used in the sense of "most likely, based on current understanding".

The hypotheses in Appendix 3 have varying degrees of uncertainty regarding the likelihood that the currently preferred one is in fact the correct one; these uncertainties are qualitatively expressed in the table as high, medium, or low (H, M, L). An "H" was assigned when model results conflicted with hydrogeologic observations, or when the EPM model could not adequately reproduce (and therefore test) a particular condition or process. An "L" was assigned when model results were supported by hydrogeologic evidence, or when the CPH gave markedly better model results than the alternatives. An "M" represents an intermediate level of uncertainty.

In some instances, no preferred hypothesis could be identified at this time - all plausible alternatives seem equally viable. No level of uncertainty was assigned, but the implication is one of very high uncertainty as to which hypothesis is correct.

Also included in Appendix 3, where appropriate, is qualification of the sensitivity of the particular condition or process with respect to the simulated hydraulic regime. This sensitivity was tested by varying boundary conditions and parameters and comparing the resulting simulated heads with observed heads. Thus, by noting the combination of uncertainty and sensitivity in Appendix 3, it is possible to define key conditions for which additional information is needed to improve understanding of the flow system. For example, discharge in the Wutach River valley is considered a highly uncertain hypothesis, and results are very sensitive to this condition; thus, additional evaluation of this condition probably is warranted. Other conditions, in which a low uncertainty exists and which have little influence on the results, can receive minimum attention in future evaluations.

For purposes of improving understanding of the regional flow system, the EPM model proved to be a satisfactory tool. Nonetheless, some simplifying assumptions were made that gave the modeling study certain limitations. For example, only a few major structural features (first-order faults) were explicitly described in the latest model version KRI3, whereas the crystalline rocks comprise a large variety of discontinuities, such as fractures, dikes, and sets of minor and major faults. Many of these features are likely to affect the groundwater flow system at smaller scales. These effects can not be tested with the EPM model at a 100-km scale and will be addressed by hybrid models at sub-regional scale. The inability of the EPM model to match some observed heads and vertical gradients, probably reflecting local flow conditions, is largely due to this factor.

An additional simplifying approach was to incorporate only spatially uniform hydraulic conductivity for the Upper and Lower crystalline units. Results of hydraulic tests indicate that this parameter is spatially variable in northern Switzerland.

No coupling of hydraulic and thermal conditions was made, although a potential for density-driven groundwater flow due to temperature variations was identified in the area. These processes were investigated by an independent 2-dimensional modeling study (RIVERA & RESELE 1992), indicating that density-driven flow occurs in the basement of Northern Switzerland but is strongly location-specific. At the regional scale, free convection is the most significant process. The largest effects of coupled groundwater flow and heat transport are expected to occur in the vicinity of deep trough and to increase with depth. Controlling factors are primarily the contrasts between K properties of hydrogeologic rock units and the regional flow regime (including faults which are known to play an important role in conducting and discharging thermal waters). The magnitude of the basal heat flux is of secondary importance and affects conduction-dominated regions only.

4 CHARACTERIZATION OF LOCAL FLOW SYSTEM IN AREA WEST

4.1 Background and objectives of the local-scale model

The approximation of an equivalent porous medium for large rock volumes in the regional model described above was satisfactory for the scale and intended purpose of the model. However, the crystalline rocks of Northern Switzerland do not in fact have uniformly distributed properties. Numerous discontinuities such as faults, joints, magmatic and ore dikes occur with wide ranges of sizes, frequencies, orientations, and hydraulic properties. Thus, for the purpose of modeling the properties and conditions of successively smaller areas and for more rigorous simulations of flow conditions, it would be desirable to describe explicitly many of these discontinuities. At the local modeling scale, the hybrid (or, double porosity) approach permits to consider prominent tectonic features as discrete permeable elements that are embedded within the relatively undisturbed blocks of crystalline rock, consisting of HPD and LPD according to the conceptual model. These intervening blocks are approximated as an equivalent porous medium and characterized by a single equivalent property (Table 2.8). It bears noting that the hybrid model is the most consequent transformation of the conceptual model of crystalline rocks (Fig. 2.4) into a numerical model.

Like the regional flow model KRI2, the hybrid models are interpretative flow-simulation tools, used for the characterization of representative hydrological conditions in an area of interest. As stressed in the introduction of this report (Section 1.3), the model areas are not necessarily related to specific geographic locations but rather describe conceptual areas that are deemed representative for the hydrogeological conditions expected at the investigation site. To account for different tectonic settings and for the observed spatial variability of the groundwater flow regime in Northern Switzerland, it was decided to discriminate two conceptual areas for the analysis of the sub-regional flow system. The area West represents hydrogeological conditions that are expected in the vicinity of the boreholes Böttstein, Leuggern and Kaisten, whereas the area East reflects the tectonic and hydrologic conditions of the Siblingen region. Each area has undergone a different tectonic deformation and is thus characterized by specific structural and hydrologic conditions. The principal features that differentiate area West from area East are summarized in Table 4.1 below.

Table 4.1 Particular features of area West and area East

	Area WEST	**Area EAST**
Tectonics	- Compressive-stress field dominates over extensive - mostly strike-slip faulting - neotectonic activity of little significance	- Extensive regime dominates - horst and graben tectonics - pronounced neotectonic activity (uplift, seismicity, young faults)
Hydrology	- "Discharge regime"; i.e., mostly upward flow - geothermal anomaly and springs - no groundwater divide - no vertical leakage across Lower Muschelkalk - gw highly evolved / mineralized	- "Recharge regime"; i.e., mostly downward flow - no thermal waters - Possible gw divide in Muschelkalk and crystalline rocks - Possible leakage across faults - low-mineralized gw

The hybrid modeling study of area West has the following objectives:

1. To increase conceptual understanding of flow on a sub-regional scale, by assessing sensitive parameters and related uncertainties.

2. To evaluate model results that are relevant as input for preliminary safety analysis, such as distribution of fluxes and gradients, flowpath lengths and travel times of particles within the host rock.

3. To link the large-scale EPM model, in which crystalline rocks are reproduced as an equivalent porous medium, and fracture-network flow models at block scale, in which discrete fractures are modeled as discontinuum (no matrix).

4. To acquire and demonstrate the ability of reproducing a geometrically complex structural pattern by a finite-element grid.

The first issue, aiming at improved conceptual understanding of flow, is related to the following questions to be addressed by the hybrid model:

- What is the effect of prominent tectonic features on the local hydrodynamic field? How significant are the existing uncertainties in geometric/hydraulic properties (parameter sensitivity)?

- To what extent can a conceptual hydrologic model be simplified and still provide a description of the system that is consistent with the observations? The objective is to establish a "robust" model with as few parameters as possible.

The task of hybrid modeling required the development of a completely new numeric algorithm that permits intersection of the conventional Finite-element grid (consisting of regular columns) by an arbitrary number of inclined planar features. The new concept of finite-element modeling, accomplished with the new computer code FRACMESH, is outlined in the following.

4.2 Approach of hybrid modeling

Recent developments in the hydrogeological modeling of hard fractured rocks have been achieved in the field of fracture-network simulation. The feasibility and validity of the fracture-network approach for characterization of groundwater flow and solute transport through fractured rock was subjected to extensive evaluations within Phase III of the international Stripa Project (HERBERT et al. 1990, GRINDROD et al. 1991, DERSHOWITZ et al. 1991). In this new family of numerical codes, the water-conducting fractures are generated as discrete two-dimensional finite elements that form a sheetwork in 3-D space. The characteristics of this network are generally specified by a statistical distribution of underlying parameters, derived from observations. None of these codes includes the rock matrix that occupies the space between the fractures in the numerical model.

In the analysis of the hydrogeology of crystalline rocks of Northern Switzerland, a need was identified for "hybrid" or double-porosity models that numerically treat the flow in discrete permeable features as well as in the interjacent rock matrix. The term "hybrid" as used in this study refers, in numerical sense, to the combination of continuum and discontinuum modeling. It allows to model explicitly a variety of discrete features that are embedded in equivalent-porous background rock. The main reasons for adopting the (relatively untried) hybrid approach for the characterization of local groundwater flow are:

- To provide a link between the regional-scale flow models that use the continuum approximation and the fracture network models at the site scale. The discrete-fracture models are limited to simulations of relatively small volumes of rock due to computational restrictions on the number of fractures. Therefore, for larger regions of rock, the minor fractures must be included implicitly into an equivalent-porous matrix, modeled as 3D-elements.

- At the intermediate scale, the hydrodynamic processes interacting between fractures and rock matrix are of interest: "Faraday cage" effect, distribution of gradient and flux between fractures and rock matrix, influence on flow path patterns, etc.

Because the complexity of the numerical mesh increases over-proportionally with the number of fractures involved, a new computer code for automatized generation of such finite-element (FE) grids was developed.

The FRACMESH code generates 3-dimensional Finite-element meshes by intersecting a volume of rock (block matrix in the conceptual model) with arbitrarily oriented planes representing faults or fractures. The principal task of the mesh generator is to completely fill the resulting space between the inclined and intersecting planes with finite elements of a simple shape (bricks, prisms, tetrahedrons, etc.). The geometric characteristics of the modeled planar features, such as orientation, vertical and lateral extent, are specified either for each feature individually or for different sets of fractures (tectonic families) in the input deck. The latter are defined by constant orientation and spacing of the single members. Additionally, the mesh-generating algorithm allows for the shaping of vertical and horizontal model boundaries (e.g., according to a natural boundary) and for zonation of the model into hydrogeological units. A detailed documentation of the FRACMESH code is given in the user's manual (HÜRLIMANN 1994).

4.3 Model structure and parameters

4.3.1 Geometric input and structure

The hybrid model West, designated HYBW 92, simulates the local groundwater flow in the conceptual area West. The structure of the numerical grid represents the geometric fault model that was defined by the structural geology for area West in AMMANN et al. (1992). The model includes a systematic classification of faults in hierarchic orders according to fault size and magnitude of displacement, based on an earlier proposal for the southern Black Forest by HUBER & HUBER (1990). The schematic fault network is displayed as plan view in Fig. 4.1. The 3-dimensional grid is obtained by including information on the dip distribution of the fault zones. Due to only a sparse and incomplete information that is available in the investigation area covered entirely by mesozoic sediments, the established structural network has a generic character and is based largely of expert judgment. A basic assumption is that observations from the southern Black Forest are also applicable to the (covered) basement of Northern Switzerland. It is evident that only a few principal features, such as the Eggberg fault and the Vorwald fault, can be attached to true locations in this model. The geometric pattern comprises five prominent systems that are characterized in the following table.

Table 4.2 Geometric characterization of the fault pattern West

Fault family (trend)	Order	Range of dip	Spacing
W1 (WNW-ESE) "Hercynian" system	1st & 2nd	55°S to 80°N	7 km between 1st order 1 km between 2nd order
W2 (N-S) "Rhenish" system	2nd	80°S to 80°N	1.5 km in west 2 km in east
W3 (NNW-SSE)	2nd	70°SW to 70°NE	1.5 km
W4 (WSW-ENE)	1st/2nd	80°SE	2 km
W5 (SW-NE), locally	2nd	80°SE	1 km, only south of Wutach

The geometric model West in Fig. 4.1 represents a relatively dense grid of inclined planar features that produce many intersections in the vertical dimension. The realization of such a complex 3-D geometry in a numerical model

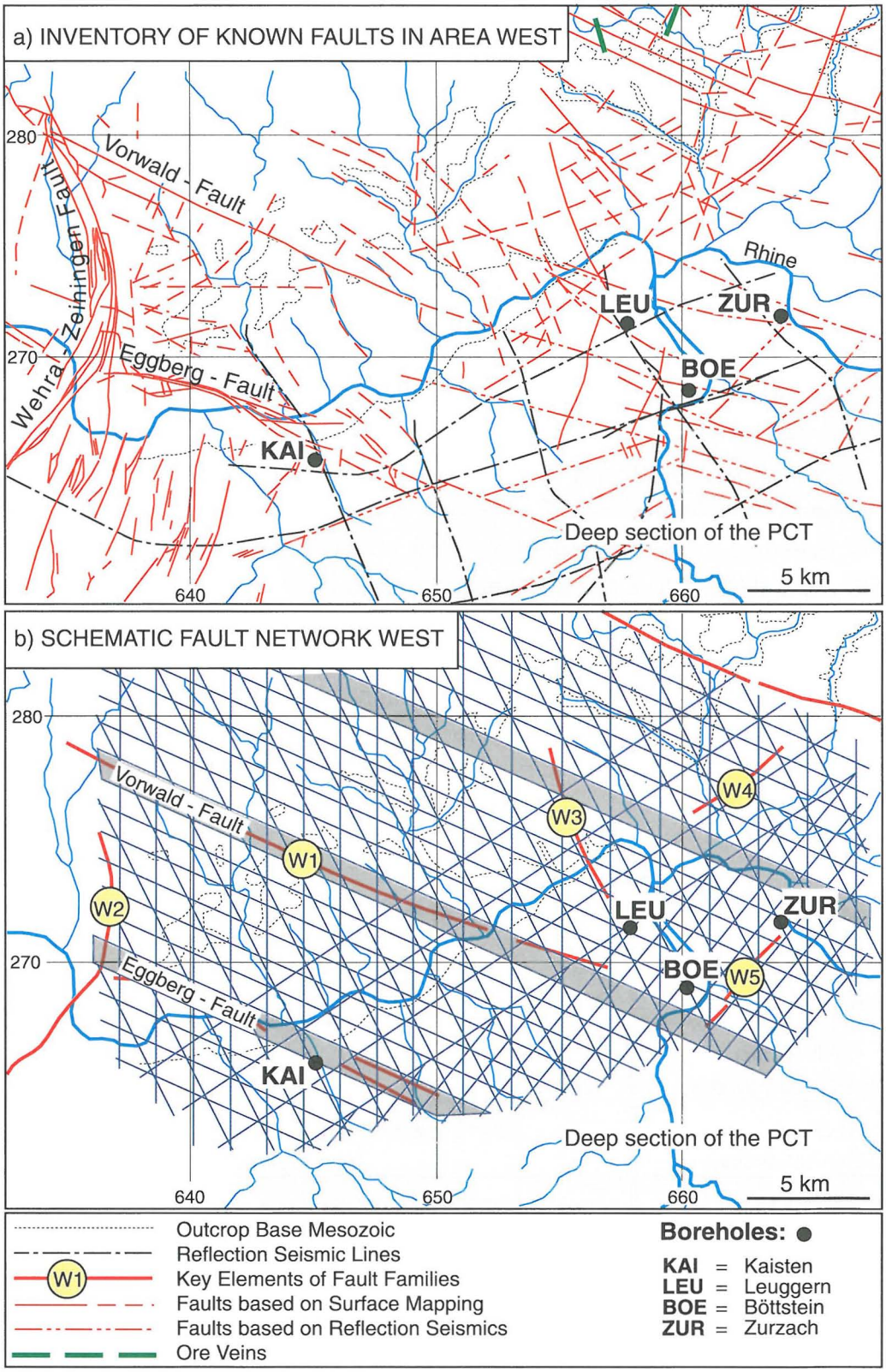

Fig. 4.1 a) Inventory of observed structures in area West (surface mapping and seismic survey)

b) Schematic fault model (THURY et al. 1994)

requires the generation of many finite elements. Accordingly, the resulting model grid consists of 23,000 nodes and 20,300 finite elements. The same computer code FEM 301 was used for solving the flow equation as in the regional model (Section 3.3.1); the size of the resulting solution file is 160 MBytes.

The geometric fault model West (Fig. 4.1) was implemented as default geometry in the initial scenario of the numerical model. The evaluation of local groundwater flow included three other alternative scenarios of fault occurrence because the frequency of **hydraulically active** faults within the population defined by the schematic geometric model is unknown. As a results, four individual Finite-element grids with variable fault geometry and frequency were constructed. The model variations are deemed to cover the expected range of plausible conditions, starting with a full fault inventory (full scenario or initial case) which is reduced to only a few active faults (sparse scenario). The performed model variations are summarized in Section 4.4 and displayed in Fig. 4.4 below.

Note that no subhorizontal faults or shear zones were included neither in the geometric model nor in the hybrid model, although the existence of such flat-lying structures cannot be excluded. It is deemed that such features could provide hydraulic connections between areas of elevated heads (Black Forest) and low heads (south of Rhine River valley) and thus generate large vertical gradients.

The structural framework of the hybrid model West is illustrated in Fig. 4.2. The plan view (*top*) shows the default model geometry derived directly from the fault pattern defined in Fig. 4.1. The model covers an area of about 50 km^2. It is bounded to the north by the Rhine River and to the south by the deep Permo-carboniferous Trough (PCT). The fault network consists of four principal families W1-W4 according to Table 4.2 above. As a simplification, the fifth system which is a local variation of the fourth set and occurs only in part of the investigation area was not included in the numerical grid. The faults are classified into a category of 1st order (MWCF-1) and 2nd order (MWCF-2) according to their tectonic significance.

A schematic cross section in Fig. 4.2 (*bottom*) shows the vertical model structure with defined hydrogeologic units and model boundaries. The upper model boundary is defined by a thin layer of Buntsandstein (BST) that occurs at the basis of low-permeable Muschelkalk sediments (not modeled). The model base was set at a depth of -2,000 m b.s.l. for the following pragmatic reasons: to limit the number of finite elements and because observations from deep boreholes

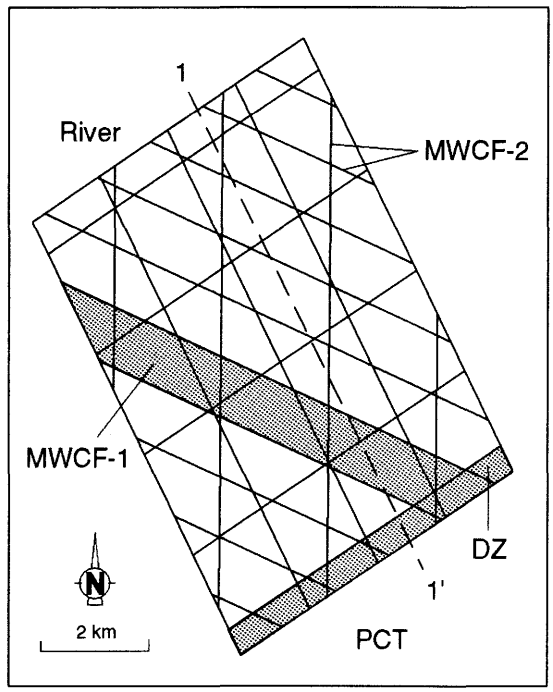

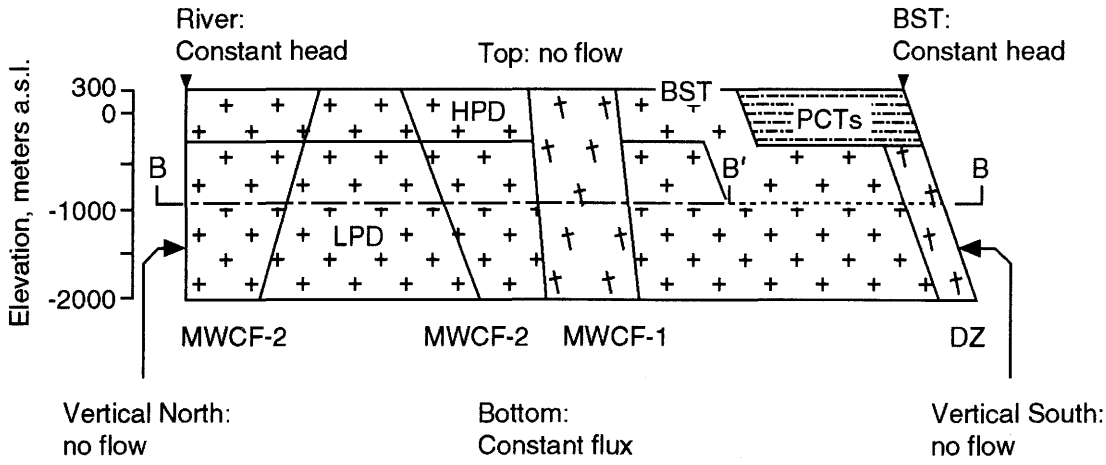

Hydrogeological units

BST Buntsandstein aquifer
PCTs Permo-Carbonif. Trough (shoulder)
HPD Higher-permeability domain
LPD Low-permeability domain
DZ Tectonically disturbed zone (MWCF-1)

Major water-conducting faults

MWCF-1 First-order (3-d elements)
MWCF-2 Second-order (2-d elements)

Additional boundary conditions

VW Vertical West: constant flux
VE Vertical East: constant flux

Fig. 4.2 Structure of hybrid model HYBW. *Top:* Plan view with main fault sets (default geometry); *Bottom:* Schematic section showing modeled unit and boundary conditions

(BOE and LEU) are limited to a depth of -1,300 m b.s.l. The imposed boundary conditions are discussed in Section 4.3.3 below.

The geological model structure is similar to that of the regional model in this area, except for the explicit faults. The thin Buntsandstein aquifer (BST) is underlain by Permian sediments that constitute the shallow trough shoulder (PCTs) in the southern part. In the remaining model area, the BST forms a single hydraulic unit with the underlying permeable crystalline rocks. The crystalline rocks are divided in hydrogeological units according to the conceptual model: the undisturbed crystalline blocks between faults (block matrix) are separated into a 500-m thick Higher-permeable domain, HPD, and the Low-permeable domain, LPD. The Major water-conducting faults, MWCF, are modeled as 3-D or 2-D elements according to their hierarchy. According to the definition in AM-MANN et al. (1992) the first-order faults in the modeled area are the Vorwald fault and the northern border of PCT, DZ (disturbed zone in the regional model). These features are represented numerically by 1,000-m and 500-m thick elements respectively. The second-order faults (MWCF-2) are reproduced by 2-D elements, characterized by transmissivity. The assigned T value implies an assumed mean thickness of 20 m for the 2nd order faults (see Table 4.3 below).

4.3.2 Input parameters

The hydraulic parameters assigned to the modeled units are based on the values derived from observations in the Nagra boreholes. One output of the borehole-data synthesis, described in Chapter 2, were analytical estimates of the effective hydraulic properties for each unit, summarized in Table 2.8. This analytical approach treated the transmissive elements by conservative means as parallel plates of infinite extent; a later investigation of the effective properties by fracture-network models (described in Chapter 5) confirmed the validity of the analytical values as the likely upper bounds of effective network permeability. Because the hybrid model HYBW 92 was developed parallel to the ongoing synthesis of borehole data, the initially adopted hydraulic parameters had to be updated in the course of the modeling study to match the final results of data synthesis. For completeness, the initial and the final input datasets are included in Table 4.3 below; the modeled hydrogeologic units are shown in Fig. 4.2 (bottom). The model results described in the following sections are based entirely on the final parameter set.

As mentioned above, the 2-D elements representing faults are assigned a transmissivity value as input parameter by considering the estimated effective hydraulic conductivity of the MWCF domain (Table 2.8) and a constant thickness of 20 m of the faults. The K_{eff} of the 2nd order faults is understood to be the same as that of the 1st order faults, both categories being part of the hydraulic domain MWCF.

Also the thin BST layer is approximated by 2-D elements with a given transmissivity. The average observed thickness in Nagra boreholes is 15 m. Due to its large permeability (K = 1·E-06 m/s), this layer exhibits horizontal flow and can thus be represented by 2-D elements.

Comment:
As a consistency check, the effective hydraulic conductivity of the modeled hybrid block is calculated for the model bottom from the total conductance values given in Table 4.4 (see Section 4.3.3.2 for explanation). The resulting "EPM conductivity" varies from 8E-08 m/s in full scenario to 5.5E-09 in sparse scenario and reflects the variable hydraulic contribution of the MWCF. These values are larger than the hydraulic conductivity assigned to the Lower Unit in the regional EPM model KRI-2 which covers a much larger area than the hybrid model. The hybrid K_{eff} values are consistent with the findings of the coupled thermohydraulic modeling study performed by RIVERA & RESELE (1992).

Table 4.3 Effective hydraulic parameters used in HYBW model

Code	Model unit	Unit	Preliminary input set	Final set
BST	Buntsandstein (d=15 m)*	T [m^2/s]	1.5E-05	1.5E-05
PCTs	Perm of the trough shoulder	K [m/s]	1.0E-09	1.0E-09
HPD	Higher-permeable domain of crystalline rocks	K [m/s]	2.0E-07	2.8E-07
LPD	Low-permeable domain of crystalline rocks	K [m/s]	9.0E-11	4.2E-11
MWCF-1	Major water-conducting faults of 1. order	K [m/s]	2.0E-07	3.2E-07
MWCF-2	Major water-conducting faults of 2. order (d=20 m)*	T [m^2/s]	4.0E-06	6.4E-06

*) assigned T corresponds to K(MWCF) and assumed thickness of 20 m of 2-D elements

4.3.3 Boundary conditions

4.3.3.1 Definition

The principal difficulty encountered during the development of the local model concerned the definition of appropriate boundary conditions. The procedures and related problems are discussed below. Initial trial runs considered constant-head conditions by using a conventional method of transferring heads from a larger model, in this case the regional model KRI2. However, due to the different scales and numerical discretization of the two models, the transfer of external heads from the EPM model to the nodes at the hybrid-model boundaries produced abnormally high fluxes within the high-permeable discrete faults intersecting the boundary. This effect is caused by the high hydraulic contrast of three orders of magnitude between the undisturbed EPM blocks (block matrix) and the intersecting discrete faults (MWCF). Under these circumstances, the definition of a "correct" head condition at each boundary node is not feasible, since it would represent the solution of the numerical model. The problem was solved by adopting prescribed-flux boundaries (Neumann condition), where a specific Darcy-flux value is assigned to each node of the boundary face. The prescription of fluxes is, according to Darcy's law, equal to imposing the value of the normal hydraulic gradient on each node of a given material unit with property K. In terms of prior knowledge, it is more convenient to provide an estimate of the representative gradients rather than discrete values of hydraulic head.

The hydraulic gradient was estimated from available head observations (borehole data, topography, etc.), as well as from the regional model KRI2. With two exceptions, the flux boundaries were used throughout, either in terms of a no-flow condition or by prescribing a non-zero flux. The applied procedure of assigning specific fluxes is outlined below. The two exceptions refer to constant-head conditions imposed along the northern edge of the model representing a river (simulating discharge conditions along the Rhine River valley), and also along the southern top edge of the model to allow a free lateral inflow into the 2-D Buntsandstein aquifer (BST) from the south. The prescribed BST heads were interpolated linearly from observations in deep Nagra boreholes.

The definition of the individual model boundaries is given in the following (see also schematic section in Fig. 4.2 *bottom*):

- **Top boundary, T:** no-flow condition, assuming no flux through the low-permeable overlying layers of Lower and Middle Muschelkalk (aquitards). Exceptions are the northern and southern top edge of the model which have prescribed hydraulic heads.

- **Bottom boundary, U:** imposed non-zero flux into the model is based on estimated vertical gradients (from environmental heads) of 0.05 in the Low-permeable domain, LPD, and of 0.003 in the MWCF domain at the sites of BOE and LEU respectively. This assumption reflects the general discharge regime of deep crystalline groundwaters that is generally observed in the region between the Rhine River and the Permocarboniferous trough (PCT), i.e., the area covered by the hybrid model. Note that this condition could not be reproduced adequately by the regional model with a no-flow boundary at the bottom (except Disturbed zone).

- **Vertical north, VN:** no-flow condition, except for the nodes at the surface to simulate discharge conditions along a river (see Top). The no-flow condition is based on the simplifying assumption that the vertical boundary underneath a principal regional discharge area is an axis of flow symmetry, that is, the boundary is oriented parallel to the flow lines.

- **Vertical south, VS:** no-flow condition, assuming that no significant lateral flow from/into the adjacent deep part of PCT occurs (in analogy to regional model). Free lateral flow is allowed within the BST layer.

- **Vertical east, VE:** imposed non-zero flow into the model, based on an mean horizontal regional gradient of 0.006.

- **Vertical west, VW:** non-zero flow out of the model, based on a horizontal gradient of 0.003. As a conceptual assumption, half of the groundwater flow entering the model through VE is allowed to leave toward west and the other half discharges into the river along the N boundary.

4.3.3.2 Procedure

As a rule, the assigned external hydraulic gradients at the boundaries, I, were kept constant in all simulations. In consequence, the corresponding flux values, q_i, being the actually prescribed boundary condition ($q_i = -K_i \cdot I$), vary from case to

case according to the variable hydraulic and geometric properties of the specific boundary face, characterized by the "conductance". In this context, the term conductance, C_i [m^3/s], is used as a quantity to describe the capacity of a planar geometric feature, i, to carry flow under an unit normal gradient (I_n=1). The conductance is equivalent to the product of the cross-flow area, A_i [m^2], and the effective hydraulic conductivity, K_i [m/s], of a geometric feature i, represented as EPM. In case of discrete 2-D elements (e.g. when intersecting a boundary face), conductance is the product of the trace length, L [m], and transmissivity, T [m^2/s]. When multiplied by an imposed external gradient, I, the conductance yields the volumetric flow, $Q_i = C_i \cdot I$, through a given planar area, A, or a 2-D element of given length L. Therefore, the volumetric flow across a model boundary scales linearly with its conductance. In turn, the bulk conductance of a given model-boundary area is controlled by 1) the cross-flow area of the high-permeable crystalline domain HPD, and 2) the presence of highly transmissive faults that carry the most of the flow within the LPD unit. Although the cross area of a given model boundary is constant in all realizations, the area of faults that is open for flow (i.e., the trace length of intersected 2-D elements) in this boundary face varies from case to case, reflecting the different frequency of active faults. The impact of this variable fault conductance on the resulting flow across the model boundaries is shown in Table 4.4 for the both bounding geometric scenarios (referring to full and sparse fault intensity, see above). Note how the reduction of fault frequency in the sparse scenario dramatically reduces the conductance (and hence Keff) of the model bottom as well as the incoming flow. This effect is much less pronounced in the lateral (vertical) model boundaries, where the overall conductance is in both cases dominated by the contribution of the HPD unit.

In technical terms, the conductance of each individual hydrogeologic unit, C_i, that constitutes a boundary face such as VE or VW is calculated. For this purpose, postprocessing tools of finite-element display (FED, see Fig. 3.1) are used to integrate the area of each EPM unit (e.g., PCTs, HPD, LPD, MWCF-1) and to calculate the length of all intersected 2-D faults (MWCF-2). The resulting volumetric flow, Q_i, through each contributing area A_i is calculated as $Q_i = C_i \cdot I$, where I is the defined external gradient for each material unit. In a second step, this flow is distributed as Darcy flux, q_i, over all nodes in that area. The Darcy flux represents here the normalized volumetric flow per unit area. The flux values are prescribed as nodal conditions to all relevant nodes in the input parameter file.

Table 4.4 Derivation of boundary conditions for model HYBW

Model boundary	Area of MWCF-1 A [m^2]	Trace of MWCF-2 L [km]	Total Conductance C [m^3/s]	External Gradient I[1)]	Volumetric Flow Q [l/s]
1. Full geometric scenario					
VE East (inflow)	7.7E+05	13.862	1.77	0.006	10.6
VW West (outflow)	4.5E+06	9.646	2.7	-0.003	-8.1
B Bottom (inflow)	10.9E+06	137.756	4.37	0.050 in LPD 0.003 MWCF	13.2
Total balance[2)]	-	-			+ 15.7
2. Sparse geometric scenario					
VE East	-	2.592	1.53	0.006	9.2
VW West	-	3.317	1.54	-0.003	-4.6
B Bottom	-	45.724	0.3	0.05 in LPD 0.003 MWCF	1
Total balance[2)]	-	-	-	-	+5.6

1) constant throughout all simulations
2) corresponding to volume of discharge along the river

The second step consisting of assigning a non-zero flux value to each boundary node represents a technical problem, because fluxes cannot be prescribed explicitly to 2-dimensional finite elements. These elements form one-dimensional trace lines across the boundary face and the corresponding nodes are common with the adjacent matrix blocks. According to the conceptual model, however, these planar tectonic features carry a volumetric flow, as defined by the equation $Q_i = T \cdot L_i \cdot I$, where T is the fault transmissivity (considering a thickness of 20 m), L_i is the individual trace length and I is the imposed external gradient. Since the total volumetric flow that would be carried by all intersected faults cannot be prescribed explicitly onto the 2-D features, it has to be "distributed" over all block-matrix nodes of that boundary area for compensation. Because the flow through permeable faults clearly dominates the bulk groundwater flow through a low-permeable block, its distribution over the boundary nodes generates over-

proportionally large hydraulic gradients within the LPD matrix as an artificial boundary effect.

4.3.3.3 Comments

The definition of boundary conditions proved to be the most critical part of the model development. A general transfer of boundary conditions from larger EPM models with single equivalent properties to a smaller hybrid (or double-porosity) model with increased numerical resolution and large contrasts in material properties is not a trivial process. It bears noting that an undifferentiated transfer of heads or gradients from an equivalent-porous medium to different hybrid-model units would generate excessive fluxes in the explicitly modeled high-permeable faults. In other words, the water-conducting faults, having a large permeability contrast to the adjacent low-permeable background rock (LPD), exhibit also much lower heads and hydraulic gradients. As a consequence, the observed regional data reflect rather the large-scale continuum properties and cannot be applied to discrete major faults representing a discontinuum.

The applied procedure permits to specify individual fluxes for each 'boundary unit' on the basis of its conductance and inferred large-scale gradients. The conductance of a planar boundary area reflects its hydraulic **and** geometric properties, and defines thus the cross flow through that area under an unit normal gradient. Although the assigned gradients are consistent with the observations and/or regional-model results, a significant uncertainty remains associated with the adopted boundary conditions. Main difficulties were experienced when trying to assign non-zero fluxes to 2-dimensional elements; from this perspective, it would be desirable to model all faults as 3-d elements.

4.4 Model variations

Model simulations focused on the impact of fault geometry and frequency on the local groundwater flow system. A key issue with respect to a potential site-characterization study is the sensitivity of the locally simulated (or observed) flow field to the proximity of major permeable faults. As mentioned above, four principal geometric scenarios were considered, in which the frequency of the water-conducting faults was successively reduced, or in other words, the size of "undisturbed" blocks that would host a repository was increased. These basic

geometric layouts are shown in Fig. 4.3. Shown are also the locations of two reference boreholes BH1 and BH2 that correspond to Nagra boreholes LEU and BOE. The four different models were designated as Series 400, 410, 420 and 430. This identification allows for realization of additional and independent parameter studies individually within each geometric scenario (designated as runs 40i, 41j, etc.). The first series represents the full scenario that includes the complete fault inventory of the geometric model (except for set 5 of Table 4.3), assuming that all these faults are hydraulically active. The other scenarios successively reduce the fault frequency, assuming that some of the faults defined by the structural model are not water-conducting. The final series 430 is defined as the sparse scenario because it represents the smallest frequency of hydraulically active faults.

The geometric scenarios shown in Fig. 4.3 are characterized as follows:

- Series 400: complete inventory of 1st and 2nd order faults

- Series 410: full set of second-order faults, first-order faults are inactive

- Series 420: only two prominent systems are active (hercynian and rhenish family of Table 4.2)

- Series 430: two prominent systems (as above) with reduced occurrence: set 1 with double spacing, set 2 with intermittent features. The latter simulate the occurrence of dikes as permeable planar features of limited lateral extent.

Two default parameter sets T and K were used with each model geometry, as indicated in Table 4.3. A first series of runs, designated 400, 410, 420 and 430, used the preliminary input data. At a later stage of the study, these input parameters were replaced by the actualized values for effective properties in runs 403, 413, 423 and 433 respectively. An additional parameter study addressed the following variations: variable direction of dip (with respect to vertical) of individual faults within the same system in order to mimic a horst-and-graben geometry, run 402; a decrease of fault permeability (all MWCFs) by a factor of 200 (run 401), and an increase of LPD permeability by a factor of 5 (run 431).

A summary of all model variations is given in a matrix form as follows.

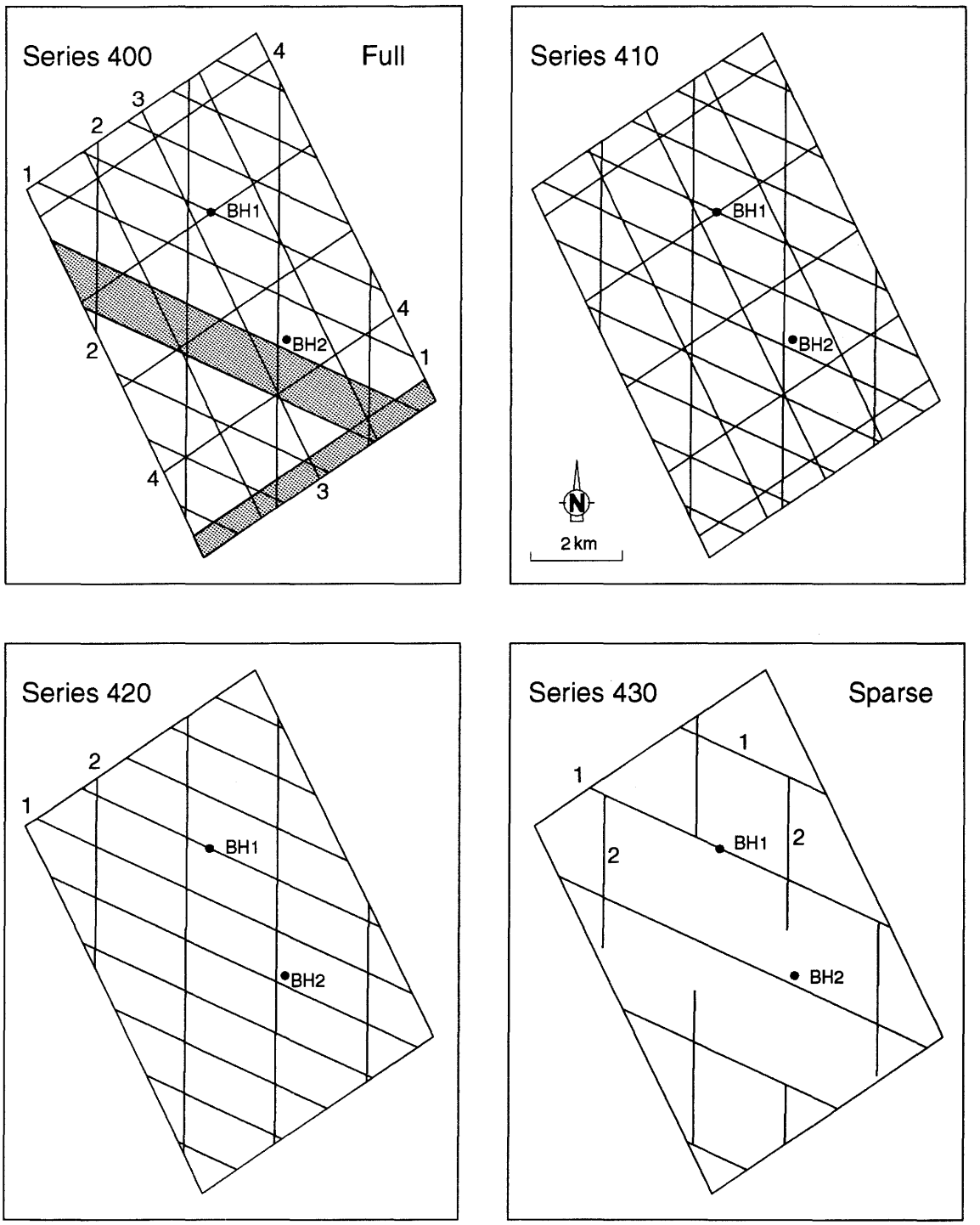

Fig. 4.3 Local model West: defined geometric scenarios with variable fault frequency

Table 4.5 Simulated scenarios in HYBW model

Parameter subject to variation	Series 400 "full"	Series 410	Series 420	Series 430 "sparse"
1. initial input set (geometry & hydraulics)	400			
2. reduced intensity of active faults		410	420	430
3. new K effective: reference case	**403**	413	423	**433**
4. variable dip direction within a family (horst-graben topology)	402			
5. K(eff) of MWCF reduced	401			
6. K(eff) of LPD increased				431

The highlighted runs represent the two key scenarios that were adopted for a detailed discussion of specific model results in the following.

4.5 Model results: description of general flow pattern

4.5.1 Methods of presentation

The output of the hybrid modeling study is presented in two parts. Section 4.5 describes the simulated flow system in general terms. The following Section 4.6 is addressed to the specific model results that are relevant to safety analysis.

The simulated flow pattern is presented generally as head contours or Darcy-flux vectors projected on two horizontal and one vertical section. The locations of the horizontal sections are shown in Fig. 4.2 (*bottom*). The lower section, B, is situated at 500 m below the top of LPD. This horizon represents the potential repository level and is referred to as "level 500" herein. However, due to the model geometry, this horizon abuts the bottom of the Upper crystalline unit (HPD) in the southern part of the model. In this area, therefore, the model results along this portion of the horizontal section are no more representative for the reference level 500 and are excluded from quantitative analysis of results in section 4.6.

An additional insight on simulated head distribution is obtained from vertical-head profiles calculated along 16 hypothetical boreholes (Fig. 4.5 *top*). This presentation allows to illustrate the effects of fault proximity on vertical gradients that are simulated in randomly located boreholes. The simulated head profiles are compared to observed heads in BOE and LEU boreholes (see Table 3.1).

A comparison of model results has indicated that no significant differences exist in the simulated flow regime between the full scenario 400 and the two intermediate geometric scenarios 410 and 420. In all three models, the spatial density of major water-conducting faults is large enough to dominate the groundwater flow through the model. Thus, the head distribution within the model is governed by the gradients within the interconnected network of faults. These gradients, in turn, generally reflect the imposed boundary condition at each extreme of the fault. An additional geometric variation in Run 402, where a horst-graben fault geometry was introduced for the hercynian system (Set 1 in Table 4.2), had no impact on the hydraulic behaviour of the already well-connected fault network.

Based on the above comparison, it is concluded that the analysis of model results can be limited to the full scenario and the sparse scenario. These are the significant runs that span the full range of anticipated simulation results. The updated parameters used in runs 403 and 433 are considered as the default set (i.e., the best estimate). In the following, the simulated flow is described for both scenarios; for completeness, the sensitivity of performed parameter variations is briefly discussed.

4.5.2 Full scenario (Run 403)

The full scenario considers all faults of the structural model West to be hydraulically active (i.e., water conducting).

The head distributions in both crystalline units HPD and LPD are displayed as head contours in two horizontal planes in Fig. 4.4 (top). In plane A, the horizontal flow in HPD merely reflects the general regional gradient, which is from the southeast toward the discharge areas in the northwest of the model. Because the hydraulic property of the faults is similar to that of the HPD blocks, the faults have no impact on the general flow. In plane B at level 500 below the top of LPD, the highly transmissive faults dominate the flow in accordance with the imposed regional gradient. Due to the dense and regular network of permeable

conduits, virtually no local flow conditions are observed in the system, which shows a behaviour similar to an equivalent porous medium.

The bottom graph of Fig. 4.4 illustrates the vertical flow pattern in the full hybrid model. The illustration shows the projection of calculated absolute Darcy-flux vectors onto a vertical section, which is oriented approximately parallel to the principal flow direction from SE to NW (section 1-1' in Fig. 4.2 top). In the south it intersects two 1st-order faults of 1.0 and 0.5 km thickness. The color of the flux vectors indicates the absolute magnitude (velocity) according to the logarithmic scale above, whereas the length corresponds to the projected value. Very short vectors, appearing as dots, represent flow in the 3rd dimension, i.e., perpendicular to the observer. Long vectors indicate flow within the plane of projection. Distinct ascending flux manifested by green vectors occurs in the 1st order faults in the southern part, representing the disturbed margin of the PCT and the Vorwald fault. Horizontal flow dominates the High-permeable domain and the upper part of LPD. The near-bottom part of the model is affected by boundary conditions that induce relatively large vertical gradients along the bottom. If the boundary effects are disregarded, no significant vertical gradients are generated in the full hybrid model. A more quantitative evaluation of gradients is performed in Section 4.6 as contribution to input for safety analysis.

The effects of fault proximity on vertical gradients is illustrated in Fig. 4.5, showing the results of synthetic head profiles that were calculated along 16 generic boreholes. Two of them, BH1 and BH2, represent the location of BOE and LEU respectively (see Fig. 4.3). A plan view at the top of the LPD unit (Fig. 4.5 top) shows the relative locations of the generic boreholes with respect to the faults. The dip direction of the faults is also given to indicate which boreholes will likely be intersected within the LPD interval. The calculated head profiles are displayed in a xy-diagram below. The head profiles are normalized to the head value at the top node in the Higher-permeable domain, HPD, i.e., the vertical gradient is visualized by relative head differences. The vertical depth is plotted from the top of the crystalline basement. The upper limit of the Low-permeable domain, LPD, is located at -500 m depth below the crystalline surface. The envisaged repository level within LPD is another 500 m below that boundary (level 500), i.e., at -1,000 m depth below 0 in Fig. 4.5. Due to the anomalous boundary effects at model bottom, the simulation results are considered relevant only to a depth of about -1,400 m, which also corresponds to the deepest observed interval in the Nagra boreholes. Similar to Fig. 4.4 (*bottom*), the vertical-head profiles indicate the general absence of significant vertical

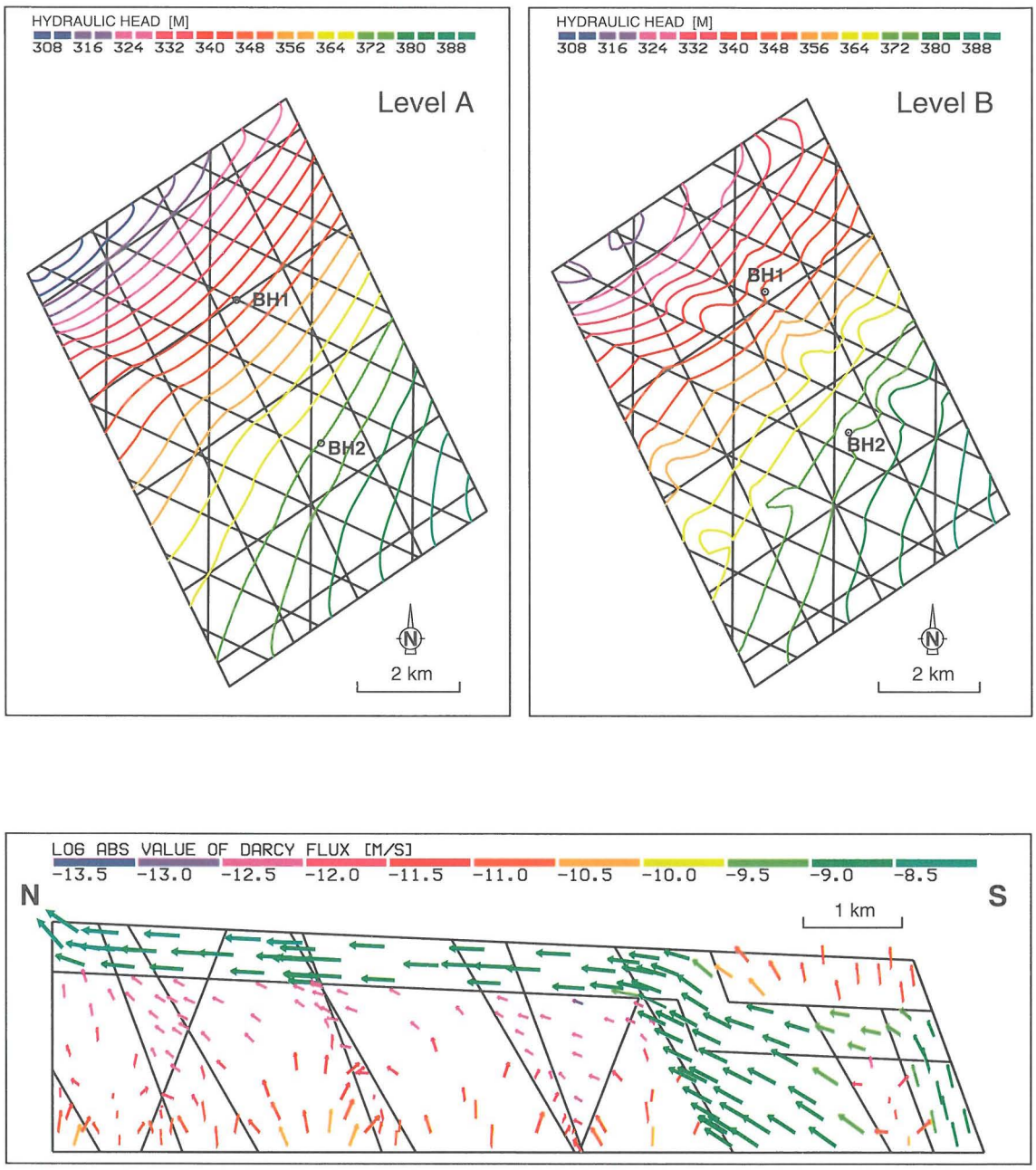

Fig. 4.4 Full scenario HYBW 403. *Top*: Plan view with head contours in HPD (level A-A) and in LPD (level B-B). *Bottom*: Vertical section 1-1' with projection of Darcy flux vectors (logarithmic scale)

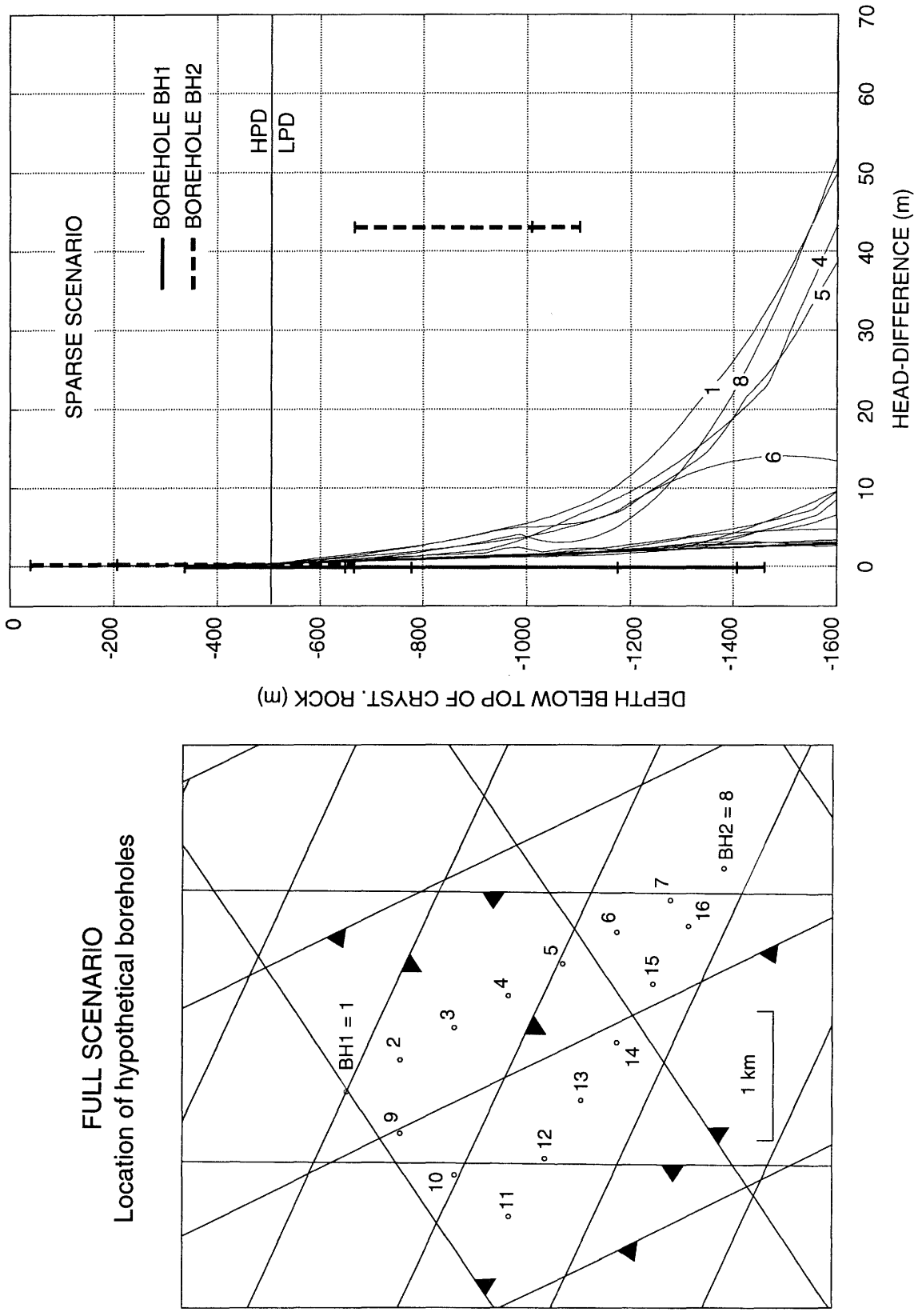

Fig. 4.5 Full scenario: Location of hypothetical boreholes with respect to faults at the top of LPD *(left);* calculated vertical head profiles (normalized) along boreholes *(right)*

gradients in the observation interval. Virtually no vertical head gradients occur in all boreholes that are intersected by faults. The faults appear as kinks in the head profiles due to the draining effect of the well-connected fault network. Gradients within this system are generally low reflecting the regional trend. These boreholes simulate in general the conditions observed in BH1 (LEU) borehole. Only the boreholes No. 1, 4, 5 and 8 are not intersected by a fault. Also here, however, the vertical gradient reproduced in the upper section of the LPD unit is negligible when compared to observed conditions in BH 2 representing BOE. It is evident that the well-interconnected full scenario cannot even approximately reproduce local vertical gradients such as observed in BH2.

4.5.3 Sparse scenario (Run 433)

The sparse scenario refers to a substantially reduced frequency of water-conducting faults with respect to the default geometry. As a net effect of the increased size of undisturbed blocks, the interconnectedness of the fault system is significantly reduced, giving rise to local flow systems that are independent of the regional trend.

Fig. 4.6 (*top*) shows the horizontal-head distributions in the model at two levels. Level A-A reflects again the regional flow regime in the HPD unit from southeast to northwest. Discharge occurs into the river along the northern boundary and farther downstream of the model. The heads and resulting gradients are smaller than in the full scenario. The LPD unit at level B-B shows a distinctly different flow pattern that is influenced by the presence of permeable faults. Note that the southern part (south of BH2) of this plan view represents the conditions of the overlying HPD (see Fig. 4.2 bottom). The horizontal flow within the permeable faults is still driven by the regional gradient imposed on the model boundaries. However, the draining effect of the faults on the adjacent blocks is limited only to a peripheral zone of these blocks. Thus, the horizontal-flow component within the blocks is directed radially toward the nearest fault. As a result, local flow systems are preserved within the blocks, and local flow directions do not necessarily coincide with the regional trend.

A similar tendency is illustrated by the projected absolute Darcy vectors in the vertical section 2-2' (Fig. 4.6 *bottom*). Horizontal flow occurs within the HPD unit and vertical flow dominates the LPD unit. Also in this dimension, the local drainage effect of permeable faults shows in radial flow directions at the periph-

ery of undisturbed blocks. Vertical flow is predominant in central areas of large blocks that are not affected by the (regional) flow regime in major water-conducting faults.

Thus, the overall flow pattern in the sparse scenario is characterized by predominantly horizontal flow in the permeable faults (driven by the regional gradient), by radial horizontal flow in the peripheral areas of intact blocks, and by vertical upward flow in the interior of large blocks. Unlike in the full scenario, the undisturbed blocks of LPD are large enough to preserve local flow conditions in the interior. Consequently, reversed flow directions may locally occur within the blocks with respect to the regional pattern.

Fig. 4.7 displays the calculated vertical head profiles along synthetic boreholes in analogy to Fig. 4.5. The location map at the top shows the relative position of boreholes to faults at the top boundary of LPD. The direction of dip of faults is also indicated. Based on the geometry, only the closest boreholes No. 9, 2, 3, and 6 are likely to be intersected within the LPD interval. The synthetic head profiles in Fig. 4.7 bottom show that significant vertical gradients are generally reproduced by the model in the LPD unit between -500 m and -1,400 m depth. The presence of permeable faults at depth strongly affects the head distribution along the borehole, as indicated by the intersected boreholes with small vertical gradients.

It is concluded that this model scenario more likely reproduces the head conditions observed at BOE for all boreholes located in the middle of LPD blocks, as well as the observation at LEU for boreholes intersecting major permeable faults. However, the model structure is too general to reproduce such local phenomena as the abrupt change of heads that is observed in BOE.

4.5.4 Sensitivity of hydraulic parameters

As stated above, investigating the impact of the fault geometry on the subregional flow was the principal objective of the model simulations. Additionally, a brief sensitivity study of the hydraulic parameters was carried out (Table 4.5).

Based on the default geometry of the full scenario, the effective conductivity of major faults was reduced to K = 1E-09 m/s in Run 401. This modification produced a small hydraulic contrast between the faults and the LPD blocks. As a

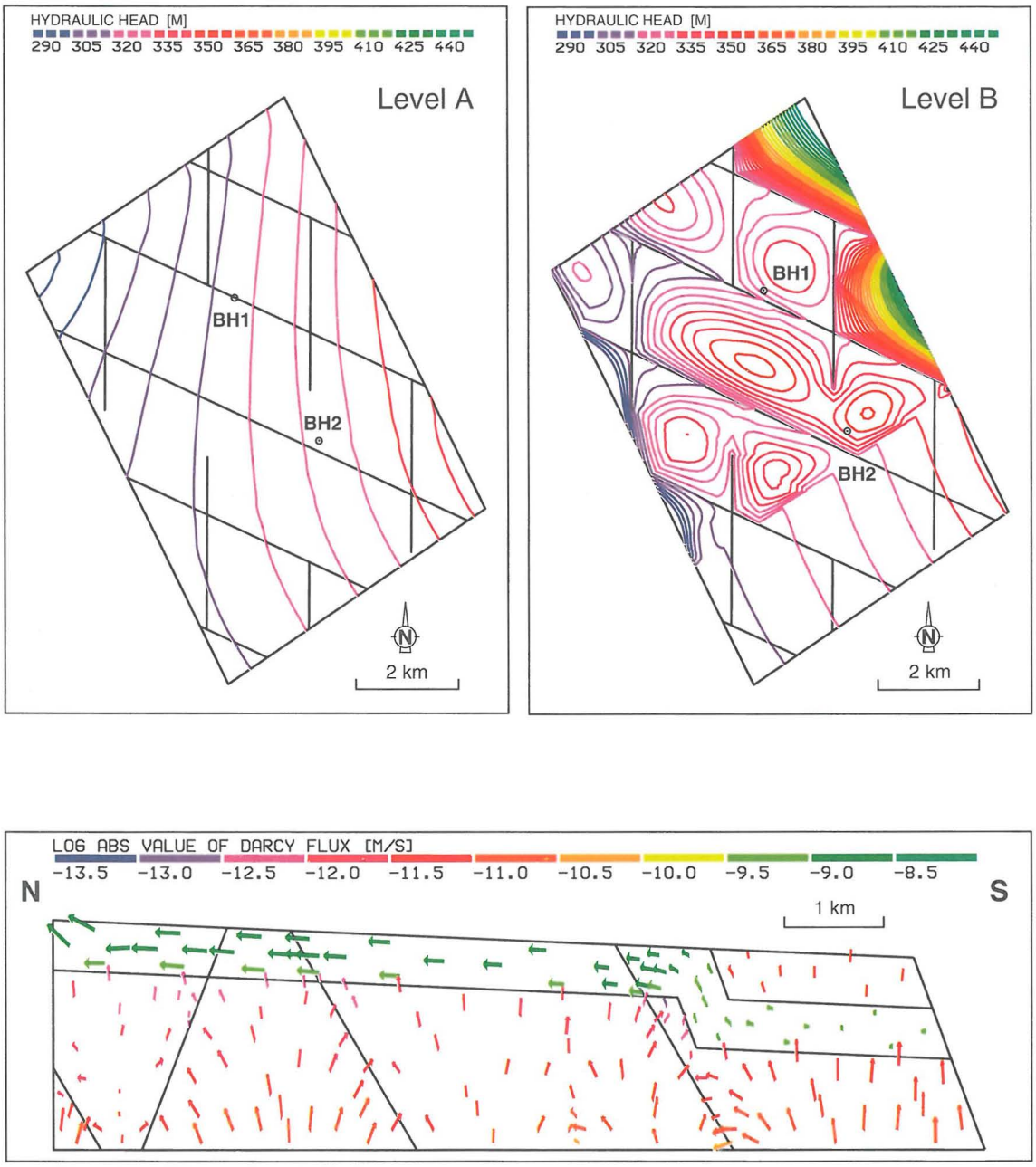

Fig. 4.6 Sparse scenario HYBW 433. *Top*: Plan view with head contours in HPD (level A-A) and in LPD (level B-B). *Bottom*: Vertical section 1-1' with projection of Darcy flux vectors (logarithmic scale)

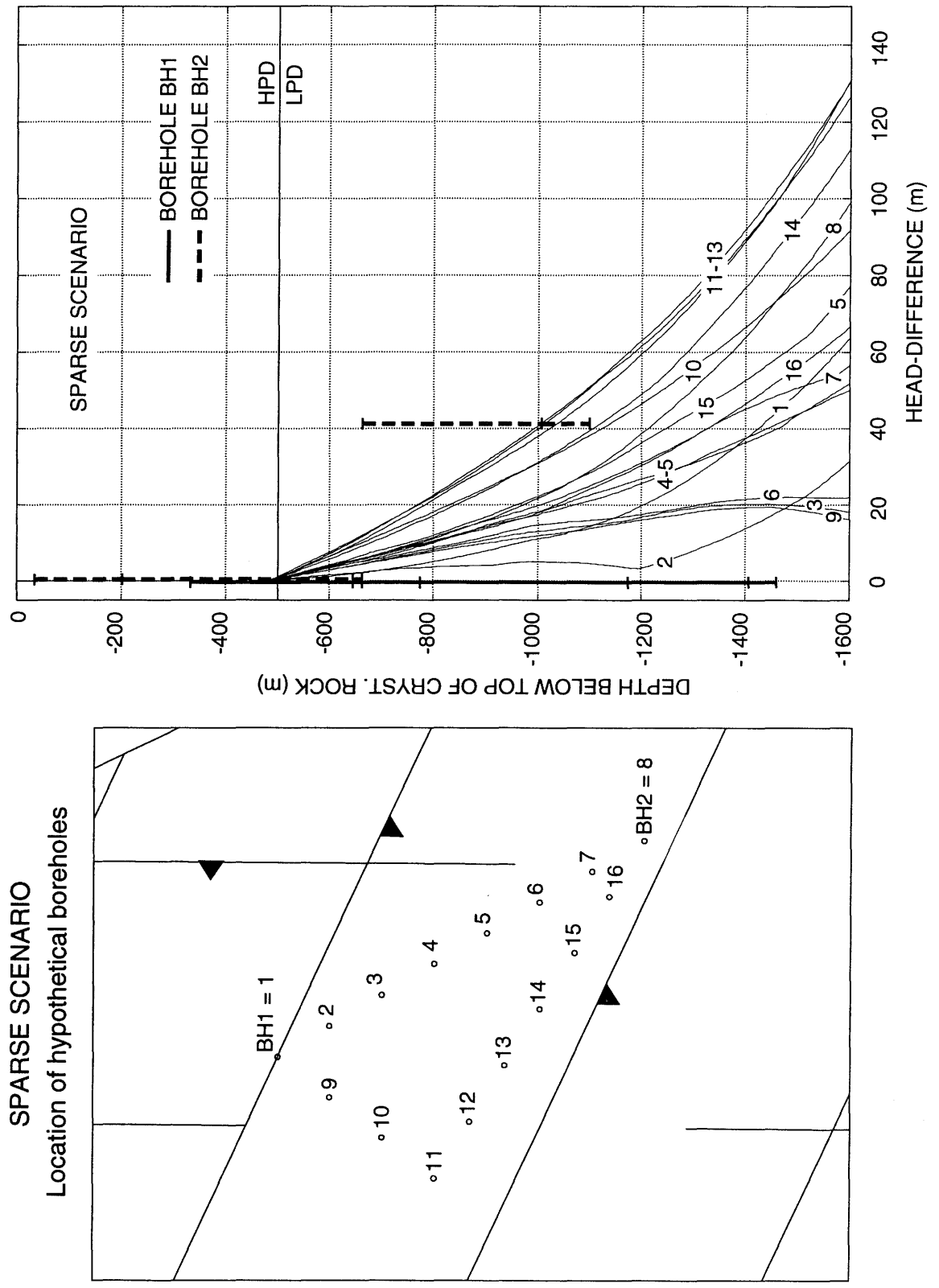

Fig. 4.7 Sparse scenario: Location of hypothetical boreholes with respect to faults at the top of LPD (*left*); calculated vertical head profiles (normalized) along boreholes (*right*).

result, only the first-order faults have a large enough transmissivity to affect the local flow, whereas the effect of the second-order faults becomes negligible. As a result, the model is divided in two large "intact" blocks, delimited by the 1st order faults; the gradient distribution within these blocks is similar to that of the sparse scenario.

Based on the geometry of the sparse scenario, the effective conductivity of the Low-permeable domain was increased by a factor of 5 in Run 431. The resulting higher conductance of the LPD blocks results generally in smaller vertical gradients and particularly in a reduced impact of boundary conditions. The overall flow pattern is the same as in the default run, that is, with prevailing upward flow in the center of intact blocks and horizontal flow in the peripheral zone.

It is concluded from the few parameter variation performed that any change in the relative hydraulic contrast between the water-conducting faults and the relatively undisturbed blocks induces similar effects on the overall connectivity of the simulated system as variations in fault frequency.

4.6 Model output relevant to safety analysis

4.6.1 Background

The principal hydrogeological information that is required for the safety analysis is the characterization of various geometric and hydraulic parameters that control the groundwater flow in the vicinity of a repository and through the geosphere. As mentioned in the introductory part of this report, this characterization involves flow analyses at different scales of interest. The relevant input that can be derived from the local-scale modeling study in area West comprises the following quantities:

- Distribution of hydraulic gradients within the LPD blocks, in particular at the level of a hypothetical repository; relation between simulated gradients and size of blocks (i.e., fault density).

- Distribution of Darcy fluxes and of integrated volumetric flow within the geosphere along the pathway; i.e., dilution of volumetric flow as it leaves the

LPD blocks (host rock) and enters a high-permeable environment, represented either by MWCF (in case of horizontal flow) or HPD (upward flow).

- Direction of flow and path lengths of particles between a release point in the interior of a LPD block and the block boundary (i.e., the point where the fluid particle enters a high-permeable environment, MWCF or HPD).

The hydraulic gradients obtained from the local-scale model serve as input for the next level of flow analyses on the block scale (Chapter 5).

Since the numerical solver calculates primarily freshwater heads at all internal nodal points, considerable post-processing efforts were required for deriving the above specified output. The codes FLUX and TRACK were applied to the first-level model results to calculate the Darcy fluxes and advective particle-flow paths respectively (see flow diagram in Fig. 3.1). The outcome of these simulations is representative for the local flow conditions of area West, which is characterized by hydrogeologic observations made in the deep boreholes of BOE, KAI and LEU. In view of the inherent uncertainties on the input side, the specific model output is expressed as the most likely range rather than a single value. As a rule, statistical distributions are provided by indicating the mean value and the 95% probability range.

The local-scale modeling results for safety analysis are described in the following. Each model output is presented as a range that spans the results of the full hybrid scenario and the sparse scenario. It was concluded in the sensitivity study that these two geometric variants cover the full range of model results; all other parameter variations (geometric or hydraulic properties) yield results within these bounds.

4.6.2 Distribution of hydraulic gradients

4.6.2.1 Approach

The distribution of hydraulic gradients in the host rock in the vicinity of a potential repository is one of the principal parameters required for the calculation of fluxes through a hypothetical repository. The gradients are derived directly from the output file of the FLUX postprocessing program. The Darcy flux is first computed

at each node within a selected volume of the host rock (represented by LPD blocks) and than scaled by the effective K property of that block to obtain the gradient vector at each node. In general, it is possible to calculate the gradient distribution resulting from all nodes randomly located within the LPD blocks. For safety-analysis purposes, however, it is appropriate to evaluate the gradient distribution that is a) representative for the designed repository depth (level 500), and b) excludes the boundary effects that were observed in Figs. 4.4 and 4.6 along the lateral and bottom model periphery. Therefore, it was decided to read out the simulated LPD gradients at level 500 from the **reduced** horizontal section B-B', i.e., excluding the southern part (see Fig. 4.2 bottom for geometry). Moreover, the peripheral area adjoin to VE and VW boundary was also excluded from the quantitative analysis. As was displayed in Figs. 4.4. and 4.6 (top right), significant boundary effects in terms of anomaly high gradients occur in the vicinity of lateral boundaries. Boundary conditions are particularly pronounced in the sparse scenario (Fig. 4.6) due to the small conductance (and resulting draining effect) of the boundary faces (see Section 4.3). Hence, only model nodes located in the interior of the model area at level 500 were used for the probabilistic analysis of hydraulic gradients.

4.6.2.2 Results

As mentioned above, the gradients are obtained indirectly by scaling the calculated Darcy flux by K. The direct model output are the vectors of 3-dimensional Darcy flux that are calculated at each node. The spatial distribution of Darcy fluxes at the 500-m level (B-B' in Fig. 4.2) is illustrated in Fig. 4.8 and 4.9. The absolute Darcy vectors are splitted into horizontal and vertical flow component to emphasize the predominant tendency of flow in each geometric scenario.

The horizontal components of Darcy flux (or gradient if scaled by K(LPD) or K (MWCF) respectively) are displayed in Fig. 4.8. The full scenario (*top*) reflects the general trend of the regional gradient from southeast to northwest which controls also the flux in the LPD blocks. The fluxes in the first-order fault are by about three orders of magnitude larger than those in the LPD blocks. The horizontal flux component in the sparse scenario (*bottom*) shows a radial direction from the block centers toward the bounding faults. Hence, the local flow direction at any point within a LPD block depends on its relative location to the nearest water-conducting fault and is no more dominated by the regional gradient.

The vertical components of Darcy flux are shown as contours of equal value (isolines) in Fig. 4.9. In the full scenario, this component is only small and limited to the centers of blocks. Again, the regional flow regime dominates within the fault network. In contrast, the sparse scenario shows the presence of distinct vertical gradients within the undisturbed large blocks where the local flow condition is preserved. The maximum upward flux occurs in the center, whereas the peripheral zones of blocks drain laterally toward the adjacent faults, as shown by the vectors in Fig. 4.8.

The gradient values were calculated from the Darcy fluxes shown in Figs. 4.8 and 4.9 for each scenario. The nodes in the vicinity of lateral model boundaries are excluded in this analysis. The resulting statistical distributions are shown as histograms in Fig. 4.10 and summarized with other relevant results in Table 4.7. Each distribution is characterized by the mean value and the 95% probability range given by the standard deviation. The full spectrum of simulated gradients in the local-scale model is defined by the minimum in full scenario and the maximum in sparse scenario.

The mean absolute gradient is 0.011 for the full scenario and 0.047 for the sparse scenario. The hydraulically well-interconnected full hybrid model is entirely drained by the fault network. In turn, the generally larger hydraulic gradients of the less connected sparse scenario are more consistent with the observed local conditions in the boreholes than the full scenario.

It is concluded that this observation, notably the general absence of vertical gradients in the highly interconnected model scenarios 400-420, suggests that not all faults in the geometric network (as identified by structural geology in Fig. 4.1) are hydraulically active, i.e., water conducting.

4.6.3 Distribution of flux between LPD blocks and major faults

4.6.3.1 Approach

The second issue of interest related to hybrid model output was the distribution of flow between the low-permeable crystalline blocks (LPD) and the bounding permeable faults (MWCF). As was previously observed in Section 4.3.3.2

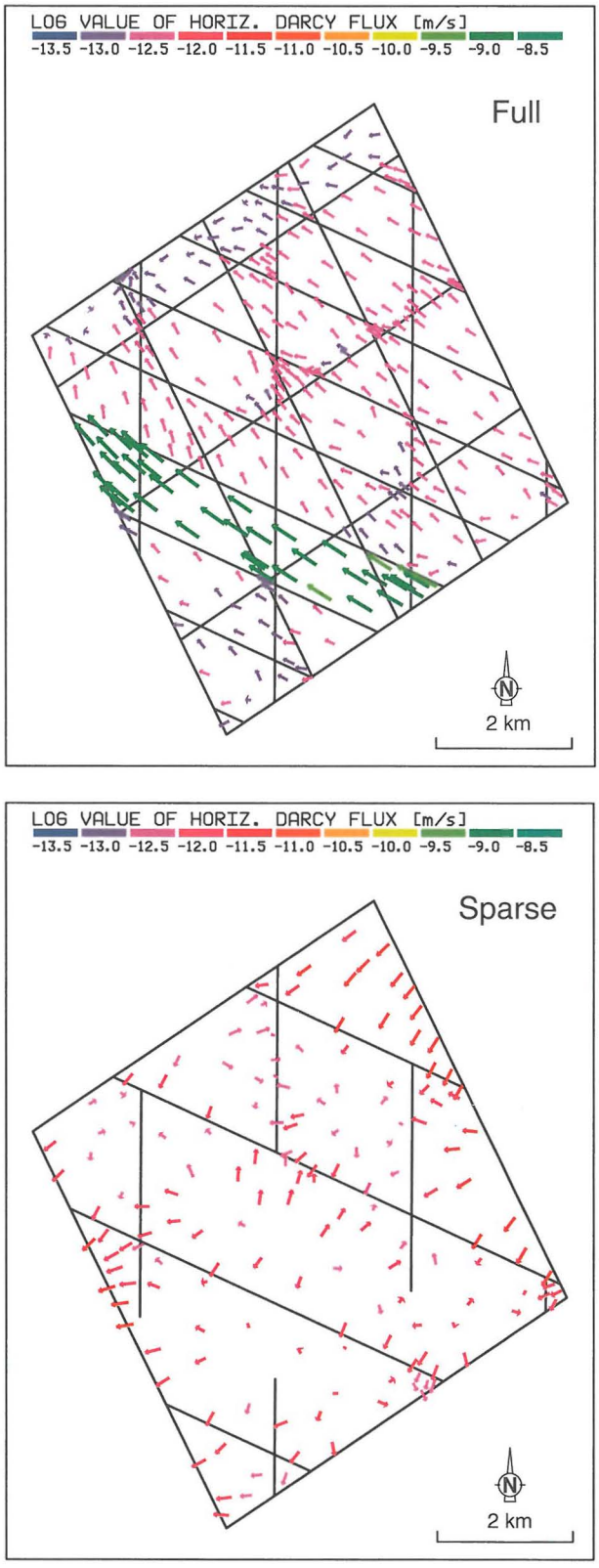

Fig. 4.8 Horizontal component of simulated Darcy flux (logarithmic scale) at 500-m level (B-B' level in Fig. 4.2). Full scenario (*top*) and sparse scenario (*bottom*)

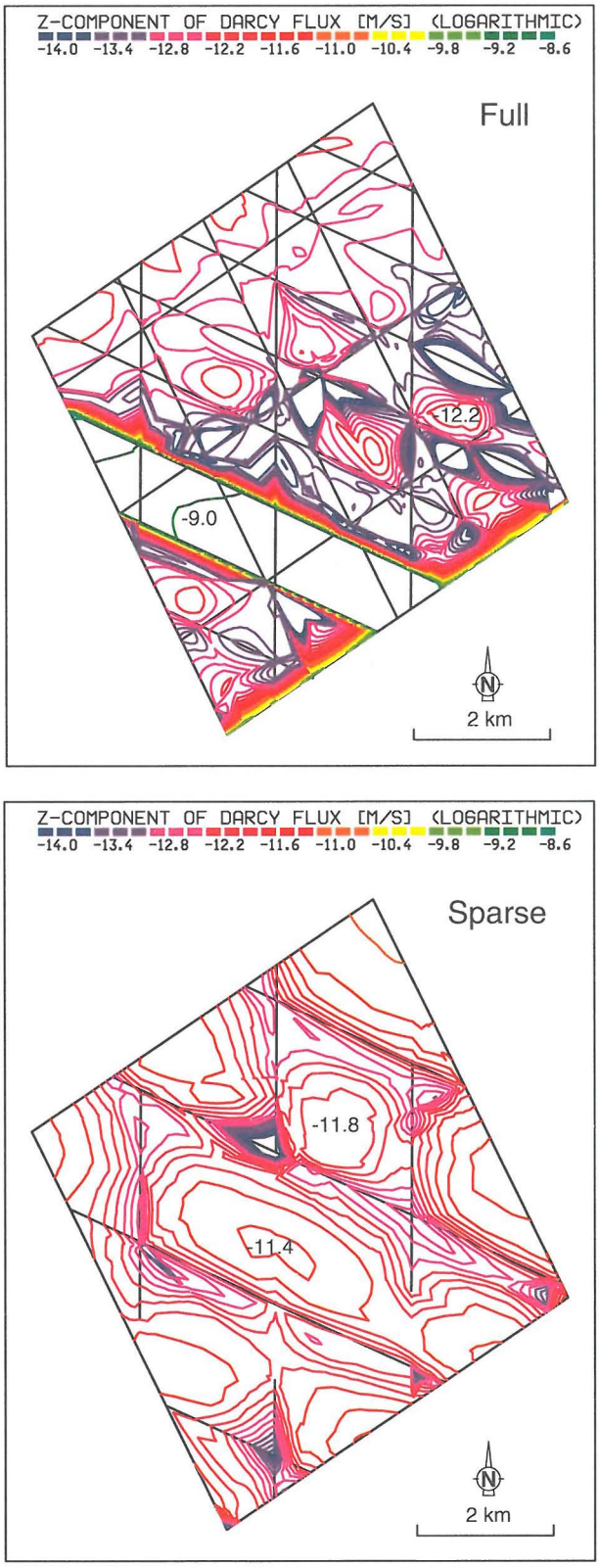

Fig. 4.9 Contours of vertical component of simulated Darcy flux (logarithmic scale) at 500-m level (B-B'). Full scenario (*top*) and sparse scenario (*bottom*)

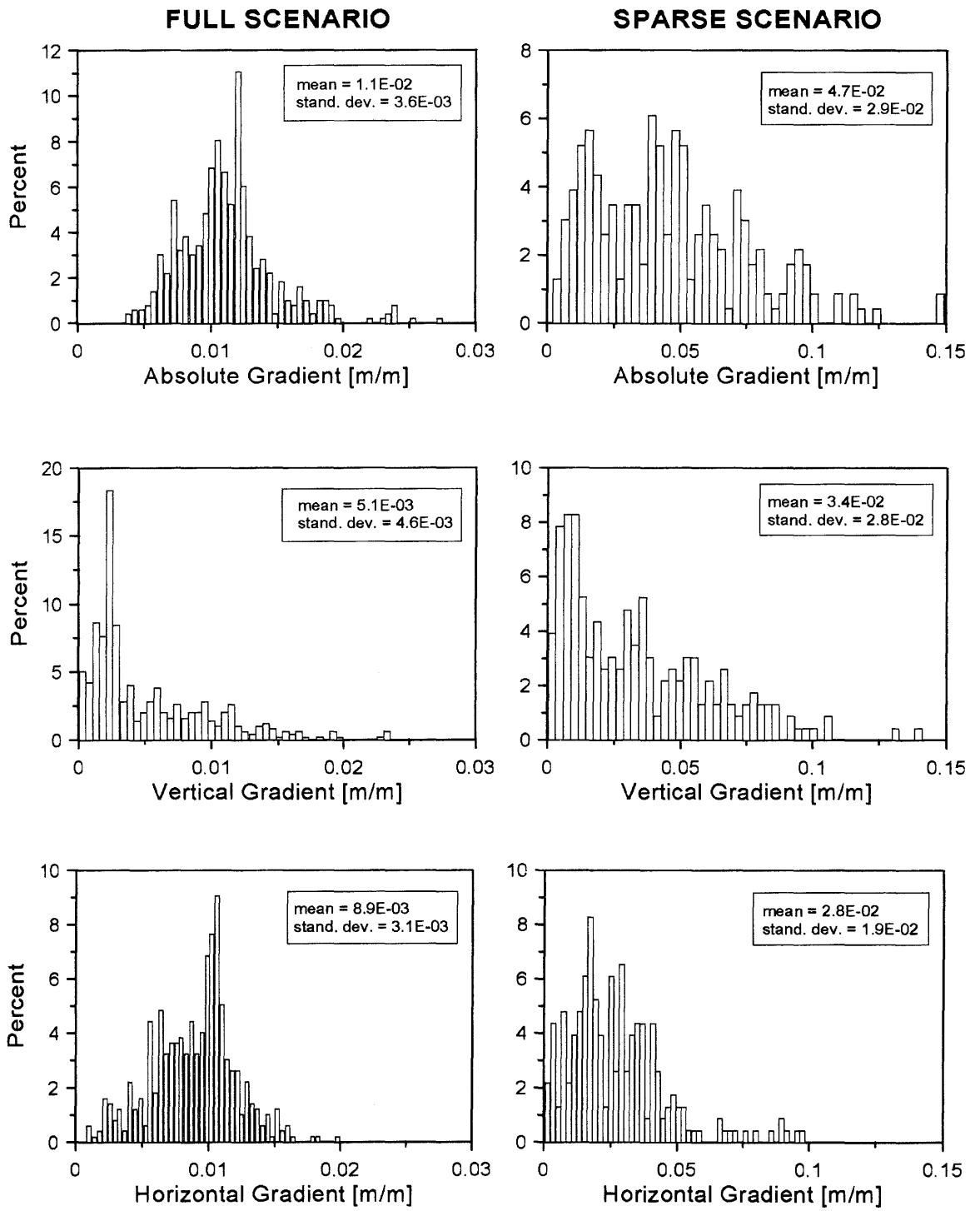

Fig. 4.10 Distribution of simulated hydraulic gradients in LPD blocks at 500-m level (B-B' in Fig. 4.2). Full scenario *(left)* and sparse scenario *(right)*.

however, the post-processing step of flux calculation is numerically not feasible in 2-D elements representing the second-order faults. In order to allow the application of the FLUX code for computation of Darcy fluxes and of integrated volumetric flow, the MWCF-2 features needed to be blown-up to 3-D elements with the correct thickness of 20 m. For computational reasons this is not possible in the full-scale model due to over-proportional increase of elements. The solution for this dilemma was found by generating small sub-models representing limited block volumes or "boxes". The limited size of these boxes with dimensions 1000 x 1000 x 500 m allows to expand the second-order faults to full 3-D elements. Numerically, each box is an independent sub-model with its own finite-element grid which is generated by the same algorithm as the HYBW model. Each box is linked to the full-size model through boundary conditions, i.e., the heads calculated by the large model are assigned as boundary conditions to all common nodes along the box surface.

In order to obtain a statistically representative database that is location-independent, up to 200 generic boxes were generated for each considered hybrid scenario. The boxes are laterally randomly distributed over the model area to provide representative results (Fig. 4.11 top). The vertical position of the boxes is constant, with the basis being fixed at level 500. Hence, the flux calculations cover the uppermost 500-m long section of the LPD unit (Fig. 4.11 bottom).

Each sub-model typically consists of 500 to 1,000 elements and the computations require about 2 minutes CPU on the STARDENT 3020 computer. Therefore, a complete analysis of all boxes for one HYBW run needs about 400 CPU minutes, or 6 to 7 hours. A new code was developed to automatize the complete process of random box generation, transfer of boundary conditions from the large model, head calculation by the FEM301 solver and post-processing.

The first level of post-processing consists of flux calculation (FLUX) for each box. This output is lumped for all generated boxes and written out in one result file. In a second step, the Darcy fluxes are categorized to the LPD and MWCF domains and subjected to statistical analysis. Since each domain is defined as equivalent porous medium of constant K property, the obtained distribution of Darcy fluxes reflects directly the variability of the hydraulic gradient within the model. As additional quantity, the so called "dilution ratio", D, of Darcy fluxes is computed at the common boundary nodes between the LPD blocks and faults. Note, that this ratio D does not involve volumetric fluxes, it merely indicates the velocity ratio of fluxes that leave the low-permeable blocks and enter the

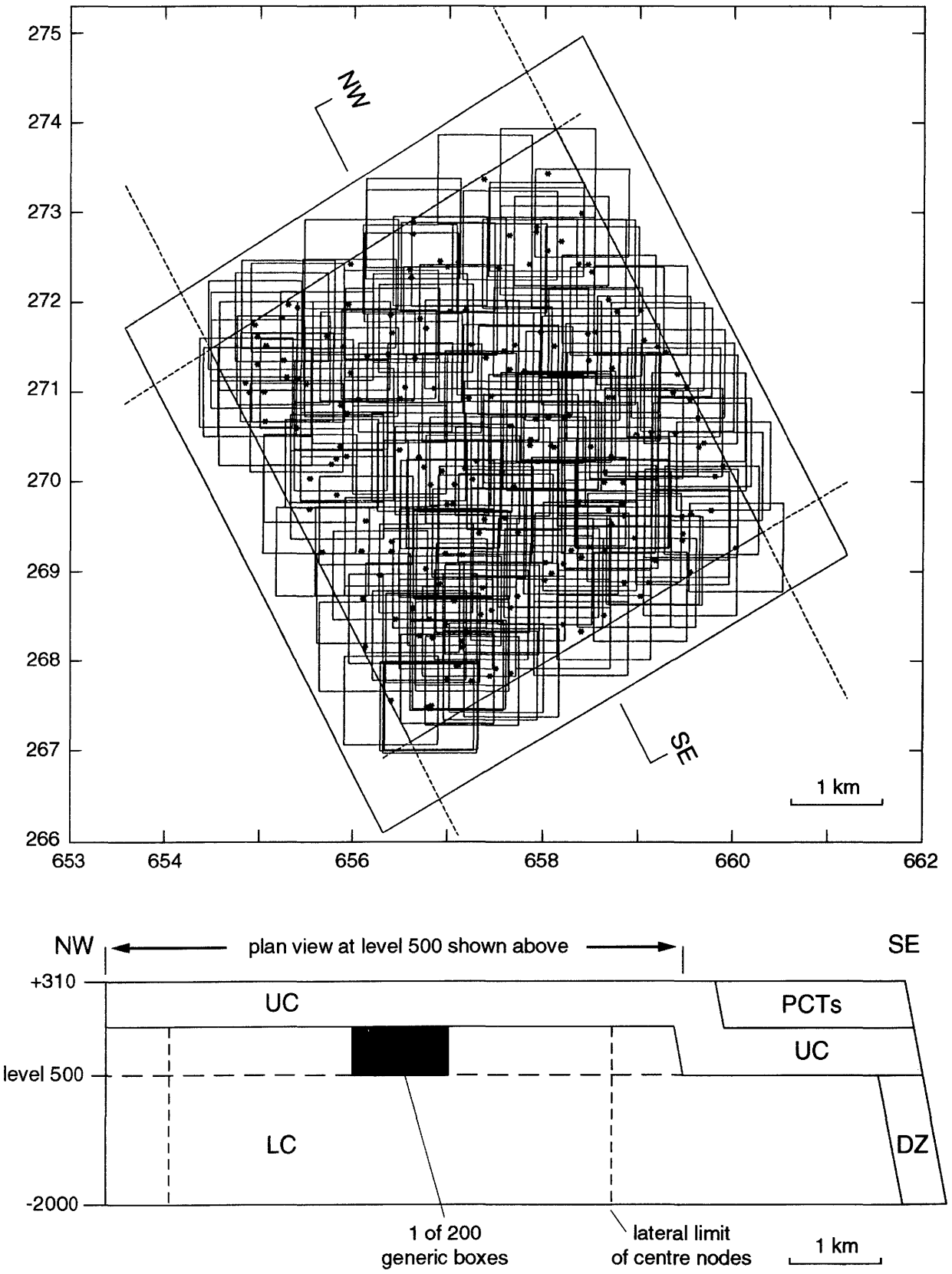

Fig. 4.11 Random locations of generic boxes (sub-models) for flux calculations. Plan view at 500-m level *(top)*, schematic section *(bottom)*.

permeable environment of MWCF. A rough estimate of the volumetric dilution rate from the Darcy fluxes requires the additional definition of a "control volume" for the mixing zone (see Section 4.6.4). The third level of the box flux evaluation consists in integrating the Darcy fluxes over the surface areas to determine the total volumetric flow (turnover) through the box.

All flux results are presented as statistical distributions over all boxes. The individual quantities are derived as follows for each single box j:

1) Darcy flux in major faults (MWCF): q_F (m/s) (16)

l = 1..N2: all nodes in faults

$$Mean: \quad \bar{q}_F^j = \frac{1}{N2} \sum_{l=1}^{N2} q_{F,l}^j$$

$$Variance: \quad \sigma_{q_F}^j = \sqrt{\frac{1}{N2} \sum_{l=1}^{N2} (q_{F,l}^j - \bar{q}_F^j)2}$$

$$Minimum: \quad q_{F,\min}^j = \min_l (q_{F,l}^j)$$

$$Maximum: \quad q_{F,\max}^j = \max_l (q_{F,l}^j)$$

2) Darcy flux in undisturbed blocks (LPD): q_M (m/s) (17)

m = 1..N1 : all nodes in LPD blocks (block matrix)

$$Mean: \quad \bar{q}_M^j = \frac{1}{N1} \sum_{m=1}^{N1} q_{M,m}^j$$

$$Variance: \quad \sigma_{q_M}^j = \sqrt{\frac{1}{N1} \sum_{m=1}^{N1} (q_{M,m}^j - \bar{q}_M^j)2}$$

$$Minimum: \quad q_{M,\min}^j = \min_m (q_{M,m}^j)$$

$$Maximum: \quad q_{M,\max}^j = \max_m (q_{M,m}^j)$$

3) Flux ratio at block-fault interface: D (-) (18)

k = 1..N3: all common nodes along LPD and MWCF boundary

$$Mean: \quad \bar{D}^j = \frac{1}{N3}\sum_{k=1}^{N3} D_k^j$$

$$Variance: \quad \sigma_D^j = \sqrt{\frac{1}{N3}\sum_{k=1}^{N3}(D_k^j - \bar{D}^j)2}$$

$$Minimum: \quad D_{\min}^j = \min_k(D_k^j)$$

$$Maximum: \quad D_{\max}^j = \max_k(D_k^j)$$

$$with \quad D_k^j = \frac{q_{F,k}^j}{q_{M,k}^j}$$

4) Integrated flow through box surface: Q_M, Q_F, Q_T (m^3/s) (19)
(turnover)

A_M = surface of blocks; A_F = surface of faults

$$Matrix: \quad Q_M^j = \int_{A_M} q_M^j(\vec{r})\, dA$$

$$Faults: \quad Q_F^j = \int_{A_F} q_F^j(\vec{r})\, dA$$

$$Total: \quad Q_T^j = Q_M^j + Q_F^j$$

The total volumetric flow through the box, Q_T, is calculated as a sum of fluxes integrated over the surface of the block matrix, Q_M, and of the faults, Q_F. Due to the small conductance of LPD blocks, the contribution of Q_M to the total turnover through the model is negligible.

4.6.3.2 Results

The results of box-flux calculations are summarized in Table 4.6 for the two principal hybrid scenarios. The results of the intermediate geometric variants are similar to those of the full-set scenario. The resulting statistical distributions of Darcy fluxes and integrated flows are presented in Fig. 4.12 and 4.13. As an additional information to Table 4.6, hydraulic gradients can be derived from the calculated Darcy fluxes by means of a scaling factor K. The resulting mean gradients within the MWCF unit vary from 0.006 (full) to 0.02 (sparse), those within the LPD blocks from 0.024 to 0.07 respectively. The latter values are by 100% and 50% larger than the mean gradients in Fig. 4.10, that were calculated directly from the hybrid model at the repository level 500. This comparison illustrates the conservative nature of the box-flow calculations, given that the generic boxes in Fig. 4.11 include also the peripheral area of the LPD unit that is affected by boundary effects.

As a general trend, the sparse scenario features generally larger flux rates and gradients, whereas the total volumetric flow is smaller in comparison with the full scenario. This result is a combined effect of imposed fluxes at the boundaries (under constant external gradients I in both cases) and reduced connectivity of the sparse model. In the full scenario, the larger volumetric flow (as a function of C and I) that is forced through the model is readily drained by the well-interconnected fault network. The incoming flux in the sparse scenario, although being smaller due to reduced boundary conductance is subjected to more flow resistance and yields larger velocities and gradients within the model.

Table 4.6 Results of box flux calculations

	Full scenario HYBW 403	**Sparse scenario HYBW 433**
1. q_F: all nodes in faults (MWCF)		
q_F (mean) [m/sec]	1.9·E-09	6.7·E-09
range: q_F(min) - q_F(max)	4E-10 - 6E-09	9E-11 - 5E-08
mean ratio min/max	0.33 (±0.15)	0.24 (±0.22)
2. q_M: all nodes in block matrix (LPD)		
q_M (mean) [m/sec]	1.0·E-12	3.2·E-12
range: q_M(min) - q_M(max)	4E-13 - 3E-12	5E-14 - 3E-11
mean ratio min/max	0.42 (±0.15)	0.07 (±0.06)
3. D: Dilution at all interface nodes i; $D(i)=q_F(i)/q_M(i)$		
D (mean)	1,920	1,950
range: Dmin - Dmax	400 - 5,000	100 - 10,000
mean ratio min/max	0.42 (±0.17)	0.38 (±0.33)
4. Q_{tot} through box [m^3/s]	3.0·E-04	1.5·E-05

4.6.4 Dilution of flow along the pathway

A complementary analysis to the above described box flux calculations is required in order to estimate the volumetric flow dilution that occurs along the flow path through the geosphere at the transition to a different hydrogeological unit. The Low-permeable domain, LPD, represents the actual geologic barrier for a flow particle released from the repository. According to the hybrid model simulations, the particle will travel under the local flow field either toward the next **active** (i.e., water-conducting) fault, MWCF, downgradient of the repository (radial flow), or rather upward to reach the higher-permeable crystalline rocks, HPD. In either environment, a significant dilution of the flow will occur before it finally reaches the biosphere in the corresponding groundwater discharge area.

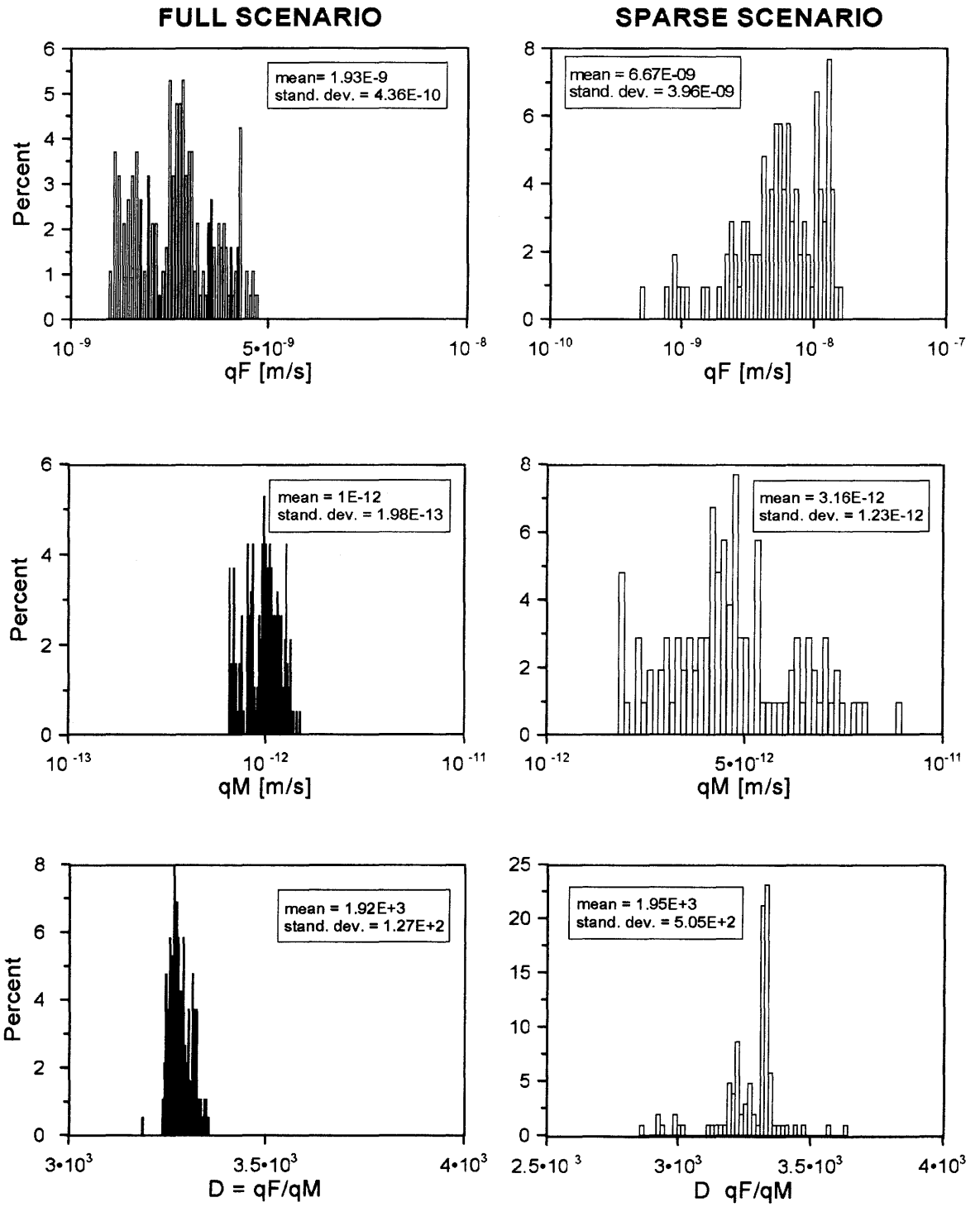

Fig. 4.12 Distribution of Darcy flux in faults (qF), LPD blocks (qM) and resulting flux ratio D=qF/qM. Full scenario *(left)*, sparse scenario *(right)*

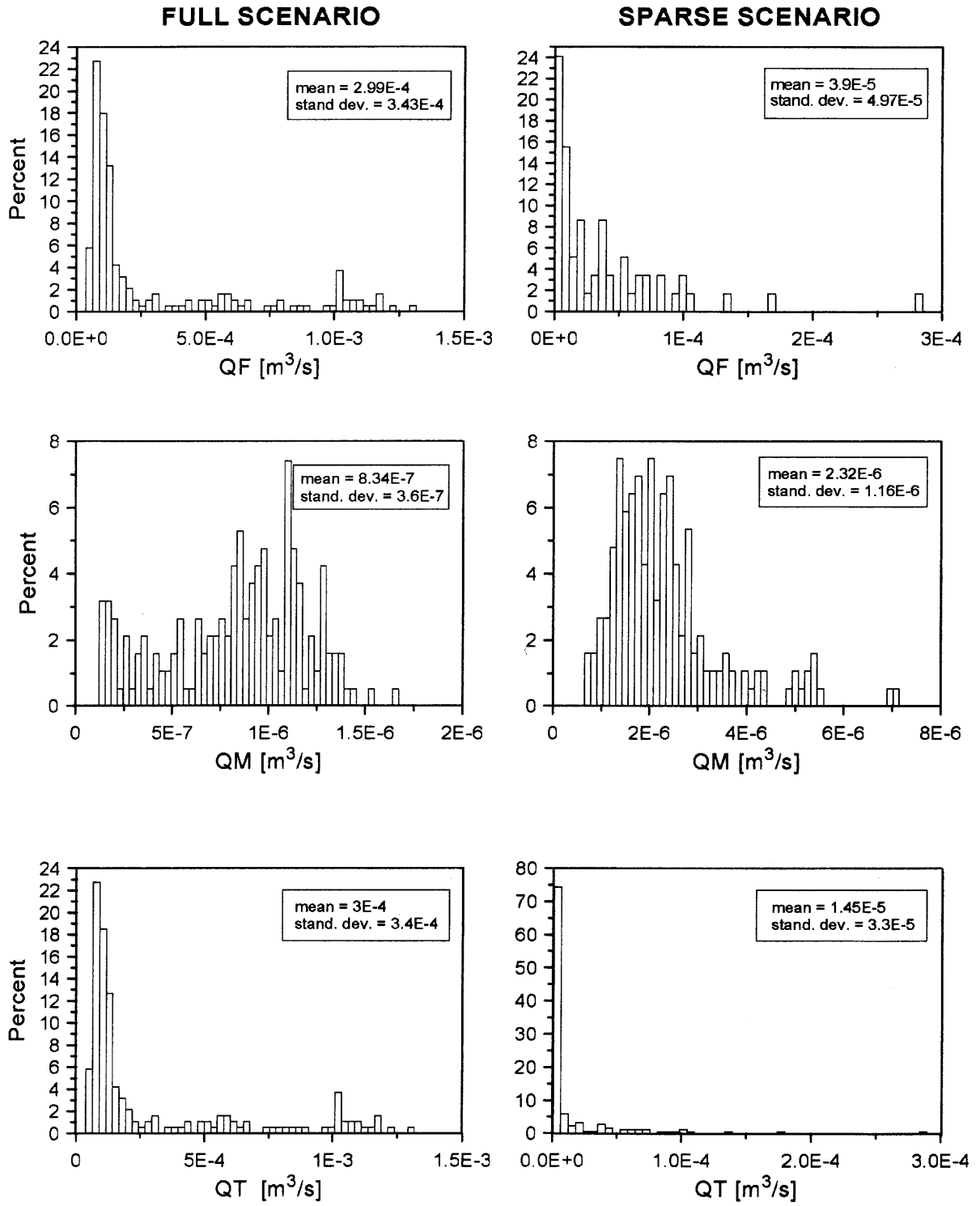

Fig. 4.13 Distribution of integrated volumetric flow through box; flow through faults (QF), blocks (QM) and total flow (QT). Full scenario *(left)*, sparse scenario *(right)*

From LPD blocks to MWCF

Based on the flux calculations described above, the volumetric dilution ratio, D_{vol}, between the flow through the Low-permeable domain (LPD) and through the major water-conducting faults (MWF) can by approximated by two means: by comparing directly the total volumetric flow, Q_M and Q_F, obtained from balance calculations in the generic boxes above, or by integration of the directly calculated Darcy fluxes q_M and q_F over an appropriate mixing volume.

A comparison of integrated volumetric flow through LPD blocks (Q_M) and faults (Q_F) in Fig. 4.13 yields a dilution ratio of 400 to 500. The derivation from Darcy fluxes (velocities) in Fig. 4.12 and in Table 4.6 requires the introduction of a "control" volume that defines the assumed mixing zone, according to a sketch in Fig. 4.14. If the water moving through the faults is assumed to be well mixed and flowing axially upward or horizontal (that is, parallel to fault walls in each case), the relevant control volume would be defined by the product of 1) thickness of the fault, b, (in this case 20 m); 2) the "width" of the plume, (i.e., the spread in the horizontal, w) of q_M entering from the LPD block, and 3) its "height" (i.e., the spread in the vertical, h).

The sketch of Fig. 4.14 shows the geometric relations for Q_F flowing upward. The volumetric flow from the block matrix entering this control volume is defined as $Q_M=q_M \cdot w \cdot h$. This flow is diluted by water flowing within faults, Q_F, through an area defined by the fault thickness and the width of the plume: $Q_F= q_F \cdot b \cdot w$. The resulting volumetric dilution $D_{vol} = Q_F/Q_M$ corresponds to the Darcy-flux ratio, D, calculated above (Table 4.6) which is scaled with the geometric ratio of fault thickness to plume height, b/h. If the height ranges from 20 m (about twice the height of the cavern plus disturbed zone) to about 200 m, the multiplicative factor of D is 1 to 0.1, resulting in dilution ratios of 200 to 2,000. In the alternative case of Q_F moving horizontally through the fault, the scaling geometric ratio in this dimension is b/w.

Conservatively, a dilution range from 100 to 1,000 is reported in Table 4.7 that summarizes all results of the local-scale model which are relevant for the safety analysis.

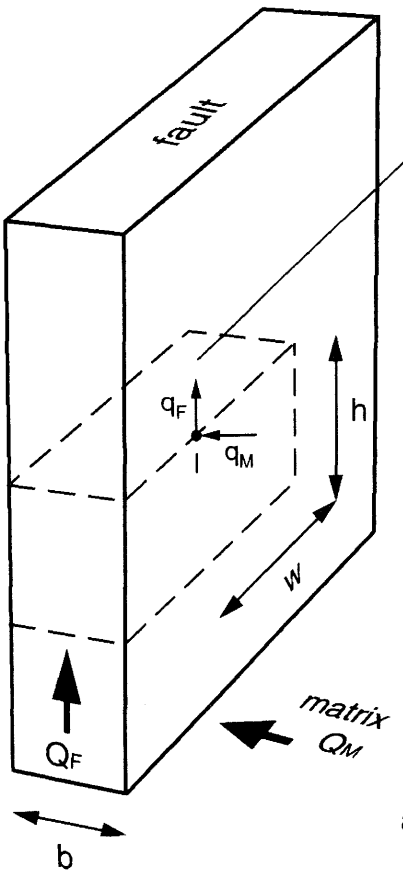

I: node at interface fault / matrix

qM, qF: Darcy flux in matrix / fault

QM, QF: volumetric flow

$$\text{at node I:} \quad \frac{qF}{qM} = D$$

$$\text{Dilution } D^* = \frac{QF}{QM} = \frac{qF \bullet b \bullet w}{qM \bullet h \bullet w} = D\,\frac{b}{h}$$

Fig. 4.14 Sketch of control volume defined for the estimate of flow dilution between LPD blocks and major faults

From LPD to HPD

In the case of an upward oriented local flow system, such as simulated in the center of LPD blocks in the sparse hybrid model, the groundwater moving from the repository would be diluted in the high permeable crystalline rocks, HPD. Based on its large transmissivity, this upper part of the crystalline basement constitutes an important regional aquifer. The dilution of volumetric flow between

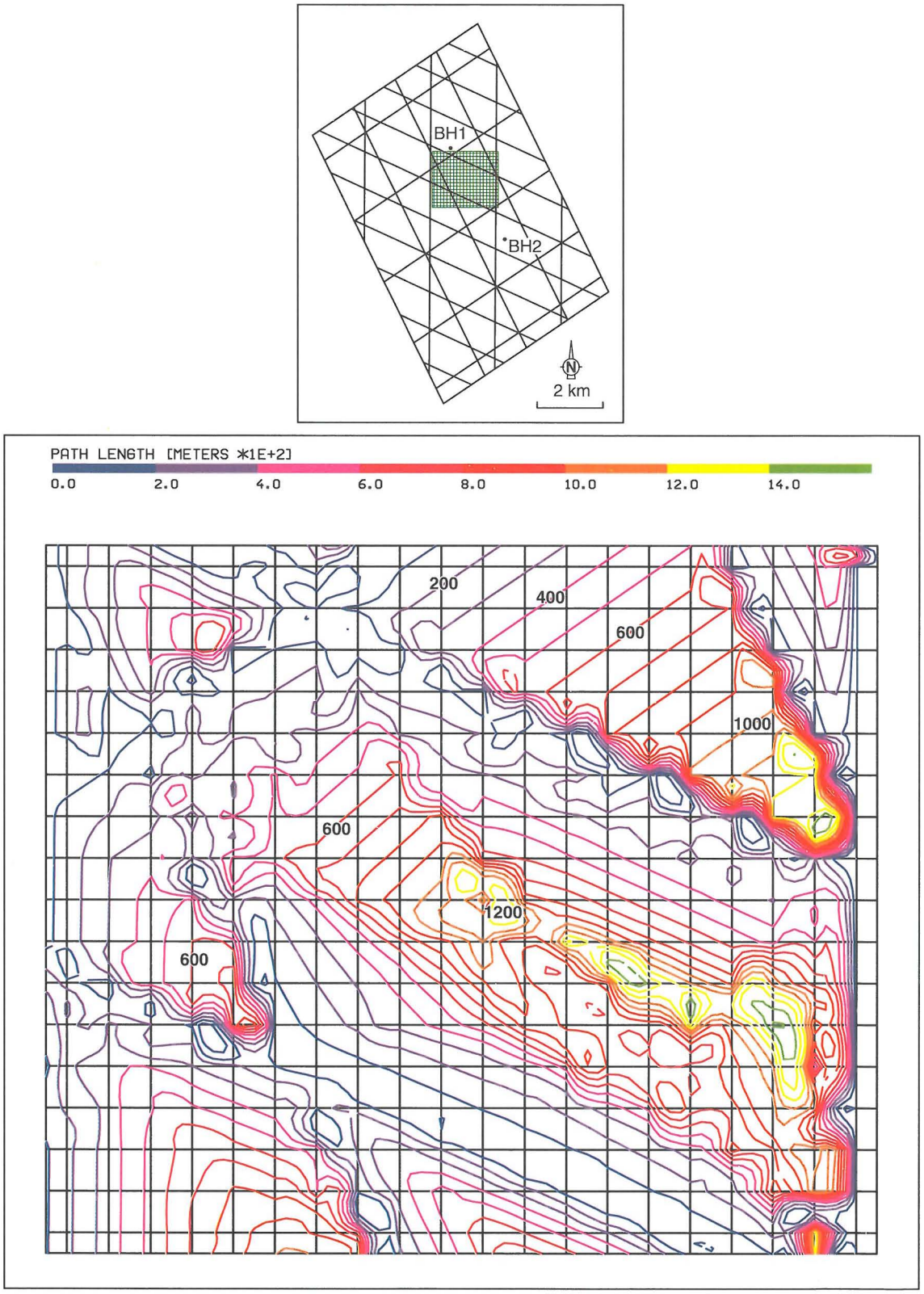

Fig. 4.15 Full scenario, particle tracking in LPD blocks: plan view at 500-m level with location of release points (*top*), contour lines of equal path lenght in LPD (*bottom*)

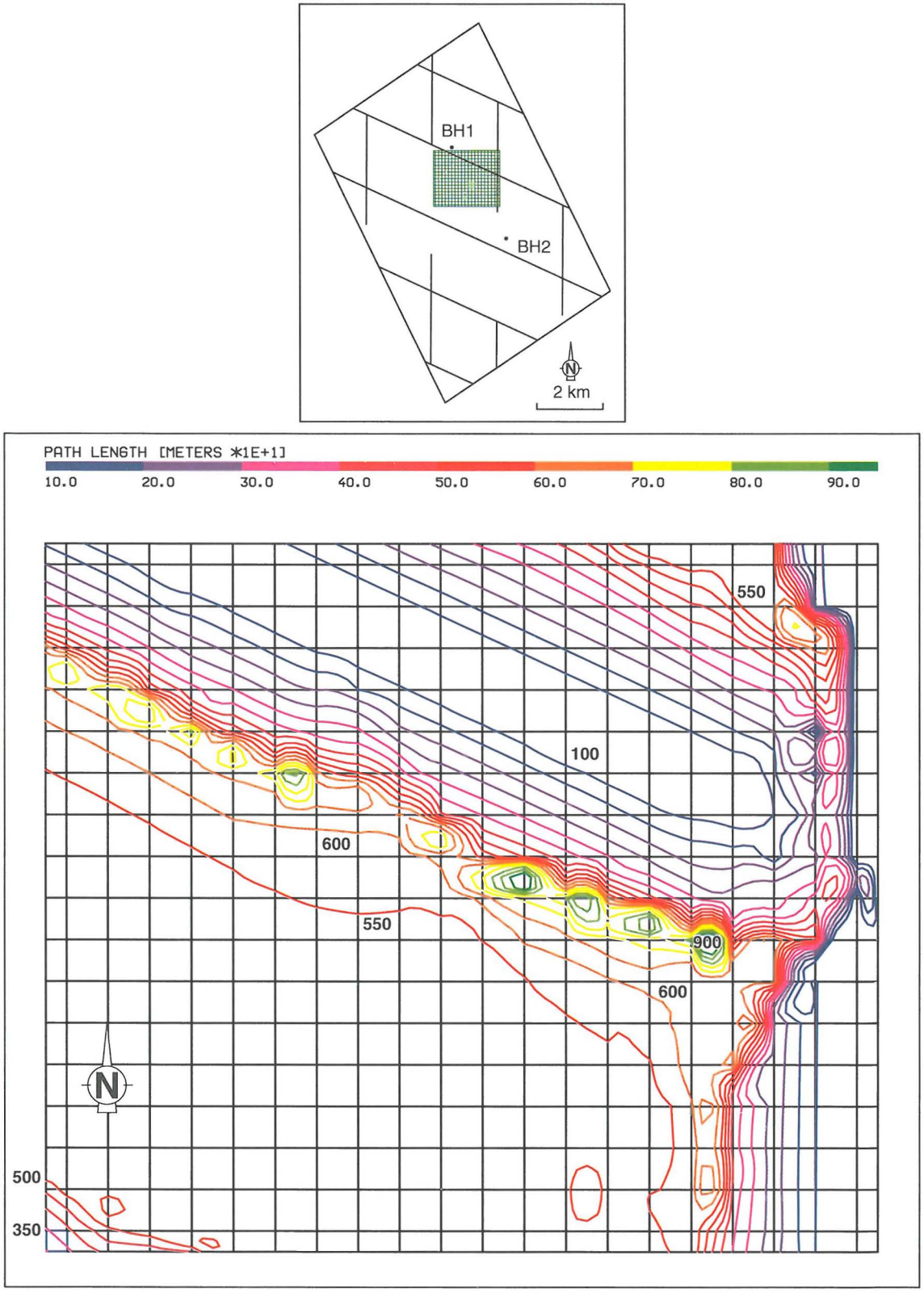

Fig. 4.16 Sparse scenario, particle tracking in LPD blocks: plan view at 500-m level with location of release points (*top*), contour lines of equal path length in LPD (*bottom*)

the two domains depends on the degree of mixing that occurs within the permeable upper layer, modeled with a thickness of 500 m. If a 20-m thick mixing zone along the bottom is assumed, then the dilution ratio is equal to that expected between the LPD blocks and faults, that is between 100 and 1,000; if all 500 m of the upper-crystalline rock layer were well mixed, then the dilution ratio would be between 2,500 and 25,000. The conservative case was assumed in Table 4.7 indicating a range similar to that of LPD/MWCF.

4.6.5 Direct flow path length in host rock

4.6.5.1 Approach

The last of the envisaged hybrid-model outputs addressed in Section 4.6.1 aims at evaluating the impact of block size (or fault spacing) on path lengths of flow within the low-permeable environment of a repository. The relation between block size and general flow direction was illustrated in Section 4.6.2.

Particle tracking calculations (TRACK, see Fig. 3.1) were applied to visualize the variability of advective path lengths as function of block size and the relative position of release points within a block. An arbitrary part of the model area was selected at two depth levels of 250 and 500 m below the top of LPD. Within this area a large number of regularly distributed particles was released. The flow particles are tracked until they reach the physical boundary of the LPD block. In numerical terms, the tracking algorithm stops as soon as the particle enters a defined material unit, in this case either MWCF or HPD block. The defined grid of release points can be moved throughout the model as to cover the entire model area. The tracking analysis was performed for both main hybrid scenarios. The results are evaluated for the 500-m level area representing a potential repository location. The results of particle tracking are displayed as contours of equal path length in Figs. 4.15 an 4.16. A plan view at the top of each contour map shows the location of the grid that defines the release points. The grids are 2x2 km in size, the release points have a constant spacing of 100 m. The calculated contour lines of equal path length are a result of the dominant flow field in each model scenario. The interpretation is facilitated in combination with the illustration of Darcy-flow directions in Figs. 4.8 and 4.9. Note also that the displayed contour lines result from interpolation between adjacent points. In areas with a heterogeneous gradient distribution (fault intersections), the inter-

polation distance of 100 m is too large and yields imprecise results. The consequence is that the minimum isolines do not show a continuous elongated shape aligned along the faults (flowpath = 0), but are disturbed by local maxima due to interpolation errors.

4.6.5.2 Results

The contour map calculated for the full scenario at level 500 is shown in Fig. 4.15 and can be interpreted as follows:

- Each block features a narrow marginal zone where the particles are directly attracted to the adjoining faults (horizontal flow with short path lengths equivalent to the direct radial distance to the faults);

- Large flowpath lengths occur generally in central parts of larger blocks (i.e., outside the influence range of radial flow), where a diagonal flow toward downstream **and** upwards predominates.

- The maximum flowpath lengths result from release points located closely on the downstream side from a fault, from where the particles move diametrally across the block toward another permeable fault that is downgradient.

- The small blocks are dominated by radial flow conditions toward the adjacent faults.

The simulated conditions in the sparse scenario are illustrated in Fig. 4.16. As shown in the situation map on the top, the grid of release points is located over a large undisturbed block and is intersected only by one diagonal fault. The results are evaluated as follows:

- Because vertical gradients dominate the local flow within the large LPD blocks, the flowpath length is basically defined by the vertical distance of the release point to the bottom boundary of the overlying HPD unit, in this case 500 m. The draining effect of faults is evident only within a relatively narrow marginal zone of the blocks.

- The absence of diagonal flow with a horizontal and vertical component results in shorter flowpaths in comparison to the results of the full scenario.

Moreover, the hydraulic gradients in the sparse scenario are generally larger than those in the full scenario.

4.6.5.3 Comments and conclusions

In general terms, the direct distance between any point in the LPD block and a higher-permeability domain (HPD or MWCF) is a function of 1) the point location relative to the permeable features, and 2) the direction of local hydraulic gradient between the release point and these features. It was shown that horizontal gradients predominate in the vicinity of major faults in the low-permeability domain, whereas vertical gradients are preserved only in the central parts of relatively large undisturbed blocks, beyond the range of influence of the MWCF.

As a consequence, a minimum lateral distance of the "release point" to the next major water-conducting fault is required as a basic layout-determining criterion. The assumption was made that a minimum horizontal setback from transmissive second-order faults will be specified on the basis of safety-analysis requirements. If the local groundwater-flow regime is well known and stable then the repository could be placed closer to hydraulically active faults upgradient. On the other hand, a more general and conservative approach is to apply the minimum horizontal direct path length uniformly away from all hydraulically active second-order faults when evaluating the area available for a repository. For preliminary design and safety analysis, it is appropriate to assume initially that all second-order faults are hydraulically active (i.e., that the full scenario is the correct description of the system).

The minimum vertical direct pathlength, which is also a design-specific criterion, is basically defined by the depth of the repository with respect to the Higher-permeability domain, HPD.

4.6.6 Summary of model results relevant to Safety Analysis

A new post-processing approach was applied to the HYBW model to derive a specific output that meets the needs of safety analysis at this modeling scale. The relevant hydrogeologic data that are required as input for safety assessment calculations are summarized in Table 4.7. These data include the magnitudes (distribution) and directions of hydraulic gradient in the host rock, Darcy fluxes in

host rock surrounding the repository cavern and in adjacent permeable faults, and estimates of flowpath length of groundwater within the low-permeability domain of the geosphere.

Table 4.7 Summary of hybrid-model results relevant to safety analysis

Type of result	Mean value (1)	Max. range (2)	Remarks
1. gradient distribution in host rock (LPD)	full sparse	full & sparse	gradients in LPD blocks at level 500, see Fig. 4.10
· Horizontal	0.009 - 0.028	0.002 - 0.086	
· Vertical	0.005 - 0.034	<E-3 - 0.07	
· Absolute	0.012 - 0.047	0.005 - 0.115	
2. Darcy-flux distribution: in LPD blocks, qM (m/s)	1E-12 - 3E-12	5E-14 - 3E-11	probabilistic analysis of 200 generic boxes, see Fig. 4.11 - 4.13
in MWCF, qF (m/s)	2E-09 - 7E-09	9E-11 - 5E-08	
ratio at interface, D	about 2,000	100 - 10,000	
3. Dilution ratio within geosphere	in the order of		see Fig. 4.14
· from LPD to MWCF	100 - 1,000		conservative assumption
· from LPD to HPD	100 - 1,000 or greater		
4. Direct path length in host rock (LPD)	minimum: defined by SA maximum: several 100 m, see remarks next column		See Fig. 4.15 - 4.16; distance depends on relative position of repository within the block and on direction of local gradient

(1) **Mean value** taken from distribution in full scenario (left) and in sparse scenario (right)
(2) Indicates the **full simulated range** covered by the full and sparse scenario

4.7 Conclusions of the hybrid study

In addition to the standard continuum models of the regional-scale flow and discontinuum models (on block scale), the hybrid modeling approach was developed as a numerical tool for simulation of the groundwater flow at the sub-regional scale. At this intermediate scale, the hydrodynamic regime is strongly controlled by flow within large permeable faults. In numerical terms, the hybrid or

double-porosity approach combines continuum and discontinuum approximations of the hydrogeological environment. In contrast to the stochastic nature of the fracture-network models, the hybrid model reproduces the discrete features in a deterministic manner. Moreover, the newly developed mesh generator allows the presentation of arbitrarily oriented faults in a 3-D FE grid (no numerical restrictions of geometry).

By testing several alternative model scenarios and comparing results with available hydrogeologic data it was concluded that not all faults in the geometrical network, as identified by structural geology, are hydraulically active, i.e., water conducting. It was shown that a certain minimum size of intact blocks is required in order to preserve local flow conditions (vertical gradients) such as observed in the boreholes of Northern Switzerland. The full scenario reflects the "best-guess" estimate on the geometrical properties of major faults based on structural geology, whereas the sparse scenario represents the most likely hydrogeological conceptual picture of *conductive* faults. This is a demonstration of how hydrodynamic modeling helps to discriminate among plausible conceptual models of deep groundwater flow in fractured crystalline rocks.

Besides of improving and testing the conceptual model, an important objective of this study was to contribute a relevant input for safety analysis calculations. The principal contribution of the hybrid model is the distribution of hydraulic gradients in the environment of a potential repository in relation to the frequency of major transmissive faults. The appropriate methodology and numerical tools have been developed. Although the outcome is representative for the modeled area of interest, the approach is applicable to any characterization study in fractured rocks.

It is emphasized, however, that considerable uncertainty is attached to the model output as resulting from this study. It is mainly derived from sparse database and equivocal nature of some hydrogeological observations. The resulting uncertainty in model parameters was partly covered by an appropriate sensitivity analysis.

5 MODELING OF FRACTURE FLOW AT THE BLOCK SCALE IN AREA WEST

5.1 Introduction

At the scale of a hypothetical repository, the groundwater flows primarily through discrete discontinuities in the rock. According to the conceptual characterization of crystalline rocks in Chapter 2, the geological environment of a potential repository is represented by the properties of the Low-permeable domain, LPD. The groundwater flow and transport through a block of LPD is controlled by the geometric and hydraulic properties of transmissive elements, TE. Hence, the key issue in describing or predicting the flow at the block scale is a quantitative characterization of fracture-flow processes. Whereas some characterization procedures are well understood, the evaluation of other fracture-flow parameters is uncertain at best (e.g., channeling, see Section 2.4.2). In order to obtain a total characterization of a fractured medium, one should know explicitly the position and orientation of fractures, their frequency, size, aperture (transmissivity) and degree of interconnectedness. It is evident that a such deterministic characterization of fracture flow is not feasible. Instead, an alternative approach is to construct probabilistic models of fracture networks which conform to statistical fracture properties as derived from borehole observations. Hence, discontinuum modeling is used as a tool of integrating statistical information into a physically realistic fracture network. By generating multiple independent networks from a given statistical input (Monte Carlo realizations), the flow through a block of low-permeable fractured rock can be predicted.

The discrete-fracture approach can be applied to a) predict flow to or from a simulated repository drift, and b) to derive the single macroscopic block property for use in continuum models.

The numerical models described herein represent a purely fractured medium, that is, the contribution of the rock matrix to flow and storage of fluid is neglected.

The modeling of fracture flow through crystalline rocks of Northern Switzerland has been performed and reported in several steps by LANYON (1992a, 1992b) and HERBERT & LANYON (1992a, 1992b). A concluding summary and discussion of results concerning the effective block properties was performed by

VOBORNY et al. (1993). The first derivation of specific results for the needs of safety analysis was presented by VOMVORIS et al. (1992). A background report on this issue - with emphasis on the adopted methods and inherent assumptions and uncertainties - is provided by VOMVORIS et al. (in prep). The following sections summarize the principal results of these studies for completeness of the present synthesis report. The mentioned background report should be consulted for a more thorough presentation and discussion of the approach and assumptions.

5.2 Approach and objectives of fracture-network modeling

Numerical methods using the NAPSAC computer code (GRINDROD et al. 1991) were utilized to characterize typical blocks of crystalline rock. The investigation focused on the Low-permeable domain (LPD) of area West that was identified as the potential host rock for a deep repository. This domain has also the lowest density of transmissive elements and warrants thus a reasonable computational effort that is required to simulate a representative crystalline block.

The objectives of the study were as follows:

1) Determine the effective hydraulic property of a typical low-permeable crystalline block that would encompass a potential repository and assess its variability with respect to uncertain model parameters;

2) Estimate the geometric and hydraulic properties of individual transmissive elements that would intersect a repository drift and hence represent discrete flowpaths for nuclide transport; and

3) By combining results of 2) and of hybrid model, predict distributions of volumetric flow through a repository drift which serve as direct input to safety-analysis calculations.

In order to assess the effective hydraulic conductivity of a representative block of LPD, multiple realizations of a cube of 500-m side length were generated by NAPSAC. The transmissive elements as defined by the conceptual model are numerically represented as square-shaped planar features in the NAPSAC model. The generated stochastic network of these elements is defined by geo-

metric and hydraulic input parameters, which were derived from statistical analysis of borehole observations in LPD (Chapter 2). The required parameters for the NAPSAC model are given in Table 5.1 below.

Table 5.1 TE parameters required as input to NAPSAC

Parameter	Property
Transmissivity [m^2/s]	Log-normally distributed Mean ($log_{10}T$) $\mu = -9.24$ Log std. dev. $\sigma = 0.4$
Strike	Isotropic, 0-360°
Dip	uniform between 45-90°
Fracture density [m^{-1}]	$P_{32C} = 0.04$ (uncorrected for channeling)
Fracture size (length)	· variable 20-200 m · constant 100 m

The uncertainty attached to the input data in Table 5.1 increases downward, i.e., the confidence in the T distributions is the highest, whereas confidence in the size distributions is the lowest. This is principally due to the one-dimensionality of the borehole observations. Therefore, the main issue in the sensitivity analysis was the variation of fracture size (mean constant lengths and length distributions) in an effort to bound the results for effective conductivity.

5.3 Effective hydraulic conductivity

5.3.1 Parameter variations

The numerical analysis of the effective block conductivity, K_{eff}, considered the following variations of geometric TE parameters:

1) constant length, constant aperture (parallel-plate model):
   independent realizations for lengths of 20, 40, 100 and 200 m

2) variable length, constant aperture; two length distributions assumed:
   - bi-modal (40 m and 200 m)
   - log-normal (mean L fixed at 100 m, realizations with variable log STD, σ)

Additionally, a simple channeling model has been implemented to show some of the possible channeling effects in a quantitative manner (HERBERT & LANYON 1992a). Each fracture was replaced by two channels with the same T property, covering in total 20% of the fracture area according to an assumed channeling factor of C=5. To maintain a constant areal density and conform the borehole observations, the fracture frequency was increased by factor of 5:

3) constant length, channeled model (aperture 1 or 0):
   -realizations for 100-m and 200-m fracture lengths
   -two different geometric arrays: 'stripe'- channel and 'cross'-channel models

The results of these simulations are summarized in the following.

5.3.2 Results

Constant length (LANYON 1992a)

The effective conductivities are slightly anisotropic, the vertical components being by less than a factor 2 larger than the horizontal values. The small-sized TE networks are virtually unconnected, notably no flow occurred in the 20-m network. The connectivity of the networks increases with fracture length, despite the decreasing number of fractures (due to a constant P_{32C}). Blocks consisting of large TE's are generally well-connected. The network conductivity of the 200-m system is only a factor of 3-4 smaller than the maximum possible equivalent property that was calculated analytically for infinite fractures in Section 2.5.3 (see Table 2.8). The analytical values were used for the hybrid models of area West as a conservative upper bound. The 100-m network shows a corresponding reduction in effective property by a factor of 6 (vert.) and 10 (horiz.) with respect to K(infinite).

Variable length (HERBERT & LANYON 1992a)

A first network with a bi-modal distribution simulated a large population of 40-m fractures and a small number of 200-m fractures. Other realizations considered

a log-normal size distribution with a constant mean length of 100 m and variable log standard deviations of 0.25, 0.75 and 1.25. The areal fracture density was kept constant throughout in conformity with the observed P_{32C} value in Table 2.8 and 5.1. Keeping the P_{32C} quantity constant implies that the density of fracture centers is inversely proportional to mean fracture area.

The simulations displayed the following general trends:

- The presence of large features in a network increases the connectivity of the system. This effect is observed even with only a small number of such large features that dominate the cross flow. In this case, however, the resulting conductivity is subjected to a larger variability (i.e., highly sensitive to the presence of these features).

- The variable-length networks, which probably represent physically more realistic systems, yield a higher effective conductivity than the equivalent constant-length networks. However, it is important to note that in no case does this simulated effective conductivity exceed the analytical value calculated for the infinite-fracture case (Section 2.5.3).

It is concluded that both the conductivity and its variability increase with standard deviation of the length distribution due to the increased likelihood of large features. The system is very sensitive to the presence of one or two large fractures that may extend across the test volume and control the bulk flow.

Channeled models (HERBERT & LANYON 1992a)

A simple channeling model was implemented by replacing each fracture by two channels of the same transmissivity, with each channel covering 10% of total fracture area. No flow occurs in the fracture plane between channels (T=0). The channels in each fracture plane are oriented either parallel or perpendicular to each other (strip and cross channel geometry).

In each case, the effective network conductivity was reduced by about a factor of 2 with respect to non-channeled (parallel-plate) models. However, this trend is not deemed representative given the simple conceptual models used, notably the random (instead of preferred) orientation of channels at fracture intersections and zero fracture transmissivity outside the channels. These two simplifying assumptions yield a systematic underestimate of the network connectivity.

5.3.3 Conclusions

The characterization of fracture flow in a typical block of low-permeable crystalline rock deals primarily with two conceptual uncertainties that affect the estimates of equivalent network properties: the true fracture-length distribution and the importance of channeling effects. Whilst the first issue was addressed by parametric studies considering a plausible range of properties, no conclusive resolution to the channeling problem was identified within the scope of this numerical study. Therefore, the former conclusions and questions in Section 2.6 regarding the understanding of fracture flow remain valid.

The numerical simulations have shown that the derived maximum theoretical conductivity for an infinite-fracture system, $K_{eff}(inf)$, as derived analytically in Section 2.5, remains a valid upper bound of the expected network properties. It was also shown that fracture networks consisting of large TE's (in the realistic range of 100 to 200 m) are highly connected. Therefore, it is appropriate and conservative to neglect the network effect in estimating the equivalent properties; i.e., to use the infinite-fracture conductivities in the analytical approach such as was proposed in Section 2.5

5.4 Principal results for safety analysis

5.4.1 Methodology

The principal input to the safety analysis is the total volumetric flow (Q_t) that passes through a given section of the repository tunnel and distribution of this flow among transmissive elements that intersect the repository. The geometric and hydraulic properties of these features define the flow of fluid from the repository to the nearest higher-permeable environment (e.g., major faults or the Higher-permeable domain). The few parameters that define the fracture-controlled flow through a repository drift are the trace length, L, transmissivity, T, and number, N, of intersected transmissive elements in the tunnel, and the imposed hydraulic gradient, I, for these TE's.

The general philosophy and overall approach adopted for deriving the relevant input required to safety analysis is extensively discussed in VOMVORIS et al. (in prep.) and only briefly outlined herein. The source and flow of information in

this approach is illustrated in Fig. 5.1. The derivation of specific fluxes corresponds to a "bottom-up" approach and consists of the following steps:

1) Determine the number and the geometric and hydraulic properties (length and transmissivity) of TE's that intersect a tunnel section.

2) In combination with hydraulic gradients obtained from the hybrid model (statistical distribution), calculate the resulting flow, Q_i, in each transmissive element intersecting the tunnel (distribution over all TE's).

3) Integrate these individual TE's fluxes over the number of intersected elements in a tunnel to calculate the total flow through a tunnel segment, Q_t. Finally, estimate the total flow through a repository with a given layout.

NAPSAC simulations were used to assess the geometric and hydraulic properties of TE's intersecting a hypothetical drift. The potential host rock is represented by the Low-permeable domain (LPD) of area West, modeled as a cube of 1,000-m side length. Based on the previous parameter studies, a constant fracture length of 100 m was selected as base case for the simulations. All other input parameters were defined according to Table 5.1. Fig. 5.2 shows a typical network realization. A hypothetical repository drift (tunnel) was incorporated as a 500-m long prism of 5x5 m cross section, assumed to represent a tunnel with diameter of 3.5 m including some excavation-damaged zone. The defined input dataset was subjected to 20 Monte-Carlo simulations to obtain a statistical database for assessing the variability of the output. The analysis of intersected TE's was based on synthetical tunnel trace maps that were calculated for each realization (Fig. 5.2c). An additional study with a reduced tunnel length (200 m) was performed to estimate the advective flowpath geometry (HERBERT & LANYON 1992b) of particles that were released from the tunnel.

All geometric and hydraulic results of NAPSAC simulations that are relevant to safety analysis are summarized in Table 5.2.

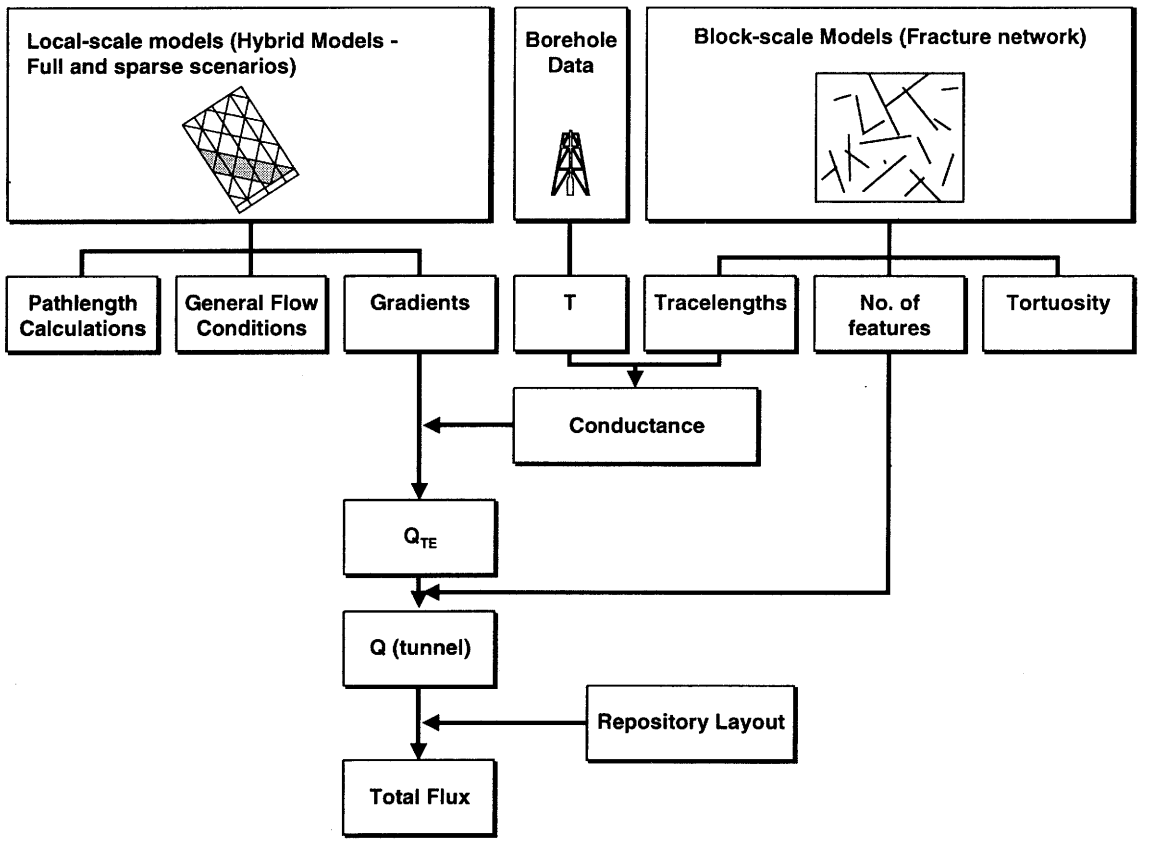

Fig. 5.1 Approach for deriving the hydrogeologic input for safety analysis in area West (VOMVORIS et al., in prep.)

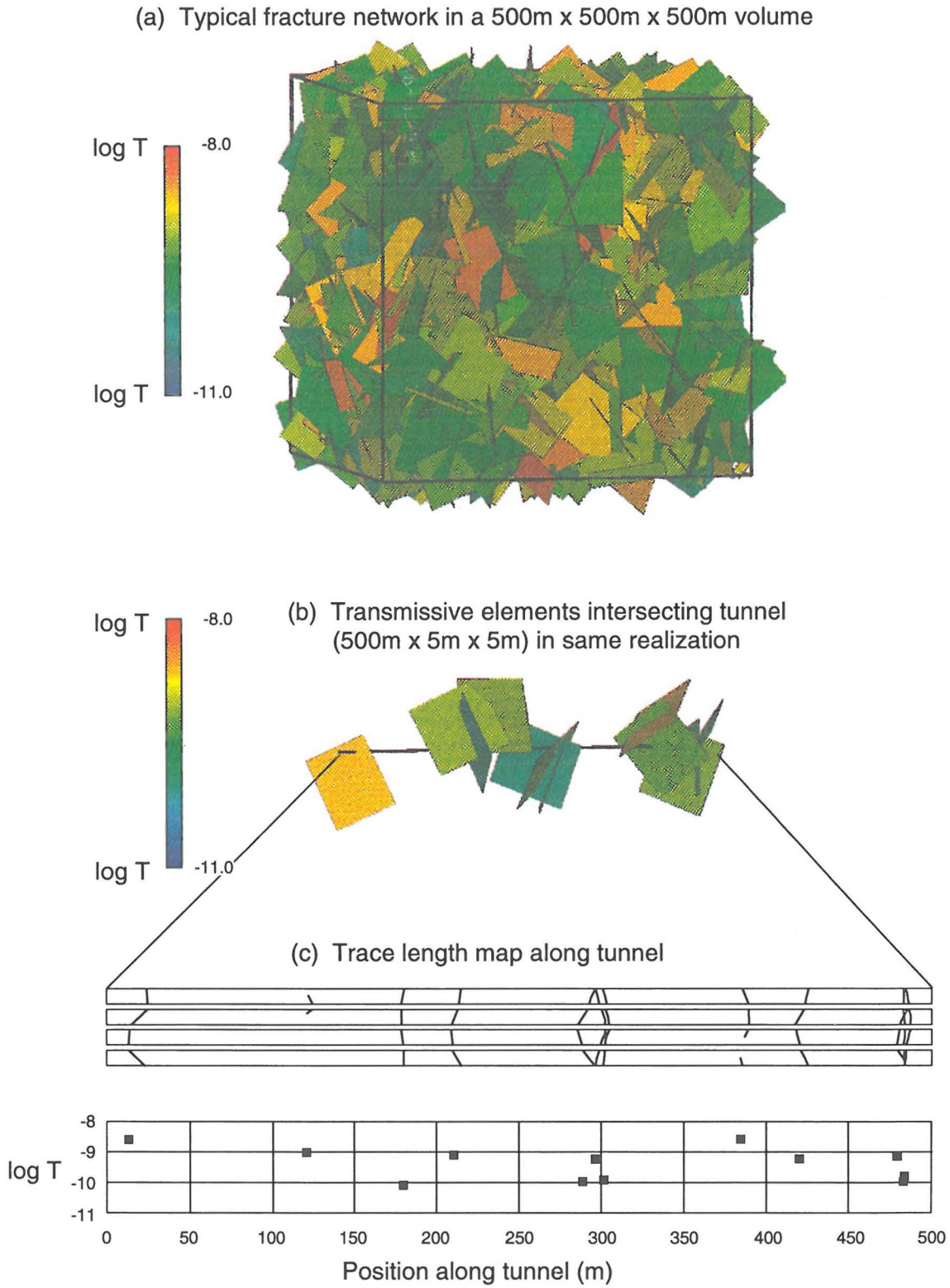

Fig. 5.2 Typical fracture network representing a block of LPD in area West. (a) full network of TE's; (b) TE's intersecting a hypothetical tunnel; (c) calculated trace length and log T of the TE's

5.4.2 Geometric and hydraulic properties of TE's around emplacement tunnels

The principal geometric results that are obtained from synthetic trace maps in 20 network realizations are displayed as probabilistic distributions in Fig. 5.3 and summarized in Table 5.2. All results refer to a 500-m long section of the emplacement tunnel. The direct model output consists of the following quantities:

Number of TE's, N

Fig. 5.3a shows the distribution of the number of TE's intersected by the tunnel. The range is from 6 to 20, and the mean is 13.7, which is consistent with analytical estimates considering similar geometric characteristics (P_{32C} and dip in Tab. 5.1).

Mean spacing, d

The mean spacing between two adjacent TE's along the tunnel wall is 35 m. About 30% of all TE's are separated by less than 10 m (Fig. 5.3b).

TE trace length, L

According to the histogram of Fig. 5.3c, most of the intersected TE's are oriented approximately perpendicular to the tunnel axis, given that most of the trace lengths are between 20 and 30 meters. Some TE's terminate within the tunnel (trace lengths smaller than 20 m), whereas large trace lengths are produced by TE's that are oriented subparallel to tunnel axis. The maximum generated trace length was 72 m. The average cumulative trace length of all TE's per tunnel section is 298 m; this corresponds to mean TE number of N = 13.7 with a mean length of L = 21.7 m.

Transmissivity and Conductance of TE

A log-normal transmissivity distribution was specified as input parameter in Table 5.1. By sampling from this distribution, the NAPSAC algorithm assigns a discrete T value to each generated transmissive element. As a consistency check, the T distribution of all TE's intersected by the simulated tunnel segment is displayed in Fig. 5.4 top.

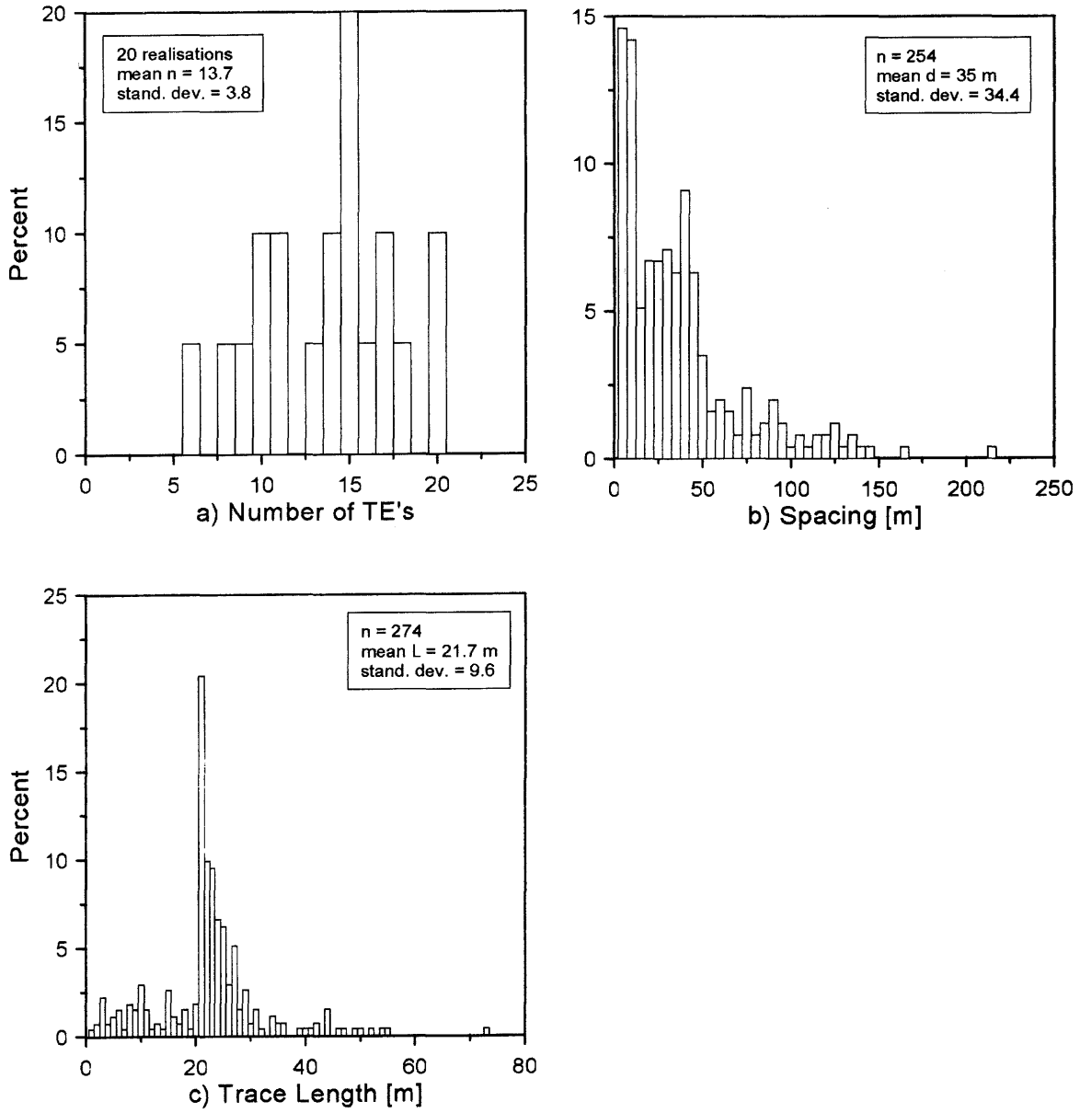

Fig. 5.3 NAPSAC output related to simulated 500-m long drift. (a) Number of intersected TE's; (b) spacing between adjacent TE's; (c) trace length of TE's along the tunnel wall.

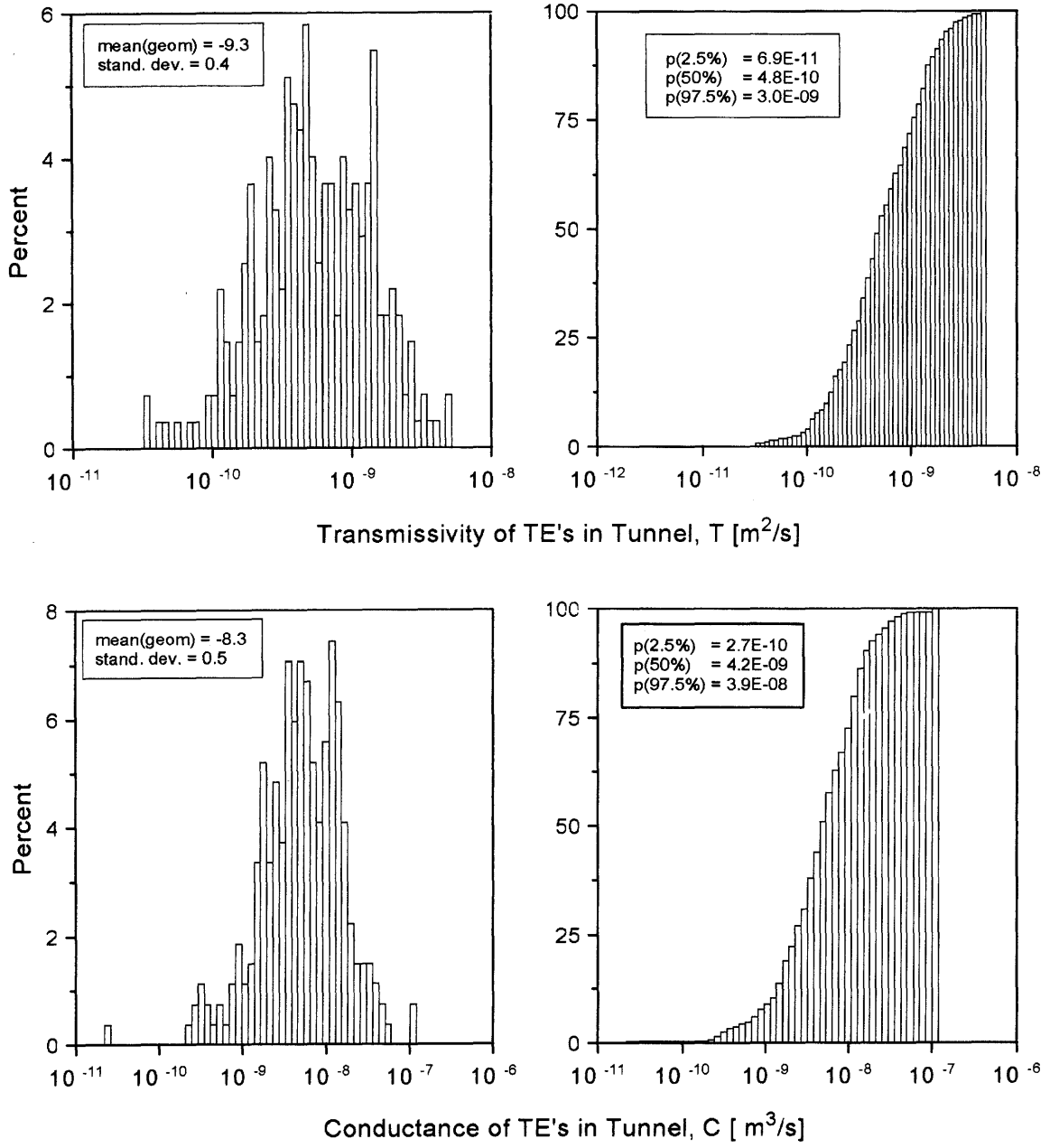

Fig. 5.4 Calculated distributions of log transmissivity T (*top*) and log conductance C (*bottom*) of TE's intersecting a 500-m long tunnel

As a direct model output, NAPSAC calculates for each of the intersected transmissive elements TE_i the hydraulic conductance, C_i, defined as the product of transmissivity (T_i) and half trace length ($L_i/2$) of that feature. The conductance (see also 4.3.3) is a specific property of each single TE that describes its capacity to carry flow under an unit gradient. The log-normal distribution of TE conductance is shown in Fig. 5.4 bottom. The geometric mean is 5E-09 m^3/s, the corresponding 95%-probability range is from 3E-10 to 4E-08 m^3/s.

Flowpath geometry

Tortuosity, or the ratio of the actual flowpath length to direct path length, was calculated by NAPSAC. For typical realizations, most of the values are between 1.4 and 2.0. For conservatism, it is assumed that the actual and the direct path lengths are the same (ratio = 1). This assumption implies that TE size is equal to or greater than the direct path length between the repository and the boundary of the low-permeable block (either to MWCF or to HPD).

Number of TE's along flowpath

Multiple TE's of variable hydraulic properties may be traversed along the travel flowpath between the release point and the entry into a higher-permeable domain. However, if a minimum direct path length of 100 to 200 m is assumed, the number of TE's probably would be small. For conservatism, it can be assumed that once a water particle enters a TE it will stay within until it reaches the more transmissive water-conducting pathway.

5.4.3 Distribution of volumetric fluxes

Flow through an individual TE

The calculation of TE flow, $Q_i = C_i \cdot I$, requires a statistical combination of the two distributions of conductance and hydraulic gradient. The procedure of "multiplying" two probability distributions is referred to as convolution. This approach assumes that the conductance and gradients are independent and that each TE intersected by the tunnel is connected to the flow network. The gradient distribution was obtained directly from the local-scale model West (Fig. 4.10). The two bounding model scenarios 403 (full fault intensity) and 433 (sparse) are considered to cover the full range of possible model output.

The resulting log-normal distributions of the individual TE flows, Q_i, are shown in Fig. 5.5 for both scenarios. The full hybrid scenario (top) yields a (geometric) mean value of 5.3·E-11 m^3/s. According to the cumulative diagram, 95% of all flux values are between 3·E-12 and 4·E-10 m^3/s. The arithmetic mean, m, is calculated from the probabilistic distribution - according to Eq. 14 in Section 2.5.3 - as 1.1E-10 m^3/s. The sparse scenario (bottom) shows flux values between 8·E-12 and 2·E-09 m^3/s, with a geometric mean of 1.8·E-10 m^3/s. The derived arithmetic mean of Q_i is 6.6·E-09 m^3/s. The larger gradients and hence fluxes in Run 433 are a direct result of the increased spacing between hydraulically active faults in the sparse scenario. Generally larger hydraulic gradients are preserved in the interior of the large low-permeable blocks.

Total flow through a 500-m tunnel segment and through the repository

The distribution of the total tunnel flow, Q_t, is obtained by a convolution of the TE-flow distribution (Fig. 5.5) and the distribution of the number of intersected TE's (Fig. 5.3a). The results for both hybrid scenarios are given in Fig. 5.6. Again, the full model (top) yields a geometric mean of 7·E-10 m^3/s, the 95% range being from 4·E-11 to 6·E-09 m^3/s. The arithmetic mean is 1.5·E-09 m^3/s. The distribution for the sparse model (bottom) is shifted by about a factor 5 toward higher values: the geometric mean of Q_t is 2.4·E-09 m^3/s with a range from 1·E-10 to 3·E-08 m^3/s; the arithmetic mean is 6.6·E-09 m^3/s.

When considering a specific geometric layout of the planned repository, the total groundwater flow through the repository, Q_{rep}, can be indicated. By assuming that the entire repository layout would include 60 tunnel segments of 500-m length, the mean (geometric) total repository flux is 4.2·E-08 m^3/s or 1.3 $m^3/year$ for the full scenario and 1.4·E-07 m^3/s or 4.6 $m^3/year$ for the sparse scenario. The arithmetic means of both distributions are 2.8 m^3/y and 12.4 m^3/y respectively.

Dilution of flow

Another relevant parameter for safety analysis is the potential dilution of the repository flux ("plume") along its pathway. The dilution in geosphere, i.e., between the low-permeable block matrix (host rock, LPD) and the higher-permeable crystalline domains (MWF, HPD) was estimated from the results of the hybrid model in Section 4.6.3. The critical parameter, however, is the final **dilution in the biosphere** that can be expected when the flux that had passed

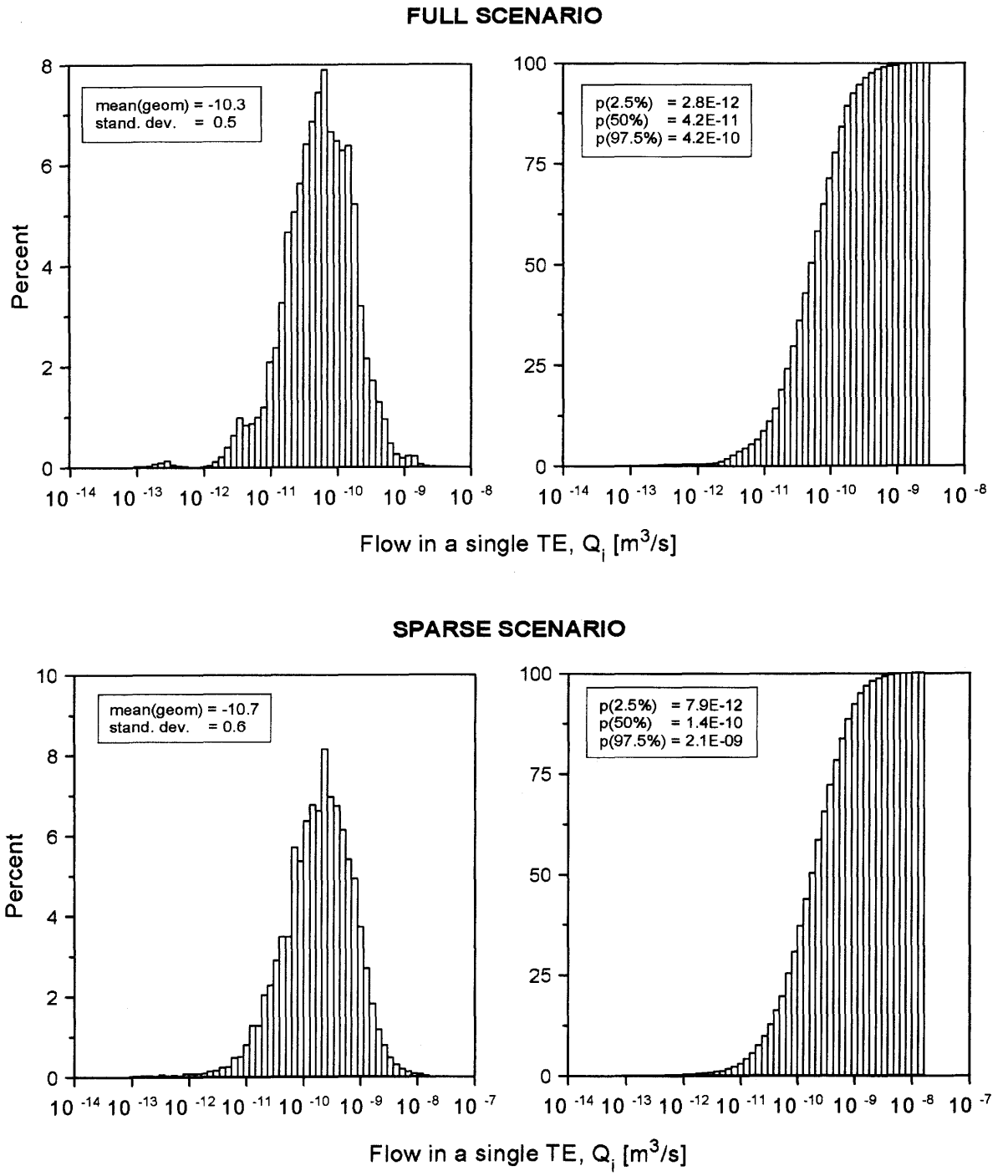

Fig. 5.5 Distribution of flow in a single TE intersected by tunnel, Q_i. Full scenario (*top*) and Sparse scenario (*bottom*)

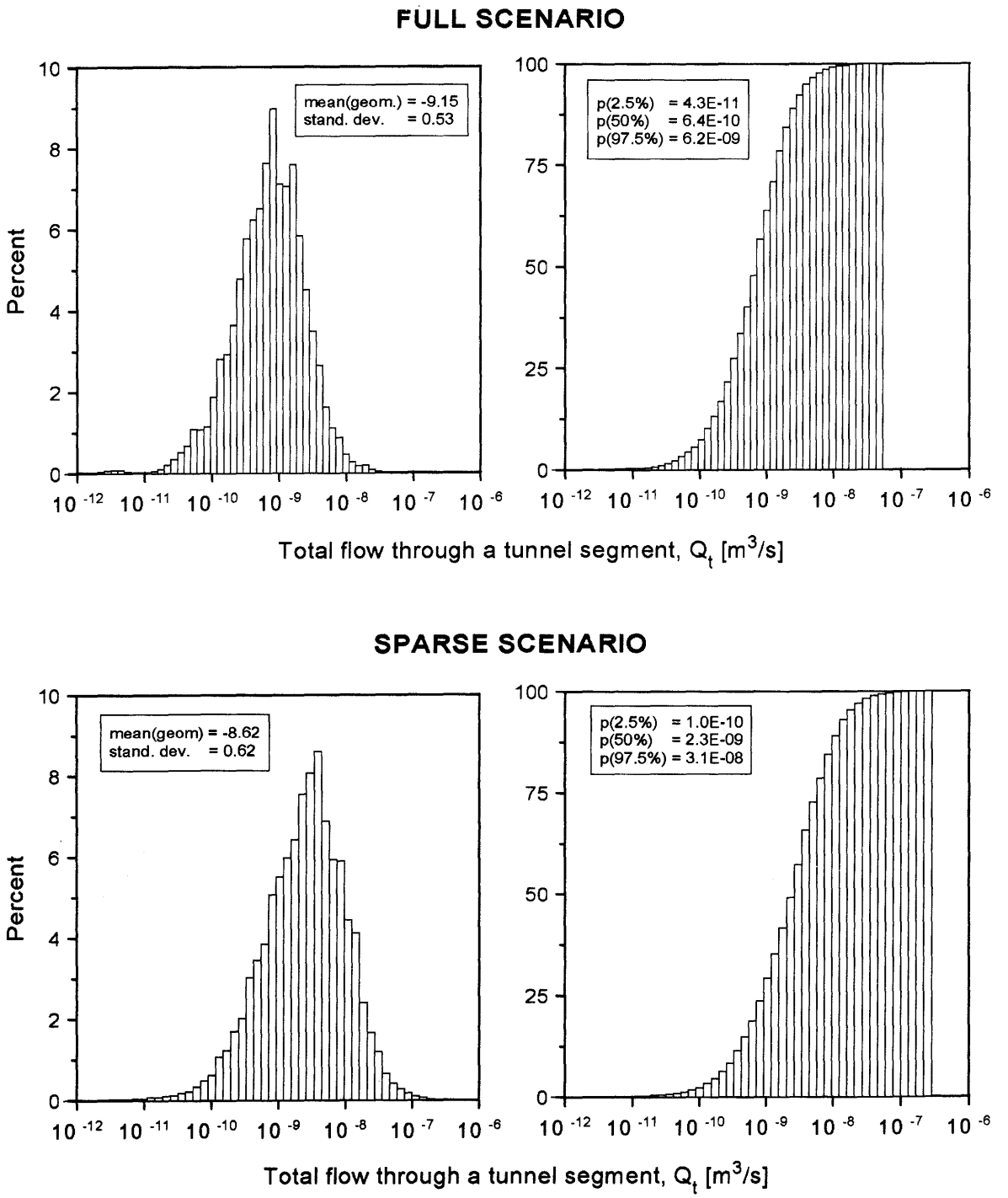

Fig. 5.6 Distribution of total flow through a 500-m long tunnel segment, Q_t. Full scenario (*top*) and Sparse scenario (*bottom*)

through the repository enters into accessible environment. For the study area, the biosphere is represented by the alluvions of the Rhine River valley that carry a broad groundwater stream.

The volumetric flow through these alluvions was estimated by an independent study (STÄUBLE 1993) as follows. At several cross sections of the Rhine River valley the flux Q was calculated according to Darcy's law $Q_j = A_j \cdot K_j \cdot i$, where A_j is the flow area of cross section *j*, K_j is the representative hydraulic conductivity for the alluvions in that cross section, and i is the hydraulic gradient. A comparison of consecutive cross sections provides insight on the lateral infiltration from bedrock. The balance estimates also consider the potential withdrawal of groundwater-supply wells in the alluvions. A cross section located downstream of the area West, which also includes the incoming lateral groundwater stream from the Frick valley, was selected for calculation of the biosphere flow, Q_{bio}. The estimated volumetric flow through this cross area is 0.65 m^3/s. By comparing this value to the maximum average volumetric flow through the repository (e.g., the arithmetic mean of the sparse scenario 433 in Table 5.2), the expected (conservative) dilution ratio in the biosphere, D, is

$$\text{mean } D = Q_{bio}/Q_{rep} \approx 2 \cdot E+06$$

The full range that spans all model results is from 3·E+08 to 4·E+05 (low tail of full-scenario distribution to high tail of sparse scenario distribution).

5.4.4 Summary and conclusions

Stochastic fracture-network models of a typical block of the low-permeable domain in area West were utilized to provide hydrogeological input that is relevant to the safety analysis of a considered repository in crystalline rocks of Northern Switzerland. The relevant results of this modeling study are summarized in Table 5.2 below. These data complement the first-level results from the hybrid model that were compiled in Table 4.7.

The input dataset provided to safety analysis is derived from numerical models at different scales. Conservative assumptions were made throughout the analysis, as long as they were internally consistent and did not contradict the observed data or general understanding of the hydrodynamic flow regime. Whenever feasible, **distributions** of values are provided that cover the expected range of alternative plausible input parameters.

Table 5.2 Block models of area West: Summary of relevant input to safety analysis

Type of result	Mean value 1)	95% Range 2)	Remarks
A. Geometry			
A1. Number of TE's in 500-m long tunnel, N	13.7	6 - 20	See Fig. 5.4 *top*
A2. Trace length of single TE's in tunnel, L_i [m] cumulative L in tunnel [m]	21.7 298	0.5 - 72 most 20-30	See Fig. 5.4 *bottom*
A3. Tortuosity, or ratio flowpath length to direct distance	Most 1.4 - 2.0	1.2 - 3.0 (approx.)	For conservatism, assume ratio = 1.0
A4. Number of TE along a flow-path	not determined		For conservatism, assume 1
B. Hydraulics			
B1. Conductance of single TE's in tunnel, C_i [m^3/s]	geo 5E-09 ar 9E-09	3E-10 to 4E-08	see Fig. 5.5 $C_i = T_i \cdot L/2$
B2. Flux in individual TE's that intersect tunnel, Q_i [m^3/s]	*Full* *Sparse* g 5E-11 2E-10 a 1E-10 5E-10	3E-12 to 2E-09	See Fig. 5.6 $Q_i=C_i \cdot I$
B3. Total flux through tunnel of 500-m length, Q_t [m^3/s]	g 7E-10 2E-09 a 2E-09 7E-09	4E-11 to 3E-08	See Fig. 5.7 $Q_t=Q_i \cdot N$
B4. Total flux through reposito-ry, Q_{rep} [m^3/s]	g 4E-08 1E-07 a 9E-08 4E-07	2E-09 to 2E-06	$Q_{rep}=Q_t \cdot 60$
B5. Dilution in biosphere, $D = Q_{bio} / Q_{rep}$	Rhine alluvions: 7E+06 - 1.6E+06 Rhine River: 1E+10 - 2.5E+09		Mean dilution of Q_{rep} (ar) for full and sparse scenario

(1) Means from distributions in *full* hybrid scenario (left) and *sparse* hybrid scenario (right)
- g: geometric mean of log-normal distribution
- a: arithmetic mean derived from log-normal distribution

(2) Full model range, defined by 2.5% minimum in Run 403 and 97.5% maximum in Run 433

The principal input to safety analysis is the distribution of volumetric flow through a hypothetic repository. Given that such a repository is sited in a low-permeable block of crystalline rocks (LPD), this distribution is controlled by 1) the frequency and the geometric and transmissive properties of discrete planar features and 2) the distance of the repository drifts to the higher-permeable zones of the geosphere (layout-determining criterion).

Emphasis is given on the conservative nature of the analyses given above that are based on the following principal assumptions:

- Each TE that intersects the repository tunnel is sufficiently large or interconnected to a network of equally transmissive features that it effectively extends in both the upgradient and downgradient directions to the significantly higher-permeable domains

- Each TE is assigned a site-scale gradient from the equivalent-porous block matrix of the hybrid model. This gradient is considered to be independent of the actual conductance of that TE. However, in a 'real' network of TE's, the gradient is in fact inversely proportional to the conductance.

- The transmissivity (and conductance) of each TE is constant, simulating parallel plates. Hence, the large spatial variability of transmissivity (aperture) of real conduits along the flowpath is neglected. It is understood that such a heterogeneity significantly reduces the bulk flow through a fracture network, which is restricted by the presence of "bottlenecks".

The conservative approach is justified by considerable uncertainties associated with the input data. The uncertainties result principally from the paucity of hydrogeologic observations, which in turn result from the few number of boreholes with reliable hydraulic and geologic information, the virtual lack of outcrops of the crystalline rocks in northern Switzerland, and the absence of in situ (underground) observations in the region.

A more comprehensive analysis of the uncertainties and discussion of their impact on the resulting dataset is presented in VOMVORIS et al. (in prep.).

6 HYDROGEOLOGICAL SYNTHESIS OF AREA EAST

6.1 Purpose and scope

A comprehensive hydrogeological characterization of crystalline rocks in the basement of Northern Switzerland is required in order to provide input to safety assessments of the planned HLW repository. Based on the synthesis of borehole data and the conceptual model of groundwater flow, two different areas of interest were defined for further characterization studies. An integral evaluation of groundwater flow at local scale and block scale in area West was provided in the preceding Chapters 4 and 5 respectively. The present chapter represents a synthesis of the current hydrogeological knowledge in area East. The final objective of this characterization study was to provide specific input data required for the safety analysis of this area; thus, the synthesis does not constitute a complete characterization of the hydrogeology of area East.

The general approach to the characterization of area East is similar to that used in area West. The principal difference that affects the analysis approach is related to the sparse data base in area East. Because there are data from only one borehole in this area, a large degree of uncertainty exists as to the representativeness of those data for the area as a whole. For this reason, it was deemed inappropriate to develop a complex hybrid model in analogon to area West to investigate local flow conditions. Instead, it was decided to modify the existing regional model KRI2 in such a manner as to better represent the specific conditions of the SIB area, in order to simulate the sub-regional flow. The results of this modified EPM model were used to evaluate the distribution of hydraulic gradients in the potential repository environment of area East. This gradient analysis also incorporated the understanding and experience that was gained from the local-flow modeling study in area West.

Principally, the input data required for safety-analysis calculations are the same as those derived for area West. For this purpose, statistical fracture-network models were also implemented in area East, representing a typical crystalline block that has the same hydraulic properties as the Lower unit observed in the SIB borehole (see Table 2.8 for characterization). In analogy to area West, the required information obtained from this modeling step comprises the geometric and hydraulic properties of transmissive elements intersected by a tunnel segment and the derived volumetric flow through this repository portion.

The key issue in evaluating the hydrogeology of area East is the representativeness of data from SIB, the only borehole in the area.The SIB data have shown, that low-permeable crystalline rocks such as observed in area West do not occur in this borehole. The basic question raised in this context in Chapter 2.3 was whether the SIB data are representative of a typical "intact" crystalline block in area East, or whether they reflect tectonically disturbed conditions of a MWCF. Since the presence or proximity of a major fault cannot be excluded at this site, both alternatives were treated as equally plausible. Consequently, the flow characterization in area East and the derivation of a relevant dataset for safety analysis has to discriminate between the two conceptual hypotheses defined in Section 2.3.3. *Pro memoria*, these hypotheses read as follows:

1. SIB data **are** representative of intact rock conditions (Block matrix) in area East.
   Consequences:
   Characterization of area East relies entirely on observations from the SIB borehole, i.e., LPD-like conditions do not exist in area East.

2. SIB data **are not** representative of a typical Block matrix in area East but reflect disturbed conditions in the proximity of a MWCF.
   Consequences:
   a) SIB conditions can occur as MWCF anywhere in the investigation area,
   b) undisturbed blocks with HPD and LPD-like properties exist also in the region surrounding the SIB site.

The characterization procedure following the 2nd hypothesis is identical to that of area West with a different orientation and magnitude of representative hydraulic gradients.

6.2 Characterization of regional and local groundwater flow

6.2.1 Results of KRI2 model (regional flow)

The regional groundwater flow system in the basement of northern Switzerland was simulated by an equivalent-porous-medium model, KRI2, described in Chapter 3. Due to the sparsity of hydrogeological observations in the eastern part of the modeled region, the regional model tested several conceptual scena-

rios of possible flow pattern in that area. The general flow system in the eastern model area is controlled by the following hydrologic elements that were partly subjected to a sensitivity analysis in the regional model KRI2:

- regional recharge in the Black Forest east and northeast of SIB site
- regional discharge in Rhine River valley west of Waldshut
- possible local discharge along the Wutach valley southeast of SIB
- possible presence of a northern segment of deep Permocarboniferous trough (NPCT) east and south of SIB
- possible groundwater divide east of SIB resulting from discharge across the Randen fault into the Muschelkalk aquifer in the region of Lake of Constance (i.e., hydraulic short-circuit of Crystalline/Buntsandstein waters with Muschelkalk waters)

The best fit with observed heads and regional hydraulic gradients was obtained in those model simulations that considered the presence of an "open" Wutach valley and a water divide east of SIB (induced by prescribed low heads long the Randen boundary). The Wutach valley proved a particularly sensitive boundary condition for the general flow pattern between the SIB and WEI boreholes. Both mentioned conceptual assumptions were designated as "currently preferred hypotheses" in the conceptual model of regional flow in Appendix 3, despite of the lack of any supporting observations. These imposed conditions yielded a substantial decrease of simulated heads in the SIB-WEI area and provided the best match with observed horizontal gradients from these sites toward the Rhine River of approximately 0.004.

6.2.2 Modified regional model KRI4

For the purpose of simulating the local flow conditions in the SIB area under the different conceptual hypotheses, a new version of the regional model was implemented, designated KRI4. As an additional feature, the model differentiates the "eastern" crystalline rocks as an independent hydrogeologic unit, and thus allows a flexible assignment of different hydraulic properties to the crystalline rocks in the eastern part of the model in accordance to the interpretation of SIB data. The lateral extent of this eastern crystalline domain is displayed as a shaded area in Fig. 6.1. The area of modified rock properties is structurally defined by the northern segment of deep trough (NPCT) to the southeast and by the rim of the Münstertal-Albtal-Graben to the southwest; both bounding tectonic units are depicted in the structural map of App. 40 in DIEBOLD et al.

(1991). Also shown in Fig. 6.1 are those finite elements that constitute the submodel of area East that is used for evaluation of specific results herein.

The default model geometry corresponds to the scenario V21 in KRI2 that considered the presence of a northern deep trough (NPCT) south of the SIB site (see Fig. 3.8), in accordance to the results of recent seismic investigations.

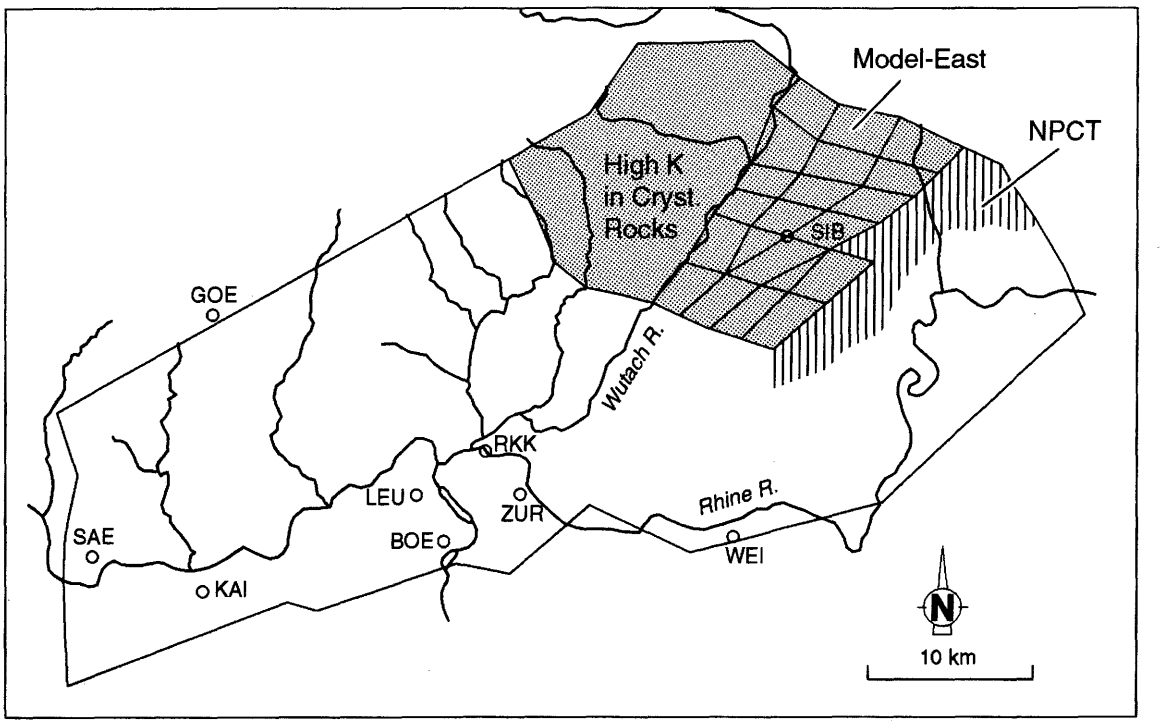

Fig. 6.1 Map showing the modified regional model KRI4 with separated eastern crystalline domain *(shaded)* and submodel representing the area East

The model parameters and boundary conditions are identical with the KRI2 model; the additional parameters for the eastern domain of the crystalline basement were defined by the estimated effective properties according to the conceptual hypothesis considered. Three parameter variations were performed with the KRI4 model in order to cover the possible range of effective hydraulic

conductivity for both conceptual scenarios. The principal results are described in the following. A comparison of simulated heads with observations in selected boreholes is given in Table 6.1.

6.2.3 Results: local flow conditions

Hypothesis 1: SIB data are representative

The assumption that SIB observations represent the properties of the average crystalline rocks in that area have the following implication on the sub-regional flow regime:

- The crystalline rocks exhibit a large bulk conductivity (no LPD-like conditions). Hence, the groundwater flow at large scale occurs through a well-interconnected network.

- Major faults play no significant role for the regional flow; i.e., their effective properties are probably similar to those of the intervening blocks.

An analytical estimate of effective rock properties in area East in Section 2.5.3 yielded K_{eff} values of approximately 1·E-06 m/s for the Upper unit and 1·E-08 m/s for the Lower unit of the crystalline block matrix at SIB (Table 2.8). These block properties are assigned to the equivalent-porous rock units of the eastern part of KRI4 in the new base case scenario, V41, under the implicit assumption that major faults have no impact on the bulk EPM properties. This assumption is supported by hydrochemical evidence; the observed high ^{14}C residence times of deep SIB groundwater speak against the presence of "fast" flow channels at regional scale.

Nevertheless, an increase of the equivalent property in the Lower unit East was considered in V40 as an extreme scenario that accounts for eventual (undetected) presence of highly permeable major faults in that area.

The simulated head distribution in the Upper crystalline unit (UC) of the eastern model area is displayed for the default scenario V41 in Fig. 6.2. The groundwater flow is driven by the recharge condition in Black Forest, north of the Wutach valley, with relatively steep gradients. The general flow toward the southeast is confined by the barrier of northern PCT; the flow follows the rim of the trough

toward the sites of Zurzach, BOE and LEU and the Rhine River downgradient of the displayed model area. Some components of crystalline groundwaters discharge into the Wutach River.

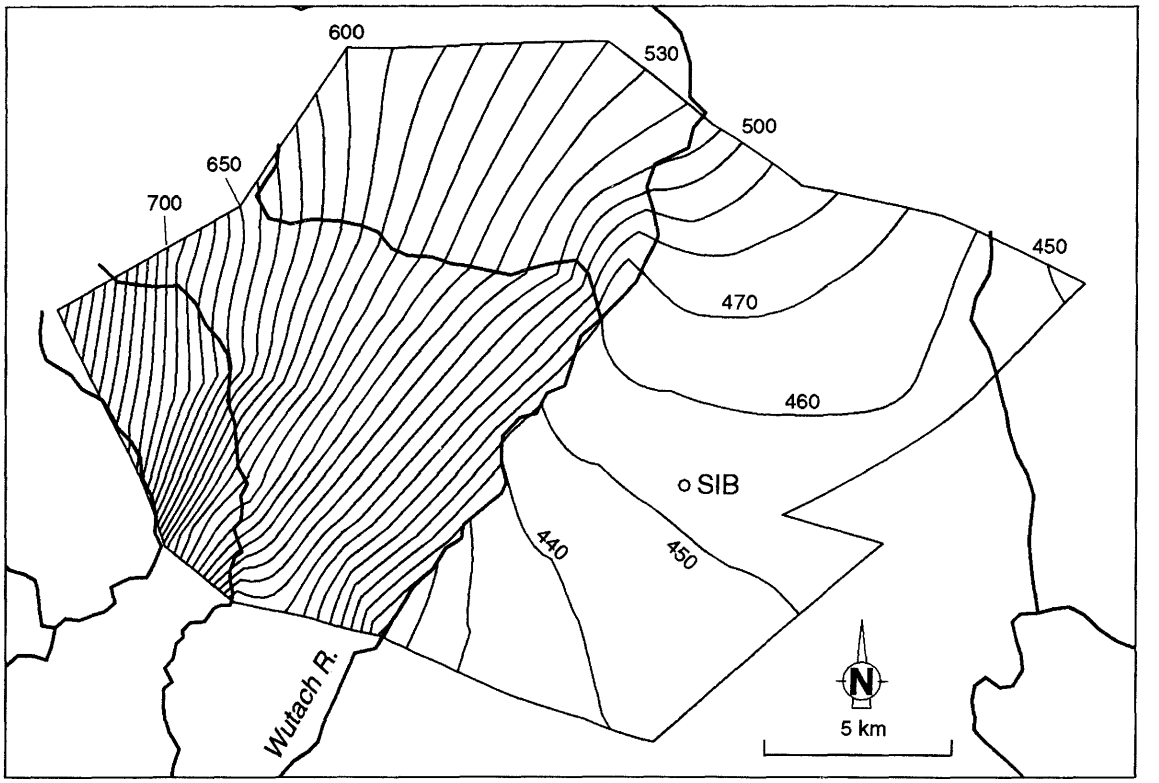

Fig. 6.2 KRI4: Map of eastern model area showing simulated heads in Upper crystalline, Base case V41

As a general trend, the increase in the bulk permeability of crystalline rocks in the eastern region yields a larger recharge capacity of the model resulting in a small increase of heads in that area. This tendency is enhanced in the high-K scenario V40. The impact of these parameter variations on the heads in the SIB and WEI boreholes and on the total flow balance through the model is shown in Table 6.1. The downstream area of the model (i.e. area West) is not affected by the variations, suggesting that the conductance of crystalline rocks in the discharge area is large enough to compensate the additional recharge simulated in southeastern Black Forest.

The default scenario V41 was used for a quantitative estimate of Darcy fluxes and hydraulic gradients in the Lower crystalline unit of area East. For this purpose, the calculated Darcy flux values were read out at each node within the second element layer from the top of the LC unit (see cross section in Fig. 3.4). This layer encompasses the relevant depth for a potential repository, similar to level 500 in the hybrid model of area West. The gradients were obtained by dividing these fluxes by the hydraulic conductivity of the LC unit. The absolute flux vector in each node was split into a horizontal and a vertical component.

The results are displayed in Fig. 6.3 as a vector map of the horizontal flux component (*top*) and a contour map of the vertical-flux component (*bottom*). Both figures indicate that the largest fluxes occur along the Wutach valley, as a result of the adjacent recharge area in the Black Forest. Due to the coarse numerical discretization in this area, the boundary effects tend to be significantly overemphasized by the simulations. Therefore, the fluxes within the first element row alongside the Wutach River boundary are considered to be non-representative for the area of interest and are excluded from the statistical assessment of simulated gradients in Section 6.3. A comparison of both figures shows that horizontal flow dominates in the SIB area, whereas the vertical component is virtually zero.

Hypothesis 2: SIB data are not representative

The second hypothesis says that the conditions observed in the SIB borehole correspond to a local anomaly, and, hence, the hydraulic data cannot be used for the characterization of the block-matrix properties. The "anomalous" rock properties are attributed to the presence of a nearby fault, or to a jointed zone with intensive hydrothermal activity, or to other phenomena. Under this hypothesis, it is assumed that the "undisturbed" crystalline blocks in area East have properties similar to those in area West.

The implications of the Hypothesis 2 for the sub-regional flow system in area East are that

- Undisturbed blocks with HPD and LPD properties exist in both areas West and East,

- SIB data are a subset of MWCF that can occur anywhere in the basement of Northern Switzerland, and

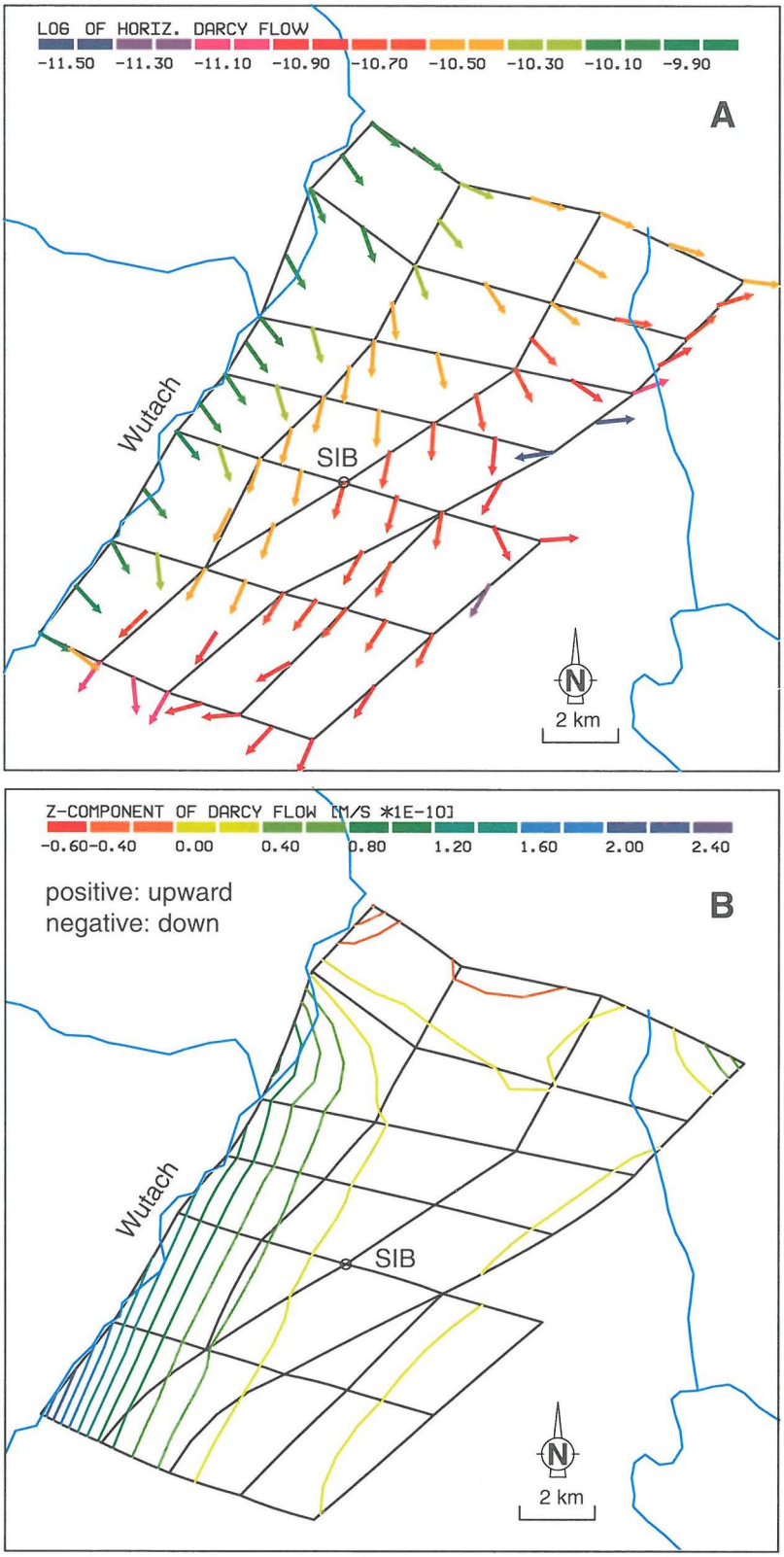

Fig. 6.3 V41: (a) maps showing vectors of horinzontal Darcy-flux component; (b) contours of vertical Darcy flux component in the LC unit East

- the MWCF dominate the large-scale groundwater flow throughout the area

This hypothesis was simulated in the run V42 by using the default parameters of the KRI2 model, i.e., by assuming that the EPM properties of crystalline rocks are homogeneous over all model area (and the same as in area West). Technically, this run is identical to the scenario V21 of KRI2 model.

The effect of the performed KRI4 variations on heads in the boreholes of SIB and WEI is shown in Table 6.1. In comparison with the Hypothesis 1 (V41), the reduced recharge into the eastern model area in V42 produces lower heads in the crystalline rocks of this region and thus a better match to observations at SIB and WEI. In general, the simulations confirmed the previous observation of KRI2 model that the head distribution within the EPM model is generally insensitive to parameter variations (Section 3.7).

Table 6.1 Principal results of KRI4 simulations

Parameter	Observed	V40	V41	V42
SIB heads [m a.s.l]	UC 440 LC 440	459 460	453 454	447 448
WEI heads [m a.s.l.]	Bs 419 P 441 UC 403 LC 385	420 " 419 "	416 " 415 "	409 " " "
Turnover (m^3/s)		1.4 260%	1.3 240%	0.539 100%
Remarks:		K(east) UC=1E-6 LC=1E-7	K(east): UC=1E-6 LC=1E-8	as KRI2: UC=1E-7 LC=1E-9

6.3 Results relevant to safety analysis

6.3.1 Approach

The adopted approach and required parameters were outlined in Section 5.4 for area West. As a difference to the flow diagram of Fig. 5.1, the local distribution of the hydraulic gradient is obtained from the modified EPM model KRI4 instead from a local hybrid model. In balance with the conceptual model, two sets of input parameters for safety analysis need to be derived for Hypotheses 1 and 2. It is expected that the consideration of these hypotheses covers the relevant spectrum of results.

The specific input required for the safety analysis in area East and the corresponding source of information depending on the conceptual alternative are summarized in Table 6.2.

Table 6.2 Required input for safety analysis

INPUT PARAMETER	Source of data	
	Hypothesis 1 SIB representative	**Hypothesis 2 SIB non representative**
Transmissive properties of TE's	Direct observation in SIB borehole	same as area W, based on BOE+KAI+LEU data
Effective K of blocks of LC unit	Analytically from observations in SIB	same as area West
Gradient distribution in LC unit at approximate repository depth	Modified regional model KRI4	Regional model KRI2 & "scaling factor"
Flowpath lengths within undisturbed blocks of LC unit	not available	not available
T, trace length and number of TE's intersected by a tunnel section	NAPSAC model with input from SIB	same as area West
Volumetric flow through tunnel section and entire repository	Combination of above parameters	Combination of above parameters
Dilution in Biosphere	Flux-balance estimates in alluvial aquifers	Flux-balance estimates in alluvial aquifers

6.3.2 Hypothesis 1: SIB data are representative

The relevant results for the safety analysis are derived from the available observations in the SIB borehole. The statistical modeling of fracture flow through the Lower crystalline unit, as defined in SIB borehole, was performed by LANYON (1992b) using the NAPSAC computer code. The input dataset defining the stochastic network properties is given in Table 6.3. Based on this input information, 20 Monte-Carlo realizations were performed. Results are compiled in Table 6.4 and discussed in the following. The repository tunnel was modeled as a 5x5-m square section, which accounts for a possible disturbed zone around the excavation of 3.5 m in diameter.

Table 6.3 Input parameters required to NAPSAC modeling of LC unit in area East

Parameter	Property
Transmissivity [m^2/s]	Log-normally distributed Mean ($log_{10}T$) $\mu = -6.94$ Log std. dev. $\sigma = 0.5$
Strike	Isotropic, 0-360°
Dip	uniform between 60-90°
Conductive fracture density [m^{-1}]	$P_{32C} = 0.112$
Fracture size (length)	constant 100 m

Geometry

The mean *number of TE's per 500-m segment of tunnel* is 40.8. This is about 3 times the mean number of TE's calculated for the LPD of area West, due to the greater P_{32C} density and generally steeper inclination of TE's in area East.

The distribution of the *trace lengths of TE's that intersect the tunnel segment* is shown in Fig. 6.4a. It is characterized by a mean of 22.8 m and a standard deviation of 13 m. The large peak near 20 m suggests that most of the TE's intersect the tunnel nearly at right angles; 50% of all intersecting features have a length of 20-24 m. The maximum length is 136 m; this TE intersects the tunnel

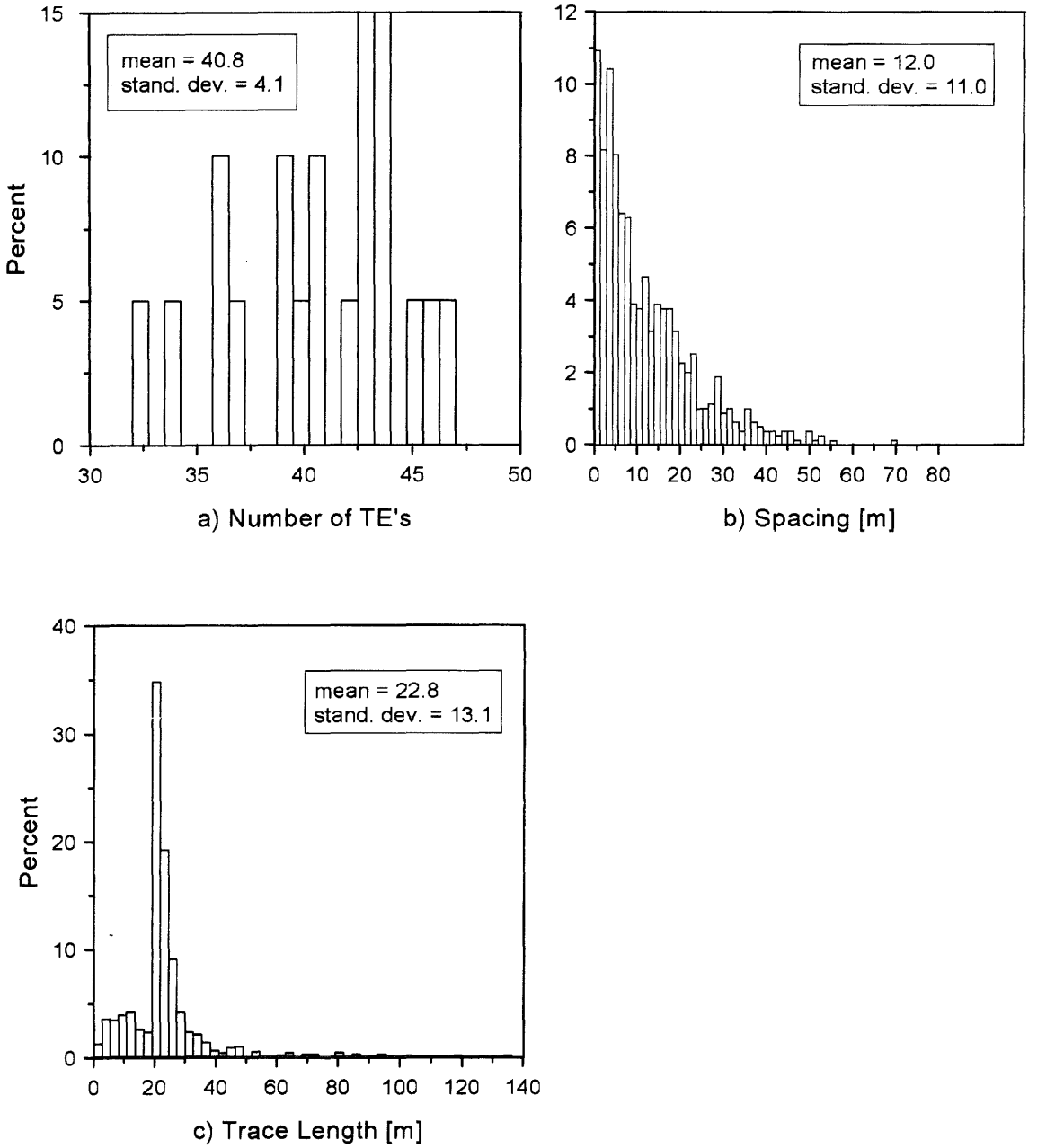

Fig. 6.4 East, Hyp. 1: number, spacing and trace-length of TE's intersected in 500-m tunnel

axis at a very small angle. Combination of the mean length with the number of TE's yields a *cumulative trace length* of 930 m for all TE's that intersect the tunnel. Fig. 6.4b shows the distribution of spacing between the intersected TE's.

No direct input is available for the estimate of the *flowpath length* of particles (nuclides) within the Lower unit to the next higher-permeable unit. However, because of the predominant horizontal flow in area East, illustrated by Fig. 6.3, the minimum flowpath is the distance from the release point to the next major fault. Based on the geometric structural model East, derived as input for hybrid modeling by AMMANN et al. (1992, Figs. 5.3, 5.4) it is concluded that, under this hypothesis, the sizes of intact blocks in area East are even smaller than in the "full-scenario" model West and, hence, the flowpath lengths are expected to be generally shorter than those simulated in area West.

Hydraulics

Figure 6.5a shows the lognormal *distribution of transmissivities* that NAPSAC assigned to each generated TE based on the input parameters in Table 6.3, derived from the SIB borehole. For each single transmissive element, i, that intersects the tunnel segment, the hydraulic *conductance*, C_i, is calculated as direct NAPSAC output. The lognormal distribution is shown in Fig. 6.5b. The geometric mean is 1.16·E-06 m^3/s and the arithmetic mean is 2.74·E-06 m^3/s. The cumulative conductance of all TE's within the tunnel section controls the volumetric flow through the tunnel under a given external gradient.

The *gradient distribution* was obtained from the results of the EPM model KRI4, described in Section 6.2. The procedure is similar to that applied to the hybrid model in area West. The basic assumption is that the gradients calculated for an equivalent-porous rock are applicable to discrete transmissive elements and are independent of their transmissive properties. The gradients were read out at model nodes located at the assumed repository depth of 500 m below the top of the Lower unit. As shown in Fig 6.3, significant boundary effects were still observed in the proximity of the Wutach River at this depth, due to coarse numeric discretization. Thus, the gradients simulated within the first element row along the Wutach River in Fig. 6.3 were excluded from the analysis. The resulting distribution is displayed as histograms in Fig. 6.6 for the base case V41.

The *volumetric flow through an individual TE*, Q_i, is calculated by a statistical combination (convolution) of the gradient distribution (Fig. 6.6) and the

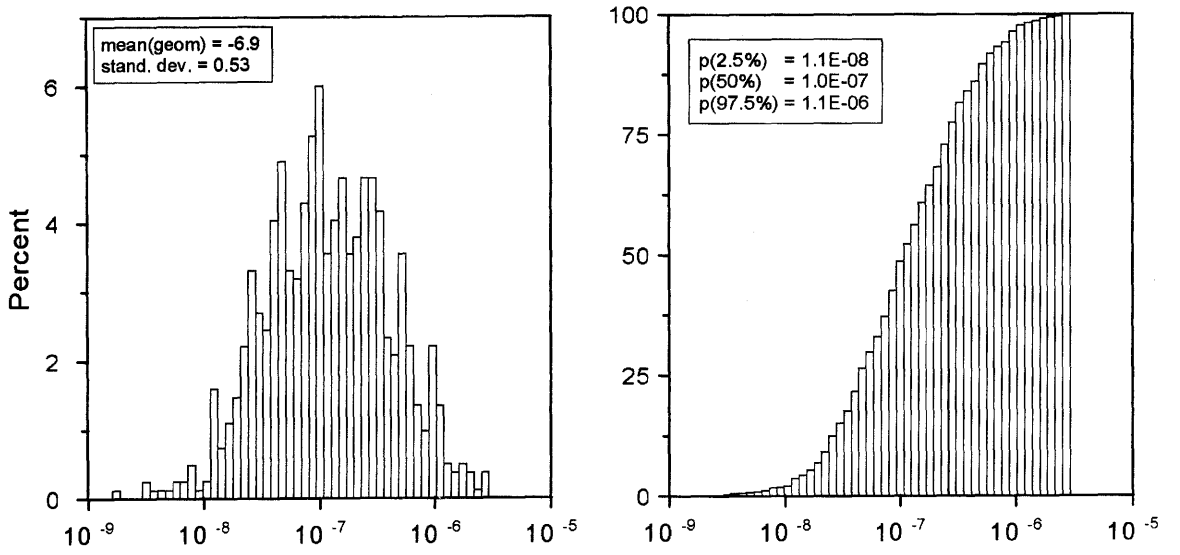

a) Transmissivity of TE's in Tunnel, T [m^2/s]

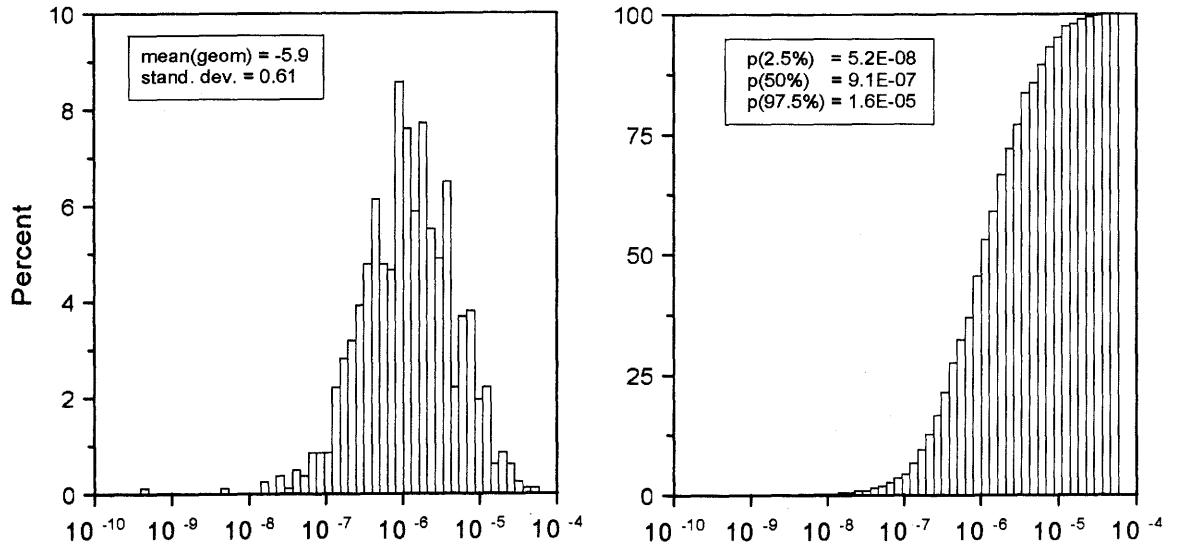

b) Conductance of TE's in Tunnel, C [m^3/s]

Fig. 6.5 (a) Log T distribution of TE's intersected by tunnel (generated by NAPSAC); (b) calculated log conductance of intersected TE's

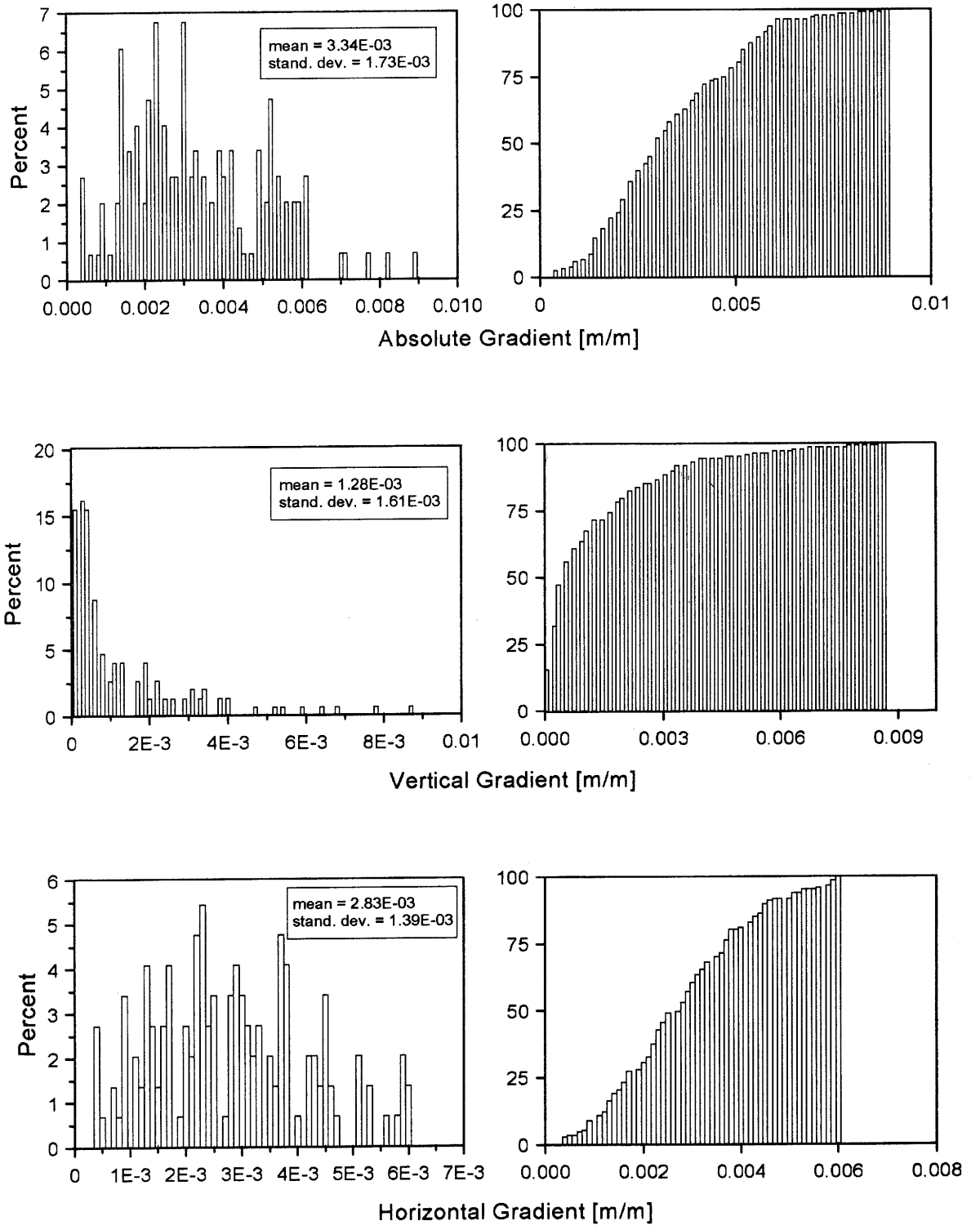

Fig. 6.6 East, Hyp. 1. Distribution of hydraulic gradients in KRI4/V1 in Lower crystalline unit at level 500

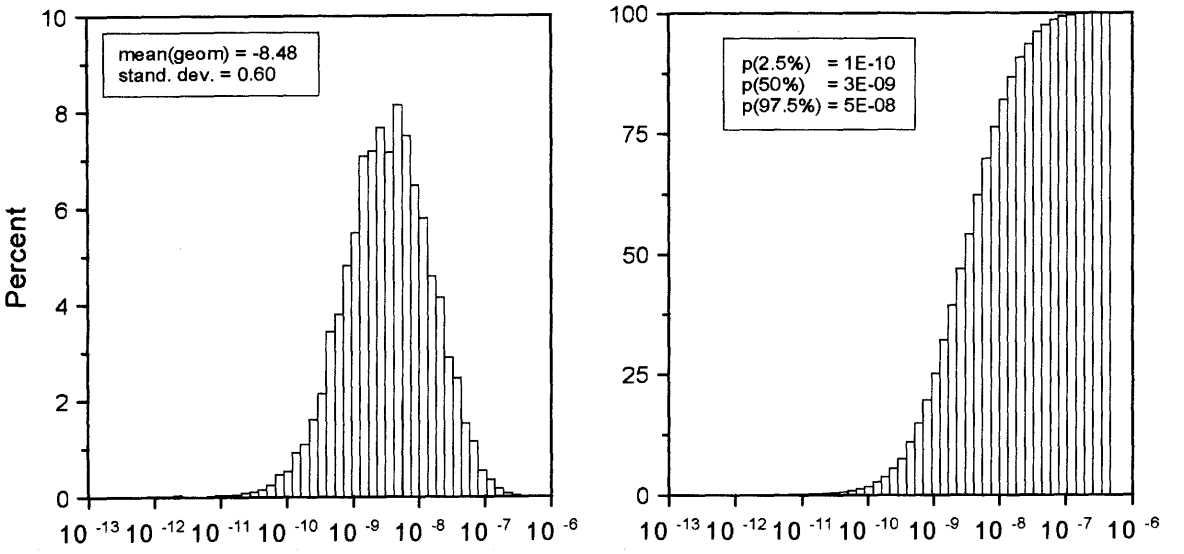

a) Flow in a single TE, Qi [m³/s]

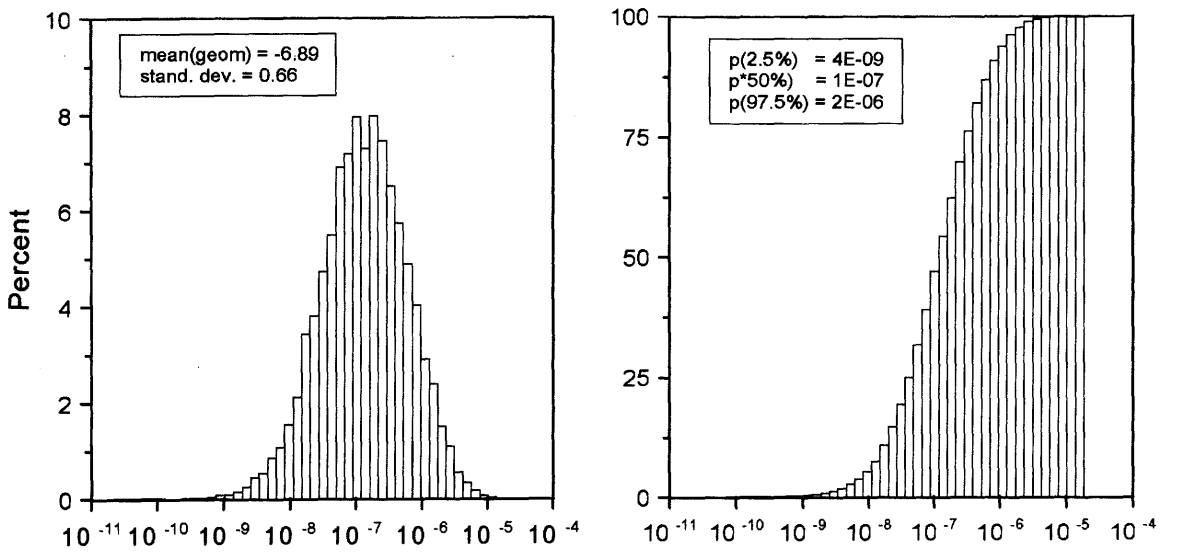

b) Total flow through a tunnel segment, Qt [m³/s]

Fig. 6.7 East, Hyp. 1: (a) flow in a single TE intersected by tunnel, Q_i; (b) total flow through a tunnel section of 500-m length, Q_t

conductance distributions (Fig. 6.5). The resulting distribution of Q_i is shown in Fig. 6.7a. The 95% probability range is from 1·E-10 to 5·E-08 m^3/s, and the geometric mean value is 3.3E-09 m^3/s. The arithmetic mean, m, is derived from the distribution as 1.1E-08 m^3/s.

Similarly, the *total flow through a 500-m tunnel segment*, Q_t, is given in Fig. 6.7b. Here again, the histogram is a result of combining the distribution of Q_i and of the number of TE's intersected by the tunnel. The range is from 4E-09 to 2·E-06 m^3/s, the geometric mean is 1.3·E-07 m^3/s. As a conservative estimate, the arithmetic mean is 4.2·E-07 m^3/s.

Because the entire repository is assumed to include 60 of 500-m tunnel segments, the *total volumetric flow through the repository*, Q_{rep}, is 2.5·E-05 m^3/s, or 790 m^3/y in average. The range is from 2.4·E-07 to 1.2·E-04 m^3/s, or about 8 to 3,800 m^3/y.

An important parameter for the safety analysis is the *dilution of flow in the biosphere* that can be expected when the flux that had passed through the repository discharges into water-bearing alluvial gravels and finally into the river itself. Two potential discharge areas are relevant for area East:

1) Assuming the Rhine River valley as the principal regional discharge for deep groundwaters from area East, the dilution ratio in the Rhine River alluvions is estimated in the following. The biosphere volumetric flow, Q_{bio}, is the same as for area West (0.65 m^3/s, see Section 5.4.3). The arithmetic mean from Table 6.4 is used as the maximum mean repository flux, Q_{rep}.

   $$D = Q_{bio}/Q_{rep} = 26{,}000 \text{ (Rhine valley alluvions)}$$

   The final dilution would occur within the Rhine River, which has an annual mean flow rate of 1,000 m^3/s, corresponding to a dilution ratio of

   $$D = 4{\cdot}E{+}07 \text{ (Rhine River)}$$

2) If the flux through the repository is assumed to discharge into the Wutach valley, the resulting dilution would be substantially smaller, because of the narrow and shallow alluvial deposits of the Wutach River. The volumetric flow through the alluvial aquifer is unknown and probably small; the annual mean flow rate of the Wutach River is about 8 m^3/s at Eberfingen, down-

stream of area East. The corresponding final dilution in the Wutach River is thus

D = 320,000 (Wutach River)

or by a factor of 100 less than in the Rhine River.

6.3.3 Hypothesis 2: SIB data are not representative

This hypothesis assumes that SIB data represent a disturbed zone (MWCF) and, consequently, that intact matrix blocks of similar quality to area West do exist in the eastern region. Because the implication that LPD-like conditions occur in area East can not be supported or rejected by other evidence so far, this hypothesis is deemed optimistic. Except for the hydraulic gradients which are different in area East, all hydraulic and geometric input parameters required for the assessment of fluxes are adopted from area West. The geometric and hydraulic properties of TE's that intersect a hypothetical repository tunnel were described in Chapter 5 and are summarized with other relevant results in Table 6.5.

The hydraulic gradients in the potential repository environment of area East were derived from run V42 of the regional model, using the default parameters of KRI2 model, i.e., by ignoring the SIB observations. In accordance to the conditions observed in area West, the presence of a strong hydraulic contrast between the major permeable faults and the low-permeable undisturbed blocks requires the discrimination of two geometric scenarios to account for the unknown density of hydraulically active faults. Hence, the assignment of mean gradients to a typical block of undisturbed rock must consider a well-connected full scenario and a poorly interconnected sparse scenario. It was shown in the hybrid-modeling study of area West that the simulated gradients in the block-matrix of the full scenario generally are low and generally reflect the regional gradients simulated in the EPM model. In turn, the sparse scenario, with a substantially reduced bulk conductance of crystalline rocks, has simulated gradients in the block matrix that are 4 to 5 times those in the same volume of equivalent porous rock in the regional model. Therefore, the *gradient distribution* for the full scenario (designated Hypothesis 2a) corresponds directly to the results of run V42 and that for the sparse scenario (2b) was obtained by the application of a "scaling factor" of 5 in analogon to HYBW results in area West.

The results are given in Table 6.5 for both alternatives.

The flux distributions through individual TE's and the repository tunnel are also summarized in Table 6.5. Corresponding histograms are shown for the full scenario only because the fluxes of the sparse scenario are scaled linearly. Fig. 6.8a shows the distribution of *flow in a single TE*, Q_i; the bottom histograms of Fig. 6.8 show the *flow through the 500-m tunnel segment*, Q_t.

The *flow through the repository*, Q_{rep}, is 3.4E-08 m^3/s for the full scenario, or 1.1 m^3/y, and 1.7E-07 m^3/s (5.4 m^3/y) for the sparse scenario. Both values are conservatively derived from the arithmetic means of corresponding tunnel flows. The mean repository flow given in the Table 6.4 is an average between both scenarios (3.2 m^3/y). This value is about 250 times smaller than that derived under Hypothesis 1 in Table 6.4, on the basis of SIB data. As a result, the *dilution ratio* in the biosphere is increased by this factor under Hypothesis 2.

6.4 Summary and conclusions regarding area East

Chapter 6 represents an attempt to characterize the hydrogeology of area East; the principal objective was to derive a relevant input-data set for the needs of safety analysis. Large uncertainties are attached to the analyses because the database for area East was derived from only one available deep borehole in Siblingen, compared to three available boreholes in area West. According to the synthesis of borehole data, the anticipated low-permeable domain, such as observed in area West (LPD), was not detected in the SIB borehole.

The key issue in evaluating the hydrogeology of area East is the representativeness of the SIB observations. The fundamental question is, whether this single borehole has sampled from a relatively undisturbed, intact block of crystalline rocks (i.e., from Block matrix of the conceptual model) or from a tectonically disturbed zone of laterally limited extent (MWCF). It is obvious that this question cannot be answered neither by the present synthesis study nor in the near future.

Therefore, both alternatives were considered as equally probable, leading to two separate sets of input parameters. This approach is deemed to cover the possible spectrum of results in area East. The conceptual Hypothesis 2, saying that SIB data are not representative for the average rock in the area East,

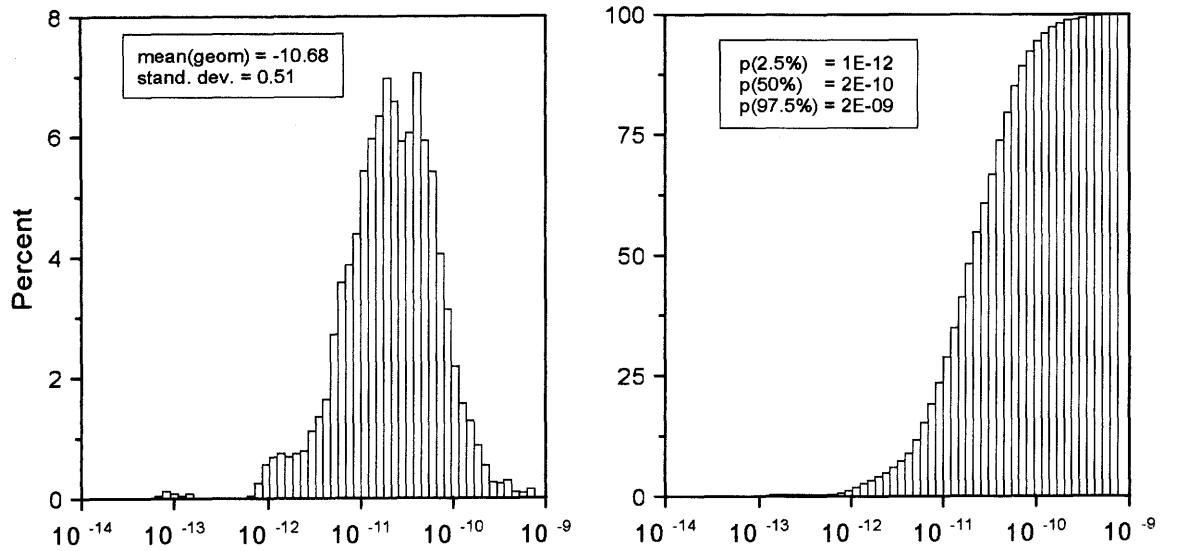

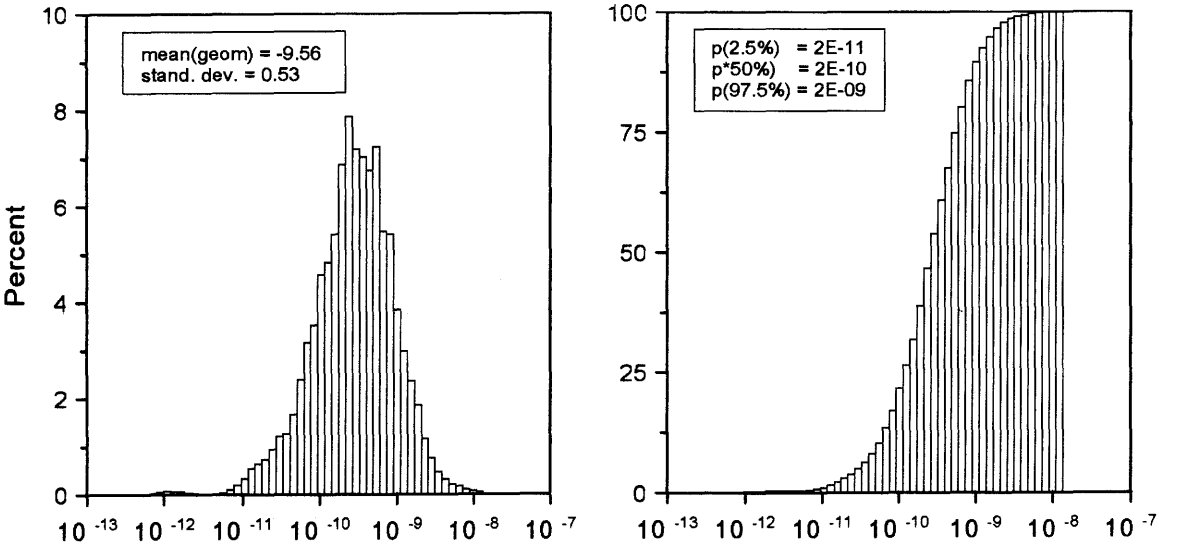

Fig. 6.8 East, Hyp. 2a: (a) flow through a single TE intersected by tunnel, Q_i; (b) total flow, Q_t, through 500-m tunnel section

assumed that undisturbed block volumes occur in this area with the same rock properties as in area West. However, the assumption of an existing LPD unit in the east (in its quality as the potential host-rock formation) is not supported by any evidence. On the other hand, the different structural and seismo-tectonic setting of area East, in particular the evidence of neotectonic activity, speak rather in favour of particular hydraulic properties in this region (see Table 4.1).

Hence, the following conclusions are made regarding the hydrogeological characterization of area East:

- The two established conceptual hypotheses on representativeness of SIB data are equally plausible, i.e., no preferred hypothesis can be indicated.

- Hypothesis 1 (SIB data representative) represents the conservative approach to derive input data for safety analysis; it extrapolates the rock properties observed at SIB site over the whole eastern sub-region.

- Hypothesis 2 (SIB not representative) represents an optimistic approach in as much as it assumes the occurrence of favorable "western" rock properties in area East.

Table 6.4 East: Summary of input to safety analysis, Hypothesis 1 (SIB data are representative)

Type of result	Mean value 1)	Range (95%)	Remarks
A. Geometry			
A1. Number of TE's in 500-m long tunnel, N	40.8	32 -47	
A2. Trace length of single TE's in tunnel, L_i [m] cumulative L in tunnel [m]	22.8 930	0.2 - 136 most 20-25	
A3. Tortuosity, or ratio flowpath length to direct distance	not determined		For conservatism, assume ratio = 1.0
A4. Number of TE along a flow-path	not determined		For conservatism, assume 1
B. Hydraulics			
B1. Gradient distribution: - horizontal component - vertical component - Absolute, I(tot)	Run V41/KRI4 0.0028 0.0013 0.0033	 <0.0004-0.006 <0.0001-0.006 <0.0004-0.007	See Fig. 6.3 for area at level 500 of LC unit; Histograms in Fig. 6.6
B2. Conductance of single TE's in tunnel, C_i [m^3/s]	geo 1.2E-06 ar 2.7E-06	5E-08 to 2E-05	NAPSAC output, C=T·L/2, see Fig. 6.5
B3. Flow in individual TE's that intersect tunnel, Q_i [m^3/s]	geo 3.3E-09 ar 1.1E-06	1E-10 to 5E-08	See Fig. 6.7a $Q_i=C_i \cdot I$
B4. Total flow through tunnel of 500-m length, Q_t [m^3/s]	geo 1.3E-07 ar 4.2E-07	4E-09 to 2E-06	See Fig. 6.7b $Q_t=Q_i \cdot N$
B5. Total flow through reposi-tory, Q_{rep} [m^3/s]	geo 7.8E-06 ar 2.5E-05	2E-07 to 1E-04	$Q_{rep}=Q_t \cdot 60$
B6. Dilution in biosphere, $D = Q_{bio} / Q_{rep}$	Rhine alluvions: 2.6E+04 Rhine River: 4E+07 Wutach River: 3.2E+05		Dilution of Q_{rep} (ar) in expected discharge areas

1) geo: geometric mean of log-normal distribution
ar: arithmetic mean calculated from log-normal distribution (Eq. 14)

Table 6.5 East: Summary of input to safety analysis, Hypothesis 2
(SIB data are not representative, rock properties as in area West)
2a: full scenario 2b: sparse scenario

Type of result	Mean value 1)	Range (95%)	Remarks
A. Geometry			
A1. Number of TE's in 500-m long tunnel, N	13.7	6 - 20	frequency and properties of TE's intersected by tunnel are adopted from West (Chapter 5)
A2. Trace length of single TE's in tunnel, L_i [m] cumulative L in tunnel [m]	21.7 298	0.5 - 72 most 20-30	
A3. Tortuosity, or ratio flowpath length to direct distance	not determined		For conservatism, assume ratio = 1.0
A4. Number of TE along a flowpath	not determined		For conservatism, assume 1
B. Hydraulics			
B1. Gradient distribution: - horizontal component - vertical component - Absolute, I(tot)	V42 5xV42 **full sparse** 0.004 0.02 0.0014 0.007 0.0043 0.022	min max **full - sparse** 0.002 - 0.032 <0.0001-0.022 0.003 - 0.033	Results from V42 for full scenario; scaled by factor of 5 for sparse scenario
B2. Conductance of single TE's in tunnel, C_i [m^3/s]	geo 5E-09 ar 9E-09	3E-10 to 4E-08	NAPSAC output for area West (Fig 5.4)
B3. Flow in individual TE's that intersect tunnel, Q_i [m^3/s]	g 2E-11 1E-10 a 4E-11 2E-09	1E-12 to 9E-10	See Fig. 6.8a for 2a $Q_i=C_i \cdot I$
B4. Total flow through tunnel of 500-m length, Q_t [m^3/s]	g 3E-10 1E-09 a 6E-10 3E-09	2E-11 to 1E-08	See Fig. 6.8b for 2a $Q_t=Q_i \cdot N$
B5. Total flow through repository, Q_{rep} [m^3/s]	g 2E-08 8E-08 a 3E-08 2E-07	1E-09 to 7E-07	$Q_{rep}=Q_t \cdot 60$
B6. Dilution in biosphere, $D = Q_{bio} / Q_{rep}$	Rhine alluvions: 2E+07 - 4E+06 Rhine River: 3E+10 - 6E+09 Wutach River: 2E+08 - 5E+07		Mean dilution of Q_{rep} (ar) for full (2a) and sparse scenario (2b)

1) geo: geometric mean of log-normal distribution
ar: arithmetic mean calculated from log-normal distribution (Eq. 14)

7 CONCLUSIONS

A comprehensive investigation of groundwater flow conditions in the crystalline basement of Northern Switzerland was performed. The final objective was to provide a quantitative characterization of hydrogeological properties and processes that are relevant for the assessment of repository performance. The investigation comprised the following stages: synthesis of hydrogeological borehole data, development of a conceptual hydrogeological model and numerical modeling of groundwater flow at three different scales of interest. The development of the conceptual model proves to be the most critical step in the chain of modeling, since it has to provide a simplified yet realistic description of the system, that, in turn, shall be in balance with a variety of field observations. In this approach, the conceptualization of flow through fractured rock is iteratively supported and improved by results of numerical models.

Due to the sparseness and irregular distribution of experimental data, considerable uncertainty is attached to the conceptualization and, consequently, to the interpretation of the models. The inherent uncertainties in this study were captured through appropriate parametric variations and consideration of different (bounding) conceptual scenarios.

Numerical models on progressively smaller scales are utilized to characterize advective groundwater flow through the geological environment of a potential deep repository. In addition to the standard continuum models at regional scale and discontinuum models at a much smaller block scale, a hybrid model was implemented at the intermediate scale to evaluate the impact of major permeable faults on the local flow regime in undisturbed crystalline blocks. Comparison of model results with available experimental data was used to discriminate among several plausible conceptual hypotheses of groundwater flow in fractured crystalline rock.

Despite the uncertainties mentioned above, the investigation provided a valuable contribution to improved understanding and increased confidence when dealing with the characterization of the groundwater flow system. The investigation focused on two different areas of interest that were identified as two potential siting regions.

Based on the available hydrogeologic database, area West is well characterized. The low-permeability domain in this area has been identified as a potential host rock. This domain forms irregular blocks of relatively undisturbed rock with an average effective hydraulic conductivity of 4E-11 m/s. These blocks are delimited by a network of large water-conducting faults that act as principal flow conduits at regional scale.

Area East is less well characterized due to ambiguous interpretation of its only deep borehole at Siblingen. The presence of a low-permeability domain such as observed in area West was not detected at Siblingen. The question, whether this observation is representative for the area East, i.e., whether or not a low-permeability domain occurs within this area, cannot be answered without additional information. Hence, the performed analyses assumed both possible alternatives as equally plausible.

At the repository scale, the fracture-controlled flow through a typical block of host rock was evaluated by stochastic fracture-network models. Multiple independent networks were employed to estimate the volumetric flow through single fractures and a repository segment, as well as to assess the effective hydraulic property of the modeled block. A simple method of combining model results from different scales to derive the required hydrogeologic input for repository-perfomance calculations was presented.

The hydrogeological synthesis indicated that favourable hydrogeological conditions exist in the crystalline basement of Northern Switzerland. The most suitable host environment for a repository is represented by sufficiently large blocks of low-permeability domain in area West, characterized by the boreholes of Böttstein, Leuggern and Kaisten.

REFERENCES

ABELIN H., NERETNIEKS I., TUNBRANT S. & MORENO L. (1985): Final report on the migration in a single fracture - Experimental results and evaluation. - Stripa Project Technical Report 85-03, May 1985. SKB Stockholm, Sweden.

ABELIN H., BIRGERSSON L., GIDLUND J., MORENO L., NERETNIEKS I., WIDEN H. & AGREN T. (1987): 3-D Migration Experiment-Report 3. Performed experiments, results and evaluation. - Stripa Project Technical Report 87-21, November 1987. SKB Stockholm, Sweden.

ABELIN H., BIRGERSSON L., WIDEN H., AGREN T., MORENO L. & NERETNIEKS I., (1994): Channeling experiments in crystalline fractured rocks. - Journal of Contaminant Hydrology, 15, 129-158. Elsevier Science B.V., Amsterdam.

AMMANN M., HUBER M. & MUELLER W.H. (1992): Geologische Grundlagen für die hydrodynamische Modellierung des Kristallins der Nordschweiz. - Nagra intern. Ber. NIB 91-30, May 1992. Nagra, Wettingen.

BLACK J., HOLMES D. & BRIGHTMAN M. (1987): Crosshole investigations - Hydrogeological results and interpretations. - Nagra tech. Rep. NTB 87-37. Nagra, Wettingen.

BOURKE P.J. (1987): Channeling of flow through fractures in rock. - Proceedings of the GEOVAL 1987 Symposium, Swedish Nuclear Power Inspectorate, Stockholm.

DERSHOWITZ W.S. (1984): Rock joint systems. - PhD Dissertation, Massachussetts Inst. of Technology, Cambridge, Mass., USA

DERSHOWITZ W.S., WALLMANN P. & KINDRED S.(1991): Discrete fracture modeling for the Stripa Site Characterization and Validation Drift inflow predictions. - Stripa Project Technical Report 91-16, June 1991. SKB Stockholm, Sweden.

DIEBOLD P., NAEF H. & AMMANN M. (1991): Zur Tektonik der zentralen Nordschweiz. - Nagra tech. Ber. NTB 90-04, Dezember 1991. Nagra, Wettingen.

DWERSTORP B. & ANDERSON J. (1990): Analysing transport in low permeable fractured rock using the Discrete fracture Network Concept. - Proceedings of the GEOVAL 1990 Symposium, Swedish Nuclear Power Inspectorate.

GEHLEN von K. (1989): Ore and mineral deposits of the Schwarzwald. In: EMMERMANN & WOHLENBERG (Ed.): The german continental deep drilling program (KTB). Springer, Berlin.

GELHAR L.W. (1987): Applications of stochastic models to solute transport in fractured rocks. - SKB Technical Report 87-05, January 1987. SKB Stockholm, Sweden.

GRINDROD J.P., HERBERT A., ROBERTS D. & ROBINSON P. (1991): NAPSAC Technical document. - Stripa Project Technical Report 91-31, December 1991. SKB Stockholm, Sweden.

GUYONNET D., MCCORD J.P. & MISHRA S. (1991): Radius of visibility evaluations for hydraulic tests performed in the LEU, KAI and BOE boreholes. - Nagra inter. Rep. NIB 91-21, March 1991. Nagra, Wettingen.

HERBERT A., DERSHOWITZ W., LONG J. & HODGKINSON D. (1990): Validation of fracture flow models in the Stripa Project. - Proceedings of the GEOVAL 1990 Symposium, Swedish Nuclear Power Inspectorate.

HERBERT A., GALE J., LANYON W. & MacLEOD R. (1991): Modeling for the Stripa Site characterization and validation drift inflow: Prediction of flow through fractured rock. - Stripa Project Technical Report 91-35, December 1991. SKB Stockholm, Sweden.

HERBERT A.W. & LANYON G.W. (1992a): Evaluation of the effect of discrete fracture flow parameters in crystalline rock. - Nagra intern. Rep. NIB 92-53, July 1992. Nagra, Wettingen.

HERBERT A.W. & LANYON G.W. (1992b): Investigation of fracture flow pathways through crystalline rock. - Nagra intern. Rep. NIB 92-66, July 1992. Nagra, Wettingen.

HUBER M. & HUBER A. (1990): Zur Tektonik des Südschwarzwaldes. - Nagra tech. Ber. NTB 90-03, 1990. Nagra, Wettingen.

HÜRLIMANN W. (1994): FRACMESH - A program for the generation of Finite-Element meshes for the hydrodynamic modeling of fractured rocks. - Nagra tech. Rep. NTB 93-36, Nagra, Wettingen.

JAQUET O. (1991a): Methodology and evaluation of OSNES probabilistic model applied to hydraulic properties of fractured rocks. - Nagra intern. Rep. NIB 91-22, March 1991. Nagra, Wettingen.

JAQUET O. (1991b): Assessment of hydrogeological characteristics of the LEU, BOE and KAI boreholes. - Nagra intern. Rep. NIB 91-24, March 1991. Nagra, Wettingen.

KIRALY, L. (1985): FEM301 - A three-dimensional model for groundwater flow simulation. - Nagra tech. Rep. NTB 84-49, Nagra Wettingen.

KLEMENZ W. (1991): Transmissivität der Zuflussstellen und Durchlässigkeit der Matrix im Kristallin der Tiefbohrungen BOE, KAI, LEU. - Nagra intern. Ber. NIB 91-20, May 1991. Nagra, Wettingen.

KLEMENZ W. & GUYONNET D. (1992): Transmissivität der Zuflussstellen und Durchlässigkeit der Matrix im Kristallin der Tiefbohrung Siblingen. - Nagra intern. Ber. NIB 92-43, June 1992. Nagra, Wettingen.

LANYON G.W. (1992a): NAPSAC modeling of crystalline fracture systems. - Nagra intern. Rep. NIB 92-52, February 1992. Nagra, Wettingen.

LANYON G.W. (1992b): Geometric simulations of fracture networks - Calculations based on data from the Siblingen borehole. - Nagra intern. Rep. NIB 92-125, December 1992. Nagra, Wettingen.

LEMCKE K. (1984): Gutachten über tiefe Grundwässer unterhlab von Tertiär (und Kreide) im Schweizer Mittelland und Jura. - Unpubl. Gutachten für Nagra vom 8.6.84.

LINDER N. & VOBORNY O. (1991): Statistische Auswertung der Matrixdurchlässigkeiten und der Transmissivitäten der Zuflussstellen im Kristallin der Tiefbohrungen BOE, KAI und LEU. - Nagra intern. Ber. NIB 91-23, May 1991. Nagra, Wettingen.

MAZUREK M. (1990): Wasser-Fliesssysteme im Kristallin der Nordschweiz: Systematik diskreter Zuflusspunkte. - Nagra intern. Ber. NIB 90-57, November 1990. Nagra, Wettingen.

MAZUREK M. (1991): Geochemical interaction between groundwater and aplitic/pegmatitic dykes and leucocratic gneisses: Geological input parameters for safety-performance analysis. - Nagra intern. Ber. NIB 91-45. Nagra, Wettingen.

MAZUREK M. (in prep.): Geology of the crystalline basement of Northern Switzerland and derivation of geological input data for hydrodynamic modeling and safety performance analysis. - Nagra tech. Rep. 93-12. Nagra, Wettingen.

MORENO L., TSANG Y.W., TSANG C.F., HALE F.V. & NERETNIEKS I. (1988): Flow and tracer transport in a single fracture: A stochastic model and its relation to some field observations. - Water Resources Res., 24(12), 2033-2048.

NERETNIEKS I., MORENO L., ABELIN H., BIRGERSSON L., WIDEN H. & AGREN H. (1990): A large scale flow and tracer experiment in granite. - Proceedings of the GEOVAL 1990 Symposium, Swedish Nuclear Power Inspectorate.

PASQUIER F., WILSON W. & VOMVORIS S. (1992): Reference set of hydraulic-head values at the Böttstein, Kaisten, Leuggern, Riniken, Schafisheim, Siblingen and Weiach boreholes, Northern Switzerland. - Nagra intern. Rep. NIB 92-51, January 1993. Nagra, Wettingen

PEARSON F.J. Jr., BALDERER W., LOOSLI H.H., LEHMANN B.E., MATTER A., PETERS Tj., SCHMASSMANN H. & GAUTSCHI A. (1991): Applied Isotope Hydrogeology - A case study in Northern Switzerland. - Nagra tech. Rep. NTB 88-01, May 1991. Nagra, Wettingen.

RESELE G. & JAQUET O. (1992): Statistik ebener Strukturen - Nagra intern. Ber. NIB 91-25, July 1992. Nagra, Wettingen.

RIVERA A. & RESELE G. (1992): Analytical and numerical evaluations of variable-density groundwater flow in Northern Switzerland. - Nagra intern. Rep. NIB 91-98, November 1992. Nagra, Wettingen.

RYBACH L., EUGSTER W. & GRIESSER J.-C. (1987): Die geothermischen Verhältnisse in der Nordschweiz. - Eclogae geol. Helv., Vol. 80/2, 521-534.

SCHMASSMANN H., KULLIN M. & SCHNEEMANN K. (1992): Hydrochemische Synthese Nordschweiz: Buntsandstein-, Perm- und Kristallin-Aquifere. - Nagra tech. Ber. NTB 91-30, Januar 1992. Nagra, Wettingen.

STÄUBLE J. (1993): Hydrogeologische Charakterisierung der Schottergrundwässer im unteren Aaretal und Rheintal. - Nagra intern. Ber. NIB 92-123, Februar 1993. Nagra, Wettingen.

STOBER I. & VILLINGER E. (1994): Hydraulisches Potential und Durchlässigkeit des höheren Malms und des Oberen Muschelkalks im baden-württembergischen Molassebecken. - Jahreshefte des Geologischen Landesamtes Baden-Württemberg, 1994.

THURY M., GAUTSCHI A., MAZUREK M., MÜLLER W.H., NAEF H., PEARSON F.J., VOMVORIS S. & WILSON W.E. (1994): Geology and hydrogeology of the crystalline basement of Northern Switzerland. - Nagra tech. Rep. NTB 93-01, May 1994. Nagra, Wettingen.

TSANG Y.W. & TSANG C.F. (1987): Channel model of flow through fracture media. - Water Resources Res., 23(3), 467-479.

TSANG Y.W., TSANG C.F., NERETNIEKS I. & MORENO L. (1988): Flow and tracer transport in fractured media: A Variable Aperture Channel Model and its properties. - Water Resources Res., 24(12), 2049-2060.

VOBORNY O., ADANK P., HÜRLIMANN W., VOMVORIS S. & MISHRA S. (1991): Grimsel Test Site: Modeling of groundwater flow in the rock body surrounding the underground laboratory. - Nagra tech. Rep. NTB 91-03, October 1991. Nagra, Wettingen.

VOBORNY O. (1992): Regional groundwater flow in crystalline rocks of Northern Switzerland: Preliminary results of a numerical model using an equivalent-porous-medium approach. - Nagra intern. Rep. NIB 91-88, May 1992. Nagra, Wettingen.

VOBORNY O., WILSON W., HÜRLIMANN W. & VOMVORIS S. (1992): Analysis of regional groundwater flow in crystalline rocks of Northern Switzerland: Results of a numerical model using an equivalent porous medium. - Nagra intern. Rep. NIB 91-95, September 1992. Nagra, Wettingen.

VOBORNY O., VOMVORIS S. & RESELE G. (1993): Hydrogeology of crystalline rocks of Northern Switzerland: Synthesis of hydraulic borehole data and assessment of effective properties. - Nagra intern. Rep. NIB 92-87, December 1993. Nagra, Wettingen.

VOMVORIS S., VOBORNY O., WILSON W., ANDREWS R. & HÜRLIMANN W. (1992): Hydrogeology of crystalline rocks of Northern Switzerland: Synthesis of results relevant to safety analysis, Reference Area West. - Nagra intern. Rep. NIB 92-65, December 1992. Nagra, Wettingen.

VOMVORIS S., VOBORNY O., WILSON W., & ANDREWS R. (1993): Hydrogeology of crystalline rocks of Northern Switzerland: Synthesis of results relevant to safety analysis, Reference Area East. - Nagra intern. Rep. NIB 92-126, February 1993. Nagra, Wettingen.

VOMVORIS S., ANDREWS R.W., LANYON G.W., VOBORNY O. & WILSON W. (in prep.): Methodology for deriving hydrogeological input parameters for safety-analysis models -- Applications to fractured crystalline rocks in Northern Switzerland. - Nagra tech. Rep. NTB 93-14. Nagra, Wettingen.

APPENDIX 1: Compilation of all identified inflow points (WCF's) in the boreholes: Definitive location and assigned T value. Data from KLEMENZ (1991) and KLEMENZ & GUYONNET (1992)

Explanation:
Column 2: Identification No. of inflow point in borehole
Column 3: Total depth below ground elevation, Z (m)
Column 4: Relative depth below the top of crystalline rocks, Zk (m)
Column 5: Definitive assigned T value to the WCF
Column 7: Assigned conceptual domain
Column 8: Classification in principal types: 1 = cataclastic zone, 2 = joints, 3 = aplitic dyke (some data points not assigned)

WEST	Inflow	Z (m)	Zk (m)	T(m^2/s)	log T	Domain	Type
1	BOE 1	388.9	73.6	1.0E-06	-6.0	HPD	2
2	2	401.4	86.1	2.0E-06	-5.7	(BOE)	3
3	3	466.3	151.0	3.0E-08	-7.5		1
4	3	479.3	164.0	5.0E-08	-7.3		
5	102	563.7	248.4	2.5E-08	-7.6		1
6	103	613.1	297.8	2.5E-07	-6.6		3
7	4	619.0	303.7	2.0E-06	-5.7		3
8	104	626.5	311.2	1.0E-05	-5.0		
9	5	638.0	322.7	1.0E-06	-6.0		3
10	105	652.0	336.7	1.0E-06	-6.0		2
11	106a	758.2	442.9	2.5E-07	-6.6		1
12	106b	765.4	450.1	2.5E-07	-6.6		1
13	6	777.7	462.4	4.0E-07	-6.4		1
14	7	790.0	474.7	2.5E-05	-4.6		1
15	8	847.5	532.2	2.5E-09	-8.6	LPD	1
16	9	964.1	648.8	1.0E-09	-9.0	(BOE)	1
17	10	970.4	655.1	2.0E-10	-9.7		1
18	11	1158.5	843.2	2.5E-10	-9.6		3
19	12	1320.0	1004.7	5.0E-09	-8.3		1
20	13	1328.0	1012.7	3.0E-10	-9.5		1
21	107	1405.5	1090.2	1.0E-09	-9.0		1
22	KAI 1	302.9	6.4	1.0E-05	-5.0	HPD	2
23	2	310.8	14.3	1.0E-05	-5.0	(KAI)	2

WEST	Inflow	Z (m)	Zk (m)	T(m^2/s)	log T	Domain	Type
24	3	327.6	31.1	2.5E-07	-6.6	HPD	1
25	4	355.4	58.9	1.5E-05	-4.8		1
26	5	382.4	85.9	1.0E-06	-6.0		2
27	6	423.5	127	1.0E-05	-5.0		1
28	7	432.0	135.5	1.0E-05	-5.0		1
29	8	446.9	150.4	5.0E-06	-5.3		1
30	9	487.0	190.5	8.0E-06	-5.1		1
31	10	502.7	206.2	1.5E-06	-5.8		1
32	11	522.2	225.7	2.5E-05	-4.6		2
33	12	540.6	244.1	5.0E-05	-4.3		2
34	107	574.4	277.9	1.0E-07	-7.0		2
35	13	620.6	324.1	2.5E-08	-7.6		2
36	14	646.9	350.4	2.0E-06	-5.7		1
37	15	648.8	352.3	2.0E-06	-5.7		1
38	16	654.6	358.1	2.0E-06	-5.7		1
39	17	664.4	367.9	2.0E-06	-5.7		1
40	18	672.0	375.5	2.0E-09	-8.7	LPD	1
41	19	686.4	389.9	2.0E-09	-8.7	(KAI)	1
42	21	697.3	400.8	6.0E-11	- 10.2		1
43	102	809.0	512.5	8.0E-08	-7.1	MWCF	
44	22	822.0	525.5	3.0E-06	-5.5	(KAI)	2
45	23	845.2	548.7	8.0E-07	-6.1		2
46	24	852.9	556.4	8.0E-07	-6.1		1
47	25	859.1	562.6	8.0E-07	-6.1		
48	26	948.8	652.3	1.5E-06	-5.8		2
49	103	996.0	699.5	5.0E-08	-7.3		
50	104	1020.0	723.5	2.5E-08	-7.6		
51	27	1040.8	744.3	4.0E-05	-4.4		3
52	28	1045.1	748.6	3.0E-07	-6.5		2
53	29	1050.9	754.4	3.0E-07	-6.5		1
54	105	1069.5	773.0	1.0E-07	-7.0		
55	30	1088.6	792.1	2.5E-06	-5.6		2
56	31	1091.7	795.2	2.5E-06	-5.6		3

WEST	Inflow	Z (m)	Zk (m)	T(m^2/s)	log T	Domain	Type
57	32	1097.3	800.8	2.5E-07	-6.6	MWCF	2
58	33	1143.5	847.0	7.5E-08	-7.1		3
59	34	1174.2	877.7	2.5E-06	-5.6		3
60	35	1181.9	885.4	2.5E-06	-5.6		3
61	36	1191.4	894.9	4.0E-07	-6.4		3
62	38	1205.1	908.6	4.0E-07	-6.4		3
63	106	1230.5	934	1.0E-08	-8.0		
64	39	1282.0	985.5	2.0E-07	-6.7		
65	LEU 2	244.3	21.5	7.5E-06	-5.1	HPD	
66	3	257.0	34.2	7.5E-06	-5.1	(LEU)	1
67	4	273.1	50.3	1.0E-07	-7.0		1
68	5	319.4	96.6	5.0E-08	-7.3		3
69	102	444.6	221.8	5.0E-07	-6.3		
70	6	458.5	235.7	2.0E-06	-5.7		2
71	7	478.9	256.1	2.0E-06	-5.7		2
72	8a	539.9	317.1	1.0E-07	-7.0		3
73	8b	540.9	318.1	1.0E-07	-7.0		1
74	8c	542.6	319.8	1.5E-06	-5.8		3
75	8d	546.8	324.0	1.0E-07	-7.0		3
76	103	580.0	357.2	3.0E-08	-7.5		
77	9	684.5	461.7	1.0E-07	-7.0		1
78	10a	704.4	481.6	3.0E-06	-5.5		1
79	10b	706.6	483.8	3.0E-06	-5.5		3
80	11	728.1	505.3	2.5E-10	-9.6		1
81	12	778.3	555.5	7.5E-07	-6.1		2
82	13	821.9	599.1	5.0E-10	-9.3		2
83	14	844.0	621.2	5.0E-07	-6.3		1
84	15	856.9	634.1	5.0E-08	-7.3		1
85	16	894.5	671.7	7.5E-10	-9.1	LPD	3
86	17a	918.1	695.3	5.0E-10	-9.3	(LEU)	1
87	17b	923.5	700.7	3.0E-10	-9.5		1
88	18	1046.1	823.3	2.5E-10	-9.6		1
89	19	1082.9	860.1	7.0E-10	-9.2		1

WEST	Inflow	Z (m)	Zk (m)	T(m^2/s)	log T	Domain	Type
90	20	1188.1	965.3	2.5E-10	-9.6	LPD	3
91	21	1199.6	976.8	1.0E-09	-9.0		2
92	22a	1215.1	992.3	1.0E-09	-9.0		2
93	22b	1222.5	999.7	1.0E-10	-10.0		1
94	23	1248.0	1025.2	7.5E-10	-9.1		2
95	24	1268.6	1045.8	2.5E-10	-9.6		2
96	25	1299.0	1076.2	1.0E-09	-9.0		3
97	26	1327.2	1104.4	5.0E-10	-9.3		2
98	28	1437.4	1214.6	1.0E-09	-9.0		1
99	30	1640.4	1417.6	2.5E-08	-7.6	MWCF	1
100	31	1659.5	1436.7	4.0E-05	-4.4	(LEU)	1

Statistics area WEST

Parameter	Upper/HPD	Lower/LPD	MWCF
Mean T (ar)	4.35E-06	9.44E-10	4.13E-06
Stand. dev.	8.50E-06	1.05E-09	1.10E-05
Mean log T (geom)	-6.17 -9.24	-6.32	
Log std. dev. (σ)	±1.10 ±0.40	±0.90	

EAST	Inflow	Z (m)	Zk (m)	T(m^2/s)	log T	Domain	Type
101	SIB 1	421.7	73.1	1.5E-03	-2.82	Top	2
102	2	460.0	111.4	4.0E-06	-5.40	Upper	
103	3	475.4	126.8	3.0E-06	-5.52	(SIB)	
104	4	498.1	149.5	5.0E-07	-6.30		
105	5	683.0	334.4	1.0E-05	-5.00		
106	6	691.9	343.3	1.0E-04	-4.00		2
107	7	700.0	351.4	3.0E-05	-4.52		
108	8	742.0	393.4	6.0E-06	-5.22		
109	9	780.6	432.0	7.0E-06	-5.15		
110	10	843.3	494.7	3.5E-05	-4.46		2
111	11	856.2	507.6	1.0E-06	-6.00		1

EAST	Inflow	Z (m)	Zk (m)	T(m^2/s)	log T	Domain		Type
112	12	879.5	530.9	3.0E-07	-6.52	Upper		1
113	13	887.5	538.9	2.0E-06	-5.70	(SIB)		2
114	14	894.0	545.4	5.0E-07	-6.30			
115	15	912.0	563.4	4.0E-06	-5.40			
116	16	917.0	568.4	4.0E-06	-5.40			
117	17	926.5	577.9	3.0E-05	-4.52			2
118	18	932.0	583.4	1.0E-06	-6.00			1
119	19	944.0	595.4	2.5E-06	-5.60			2
120	20	954.6	606.0	1.0E-06	-6.00			2
121	21	967.2	618.6	3.0E-07	-6.52	Lower		2
122	22	1070.4	721.8	1.0E-07	-7.00			2
123	23	1078.7	730.1	7.0E-07	-6.15			2
124	24	1082.6	734.0	5.0E-07	-6.30			1
125	25	1162.6	814.0	1.5E-07	-6.82			2
126	26	1223.6	875.0	6.0E-08	-7.22			
127	27	1236.4	887.7	1.0E-07	-7.00			1
128	28	1250.1	901.5	2.5E-07	-6.60			1
129	29	1308.6	960.0	3.0E-08	-7.52		Lower	1
130	30	1385.4	1036.8	1.5E-07	-6.82			1
131	31	1410.1	1061.5	4.0E-08	-7.40			2
132	32	1419.4	1070.8	4.0E-08	-7.40			1
133	33	1472.9	1124.3	5.0E-09	-8.30			2
134	34	1477.9	1129.3	1.5E-07	-6.82			1
135	35	1502.2	1153.6	4.0E-07	-6.40			3
136	36	1512.7	1164.1	1.5E-07	-6.82			2

Statistics area EAST

Parameter	Top	Upper	Lower
Mean T (ar)	1.5E-03	1.3E-05	2.0E-07
Stand. dev.	(1 value)	2.3E-05	1.9E-07
Mean log T (geom)		-5.42	-6.94
Log std. dev. (σ)		±0.7	±0.5

APPENDIX 2: Compilation of all identified matrix properties in the boreholes: Location and assigned conductivity value. Data after KLEMENZ (1991) and KLEMENZ & GUYONNET (1992)

Explanation:
Column 2: Total depth of **interval center** below ground elevation, Z (m)
Column 3: Depth of center below top of crystalline rocks, Zk (m)
Column 4: Length of interval, L, in m
Column 5/6: Definitive K value assigned to the interval

No.	Z (m)	Zk (m)	L (m)	K(m/s)	log K
1 BOE	347.7	32.4	7.1	3.0E-12	-11.52
2	368.2	52.9	16.2	5.0E-12	-11.30
3	411.6	96.3	11.2	2.0E-12	-11.70
4	421.7	106.4	9.0	1.3E-11	-10.89
5	457.0	141.7	12.4	2.0E-11	-10.70
6	518.5	203.2	30.4	3.4E-13	-12.47
7	538.7	223.4	10.0	1.0E-13	-13.00
8	552.1	236.8	16.8	3.4E-13	-12.47
9	585.6	270.3	12.6	1.0E-12	-12.00
10	600.8	285.5	17.8	4.1E-12	-11.39
11	665.0	349.7	23.0	3.9E-13	-12.41
12	679.6	364.3	6.2	1.0E-12	-12.00
13	684.7	369.4	4.0	3.9E-13	-12.41
14	703.9	388.6	33.2	1.0E-12	-12.00
15	726.3	411.0	11.5	4.9E-13	-12.31
16	735.8	420.5	7.7	1.0E-13	-13.00
17	746.7	431.4	14.0	4.9E-13	-12.31
18	754.5	439.2	1.5	3.2E-11	-10.49
19	797.1	481.8	8.3	2.5E-11	-10.60
20	807.6	492.2	12.5	7.0E-13	-12.15
21	820.1	504.8	12.6	6.0E-12	-11.22
22	832.7	517.4	12.6	6.0E-12	-11.22
23	873.8	558.5	25.0	2.0E-13	-12.70

No.		Z (m)	Zk (m)	L (m)	K(m/s)	log K
24		898.8	583.5	25.1	1.0E-12	-12.00
25		916.9	601.6	11.0	1.0E-11	-11.00
26		928.7	613.4	12.7	6.3E-13	-12.20
27		937.0	621.7	3.9	3.0E-12	-11.52
28		943.2	627.9	8.4	6.3E-13	-12.20
29		985.0	669.7	25.0	1.0E-13	-13.00
30		1010.0	694.7	25.1	4.0E-13	-12.40
31		1035.1	719.8	25.0	2.0E-13	-12.70
32		1060.1	744.8	25.0	1.0E-12	-12.00
33		1085.1	769.8	25.0	6.0E-13	-12.22
34		1110.2	794.9	25.1	3.0E-12	-11.52
35		1135.2	819.9	25.0	2.0E-12	-11.70
36		1185.3	870.0	25.1	6.0E-13	-12.22
37		1210.3	895.0	25.0	9.0E-12	-11.05
38		1235.3	920.0	25.0	6.0E-12	-11.22
39		1260.4	945.1	25.0	3.0E-12	-11.52
40		1285.4	970.1	25.0	1.0E-13	-13.00
41		1344.8	1029.5	20.8	2.0E-12	-11.70
42		1362.1	1046.8	13.8	2.5E-12	-11.61
43		1381.5	1066.2	25.1	4.0E-13	-12.40
44		1397.2	1081.9	6.3	4.7E-12	-11.33
45		1416.0	1100.7	10.4	2.0E-13	-12.70
46		1432.7	1117.4	19.9	2.2E-12	-11.66
47		1456.6	1141.3	28.1	3.0E-12	-11.52
48		1481.7	1166.4	25.0	1.0E-12	-12.00
49		1497.8	1182.5	7.1	2.0E-13	-12.70
50	KAI	407.0	110.5	24.8	1.0E-10	-10.00
51		555.3	258.8	25.0	1.0E-11	-11.00
52		604.8	308.3	25.0	3.0E-12	-11.52
53		728.5	432.0	24.7	5.6E-11	-10.26
54		753.1	456.6	24.5	1.0E-10	-9.99
55		777.9	481.4	24.9	5.0E-11	-10.30
56		798.2	501.7	9.7	5.0E-12	-11.30

No.		Z (m)	Zk (m)	L (m)	K(m/s)	log K
57		876.8	580.3	24.9	1.0E-12	-12.00
58		901.5	605.0	24.5	2.0E-11	-10.69
59		920.9	624.4	14.3	7.2E-12	-11.14
60		935.3	638.8	14.6	2.0E-12	-11.70
61		971.2	674.7	24.9	5.0E-11	-10.30
62		1128.8	832.3	25.0	5.0E-11	-10.30
63		1251.0	954.5	4.1	4.1E-11	-10.39
64	LEU	267.8	45.0	1.0	6.0E-13	-12.22
65		292.5	69.7	24.8	6.0E-10	-9.22
66		341.6	118.8	24.8	1.5E-12	-11.82
67		364.4	141.6	20.8	3.1E-11	-10.50
68		385.4	162.6	22.1	1.0E-10	-9.99
69		407.3	184.5	22.7	1.0E-12	-12.00
70		429.8	207.0	22.5	1.0E-12	-12.00
71		496.0	273.2	22.7	1.0E-10	-10.00
72		606.2	383.4	28.0	1.0E-12	-12.00
73		630.7	407.9	21.0	3.1E-11	-10.50
74		653.7	430.9	25.0	6.0E-12	-11.22
75		745.2	522.4	25.5	1.0E-11	-11.00
76		769.9	547.1	18.2	3.0E-11	-10.52
77		940.1	717.3	23.7	6.2E-12	-11.21
78		962.8	740.0	21.6	2.3E-12	-11.64
79		986.0	763.2	24.9	3.0E-13	-12.52
80		1006.3	783.5	15.6	7.8E-13	-12.11
81		1026.6	803.8	25.0	2.0E-13	-12.70
82		1064.6	841.8	24.9	3.0E-12	-11.52
83		1101.1	878.3	23.0	2.1E-12	-11.68
84		1125.0	902.1	24.7	1.0E-12	-12.00
85		1149.8	927.0	25.0	3.0E-13	-12.52
86		1174.7	951.9	24.7	1.0E-11	-11.00
87		1283.8	1061.0	24.9	1.0E-13	-13.00
88		1349.2	1126.4	25.0	2.0E-12	-11.70
89		1370.7	1147.9	18.0	3.6E-12	-11.44

No.		Z (m)	Zk (m)	L (m)	K(m/s)	log K
90		1392.1	1169.3	24.9	1.0E-13	-13.00
91		1414.8	1192.0	20.4	5.9E-13	-12.23
92		1455.9	1233.1	23.1	3.2E-12	-11.49
93		1480.0	1257.2	25.0	1.0E-13	-13.00
94		1504.7	1281.9	24.5	2.0E-12	-11.69
95		1529.2	1306.4	24.3	6.1E-13	-12.21
96		1553.8	1331.0	25.0	3.0E-13	-12.52
97		1578.7	1355.9	24.7	5.0E-12	-11.30
98		1603.5	1380.7	25.0	1.0E-13	-13.00
99	SIB	438.9	90.3	7.7	5.1E-11	-10.29
100		487.3	138.7	7.2	5.3E-11	-10.28

Statistics Matrix (all boreholes)

Parameter	
Mean K (ar)	1.74E-11
Stand. dev.	6.3E-11
Mean log K (geom)	-11.63
Log std. dev. (σ)	±0.86

Appendix 3 Conceptual model of the groundwater flow system in crystalline rocks of Northern Switzerland.

EXPLANATION

Columns No. 1 & 2: Hypotheses

- CPH Currently preferred hypothesis
- PAH Plausible alternative hypothesis

Column No. 3 Uncertainty: Degree of uncertainty that the CPH is correct

- L Low uncertainty
- M Medium uncertainty
- H High uncertainty

Column No. 4 Sensitivity: Sensitivity of model results to hypothesis

- ⊕ Relatively large sensitivity
- O Sensitivity not tested or not applicable
- ⊖ Relatively small sensitivity

EPM Equivalent porous medium
K Hydraulic conductivity
SBF Southern Black Forest

Nagra boreholes:

BOE Böttstein
KAI Kaisten
LEU Leuggern
SIB Siblingen
WEI Weiach

Hydrogeologic model units:

BST Buntsandstein
PCT Permocarboniferous trough (not modeled)
P Permian units (Rotliegend) of PCT shoulder
UC Upper crystalline unit
LC Lower crystalline unit
DZ Disturbed zone along PCT

Hypotheses concerning conceptual-model elements		3. Uncer-tainty	4. Sensi-tivity	5. Comments
1. Currently Preferred Hypotheses (CPH)	**2. Plausible Alternative Hypotheses (PAH)**			
A. Hydrogeologic framework				
1. Distinct UC (with relatively large K) and LC (with relatively small K) units exist.	1a. K of crystalline rocks gradually decreases with depth. 1b. K of crystalline rocks is relatively uniform with depth. 1c. K of crystalline rocks is highly variable and shows no consistent change with depth.	M	⊕	· Test results from all Nagra boreholes in crystalline rocks show general decrease in K with depth. CPH 1 gives a better match of simulated and observed heads in LC unit than does PAH 1b. PAH 1a provides similar results as CPH1. PAH 1c was not tested.
2. Each crystalline unit has spatially variable K	2a. K of each crystalline domain is spatially relatively uniform.	L	○	· CPH 2 not tested with EPM model. PAH 2a was assumed to be a satisfactory representation for regional EPM model.
3. K of PCT shoulder is isotropic and substantially less than K of UC.	3a. K of PCT shoulder is about the same as K of UC unit. 3b. K of PCTs is highly anisotropic with relatively large K(horizontal) and low K(vertical)	M	⊖	· In EPM model, PAH 3a shows no significant effect on flow in crystalline rocks. PAH 3b was not tested.
4. A northern segment of deep PCT exists but has little impact on regional flow system.	4a. A large segment or multiple segments of deep PCT exist and have substantial impact on flow in crystalline basement.	L	⊖	
5. A disturbed zone of relatively large K (DZ) exists in LC along the margin of the PCT	5a. Undisturbed LC unit adjoins PCT, and no DZ exists.	H	⊖	· DZ is proposed to accomodate postulated basal flux (see PAH B5b).
6. Horizontal anisotropy of K in BST has little or no effect on flow in crystalline rocks.	6a. Horizontal anisotropy of K in BST has substantial effect on flow in crystalline rock.	L	⊖	

Hypotheses concerning conceptual-model elements		3. Uncer-tainty	4. Sensi-tivity	5. Comments
1. Currently Preferred Hypotheses (CPH)	**2. Plausible Alternative Hypotheses (PAH)**			
A7. Large-scale horizontal anisotropy of K occurs in crystalline rocks, K(NW)>K(SW), and substantially affects flow.	7a. Large-scale horizontal anisotropy of K occurs in crystalline rocks, K(SW)>K(NW), and substantially affects flow. 7b. No large-scale horizontal anisotropy of K occurs in crystalline basement.	H	⊖	· CPH 7 is in accordance with known tectonic stress field, but PAH 7a produces better model results. Anisotropy probably is related to major structural features, such as those explicitly considered in KRI3 model.
B. Boundary conditions				
1. <u>Top (exposed crystalline rocks, T1)</u> · Infiltration occurs in upland areas of exposed crystalline basement. · Local discharge occurs at tributaries to Rhine River, north of Rhine. · Principal discharge occurs at Rhine River west of Aare River.	1a. No PAH identified.	L	O	
2. <u>Top (covered crystalline rocks, T2)</u> · No significant vertical leakage occurs through Mesozoic rocks that overlie BST and UC units.	2a. Significant vertical leakage occurs locally between Mesozoic sediments and underlying BST and UC units, along major fault zones.	L	⊖	· Any downward leakage that might occur tends to be drained by BST/UC aquifer. · The CPH is supported by hydrochemical evidence
3. <u>Top (covered crystalline rocks)</u> · In the SIB-WEI area, Wutach River valley is a principal discharge area.	3a. In the SIB area, no major discharge occurs to the Wutach River valley.	H	⊕	· Inclusion of Wutach as a discharge area substantially improves match of simulated and observed heads in SIB & WEI, but field evidence is lacking.

Hypotheses concerning conceptual-model elements		3. Uncer-tainty	4. Sensi-tivity	5. Comments
1. Currently Preferred Hypotheses (CPH)	**2. Plausible Alternative Hypotheses (PAH)**			
B4. Bottom of LC (B1) · No CPH identified.	4a. No flow occurs across B1 boundary. 4b. Significant density-driven groundwater flow due to thermal variations occurs across B1.	--	○	· PAH 4a was the default condition in all simulation runs. PAH 4b was not tested with EPM model.
5. Bottom of DZ (B2) · No CPH identified.	5a. No flow occurs across B2 boundary. 5b. Significant upward groundwater flow (basal flux) occurs across bottom boundary of DZ. Basal flux is driven by variations in groundwater density that are due princpally to temperature variations.	--	⊕	· Both PAH's were tested in the EPM model; PAH 5b gives slightly better results in terms of matching simulated and observed heads in the W part of the model area. However, inclusion of basal flux is not supported by hydrochemical evidence from UC at BOE. Effects of thermal variations on density-driven flow were not tested with this EPM model.
6. North, VN · Southward inflow in UC+LC occurs across VN boundary from the central Black Forest	6a. No lateral inflow occurs across northern vertical boundary, VN.	L	⊖	· EPM model suggests that inflow across northern boundary is minor compared to total surface recharge into UC unit.
B7. South, VS · No significant lateral inflow occurs from PCT into crystalline rocks.	7a. Significant northward lateral flow occurs from deep PCT into crystallines rocks across the southern model boundary, VS.	M	⊕	· Substituting lateral flux from PCT (without DZ) for basal flux (with DZ) significantly improves match of heads in LC. - However, this lateral migration of saline waters into adjacent crystalline rocks is not supported by hydrochemical evidence.

Hypotheses concerning conceptual-model elements		3. Uncer-tainty	4. Sensi-tivity	5. Comments
1. Currently Preferred Hypotheses (CPH)	**2. Plausible Alternative Hypotheses (PAH)**			
8. <u>West, VW</u> · Lateral inflow occurs westward across the western boundary, into or across a permeable fault zone.	8a. The western boundary VW is a fault zone that has very small K (no-flow boundary) and thus forces virtually all westward-flowing groundwater to discharge to the Rhine River before leaving the model area. 8b. Inflow occurs **eastward** across the fault	H	⊖	· Inclusion of PAH's 8a and 8b in EPM model has little impact on heads at KAI site.
9. <u>East, VE</u> · Eastern boundary is a permeable fault zone that allows outflow eastward from the model	9a. Eastern boundary, VE, is a fault zone with small K that virtually prevents groundwater flow across the boundary.	M	⊕	· No-flow VE boundary in the EPM model results in higher heads at WEI and SIB but has little effect west of these sites.
10. <u>East, VE</u> · BST/UC heads along the fault zone at eastern boundary are relatively low, because they are affected by a potentiometric trough in Upper Muschelkalk in the Lake Constance area.	10a Potentiometric trough in the Lake Constance area has no effect on crystalline heads in the SE part of the model area; heads there are relatively high. 10b Potentiometric trough in the Lake Constance area results in very low head in the SE part of the model area.	M	⊕	· High head in SE (PAH 10a) results in substantially higher simulated heads in SIB-WEI area and is not supported by the observed horiz. gradients in UC; a very low head of about 300 m (PAH 10b) is hydraulically possible but not likely.
C. Flow paths and groundwater origins: Siblingen-Weiach area.				
1. Groundwater originates as recharge in the Black Forest.	1a. No PAH identified.	L	O	
2. A groundwater divide exists; it separates flow toward the SE from flow toward the SW.	2a. No groundwater divide exists; all flow is toward the SW (i.e., the Rhine River discharge area)	M	⊕	· CPH in the EPM model results in much better match of heads at the SIB and WEI sites.

Hypotheses concerning conceptual-model elements		3. Uncer-tainty	4. Sensi-tivity	5. Comments
1. Currently Preferred Hypotheses (CPH)	**2. Plausible Alternative Hypotheses (PAH)**			
C3. Groundwater divide is east of SIB; flow from SIB site is toward SW.	3a. Groundwater divide is west of SIB; flow from SIB site is toward SE.	L	O	· In the EPM model, a head of about 300 m is required to shift the divide west of the SIB site; possible, but not likely (see PAH B10b above).
D. Flow paths and groundwater origins: BOE-LEU-KAI area.				
1. Groundwater in the upper crystalline unit north of the PCT originates as recharge in the southern Black Forest (SBF).	1a. No PAH identified	L	O	· CPH is based on hydrochemical evidence.
2. Groundwater in upper crystalline unit (UC) at BOE site belongs to the regional flow system of SBF (according to CPH D1 above). The influence of saline groundwaters of PCT domain (i.e., with origin from beneath, beside or within the PCT) is minor (a few percent by volume).	2a. Groundwater in UC at BOE consists of a mixture of low-mineralized SBF water and saline water of PCT domain (in EPM model represented by the DZ water with origin as basal flux, Weiach water or PCT water)	L	O	· In the EPM model, a flux analysis was made to discriminate among the CPH and PAH. Results indicate that the CPH conditions are reproduced when no external fluxes (basal flux or PCT water) are introduced into the model. · PAH 2a is reproduced if areal fluxes are prescribed at bottom or south model boundary. Both cases provide a better head match (see PAH's B5b+B7a.); however, the simulated high proportion of saline water in UC contradicts the hydrochemical evidence at this site.

Hypotheses concerning conceptual-model elements		3. Uncer-tainty	4. Sensi-tivity	5. Comments
1. Currently Preferred Hypotheses (CPH)	**2. Plausible Alternative Hypotheses (PAH)**			
D3. Groundwater in UC and LC at LEU site belongs entirely to the flow system of SBF (CPH D1). The influence of saline groundwaters of PCT domain is not significant.	3a. No PAH identified	L	O	· EPM model results are in balance with hydrochemical evidence.
4. No CPH identified	4a. Highly mineralized groundwater in LC at BOE results predominantly from in-situ rock-water interaction. 4b. Highly mineralized groundwater in LC at BOE results predominantly from a mixing of more saline PCT water with low-mineralized waters from SBF.	-	O	
E. Travel time				
1. Travel times from LC at the sites of BOE, LEU, and KAI to the discharge area in the Rhine River valley are on the order of thousands to tens of thousands of years.	1a. Travel times from LC at the sites of BOE, LEU and KAI to the Rhine River are on the order of hundreds of years, due to existence of major permeable structural features.	H	O	· EPM model did not fully evaluate influence of structural features. Travel times are highly sensitive to K, porosity, distance and gradients that are selected for the calculations.